Quantifying sedimentation in extensional basins and magmatism during continental collision

Kwantificering van sedimentatie in extensiebekkensenmagmatismetijdenscontinentalebotsing

(met een samenvatting in het Nederlands)

Квантификовање процеса седиментације у екстензионим басенима и магматизма током континентале колизије

(са резимеом на српском језику)

Proefschrift

ter verkrijging van de graad van doctor aan de Universiteit Utrecht op gezag van de rector magnicus, prof.dr. G.J. van der Zwaan, ingevolge het besluit van het college voor promoties in het openbaar te verdedigen op donderdag 5 oktober 2017 des morgens te 10.30 uur

door

Nevena Andrić

geboren op 5 februari 1988 te Kragujevac, Servië

Promotoren: Prof. dr. L.C. Matenco

Prof. dr. V. Cvetković

Prof. dr. S.A.P.L. Cloetingh

This study was financially supported by the Netherlands Research Centre for Integrated Solid Earth Sciences (ISES) and Ministry of Education, Science and Technological Development of Serbia.

На крају, на правом и коначном крају, све је ипак добро и све се решава хармонично.

Иво Андрић

Members of the Reading Committee:

Prof. dr. H.D. Sinclair	University of Edinburgh, United Kingdom
Prof. dr. T. Ehlers	University of Tuebingen, Germany
Prof. dr. S.D. Willett	Swiss Federal Institute of Technology (ETH) Zurich, Switzerland
Prof. dr. C. Faccenna	University Roma Tre, Italy
Dr. A. von Quadt	Swiss Federal Institute of Technology (ETH) Zurich, Switzerland

The research presented in this thesis was carried out at:

- Tectonics Research Group, Department of Earth Sciences, Faculty of Geosciences, Utrecht University, The Netherlands;
- Department of Petrology and Geochemistry, Faculty of Mining and Geology, University of Belgrade.

This is Utrecht Studies in Earth Sciences volume 136.

ISBN: 978-90-6266-479-5

Printed in the Netherlands by Proefschrift-AIO, typset in inDesign by the author.

Cover: photo collage includes field photos and photograph of strain rate of one of the numerical modelling experiments, which are presented in the following chapters.

Contents

Acknowledgements

This thesis is the culmination of three years of intensive research as well as professional and personal development. My thesis was based on an integrated approach, which involved intensive interactions with scientists from various fields. I am grateful for their contribution and support. This interaction went beyond scientific discussions: As Sierd likes to say: "You cannot be serious If you are not having fun…", therefore big thanks also goes to people who dragged me away from my computer to relax and have fun.

Firstly, I would like to thank Sierd Cloetingh, Liviu Matenco and Vladica Cvetković for giving me a chance to pursue my research and work on a very challenging subject in such an excellent professional environment. Also, thank you very much for your time, patient guidance, support and the confidence you gave me.

Sierd, thanks for always being helpful and enthusiastic about my extracurricular activities such as the idea to organize a student workshop in Serbia. I am very grateful to you for opening the door of the **FACULTY CLUB** for the **Tectos**! Lectures and events at the Faculty club were an inevitable part of my visits in Utrecht. There I had great opportunity to meet wonderful people and enjoy excellent music, geofluids and food.

Liviu's enthusiasm on the field was fantastic and really motivating. Every day was a learning process leading to new ideas. I really appreciated our long discussions from which I learned a lot. Thank you for teaching me to slow down and be patient sometimes, and for giving me the freedom to choose my own path.

Vladica, I am really grateful for your long term support on my scientific development, even when I decided to peruse my career in the `boring` soft rock. Your sharp comments and suggestions have been crucial since the early stages of my scientific career (remember my first proposal).

Further, I would like to express my gratitude to the members of the reading committee: Prof. Hugh Sinclair, Prof. Claudio Faccenna, Prof. Todd Ehlers, Prof. Sean Willett and Dr. Albrecht von Quadt. Thank you for taking the time to review my thesis and for your feedbacks.

Bruno, Davor, Oleg and Wout thank you for the time on the field, excellent discussions and great fun! I really enjoyed and learned a lot. Bruno, thank you for discussions and warm hospitality in Zagreb.

My sincere thanks also goes to Prof. dr. Hazim Hrvatović, who helped Karin and me during our work in the Sarajevo-Zenica Basin, Bosnia. Hazime, hvala Vam for sharing your huge experience and knowledge about the geology of Bosnia. I am grateful to his team in the Federal Institute for Geology of Bosnia and Herzegovina, Vedad Demir, Alojz Filipović, Ćazim Šarić and Toni Nikolić for discussions and logistic support on the field.

Frits, Chris, Liviu and Hans, thank you for accepting me as a part of your fieldwork crews. It came in the right moment and really meant to me! I enjoyed a lot and learned enormously about geology and teaching.

One very important aspect of my PhD experience is being a part of **TECTOS**

and **USUAL SUSPECTS**. Dear **TECTOS**, Alessio, Antoine, Attila, Damien, Dimi, Elisa, Ernst, Eszter, Fausi, Fred, Inge, Jeroen, Jon, Katharina, Kristof, Lindsay, Lukman, Magdala, Martje, Miloš, Thomas thank you for moral support, long discussions in front of the coffee machine and/or in the boulder sterk, beers, dinners and excellent company during conferences.

Dear **SUSPECTS**, thank you for luring me away from my computer and helping me to refresh my mind with various activities, dancing, hikes, dinners, post-conference trips (`m honored for being a pioneer with you guys of the post NAC conference field trips :D). Thanks for emitting inexhaustible positive energy!

Typical life of the PhD includes bad days at the office and various and unfortunately numerous obstacles. Luckily, I had the wonderful office mate, Attila to share the heavy burden of geological and administrative problems and doubts, code/scripts issues, and unreadable and incomprehensible drafts of our manuscripts. Certainly, I cannot forget our long funny discussions, sometimes about geology and tons of laughs (e.g. does Estonian forest rings a bell). Thank you a lot for establishing the climbing Tecto group and introducing the world of climbing to me! Since then, I became a passionate climber.

Katharina, thanks for pushing me beyond what I thought were my limits! The time I spend working with you significantly improved my scientific thinking and writing.

Jeroen, first thank you for translating my summary into Dutch and sorry for being too picky. Also, thank you for long discussion, insightful comments and encouragements, but also for the difficult questions which stimulated me to stop working and start thinking. Your presence on my roasting events in Serbia was inevitable for the great atmosphere and fun, thanks!

Karin and Alex thanks for being my fantastic paranymphs. Karin, I spent great time on the field in Bosnia with Vedad and you. Our field crew endured long days on the field, complex geology, and even weird weather condition such as snow and devastating flooding. During these months I learned a lot from you about geology but also about Dutch directness and self-confidence which I see as very useful qualities in life. Your energy (although you are not drinking coffee) and enthusiasm was really inspiring and important in difficult moments.

Alex thanks for your patient ear and advices, and especially hilarious and awesome craziness, cooking and dancing parties, I loved it all! ☺

Dragana i Vlado, hvala puno for your constant support and encouragements, geological discussions, fieldworks and lab work, and fun since my bachelor studies.

Sacha, thanks for being excellent landlord and friend during my Utrecht visits.

Last but not the least, I would like to thank all my family and friends back home, especially my parents, sister and boyfriend for being always with me and encouraging me in difficult moments but also being there to celebrate my successes.

Summary

Continental collision is one of the main tectonic processes responsible for the formation of mountain ranges and plays an important role in the overall crustal growth, i.e. in the creation of new crust. The structural modifications along colliding continents result in a distinctive distribution of structural styles, sedimentary facies and metamorphic patterns, which are often associated with a migration of deformation and magmatism. Understanding the processes operating during collision requires an integrated approach in which the interaction of the lithospheric-, crustal- and basin-scale processes are analyzed at various time scales.

This thesis focuses on understanding the migration of deformation and its influence on deposition and magmatism in collisional orogenic systems. Firstly, the aim is to understand and quantify the sedimentation in basins driven by normal faulting, with particular focus on asymmetric extensional basins formed during the final stages of collision. Secondly, the thesis analyzes the relationship between magmatism and tectonic processes during continental collision by the means of process-oriented numerical modelling at lithospheric scale. Two key areas of the Alpine - Mediterranean region: the Dinarides of Central Europe and the Betic Cordillera of SE Spain are taken as natural laboratories where such relationships were studied.

Chapter 2 addresses the tectono-sedimentary evolution of the extensional asymmetric Sarajevo-Zenica Basin located in the Dinarides of Bosnia and Herzegovina. This intra-montane basin recorded Oligocene – Pliocene sedimentation in an isolated lake environment during the late stage of Dinarides orogenic evolution. The novel sedimentological and kinematic results demonstrate a close correlation between periods of normal faulting and sedimentological cycles at the scale of individual normal faults, which are consider as high-order cycles. The SW-ward migration of listric normal faults was associated with a gradual shift of the sedimentological environment, enabling the formation of sedimentological cycles at the basin scale, which are considered as low-order cycles. This is reflected by a largely uni-directional sediment supply from the neighbouring mountain belt located along the SW-ward basin margin. The high- and low-order cycles are used to define a new sedimentological model for such asymmetric extensional basins. Moreover, the study documents a novel succession of deformation events with important inferences for the evolution of the Dinarides mountain chain. Early - Middle Miocene extension that affected the central part of the Dinarides was associated with the opening of the neighbouring Pannonian Basin. The extension was preceded and followed by two phases of contraction, during the Oligocene – Early Miocene and the post-Middle Miocene, respectively. The Oligocene - Early Miocene thrusting took place during the final stages of the Dinarides collision, whereas the post-Middle Miocene contraction is correlated with the regional indentation of the Adriatic continental unit. This latter phase inverted the extensional basin by reactivating inherited basal listric detachment.

The relationship between magma generation and tectonic evolution of orogens during subduction and subsequent collision is investigated form lithosphere-to-basin scale in Chapter 3. A 2D magmatic-thermomechanical numerical modelling approach was used to analyze the volumes and compositions of

produced magmatic rocks during the relatively rapid subduction of a narrow ocean and subsequent continental collision. The results suggest that magmatism has a large-scale effect on geodynamic evolution of an orogen by focusing deformation during the entire subduction and collision process. The rheological structure and compositional layering of the crust impose a key control on the distribution of magmatic rocks within the orogen. Compared to previous models that adopted a simplified homogeneous crust, the here tested compositionally layered crust causes an increase of felsic material influx during continental collision and results in shallower magmatic sources that migrate with time towards the foreland. Changes in deformation style may be locally driven by magma emplacement rather than by slab movement processes. The modelling also demonstrates that the pattern of migration of deformation front and the magmatic arc relative to the location of the suture zone may be driven by the indentation of the lower crust of the upper plate into the orogenic wedge during the early stages of collision. Moreover, the modelling predicts a gradual temporal change in magma source composition from predominantly mafic to more felsic during subduction, subsequent collision and eduction stages. This transition explains the migration of magmatism and compositional changes of magmas, as well as the observed link with deformation in the Dinarides orogen of Central Europe.

Chapter 4 analyses the interplay between tectonic deformation and sedimentation during the onset of extension in one of the best exposed asymmetric extensional system, the Sorbas Basin in the Betic Cordillera of SE Spain. The Upper Serravallian-Tortonian interplay between extension and deposition is analyzed in the SE part of the basin, by the means of a detailed sedimentological and field kinematic study. The new kinematic and sedimentological results indicate that the basin evolution is characterized by low – order tectonic cycles driven by the change of deformation style and higher – order cycles driven by individual phases of fault activity. After extension initiation, syn – kinematic deposition was characterized by a wide spectrum of subaqueous gravity flows. The types of gravity flows and their transformation mechanisms were controlled by the sediment supply and basin physiography.

Samenvatting

Continentale botsing is een van de belangrijkste tektonische processen die verantwoordelijk zijn voor de vorming van bergketens en speelt een belangrijke rol in de vorming van nieuwe aardkorst. De structurele modificaties langs de randen van botsende continenten resulteren in een typische verdeling van structurele stijlen, sedimentaire facies en metamorfe patronen die vaak verband houden met een migratie van deformatie en magmatisme. Het begrijpen van de processen die tijdens de botsing actief zijn vereist een geïntegreerde aanpak waarbij de interactie van de lithosferische, korst- en bekkenschaal processen worden geanalyseerd op de verschillende tijdschalen waarop ze functioneren.

Dit proefschrift richt zich op het begrijpen van de migratie van deformatie en de invloed ervan op afzetting en magmatisme in orogene botsingsystemen. Enerzijds is het doel het kwantificeren van de sedimentatie in bekkens die wordt gedreven door afschuivingen, met bijzondere aandacht voor asymmetrische extensieve bekkens die zijn gevormd tijdens de laatste fasen van de botsing. Anderzijds analyseert het proefschrift de relatie tussen magmatisme en tektonische processen tijdens continentale botsing door middel van procesgeoriënteerde numerieke modellering op lithosfeer schaal. Twee belangrijke gebieden van het Alpen-Middellandse-Zeegebied: de Dinariden van Midden-Europa en de Betische Cordilleren van zuidoost Spanje zijn de natuurlijke laboratoria waar dergelijke relaties werden bestudeerd.

Hoofdstuk 2 bestudeert de tektono-sedimentaire evolutie van het extensieve asymmetrische Sarajevo-Zenica Bekken in de Dinariden van Bosnië en Herzegovina. Dit intra-montane bekken registreerde Oligoceen-Pliocene sedimentatie in een geïsoleerde lacustrine omgeving tijdens het late stadium in de evolutie van het Dinariden gebergte. De nieuwe sedimentologische en kinematische resultaten tonen een nauwe correlatie tussen perioden van breukbeweging en sedimentologische cycli op de schaal van individuele afschuivingen, d.w.z. hoge-orde cycli. De zuidwestwaartse migratie van de listrische afschuivingen was geassocieerd met een geleidelijke verschuiving van de sedimentologische omgeving, waardoor de vorming van sedimentologische cycli op de bekkenschaal, d.w.z. lage-orde cycli, mogelijk was. Dit wordt weerspiegeld door een grotendeels uni-directionele sedimenttoevoer vanaf de naburige gebergtegordel die zich langs de zuidwestelijke bekkenmarge bevindt. De hoge en lage orde cyclussen worden gebruikt om een nieuw sedimentologisch model te definiëren voor dergelijke asymmetrische extensie bekkens. Bovendien documenteert deze studie een nieuwe opvolging van deformatie fasen met belangrijke gevolgen voor de evolutie van de Dinariden. De Vroeg - Midden Miocene extensie die het centrale deel van de Dinariden beïnvloedde was geassocieerd met de opening van het naburige Pannoonse Bekken. De extensie werd voorafgegaan en gevolgd door twee fasen van compressie, respectievelijk tijdens het Oligoceen - vroeg Mioceen en het post-Midden Mioceen. Tijdens de laatste fasen van gebergtevorming in de Dinariden vond de Oligoceen -vroeg Miocene compressie plaats, terwijl een post-Midden Miocene compressie gecorreleerd is met de regionale indentatie van de Adriatische continentale eenheid. Deze laatste fase inverteerde het extensieve bekken door reactivatie van het geërfde basale listrische detachment.

De relatie tussen magmageneratie en de tektonische evolutie van gebergten tijdens subductie en de daaropvolgende botsing wordt onderzocht van lithosfeer- tot bekkenschaal in Hoofdstuk 3. Door middel van 2D magmatisch-thermomechanische numerieke modellering zijn de volumes en composities geanalyseerd van de magmatische gesteenten die tijdens de relatief snelle subductie van een smalle oceaan en daaropvolgende continentale botsing worden geproduceerd. De resultaten suggereren dat magmatisme een grootschalig effect heeft op de geodynamische evolutie van een orogeen door deformatie te concentreren gedurende het gehele subductie- en botsingsproces. De rheologische structuur en de compositionele gelaagdheid van de korst drukken een belangrijk stempel op de verdeling van magmatische gesteenten in het orogeen. In vergelijking met eerdere modellen die een vereenvoudigde homogene korst aannamen, veroorzaakt de hier geteste compositionele gelaagdheid van de korst een toename in de toevoer van felsisch materiaal tijdens continentale botsing en resulteert in ondiepere magmatische bronnen die in de tijd naar het voorland migreren. Veranderingen in deformatiestijl kunnen lokaal worden aangedreven door magmatoevoer, in plaats van door bewegingsprocessen. De modellen tonen ook aan dat het migratiepatroon van het deformatiefront en de magmatische boog ten opzichte van de locatie van de sutuurzone kan worden aangedreven door de indentatie van de onderkorst van de bovenplaat in de orogene wig tijdens vroege botsingsfasen. Bovendien voorspelt de modellering een geleidelijke temporale verandering in de magmabron samenstelling van overwegend mafisch tot meer felsisch tijdens de subductie en de daaropvolgende botsings- en eductiestadia. Deze overgang verklaart de migratie van magmatisme en compositieveranderingen van magmas, evenals de waargenomen gelijkenissen met de deformatie in de Dinariden van Centraal-Europa.

Hoofdstuk 4 analyseert de wisselwerking tussen tektonische deformatie en sedimentatie tijdens het ontstaan van afschuivingen in een van de best ontsloten asymmetrische extensiesystemen, het Sorbas Bekken in de Betische Cordilleren van zuidoost Spanje. De interactie tussen extensie en sedimentatie tijdens het Boven Serravalien en Tortonien is geanalyseerd door middel van een gedetailleerde sedimentologische en veldkinematische studie in het zuidoostelijke deel van het bekken. De nieuwe kinematische en sedimentologische resultaten wijzen erop dat de bekkenevolutie wordt gekenmerkt door lage orde tektonische cycli die worden gedreven door de verandering van deformatiestijl en hogere orde cycli die worden aangedreven door individuele fasen van breukactiviteit. Na de initiële extensie fase worden de synkinematische afzettingen gekenmerkt door een breed spectrum aan onderwater zwaartekrachtstromen, waarvan het karakter en transformatie mechanismen werden bepaald door de sedimentvoorziening en bekkenfysiografie.

Резиме

Континентална колизија је један од главних процеса одговорних за формирање планинских венаца и игра важну улогу у целокупном расту континенталне коре, тј. у формирању нове коре. Структурне модификације дуж сучељених континената доводе до карактеристичне расподеле структурних стилова и, типова седиментних и метаморфних фација, која је често повезана са миграцијом фронта деформације и магматизма. Разумевање процеса колизије захтева интегрални приступ којим се анализира међусобна условљеност догађаја на нивоу литосфере, коре и басена, и то у различитим временским скалама.

Ова теза се усредсређује на разумевање мигрирања деформације и њеног утицаја на процесе депозиције и магматизма у колизионим орогеним системима. У првом делу, теза има за циљ разумевање и квантификацију процеса седиментације у басенима контролисаним гравитационим раседима, са посебним фокусом на асиметричне екстензионе басене формиране током завршне фазе колизије. Други део тезе анализира однос између магматизма и тектонских процеса током континенталне колизије помоћу нумеричког моделирања на литосферном нивоу. Као природне лабораторије за проучавање наведених односа проучаване су две кључне области Алпско-медитеранске регије: Динариди централне Европе и Бетски Кордиљери у југоисточној Шпанији.

Поглавље 2. истражује тектонско-седиментациону еволуцију асиметричног екстензионог Сарајевско-зеничког басена који се налази у Динаридима Босне и Херцеговине. У овом интрамонтанском басену депозиција се одвијала у изолованој језерској средини током касне фазе развоја Динаридског орогена од олигоцена до плиоцена. Нови резултати седиментолошких и кинематских испитивања показују блиску корелацију између периода активности гравитационих раседа и седиментационих циклуса на нивоу појединачних нормалних раседа, који се сматрају циклусима вишег реда. Миграција листричних нормалних раседа ка југозападу је праћена постепеним мигрирањем седиментационе средине, што је омогућило формирање седиментационих циклуса на нивоу басена, који се сматрају циклусима нижег реда. Овај процес је рефлектован углавном једносмерним приносом седимената са суседног планинског појаса који се простире дуж југозападне маргине басена. Циклуси вишег и нижег реда су коришћени за дефинисање новог седиментолошког модела за овакве асиметричне екстензионе басене. Осим тога, ова студија документује и нову сукцесију деформационих догађаја и пружа важне закључке о еволуцији планинског ланца Динарида. Рано – средњомиоценска екстензија која је утицала на централни део Динарида повезана је са отварањем Панонског басена. Овој екстензији је и претходила а и следила јој је по једна фаза контракције, током олигоцена и доњег миоцена, односно након средњег миоцена. Олигоценско – доњомиоценско навлачење се одвијало током завршне колизионе фазе у Динаридима, док се пост-средњомиоценска контракција може корелисати са регионалном индентацијом Адријске континенталне јединице. Током ове касније фазе дошло је до инверзије екстензионог басена реактивацијом

постојећег базалног листричног раседа.

Однос између формирања примарне магме и тектонске еволуције орогена током субдукције и касније колизије проучаван је у 3. поглављу. 2Д магматско-термомеханичко нумеричко моделовање коришћено је за анализу количине и састава магматских стена формираних током релативно брзе субдукције уског океана која је праћена континенталном колизијом. Резултати сугеришу да магматизам утиче на фокусирање деформације током процеса субдукције и колизије и тако има велики ефекат на свеукупну геодинамичку еволуцију орогена. Модел показује да реолошка структура и састав слојева коре имају кључну улогу у контролисању расподеле магматских стена унутар орогена. У поређењу са претходним моделима који били базирани на кори поједностављеног хомогеног састава композитна слојевита кора, која је примењена у овом моделу узрокује повећање прилива магми фелзичног карактера током континенталне колизије и резултира стварањем плитких магматских извора који временом мигрирају према форланду. Промене у стилу деформације могу локално бити проузроковане утискивањем магме, пре него процесом везаним за кретање субдукујуће плоче. Резлтати моделовања такође показују да мигрирање фронта деформације и магматског лука у односу на локацију сутуре (шавне зоне) могу бити последица идентације доње континенталне коре горње плоче у језгро орогена током раних фаза колизије. Поврх тога, моделирање предвиђа постепену промену састава извора магме са временом од претежно мафичног до фелзичног састава током континуираних процеса субдукције, колизије и едукције. Ова транзиција објашњава мигрирање места магматских догађаја и промене у саставу магме, као и везу ових процеса са деформацијама у Динаридима централне Европе.

Поглавље 4. анализира интеракцију између тектонске деформације и процеса седиментације током почетка екстензије у једном од најбоље откривених асиметричних екстензионих система, Сорбас басена који се налази у Бетским Кордиљерима у југоисточној Шпанији. Интеракција екстензије и седиментације током горњег серавалијана и тортона анализирана је помоћу детаљне седиментолошке и теренске кинематске студије у југоисточном делу басена. Нови резултати кинематских и седиментолошких испитивања указују да се еволуција басена карактерише тектонским циклусима ниског реда захваљујући променама стила деформације и циклусима вишег реда, који су контролисани појединачним фазама активности гравитационих раседа. Након иницијације екстензије, синкинематска депозиција је представљена широким спектаром подводних гравитационих токова. Типови ових токова, и механизми њихове трансформације, контролисани су приносом седимената и физиографијом басена.

Chapter 1. Introduction

Most orogenic systems (e.g., Alpine-Himalayan belt, Appalachian–Caledonian orogen, Grenville orogen) are located at convergent plate boundaries delineating the sites of ancient oceans that closed during subduction and subsequent continental collision (e.g., Dewey and Bird, 1970, Royden, 1993; Gower, 1996; Schmid et al., 2008). Collisional orogens represent major elongated zones of the Earth surface of intensively deformed and thickened crust preserved as mountain belts through large-scale shortening, magmatism and metamorphism (e.g., Dewey, 1980).

Crustal deformation along continent-continent collision zones involves a complex interplay between numerous external and internal forcing factors. Since, most continent-continent collisions follow subduction of the oceanic lithosphere, the history of oceanic subduction (e.g., steep, flat, oblique, detachment, slab tearing) and character of the oceanic lithosphere (e.g., age, length) may lead to significantly different processes during mountain building and subsequent post – collisional stages (e.g., Duretz et al., 2011; Li et al., 2011; Gerya and Meilick, 2011; Sizova et al., 2012; Dymkova et al., 2015; Menant et al., 2016a). Other important factors controlling collisional dynamics are crustal rheology, lithospheric thermal structure, lateral heterogeneities of the colliding continents, convergence rate, fluid/melt weakening and propagation rate (e.g., Burov and Yamato, 2008; Faccenda et al., 2008, 2009; Sokoutis and Willingshofer, 2011; Duretz and Gerya, 2013; Vogt et al., 2017; Liao and Gerya, 2017).

The variability of modern and ancient orogens in terms of overall structure, evolution and magmatism demands better understanding of the link between deep and shallow Earth processes governing the collisional dynamics. This requires an integration of observational and process – oriented modelling studies (e.g., Cloetingh and Wilett, 2013; Matenco et al., 2016), which focus on the quantitative assessment of the deep and shallow Earth processes underpinning the regional evolution of collisional orogens.

1.1. The link between sedimentation and tectonics in asymmetric extensional basins

To date, numerous studies have been focused on the structural and (sequence) stratigraphic patterns in the syn-rift successions of extensional basins developed in intracontinental rift settings (Fig. 1.1; e.g., Suetz Rift, North Sea, Espinhaço Basin, Brazil, Leeder and Gawthorpe, 1987; Prosser, 1993; Nottvedt et al., 1995; Young et al., 2000; Sharp et al., 2000; Jackson et al., 2005; Martins-Neto and Catuneanu, 2010; Lewis et al., 2015). However, the link between sedimentation and tectonics in asymmetric extensional basins developed during the late stage of orogenic evolution is poorly understood. Asymmetric basins are developed by a major low-angle normal fault or by systems of such faults which are favoured by pre-existing structures. The mountain building process leaves an imprint of numerous discontinuities such as sutures, nappe stacks and thrusts, which represent the critical rheological contrasts within the continental crust (e.g., Le Pourheit et al., 2004; Sokoutis et al., 2007; Balazs et al., 2017). These rheological contrasts control the heterogeneous mechanical behavior of the over thickened lithosphere during

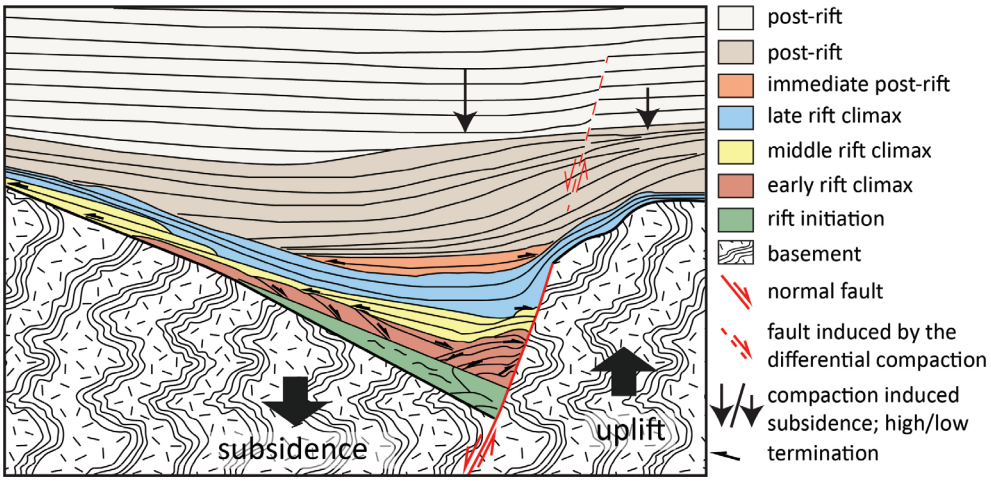

Figure 1.1: Idealized rift sequence based on seismic interpretation (modified after Prosser, 1993).

subsequent geological event(s) (e.g., Cloetingh and Ziegler, 2007). Such complex inheritance is often a prerequisite for the initiation and evolution of late orogenic extensional basins when extension reactivates pre-existing fabrics as detachments or low-angle normal faults (e.g. Jolivet et al., 1998; Jolivet and Brun, 2010).

In tectonically active basins, faulting exerts the first-order control on accommodation space and sediment supply through hanging-wall subsidence and footwall uplift (i.e. rejuvenation of the source area, erosion and deposition e.g., van Wagoner et al., 1990; Withjack et al., 2002; Burov and Poliakov, 2003; Ballato et al., 2014). This result in tectonically driven depositional cycles which range from millions to several thousand years (e.g., Cloetingh et al., 1985; Peper and Cloetingh, 1992; Petersen et al., 2010; Balazs et al., 2016). However, asymmetric extensional basins are characterized by the gradual migration of the deformation in space and with time (e.g., Wernicke, 1992; Bargnesi et al., 2013), that creates a complex basin architecture, and therefore tectonic cycles at different orders of magnitude.

Moreover, the structural geometry of asymmetric basins influences contrasting fault-perpendicular drainage networks that play an important role in the net growth of the alluvial or delta fan systems in the immediate hanging-wall of normal faults (e.g., Collela, 1988; Jackson et al., 2005; Leppard and Gawthorpe, 2006). The close proximity to the active margin enables these relatively small depositional systems to record the faulting activity (e.g. Steel, 1976; Glopen and Steel, 1981) and permits direct observation and correlation between erosion of the uplifting footwall and deposition in the immediate hanging-wall. Furthermore, it is poorly understood how far tectonic pulses could be transmitted to the basin, how their signature can be recognized and distinguished in a distal environment from a 'background' sedimentation controlled by the different allotigenic and autigenic factors such as eustasy, climate, avulsion or, depositional compensation.

Finally, the interplay between faulting and sedimentation in asymmetric

extensional basins has major impact on genesis and preservation of numerous mineral and energy resources. Therefore, better understanding of tectonically induced depositional cycles may serve as a predictive tool for assessing their potential.

1.2. Magmatic pulses in collisional settings

Collisional zones are the important sites of the System Earth, where mass transfer and interaction between upper mantle and crust takes place (e.g., Condie, 2014). In this system, magmatism plays significant role in crustal growth and recycling through partial melting of various rocks and subsequent emplacement of magmas within the crust (e.g., Rudnick and Gao, 2003; Vogt et al., 2012). The magmatism occurs through all collisional stages i.e. during the ocean closure, subduction of the continental crust, exhumation and uplift after the detachment of the oceanic lithosphere (e.g., Rudnik, 1995; Condie and Aster, 2010). It differs in terms of volume, composition, spatial extent and temporal distribution of magmas during different stages of continent-continent collision but also among different orogens (e.g., Dilek and Altunkaynak, 2009; Cvetković et al., 2013). Therefore, magmatism significantly influences the compositional evolution and variability of the crust (e.g., Harker et al., 2011).

The magmatic activity during collisional stages is not continuous, but rather cyclic (e.g. Zhu et al., 2014; Gallhofer et al., 2015). In various collisional orogens it has been documented that magmatism migrates across the collisional zone. In some orogens of the Mediterranean domain (Apennines, Aegean, Betic - Rif, Carpathians, etc) magmatism migrates towards the foreland following the retreat of the subducting slab (e.g., Brun and Faccenna, 2008; Faccenna et al., 2014; Matenco et al., 2016; Menant et al., 2016b). Such scenarios are commonly followed by chemical diversity of igneous rocks across the orogen from more mafic to more felsic rocks (e.g. Seghedi et al., 2004; Duggon et al., 2005; Dilek and Altunkaynak, 2009; Seghedi et al., 2011; Lavecchia and Bell, 2012). However, there are collisional orogens where magmatism migrates in the upper plate direction and without significant changes in the composition, which is most likely controlled by flat slab subduction (e.g. Zagros Mountains, Verdel et al., 2011 and references therein).

The tectonic mechanisms driving a large magmatic diversity observed in many continental collisional systems are not fully understood and are difficult to quantify by conventional observations or geochemical techniques. Better understanding and quantitative assessment of these mechanisms demands a more generic approach, such as thermo-mechanical geodynamic modeling.

1.3. The Dinarides and Betic Cordillera in the context of the Alpine – Mediterranean system

The Alpine - Mediterranean system is part of the broad Eurasia - Africa convergent plate boundary zone (Fig. 1.2; Rosenbaum et al., 2002). This mobile belt underwent a complex evolution exhibiting the interaction between mountain building processes, widespread extension and plate fragmentation by major

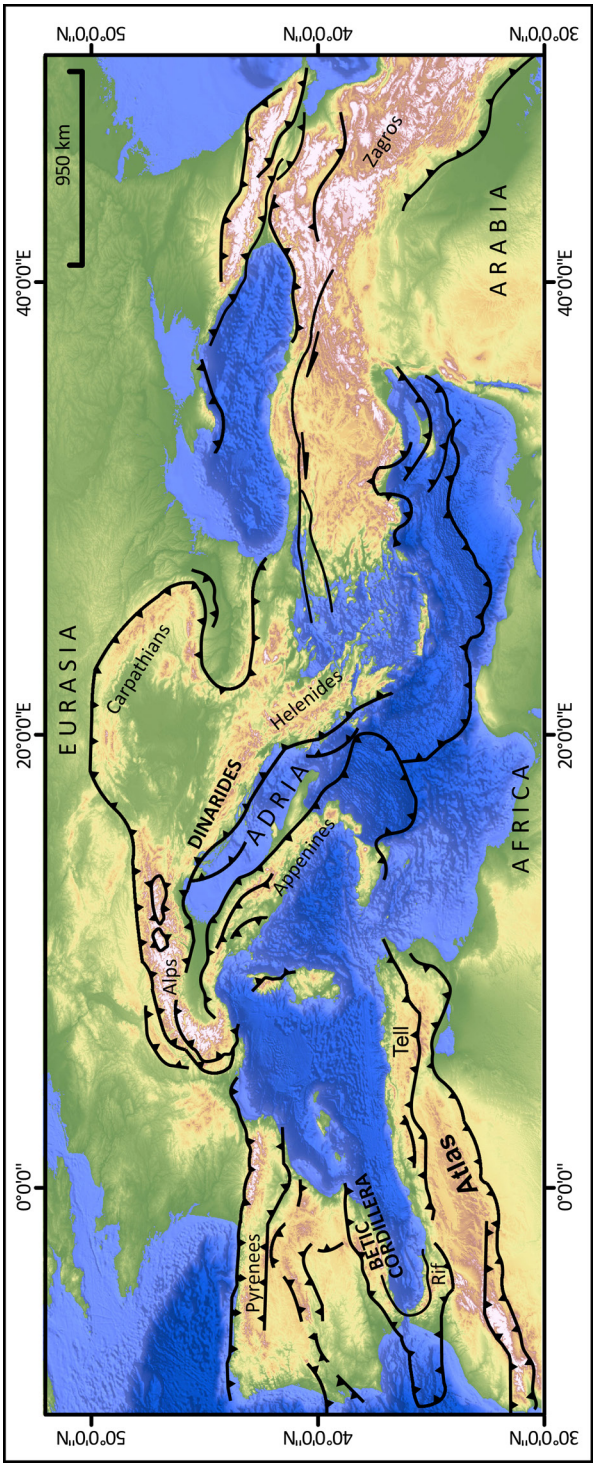

Figure 1.2: Simplified map of the Alpine – Mediterranean system.

strike - slip zones. The crustal deformation was driven by the interplay between subduction related mechanisms and associated mantle flow (e.g. slab roll-back, tearing, detachment), and collisional processes (e.g., Dewey, 1988; Royden, 1993; Jolivet et al., 2009; Faccenna and Becker, 2010; Faccenna et al., 2014).

In this context, the Alpine - Mediterranean region represents an excellent natural laboratory to study collisional dynamics. The Dinarides and Betic Cordillera are two key areas of the Alpine - Mediterranean region, where the concepts regarding the tectonic control on sedimentation and magmatism along colliding margins can be tested.

1.3.1. The Dinarides

The Dinarides represent the southeastern branch of the complex Alpine orogen which continues further to the south into the Hellenides (Fig. 1.2; e.g., Schmid et al., 2008; Handy et al., 2015). These mountains resulted from the late Mesozoic – earliest Cenozoic closure of the Neotethys Ocean followed by continental collision between the Europe and the Adria microplate (Fig. 1.3a, e.g., Dimitrijević, 1997; Karamata, 2006; Schmid et al., 2008). Starting with Miocene times, the northern and southern parts of the Dinarides were strongly overprinted by the interaction with surrounding slabs in the Carpathian and Aegean regions (e.g., Matenco and Radivojević, 2012).

In more detail, the initial thrusting geometry was significantly modified by the Miocene Pannonian back-arc extension and subsequent latest Miocene – Quaternary inversion (e.g., Horváth and Cloetingh, 1995; Balázs et al., 2016). The Miocene extensional phase was marked by the development of numerous lacustrine intramountain basins whereas most of them were isolated displaying an endemic fauna (e.g., Krstić et al., 2003; Mandic et al., 2008; de Leeuw et al., 2012). These basins originated as a combination of orogenic collapse and slab retreat (Carpathian and Dinaridic slabs, e.g., Matenco and Radivojević, 2012) by reactivating weak zones inherited from orogenic nappe stacking (e.g., Schefer et al., 2011; Stojadinović et al., 2014). Therefore, these basins are excellent places to study the link between sedimentation and tectonics outside the influence of eustasy.

The tectonic collisional evolution of the Dinarides was associated with significant magmatic activity during Late Cretaceous-Miocene times (Cvetković et al., 2013 and references therein). The resulting magmatic belts were aligned approximately parallel to the strike of the orogen showing the overall youngening trend and increase of the crustal input into the foreland direction (e.g., von Quadt et al., 2003; Cvetković et al., 2013; Gallhofer et al., 2015). In order to better understand the variability of the magmatism in the subduction - collisional systems, the Dinarides holds a number of key advantages when compared with

Figure 1.3a (facing page): Tectonic map of the Alps – Carpathians – Dinarides system (simplified after Schmidt et al., 2008). Blue and transparent polygons delineate Neogene basins. Red polygons delineate magmatism associated with the evolution of the Dinarides.

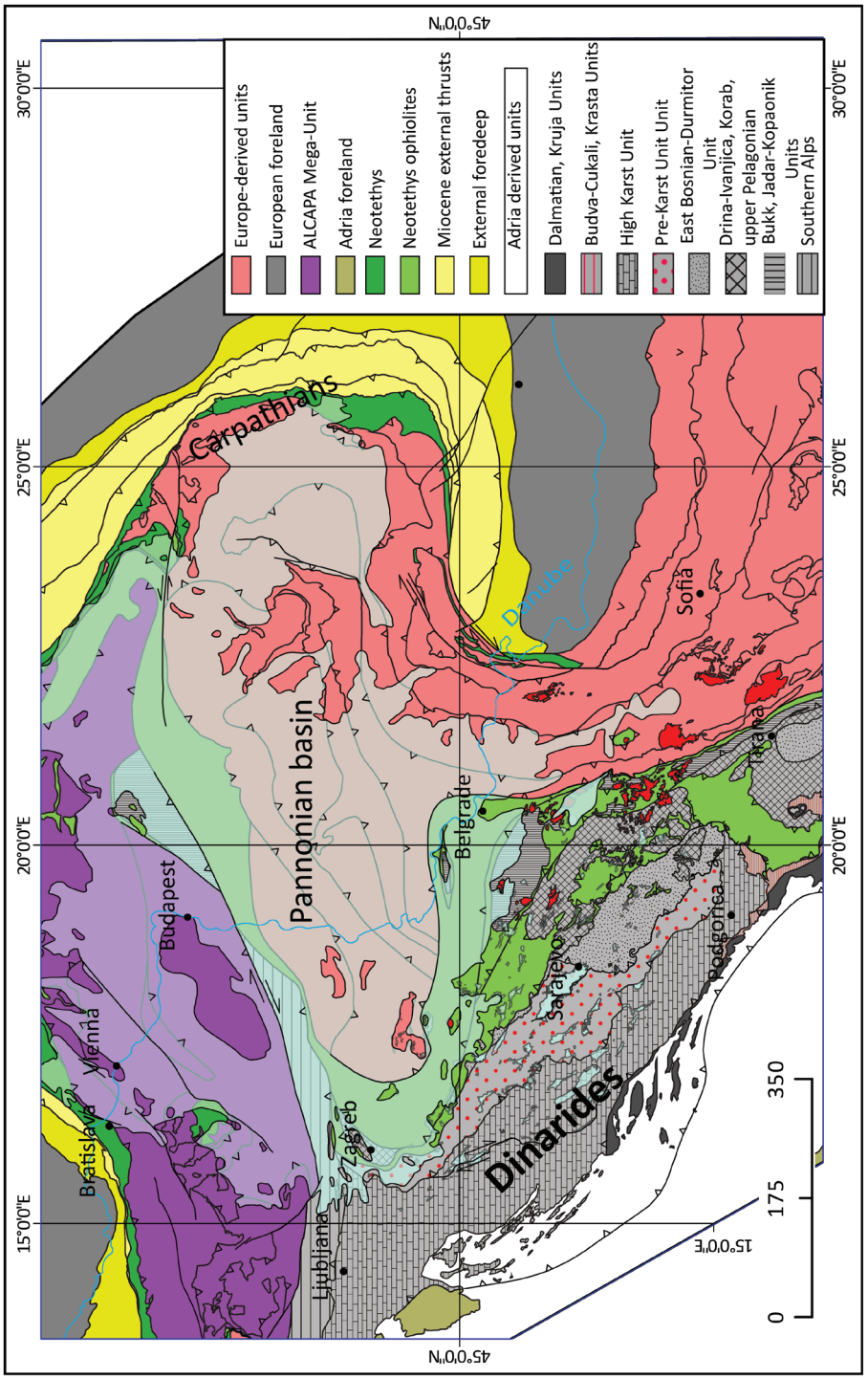
Europe-derived units
European foreland
ALCAPA Mega-Unit
Adria foreland
Neotethys
Neotethys ophiolites
Miocene external thrusts
External foredeep
Adria derived units
Dalmatian, Krujа Units
Budva-Cukali, Krasta Units
High Karst Unit
Pre-Karst Unit Unit
East Bosnian-Durmitor Unit
Drina-Ivanjica, Korab, upper Pelagonian
Bukk, Jadar-Kopaonik Units
Southern Alps
Carpathians
Pannonian basin
Dinarides
Danube
Vienna
Bratislava
Budapest
Ljubljana
Zagreb
Belgrade
Sarajevo
Podgorica
Sofia
Tirana
15°0'0"E
20°0'0"E
25°0'0"E
30°0'0"E
45°0'0"N
0
175
350

neighboring orogens. First, since Late Cretaceous to Miocene times the process of orogenic building and collapse seem to have mainly been controlled by subduction and subsequent closure of the Neotethys ocean (e.g., Dimitrijević, 1997; Pamić et al., 2002; Karamata, 2006; Schmid et al., 2008). After Miocene structural reorganization, the central part of the Dinarides remained unaffected and they still have preserved the original magmatic rock record including an important evidence of migration of magmatic fronts and compositional changes. Second, in the last two decades numerous studies provide an excellent basis for understanding geochemistry, petrogenesis and crystallization time of orogen-related magmatism in the Dinarides. (e.g. Gallhofer et al., 2015; Borojević-Šoštarić et al., 2012; Kolb et al., 2012; Schefer et al., 2011; Banješević, 2010; Cvetković et al., 2013, 2007ab, 2004ab; Prelević et al., 2013, 2010, 2005).

1.3.2. The Betic Cordillera

The Betic Cordillera is part of the Betic – Rif orogenic arc that formed during convergence between, Africa and Iberia continental units (Fig. 1.3b, e.g., Platt et al., 2013). Comparably to the Dinarides, in the Betic Cordillera numerous intramountain basins were formed after the main phase of mountain building process during Miocene times (e.g., Garcia-Dueñas et al., 1992; Lonergan and Platt, 1995; Crespo-Blanc, 1995; Platt et al., 2005; Augier et al., 2005). In addition, the initiation and

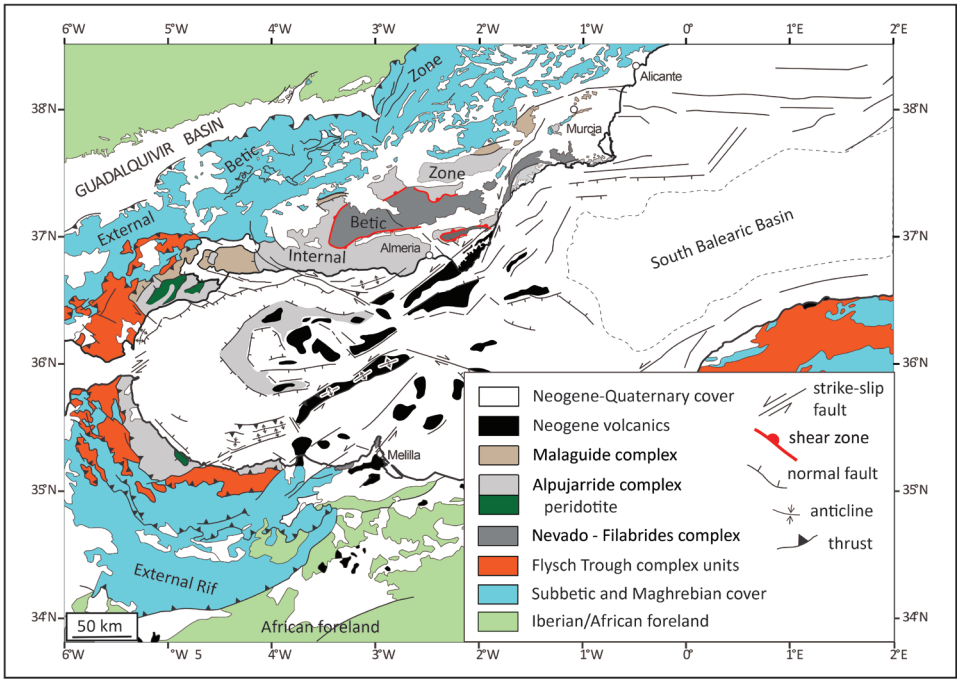

Figure 1.3b: Tectonic map of Betic – Rif system (modified after Comas et al., 1999).

evolution of these basins were strongly influenced by inherited orogenic fabrics, i.e. thrusts and nappe stacks that are reactivated as low angle normal faults (e.g., Meijninger and Vissers, 2006; Augier et al., 2013). The resulting half-graben basin geometries were controlled by syn-depositional normal faults (Do Couto et al., 2014; Meijninger and Vissers, 2006 and references therein).

Conversely, the dominant depositional environment in these basins was marine, and a large number of them was likely connected during certain stages of their evolution (e.g., Vera, Sorbas and Tabernas, Haughton, 2001). Therefore, these basins are optimal places to study depositional cyclicity controlled by tectonics and eustasy, and for testing ideas derived from similar non-marine basins.

1.4. Scope of the thesis

Most collisional orogens are characterized by foreland-directed deformation migration followed by the deposition in specific sedimentary environments within intramountane extensional basins, and magmatism across the orogen. These key features provide the motivation for undertaking investigations aimed at improving the understanding of (1) the link between tectonic and sedimentation in extensional basins and (2) the link between tectonic and magmatism in orogenic systems.

First, this thesis focuses on constraining the influence of normal faulting on deposition in asymmetric extensional basins that are typical for the late stage collisional orogen evolution. In more detail, the thesis will pertain in answering the following questions: how the sedimentary environment responds to faulting events; how the time-space migration of extensional deformation controls the basin architecture, and how the fault-controlled slopes control the generation and transformation mechanisms of subaqueous flows?

Second, the thesis focuses on better understanding the interaction between tectonic and magmatic processes with the aim to address the following questions: what drives migration of magmatism across the collisional orogens; how do magma sources change during collision; what are the physical processes governing these changes and how magmatism influences deformational styles?

To address these questions and improve the present-day knowledge of the geodynamical evolution of collisional zones, field and numerical modelling data were combined with pre-existing extensive knowledge from two natural analogues in the Dinarides of the SE Europe (Chapter 2 and 3) and the Betic Cordillera of SE Spain (Chapter 4).

1.5. Thesis outline

This thesis consists of 5 chapters. The introduction is followed by Chapter 2 that aims at analyzing tectono-sedimentary evolution of one asymmetric extensional basin, i.e. the isolated intramountain Sarajevo - Zenica basin located in the Dinarides. As such, the basin allowed studying the influence of extensional tectonics as the major external factor controlling the accommodation space and sedimentation, as eustasy could be ruled out by the absence of a marine influence.

The novel results of kinematic and sedimentological studies demonstrate close relationship between high-order sedimentological cycles and moments of faulting of individual normal faults. Additionally, the gradual source-ward migration of the extensional deformation controlled the lower order depositional cyclicity. Building on previous knowledge, this study provides a high-resolution evolutionary model of the Sarajevo-Zenica Basin. Furthermore, it documented a new succession of deformation events, with critical implications for the evolution of the Dinaridic mountain chain.

The relationship between magma generation and the tectonic evolution of orogens during subduction and subsequent collision is discussed in Chapter 3 by presenting a series of 2-D magmatic-thermomechanical models. The results demonstrate that magmatism has an important influence of the broad geometry and dynamics of the orogen by focusing deformation throughout subduction – collision process. Also, it may control the local deformational styles such as smaller-scale extension within the arc, which can be coeval with the main phase of shortening. Modelling also demonstrates that the rheological structure and compositional layering of the crust impose a key control on the distribution of magmatic rocks within the orogen. Results indicate that the indentation of the overriding plate`s lower crust into the orogenic wedge can explain the migration pattern of deformational and magmatic fronts. Furthermore, the modelling shows a gradual change in magma source compositions with time from dominantly mafic to felsic. Finally, modelling result lead to a new model for the lithospheric scale processes driving the evolution of the Dinarides.

Chapter 4 focuses on tectonically induced depositional cyclicity during initiation of extension based on outcrop examples studied in the Sorbas Basin, the Betic Cordillera of SE Spain. The results kinematic and sedimentological analysis demonstrate that the change in deformational style during the basin evolution strongly controls the low-order tectonic – induced cyclicity. Similar to the Sarajevo – Zenica Basin of the Dinarides, the Sorbas Basin has an internal architecture composed of high order cycles controlled by individual stages of fault activity. During later stages of extension, sedimentation was predominantly controlled by submarine gravity flows transported along the hanging-wall slopes created by the activity of intra-basinal normal faults. The results also demonstrate a complex mechanisms of sediment deposition and flow transformation in relation to the steepness of the depositional slope. Moreover, these results show strong influence of the fault mechanics on the formation of a heterogeneous basin fill during multiple extensional events.

Finally, Chapter 5 summarizes the results and provides a synthesis of the inferred links between lithospheric- and crustal-scale processes operating during collision based on the studied examples in the Dinarides and Betic Cordillera.

Chapter 2. The link between tectonics and sedimentation in asymmetric extensional basins: inferences from the study of the Sarajevo-Zenica Basin

This chapter is based on Andrić, N., Sant, K., Matenco, L., Mandic, O., Tomljenović, B., Pavelić, D. , Hrvatović, H., Demir, V., Ooms, J., 2017. Marine and Petroleum Geology, 83, 305-332.

2.1. Introduction

Depositional geometries are controlled by the balance between sediment supply and accommodation space, which is enhanced in tectonically active basins (e.g., Schlager, 1993; Miall and Miall, 2001; Cloetingh and Haq, 2015; Balázs et al., 2016). The relationship between tectonic and sedimentation has been extensively studied in rift systems by the means of seismostratigraphic interpretations correlated with wells and/or observations in outcrops, either in extensional structures buried beneath passive continental margins, or in similar basins exposed onshore (e.g., van Wagoner et al., 1990; Nottvedt et al., 1995; Hinsken et al., 2007; Martins-Neto and Catuneanu, 2010). These studies have demonstrated that moments of deformation are associated with a depositional cyclicity. The creation of accommodation space is enhanced in the hanging-wall of normal faults, while footwall erosion is a good indicator for regressive patterns. Such relationships are less obvious in the case of asymmetric extensional basins, i.e. basins where sedimentation is controlled by either a major extensional detachment, or by a system of uni-directional dipping listric normal faults that are connected at depth to one major shear zone, as observed, for instance, in extensional break-away or supra-detachment basins (e.g., Wernicke, 1992; Friedmann and Burbank, 1995; Ziegler and Cloetingh, 2004; Rosenbaum et al., 2005; Tugend et al., 2014). Asymmetries are favoured when pre-existing crustal rheological contrasts are inherited, such as thrusts, orogenic nappe stacks or suture zones, frequently observed in extensional back-arc basins during the evolution of detachment faults that exhume rocks previously buried at high depths (e.g., Bertotti et al., 2000; Brun and Faccenna, 2008; van Wijk et al., 2008). Numerous examples are observed during the Paleogene - Miocene evolution of orogens in the Mediterranean region, when slab rollback was associated with back-arc extension and the formation of a large number of core-complexes and extensional basins bounded by detachments or low-angle normal faults (Jolivet and Faccenna, 2000; Faccenna et al., 2004; Jolivet and Brun, 2010). In such basins, sedimentation is not only controlled by the position of the central subsiding area, but also by the gradual migration in space and time of normal faulting combined with enhanced exhumation of footwalls (Lister and Davis, 1989; Martín-Barajas et al., 2001; Bargnesi et al., 2013).

One area where the formation of asymmetric extensional basins was controlled by detachments reactivating pre-existing thrusts is the Dinarides - Pannonian system (Fig. 2.1a,b, e.g., Balázs et al., 2016). For instance, the inherited Cretaceous suture zone between Adria and Europe (i.e. the Sava Zone) was reactivated by extension along its entire strike (e.g., Ustaszewski et al., 2010; van Gelder et al., 2015). This extension created (Oligocene-) Miocene extensional basins that are either parts of the larger Pannonian Basin system (e.g., Tari et al., 1992; Horváth et al., 2015), or evolved in an endemic and/or geographically isolated environment within the Dinaride Lake System (Harzhauser and Mandic, 2008). In this latter system, the largest basin is Sarajevo-Zenica that formed on the northern flank of the Mid-Bosnian Schist Mountains, near the inherited nappe contact between the Pre-Karst and East Bosnian - Durmitor units (Fig. 2.1b). The basin was filled with alluvial-fluvial and lacustrine sediments deposited during Oligocene - Pliocene times and has a highly asymmetric stratigraphic geometry

controlled by a large fault, or a system of faults, located at its SW margin (Fig. 2.1b, the Busovača Fault of Hrvatović, 2006). Interesting is the isolated nature of the basin, which evolved entirely in an isolated and endemic environment during its entire existence (Milojević, 1964). This allows a direct correlation between erosion in the neighbouring source area and deposition inside the basin, although lake-level variations, controlled by the local balance between precipitation and evapo-transpiration, are rather frequent in such systems (e.g., Garcia-Castellanos et al., 2003; Leever et al., 2011).

The kinematic and sedimentological field observations performed on existing outcrops were correlated with previous local and regional studies (e.g., Hrvatović, 2006 and references therein) in order to derive a high-resolution evolutionary model of the Sarajevo-Zenica Basin. These observations were taken along a number of transects and isolated outcrops that were correlated based on field mapping, synchronicity of faulting events and associated sedimentary wedges in the basin and, whenever available, existing biostratigraphic information. Field observations were used to separate kinematic phases of deformation and individual episodes of faulting. This kinematics was coupled with sedimentological observations for the period of extensional deformation by following a standard approach including the definition of facies units, facies associations, sedimentological environment and systems tracts. Systems tracts are fault-controlled and were used to correlate the kinematic episodes and quantify the evolution of accommodation space in the basin. The ultimate target is to define a new tectonic model of coupled tectonic and depositional evolution for asymmetric extensional basins. This model is still specific to the Sarajevo-Zenica Basin, but the principles of its construction are generic and can be applied to similar basins worldwide. Furthermore, the kinematic model of basin evolution has significant novel inferences for understanding the tectonics of the Dinarides.

2.2. The Sarajevo-Zenica Basin in the context of the larger Dinarides evolution

The Dinarides formed in response to the Triassic opening of the Neotethys Ocean between Europe- and Adriatic- derived continental units and its subsequent closure that started during Middle - Late Jurassic times (Fig. 2.1, Pamić, 2002; Schmid et al., 2008; Handy et al., 2015). The internal parts of Dinarides were tectonically overlain by ophiolites and genetically associated ophiolitic melanges during the Late Jurassic - earliest Cretaceous obduction stages (e.g., Dimitrijević and Dimitrijević, 1991; Đerić et al., 2007; Schmid et al., 2008; Robertson, 2011). The orogen was subsequently built-up during subsequent Cretaceous - Eocene shortening events that created an overall nappe stack where deformation generally migrated in time towards the Adriatic foreland (Fig. 2.1, e.g., Dimitrijević, 1997; Schmid et al., 2008). The contraction is still active at present (e.g., Bennett et al., 2008; Herak et al., 2009). The nappes are made up by a Paleozoic basement affected by various degrees of Variscan deformation and metamorphism that was unconformably covered by a dominantly carbonatic Permian - Eocene succession (e.g., Đoković, 1985; Korbar, 2009).

2.2.1. Available constraints from the tectonic and sedimentary evolution

The Late Jurassic - Eocene contraction was locally associated with the deposition of syn-contractional trench turbidites (i.e. flysch deposits). Elongated areas of such highly-deformed sediments follow thrust contacts along the Dinarides strike (e.g., Dimitrijević and Dimitrijević, 1987). Among them, the Bosnian Flysch recorded a Late Jurassic - latest Cretaceous deposition of mixed carbonate and siliciclastic sediments (e.g., Aubouin et al., 1970; Rampnoux, 1970; Mikes et al., 2008b), which overlies the upper and internal parts of the Pre-Karst unit (Fig. 2.1). Thrusting over the Bosnian Flysch separates the dominant Triassic - Lower Eocene shallow-water Adriatic carbonate platform deposition observed in more external Dinarides units (Dalmatian, Budva - Cukali, High Karst, and Pre-Karst units) from more internal units carrying obducted ophiolites in an upper structural position (East Bosnian - Durmitor, Drina - Ivanjica and Jadar – Kopaonik units) and recorded

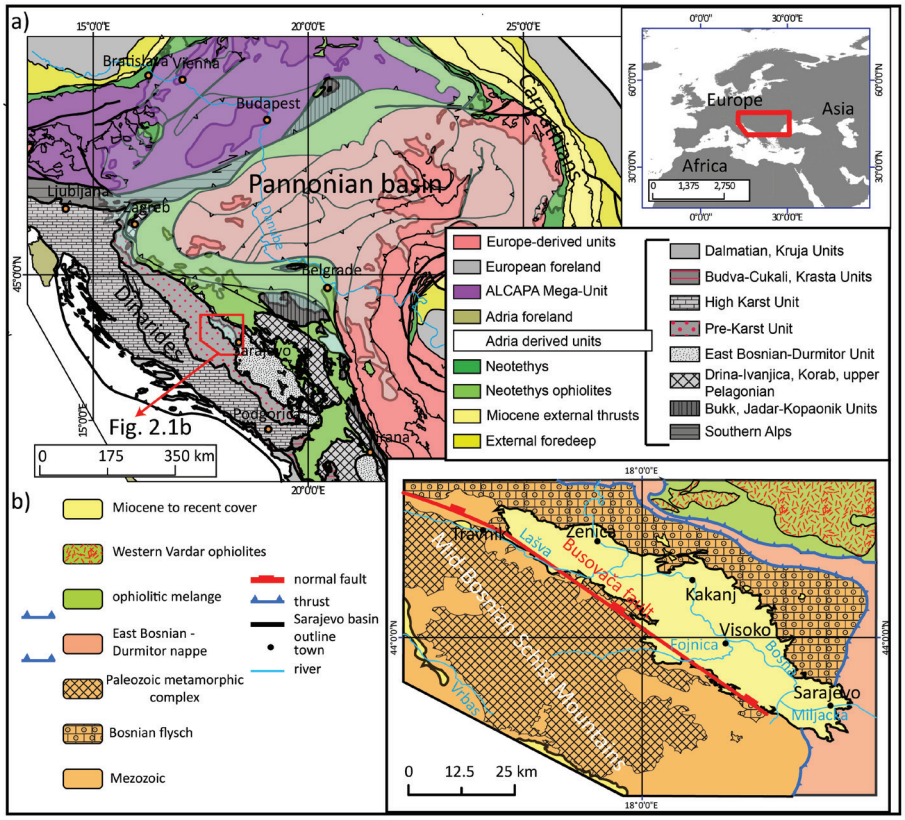

Figure 2.1: a) Tectonic map of the Alps - Carpathians - Dinarides system (simplified after Schmid et al., 2008). White and transparent white polygons show the locations of Miocene basins, such as the Pannonian. Red polygon outlines the location of the Sarajevo-Zenica Basin. Inset represents the location of the map. b) Simplified tectonic map of the Central Dinarides with the outline of the Sarajevo-Zenica Basin (after Jovanović et al., 1971; Sofilj et al., 1971; Olujić et al., 1978; Živanović et al., 1975).

a late Middle Triassic - Early Jurassic gradual deepening of their carbonatic facies (Fig. 2.1, Dimitrijević, 1997; Pamić, 2002; Schmid et al., 2008). The Bosnian Flysch was significantly deformed in successive phases of thrusting and is divided into two units separated by local unconformities: an older and more internal Late Jurassic - Berriasian Vranduk Flysch, and a younger and more external Turronian - Senonian Ugar - Durmitor Flysch unit that extends ESE-wards until the junction with the Albanides (Rampnoux, 1970; Dimitrijević, 1997; Hrvatović and Pamić, 2005).

The internal part of the Dinarides was affected by significant extension, which is generally related with the back-arc opening of the Pannonian Basin starting at ~20Ma, driven by the rapid Miocene retreat of the Carpathian subduction zone (Fodor et al., 1999; Horváth et al., 2015 and references therein). The extension in the north – eastern Dinarides started during the Late Oligocene, migrated in space and time and recorded peak moments during the Middle Miocene (~14-15Ma) (de Leeuw et al., 2012; Matenco and Radivojević, 2012). Large-scale extensional detachments inverted the Adria - Europe suture zone (i.e. the Sava zone), as well as various thrust contacts in the Dinarides and thus exhumed parts of tectonic units previously deeply buried in their footwalls (Ustaszewski et al., 2010; Schefer et al., 2011; Stojadinović et al., 2013; Toljić et al., 2013; van Gelder et al., 2015). These detachments are locally observed along the strike of the Dinarides near their NE margin and are also buried beneath the Miocene sediments of the Pannonian Basin (Matenco and Radivojević, 2012). The systems of low-angle normal faults, their exhumed footwalls and hanging-wall basins have similar structural geometries and have also comparable mechanisms with the Miocene extension affecting the transition between the Alps and the Pannonian Basin (Ratschbacher et al., 1991; Tari et al., 1992; Cao et al., 2013).

The contraction near the frontal part of the Dinarides and the coeval extension in more internal areas created the accommodation space for the formation of many Miocene lakes, which recorded shallow water lacustrine to continental alluvial deposition in a mostly endemic and/or geographically isolated environment (Krstić et al., 2003; Harzhauser and Mandic, 2008; de Leeuw et al., 2012). The endemic and often isolated nature of these basins provided important constraints for the palaeoenvironmental and palaeobiogeographic evolution of the Dinarides region (Jiménez-Moreno et al., 2009; de Leeuw et al., 2010; Mandic et al., 2011). Some basins formed and evolved separately as individual and isolated depocentres (the Dinaride Lake System of de Leeuw et al., 2012), while others are interpreted as remnants of a single lake (Lake Serbia, Krstić et al., 2003). While the isolation of northern basins ceased during a Middle Miocene marine transgression, the deposition in smaller basins in the External Dinarides apparently stopped at the same time (de Leeuw et al., 2012; Mandic et al., 2012). The Neogene deposits of the Dinarides have been deformed by contraction during the Adria indentation starting during latest Miocene times (e.g., Ustaszewski et al., 2014). Although a number of tectonic hypotheses have been suggested for the formation of the entire lake system, such as transtensional opening due to the movements along the Peri-Adriatic lineament (Hrvatović, 2006) or wedge-top basins (Korbar, 2009), the detailed tectonic and sedimentary evolution of most of these Oligocene - Miocene basins is largely unknown (Mikes et al., 2008a).

2.2.2. The geological evolution of the Sarajevo - Zenica Basin

The Sarajevo-Zenica Basin (Fig. 2.1) is the largest in the Dinaride Lake System and has received little attention in published geological studies. It overlies a paleorelief formed during successive Late Jurassic - Cretaceous thrusting events at the contact between the East Bosnian - Durmitor and Pre-Karst units, the latter including a thick sequence of highly deformed Bosnian Flysch that outcrops dominantly along the NE basin flank (Fig. 2.1b, e.g., Hrvatović, 2006; Schmid et al., 2008). The strike of this contact swings in map view from NW-SE in Montenegro and eastern Bosnia and Herzegovina to N-S and further back to NW-SE westwards, coinciding with a significant reduction in the exposed width of the East Bosnian - Durmitor unit (Fig. 2.1, the Sarajevo sigmoid of Dimitrijević, 1997). Outside the Bosnian Flysch sediments described above, the SW basin margin is made up by the Paleozoic metamorphic complex of Mid-Bosnian Schist Mountains overlain by an undifferentiated Mesozoic cover (Fig. 2.1b). The Mid-Bosnian Schist Mountains include Variscan meta-sediments and meta- volcanics together with limestones, dolomite and Permian post-Varisan continental sediments (e.g., Hrvatović, 2006). The Mesozoic cover contains clastics and carbonate sediments deposited on the passive continental margin during Triassic times together with Middle Triassic rifting magmatics (diabases, diorites, gabbros, syenites, spilites and quartitic andesites).

Existing biostratigraphic constraints of the Sarajevo-Zenica Basin were derived from regional geological correlation of pollen and mollusk records (e.g. Hrvatović, 2006). This stratigraphic scheme is less accurate (see details in de Leeuw et al., 2012) and may be further updated through independent geochronological methods.

Starting with Late Oligocene times, the evolution of the Sarajevo-Zenica Basin is thought to be controlled by the large NW-SE striking Busovača Fault recognized near the SW margin from surface mapping, well data and geophysical interpretations (Fig. 2.1, Hrvatović, 2006). Along the northern margin of the basin, Upper Oligocene - Miocene sediments were deposited unconformably over the Bosnian Flysch sediments (Hrvatović, 2006). South of the Busovača Fault, exhumed areas of the Mid-Bosnian Schist Mountains expose their Paleozoic core made up by sediments affected by various degrees of Caledonian, Variscan and Cretaceous metamorphism that are covered along their strike by Mesozoic sediments of the Adriatic carbonate platform (Pamić et al., 2004; Hrvatović and Pamić, 2005). Low temperature thermochronological dating of the exhumation that have inferred ages ~42-27 Ma and 29-24 Ma for zircon fission tracks and U-Th/He, and ~7-5 Ma for apatite U-Th/He (Casale, 2012; Hrvatović et al., 2015). These ages have been interpreted to reflect the exhumation of a Cordilleran-type core complex, although the location and kinematics of the controlling detachment and its relationship with the Busovača Fault are largely unknown. This Miocene fault was inferred to be inverted with a dextral transpressive component during Pliocene times (Hrvatović, 2006).

Figure 2.2 (facing page): Tectonostratigraphic column of the Sarajevo – Zenica Basin. Stratigraphic ages, description, depositional cycles, thickness and lithostratigraphy modified after Milojević (1964). Tectonic system tracts and events are results of the present study.

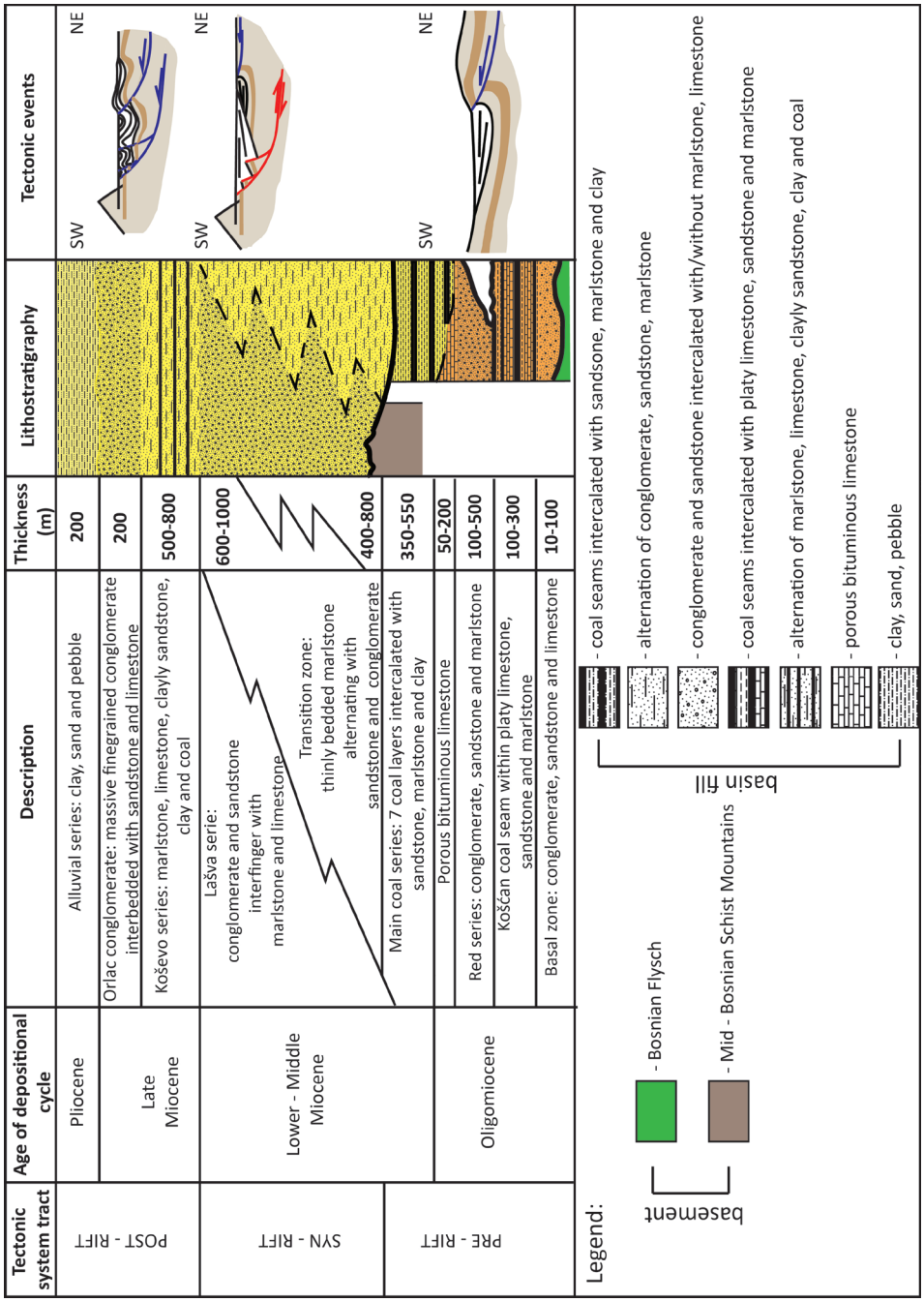
Tectonic system tract
Age of depositional cycle
Description
Thickness (m)
Lithostratigraphy
Tectonic events
POST - RIFT
SYN - RIFT
PRE - RIFT
Pliocene
Late Miocene
Lower - Middle Miocene
Oligomiocene
Alluvial series: clay, sand and pebble
Orlac conglomerate: massive finegrained conglomerate interbedded with sandstone and limestone
Koševo series: marlstone, limestone, clayly sandstone, clay and coal
Laša serie: conglomerate and sandstone interfinger with marlstone and limestone
Transition zone: thinly bedded marlstone alternating with sandstone and conglomerate
Main coal series: 7 coal layers intercalated with sandstone, marlstone and clay
Porous bituminous limestone
Red series: conglomerate, sandstone and marlstone
Koščan coal seam within platy limestone, sandstone and marlstone
Basal zone: conglomerate, sandstone and limestone
200
200
500-800
600-1000
400-800
350-550
50-200
100-500
100-300
10-100
SW
NE
Legend:
basement
- Bosnian Flysch
- Mid - Bosnian Schist Mountains
basin fill
- coal seams intercalated with sandsone, marlstone and clay
- alternation of conglomerate, sandstone, marlstone
- conglomerate and sandstone intercalated with/without marlstone, limestone
- coal seams intercalated with platy limestone, sandstone and marlstone
- alternation of marlstone, limestone, clayly sandstone, clay and coal
- porous bituminous limestone
- clay, sand, pebble

Previous studies (e.g., Milojević, 1964) have inferred that the continental basin fill was deposited during four main cycles, the timing of their deposition being constrained by an incomplete biostratigraphy (Fig. 2.2). The deposition of the ~800 m thick Oligocene - Lower Miocene sediments outcropping in the NE part of the basin (Figs. 2.2 and 2.3) started with an overall transgression of continental alluvial clastics deposited over an unconformity above the Bosnian Flysch turbidites. The transgression established gradually a lacustrine environment with widespread carbonatic deposition in the basin centre, while thick sequences of coal (i.e. Košćan coal, Fig. 2.2) alternating with alluvial sediments were deposited in transitional areas. This was followed by a generalized regression and deposition of red alluvial clastics locally overlain by bituminous and porous limestones, as observed in the northern part of the basin. Superposed over this overall pattern, a higher order cyclicity inside these Oligocene - Lower Miocene sediments is suggested by the observed alternation between alluvial clastics, coal deposition and shallow water carbonates. Previous interpretations have inferred the deposition of at least two cycles during this time span, separated by a sub-aerial unconformity (Muftić, 1965; Milojević, 1964).

The deposition of the second, ~1500m thick, Lower-Middle Miocene sedimentary cycle (Fig. 2.2) started most probably not earlier than 17 Ma (de Leeuw et al., 2012). The onset of a new transgression is documented by the dominant deposition in a paludal and marshy environment, where nine coal seems were accumulated and are intercalated with continental clayey sandstones and mudstones that are ultimately overlain by shallow water lacustrine limestones. These are further overlain by the gradual onset of a laterally variable sequence that starts with thin bedded marls and silts. These are gradually and laterally replaced by sandstones and conglomerates in a coarsening upwards pattern. This coarse part of the basin fill is named Lašva Series and changes laterally from thick conglomerates of up to 1000 m thick to a few hundred metres thick alternations of sandstones and marls towards the SE (Milojević, 1964). The clastic material was derived from the Bosnian Flysch in the NE and Mid-Bosnian Schist Mountains in the SW (Jovanović et al. 1971). These sediments are overlain by the Koševo Series composed of marls, coals and limestones that indicate a gradual drowning of a swamp environment and the creation of a perennial lake (Milojević, 1964). These deposits are overlain by the 200 m Orlac conglomerates and 200 m Pliocene alluvial sediments. The latter were deposited over a larger area transgressing over the Mid-Bosnian Schist Mountains (Milojević, 1964). The present geometry of the basin shows generally younger sediments towards the SW. The exception is the Upper Miocene - Pliocene deposits that are observed in synforms (or “depressions”) in the north, south and western margin of the basin (Fig. 2.3).

2.3. Methodology

The excellent exposures together with good lateral continuity of outcrops in the Sarajevo-Zenica Basin have allowed the correlation of fault kinematics with depositional history. The mapping was performed along cross-sections by following the main valleys cross-cutting the basin. These were correlated by a large number of isolated outcrop observations (Fig. 2.3). The sense of shear along faults and

shear zones was derived from common kinematic indicators such as Riedel shears, drag folds or slickensides. The relative timing of deformation was defined based on cross-cutting, stratigraphic and offset relationships. The syn-kinematic deposits are commonly observed as clastic wedges in the hanging-wall of normal faults, footwall or hanging-wall of thrusts sealed by fine-grained sediments. Whenever the size of syn-kinematic wedges was larger than the outcrop (i.e. the post-kinematic sedimentation not visible in outcrop), the wedges were detected based on variable offsets across faults, which decrease upwards in the stratigraphy. When deformation structures and their associated syn-kinematic wedges were tilted by subsequent tectonic events, their geometry was restored by using the positions of conjugate normal or reverse faults and/or the attitude of immediately overlying strata. Note that this original attitude could have been close to horizontal in the case, for instance, of a deltaic plain or prodelta, or inclined up to 30° in the case of original sedimentological slopes such as deltaic fronts. We have separated tectonic phases based on the type of deformation and higher-order tectonic events based on consistency of kinematics with stratigraphic time (Fig. 2.4).

The detailed sedimentological study was based on field mapping and logging of facies units in cross-sections across the basin with special focus on lateral prolongation of facies units, the geometry of syn-kinematic deposits and stratigraphic surfaces. Facies units were defined based on sedimentary structures and textures, geometry, upper/lower boundaries, thickness, fossil content and colour (Table 2.1, e.g., Leppard and Gawthorpe, 2006; Ielpi, 2012). These facies units were subsequently grouped in facies associations (Table 2.2, e.g., Melchor, 2007; Strachan et al., 2013). Following a typical sequence stratigraphic approach (e.g., Jackson et al., 2005), stratigraphic surfaces were identified based on the contact type between facies associations, associated depositional trends and subsequent stratal terminations across boundaries.

Similar with other sequence stratigraphic studies in tectonically active regions (e.g., Hinsken et al., 2007; Răbăgia et al., 2011; Pereira and Alves, 2012), we have used a combination of different sequence stratigraphy techniques to define genetically related strata (i.e. systems tracts) and to correlate them with observed tectonic events. The evolution of the depositional environment during episodes of enhanced tectonic activity was defined using transgressive-regressive sequences (sensu Embry and Johannessen, 1992). The first step was grouping retrogradational-progradational facies associations. Converting these geometrical patterns into transgressive-regressive stratigraphic sequences relies on the specific structural evolution of asymmetrical extensional systems that creates continuous footwall exhumation and a gradual migration of faulting in time and space. As long as erosion is detected over the footwall, the onlap of the lacustrine facies units is coastal. This corresponds generally with the sub-aerial erosion and coastal deposition observed in studied outcrops. Therefore, a direct interpretation of these geometrical patterns in stratigraphic sequences is possible: the sub-aerial erosion, combined with the coastal onlap and the correlative maximum regression surface, defined by the geometry of the facies associations (e.g. Helland-Hansen and Martinsen, 1996), is an expression of the composite surface that bounds a Transgressive – Regressive (TR) sequence (Embry and Johannessen, 1992). The syn-kinematic deposition against gradually migrating normal faults provides the

control over the coeval nature of erosion and sedimentation, whenever available. The maximum flooding surface was defined in the field by downlapping patterns of distal facies associations (e.g., Posamentier and Allen, 1993; Jackson et al., 2005). Such a downlapping surface was observed only in a few places. Whenever this was not available, the maximum flooding surface was approximated as the transition between retrogradational and progradational depositional trends. Such an approximation affects inherently the definition of individual systems tract, but not the one of sequences.

The correlation between kinematic and sedimentological observations was done extensively for the Middle - Late Miocene extensional phase that still retains a large number of syn-kinematic deposits observed in outcrops. The Oligocene - Early Miocene and Latest Miocene - Pliocene contractional phases retained just a few syn-kinematic geometries and, therefore, are less described in our sequence stratigraphic analysis.

2.4. Basin kinematics

Three phases of deformation were recognized in the basin. The first NE-SW oriented phase of thrusting (Fig. 2.5) and basin subsidence was followed by large scale NE-SW and E-W extension (Figs. 2.6-2.8). The last N-S shortening phase (Fig. 2.9) was characterized by variable structures across the basin.

2.4.1. Initial shortening

The first deformation phase (Fig. 2.4a) was characterized by NE-SW contraction observed only in Oligocene - Lower Miocene strata that outcrop along the NE basin margin. Locally, clear syn-kinematic depositional wedges and onlaps over the flank of thrusts and anticlines demonstrate that shortening was coeval with sedimentation. Typical structures can be observed in the Bijele Vode profile (NE of Kakanj, Figs. 2.3 and 2.5a), where contraction along oblique-slip NNW-SSE trending thrusts with a top SW sense of transport was associated with syn-kinematic deposits onlapping the hanging-wall of faults (Fig. 2.5a,b). These syn-kinematic wedges thin and pinch-out in the hanging-wall of thrusts. The reverse fault concentrated its slip along the rheological contrast between basin limestones and soft mudstones and is observed as a fine-grained foliated fault gouge with shear-bands characterized by a brittle S-C fabric (Fig. 2.5c). Other thrusts are associated with the formation of clastic wedges and are sealed by subsequent deposition of finer grained sediments,

Figure 2.3 (facing page): Simplified kinematic and sedimentological map of the Sarajevo-Zenica Basin (modified from Milojević, 1964 with the results of the present study) with structures active during different deformation events. The Oligocene - Lower Miocene depositional cycle formed in response to the first phase of contraction. The Lower-Middle Miocene depositional cycle formed in response to the phase of extension. The post-Middle Miocene depositional cycle formed in response to the last phase of contraction. Thin black arrows, lines and green dots mark the locations of the profiles and outcrops in Figs. 2.5-2.9 and 2.14.

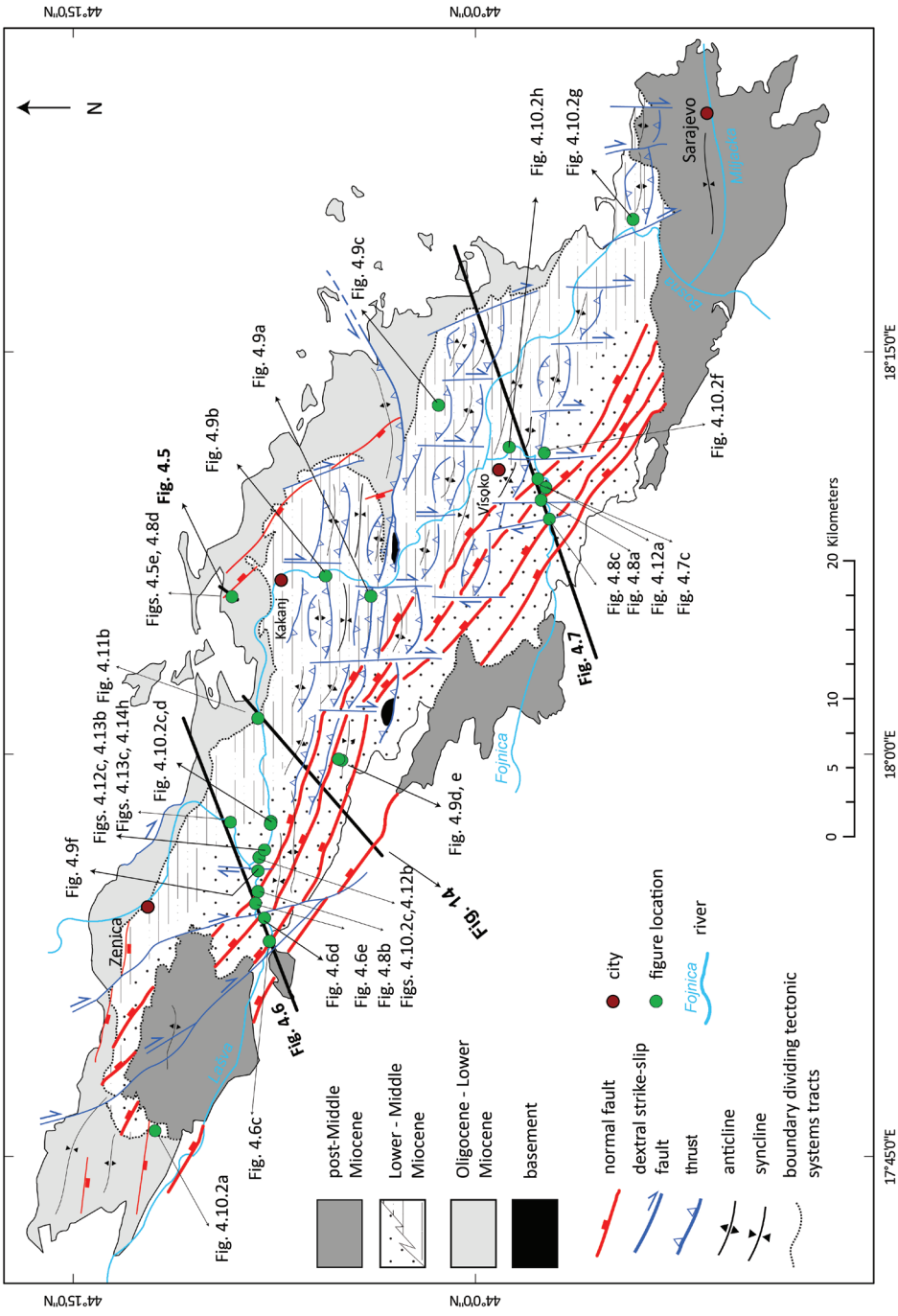
N
17°45'0"E
18°0'0"E
18°15'0"E
44°15'0"N
44°0'0"N
0
5
10
20 Kilometers
Fig. 4.5
Fig. 4.7
Fig. 14
Fig. 4.9f
Figs. 4.12c, 4.13b
Figs. 4.13c, 4.14h
Fig. 4.11b
Fig. 4.10.2c,d
Figs. 4.5e, 4.8d
Fig. 4.9b
Fig. 4.9a
Fig. 4.9c
Fig. 4.10.2h
Fig. 4.10.2g
Fig. 4.10.2f
Fig. 4.9d, e
Fig. 4.6d
Fig. 4.6e
Fig. 4.8b
Figs. 4.10.2c,4.12b
Fig. 4.6c
Fig. 4.10.2a
Fig. 4.8c
Fig. 4.8a
Fig. 4.12a
Fig. 4.7c
Zenica
Kakanj
Visoko
Sarajevo
Bosna
Fojnica
Lašva
post-Middle Miocene
Lower - Middle Miocene
Oligocene - Lower Miocene
basement
normal fault
dextral strike-slip fault
thrust
anticline
syncline
boundary dividing tectonic systems tracts
city
figure location
river

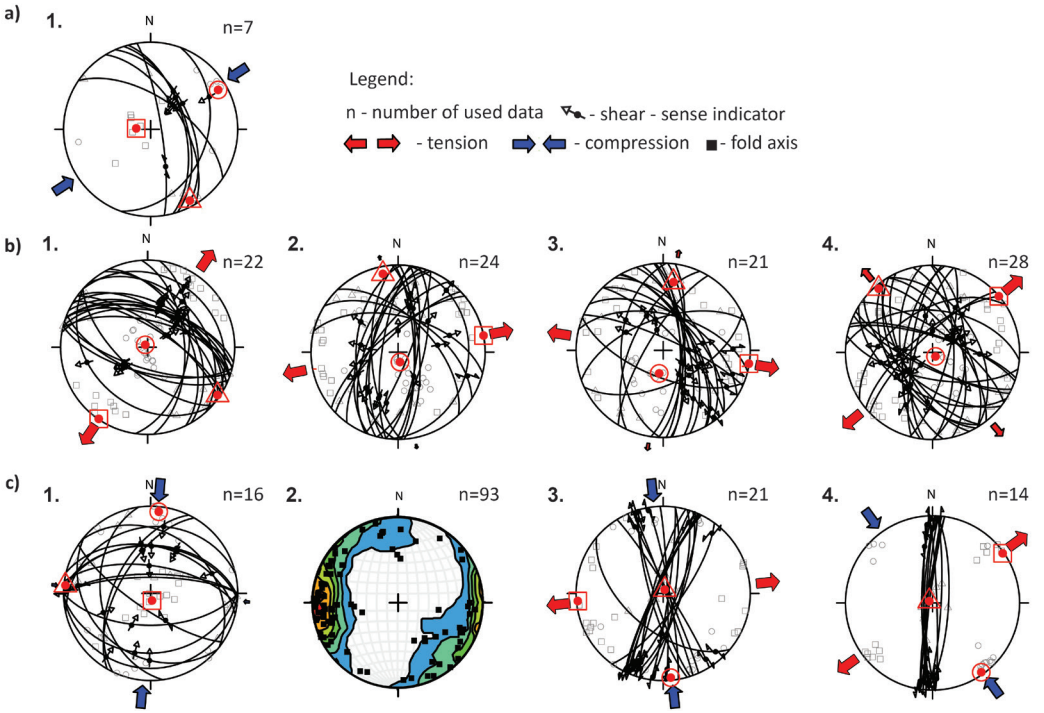

Figure 2.4: Kinematics of deformation phases and individual tectonic events recorded in the Sarajevo – Zenica Basin. a) Stereoplot with faults associated with the Oligocene – Lower Miocene phase of contraction; b) Stereoplots with faults formed during the Middle Miocene phase of extension. 1 - 3 are the individual normal faulting events detected by our study: 4 – normal faults observed in older sediments without separating individual events; c) Stereoplot of structures formed during the Late Miocene – Pliocene phase of contraction, 1 – stereoplots of reverse faults; 2 – stereoplots of fold axes; 3 – stereoplots of strike-slip faults; 4 – stereoplots of transfer/tear strike-slip faults formed due to the inversion along oblique ramps.Red circles, triangles and squares are projections of the mean compressional, intermediate and tensional stress for each fault set calculated using PBT method (e.g., Delvaux and Sperner, 2003). Grey circles, triangles and squares are projections of the measured p, b and t axes, respectively, for each fault in the data set.

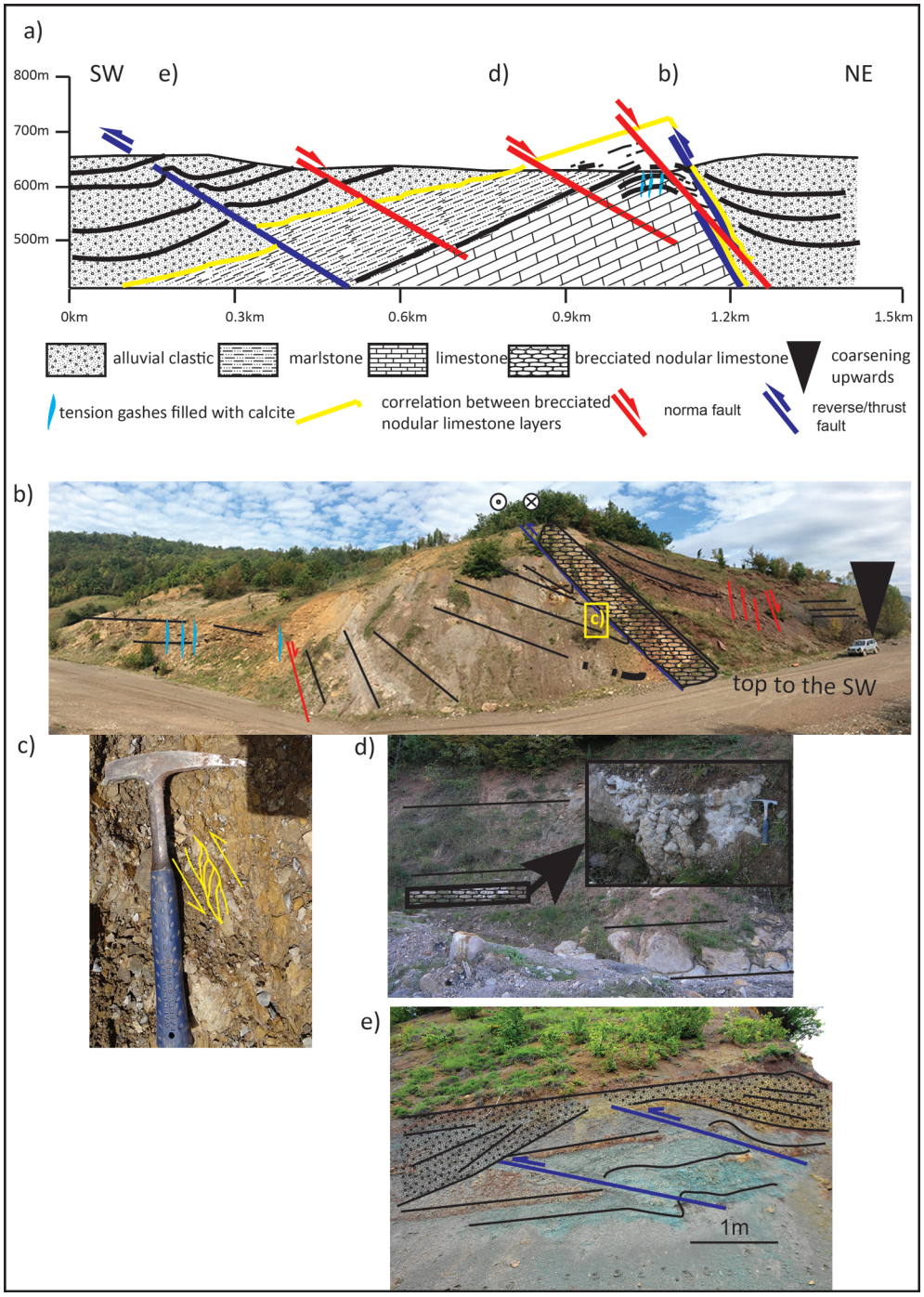

Figure 2.5: Example of syn- and post- depositional structures formed during the first phase of thrusting. a) geological cross-section along the Bijele Vode profile, location in Fig. 2.3. Note the syn-depositionalreverse faulting; b) Reverse - sinistral fault (top SW) in Oligocene – Lower Miocene sediments with onlapping of syn-kinematic siliciclastic sediments over the

Figure 2.5 (continued): earlier deposited shallow-water limestones. Oblique slip normal faults with lower offsets post-date the deposition. Location in Fig. 2.5a; c) Detail on the kinematics of the main reverse fault in Fig. 2.5b with layer parallel slip accommodating the shearing along brittle shear-bands with S-C fabrics developed in poorly consolidated sediments; d) Brecciated nodular limestone intercalated within a mudstone matrix that was deposited at the same time with the limestones in Fig. 2.5b. The overall structural geometry shows asymmetric folding with SW vergence. e) Syn-depositional reverse faulting within the Oligocene – lower Miocene alluvial sediments. Location in Fig. 2.5a.

while onlaps and pinch-outs show syn-kinematic character (Fig. 2.5e). The overall profile shows intense deformation with tilted strata (Fig. 2.5b). Similar thrusts or high-angle reverse faults with oblique components of movement were observed also elsewhere along the NE margin of the basin (Fig. 2.4a), although syn-kinematic indicators of deposition were not always obvious.

2.4.2. Large scale extension

The second phase of deformation observed (Figs. 2.3 and 2.4b) was extensional and resulted in the formation of normal faults that rarely display an oblique component of movement, either sinistral or dextral. Exceptionally well-developed Lower - Middle Miocene syn-kinematic sediments were observed in the Lašva Series, where the normal faults were buried beneath uppermost Miocene - Pliocene deposits and exhumed by subsequent inversion. The syn-depositional character of faults is recognized by the observation of clastic wedges in the hanging-wall, usually covered by fine-grained sediments (Figs. 2.6, 2.8). Faults have variable orientations and gradually changed kinematics with time and along their strike (Fig. 2.4b), but the dominant strike of large offset faults that control the variations in thicknesses and formation of large sedimentary wedges is NW-SE and N-S with a dominant top-NE to E sense of tectonic transport. Normal faults cross-cutting older pre-kinematic sediments generally show a large spread of extension directions (Fig. 2.4b4). The stratigraphic correlation of syn-kinematic wedges has allowed the separation of three successive events during this extensional phase (Fig. 2.4b1-3). These events are in fact the progressive evolution of a normal fault set (consisting of three main faults) branching from a common, nearly horizontal detachment located at the base of the Bosnian Flysch (see below). Such a high-resolution mapping of

Figure 2.6 (facing page): Example of syn-depositional structures formed during the middle Miocene extensional phase. a) Geological cross section along the Lašva valley with normal faults formed during the three individual events. Note that structure 2.3b is the Busovača Fault that is not exposed along the profile. This fault was interpreted based on basin geometry and geophysical surveys by previous studies (Hrvatović, 2006). The numbering reflects the evolution in time of normal faulting; b) Stereoplots of normal faults formed during the extensional phase for extensional deformational phase, 1 – first event of normal faulting; 2 – second event of normal faulting; 3 – third event of normal faulting. Orange dots represent pole of the bedding plane used to back-tilt the fault; c) syn-kinematic wedge formed against a normal fault in coarse conglomeratic deposits; d) Listric normal fault with a low degree of subsequent tilting; e) Normal fault with a high degree of subsequent tilting.

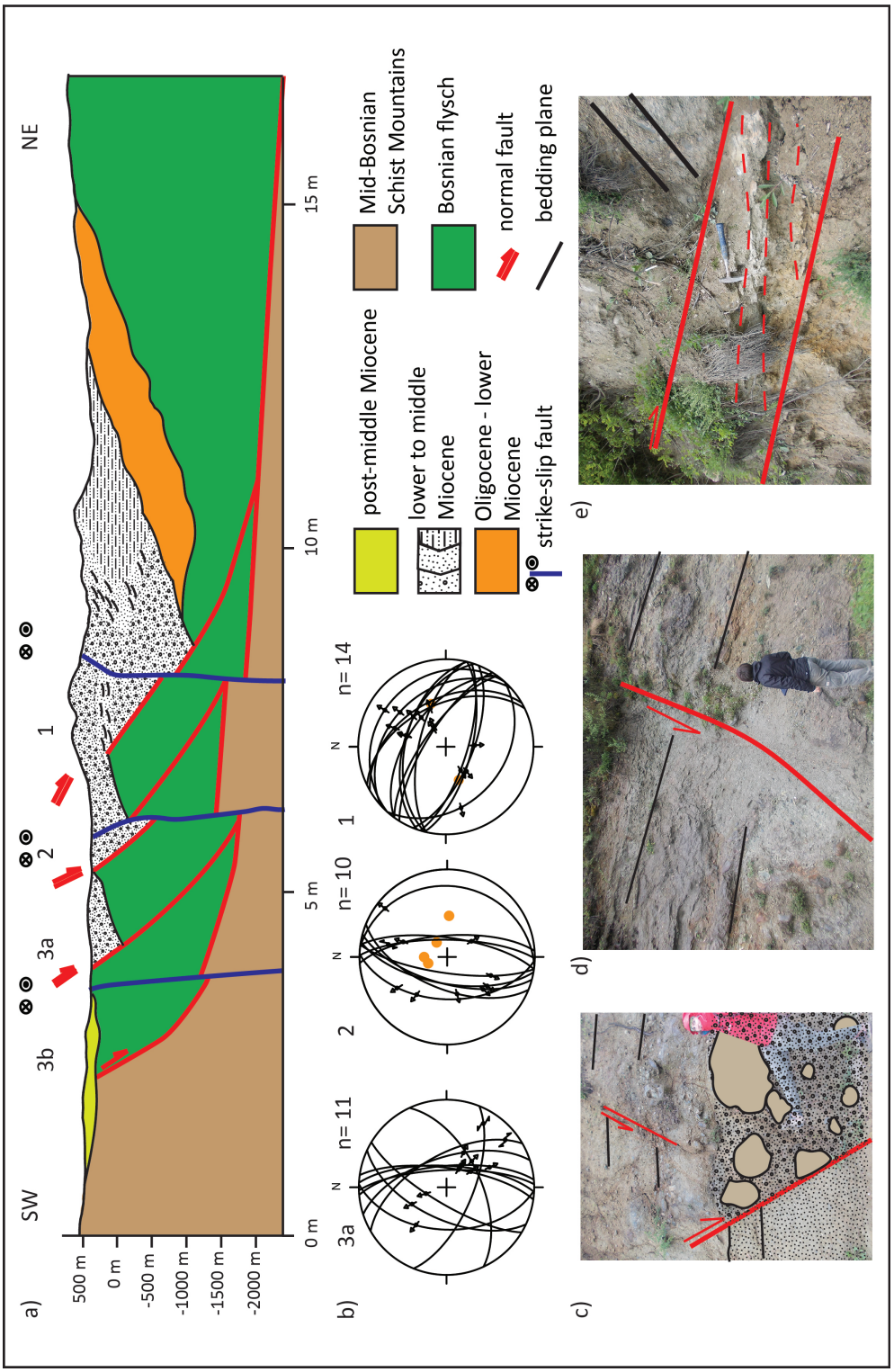
a)
SW
NE
3b
3a
2
1
500 m
0 m
-500 m
-1000 m
-1500 m
-2000 m
0 m
5 m
10 m
15 m
b)
3a
n= 11
2
n= 10
1
n= 14
N
post-middle Miocene
lower to middle Miocene
Oligocene - lower Miocene
strike-slip fault
Mid-Bosnian Schist Mountains
Bosnian flysch
normal fault
bedding plane
c)
d)
e)

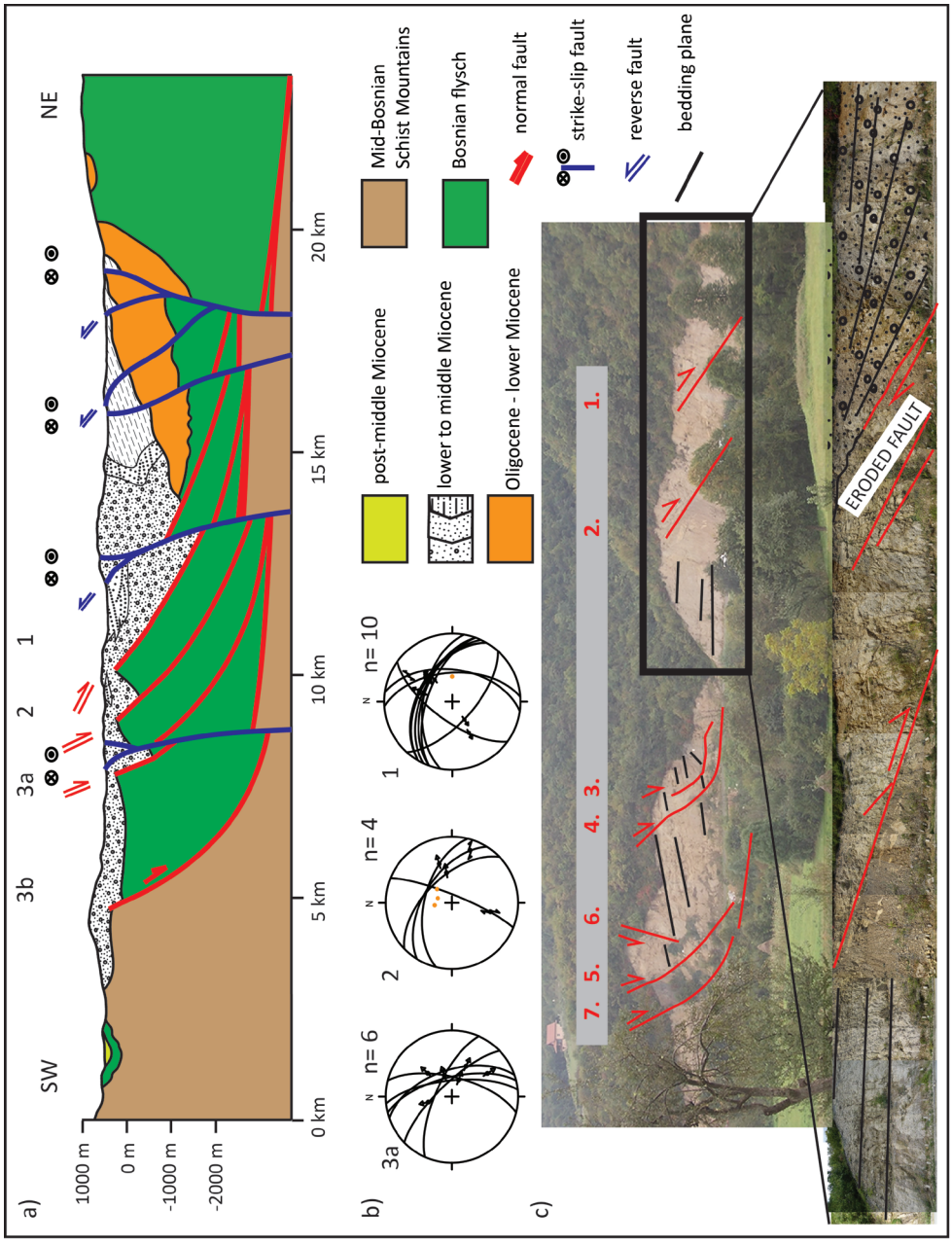
a)
SW
NE
3b
3a
2
1
1000 m
0 m
-1000 m
-2000 m
0 km
5 km
10 km
15 km
20 km
b)
3a
n= 6
2
n= 4
1
n= 10
N
Mid-Bosnian Schist Mountains
Bosnian flysch
post-middle Miocene
lower to middle Miocene
Oligocene - lower Miocene
normal fault
strike-slip fault
reverse fault
bedding plane
c)
1.
2.
3.
4.
5.
6.
7.
ERODED FAULT

Figure 2.7 (opposing page): Example of syn-depositional structures formed during the middle Miocene extensional phase. Location of the profile and outcrops are marked in Fig. 2.3. a) Geological cross section along the Fojnica valley with the normal faults formed during the three extensional events. Note that structure 2.3b is the Busovača Fault that is not exposed along the profile. This fault was interpreted based on the basin geometry and geophysical surveys by previous studies (Hrvatović, 2006). The numbering reflects the gradual evolution in time of normal faulting; b) Stereoplots of normal faults formed during extensional events, 1 – first event of normal faulting; 2 – second event of normal faulting; 3 – third event of normal faulting. Orange dots represent pole of the bedding plane used to back-tilt the fault; c) Interpreted photo illustrating a syn-kinematic clastic wedge formed above an eroded normal fault footwall.

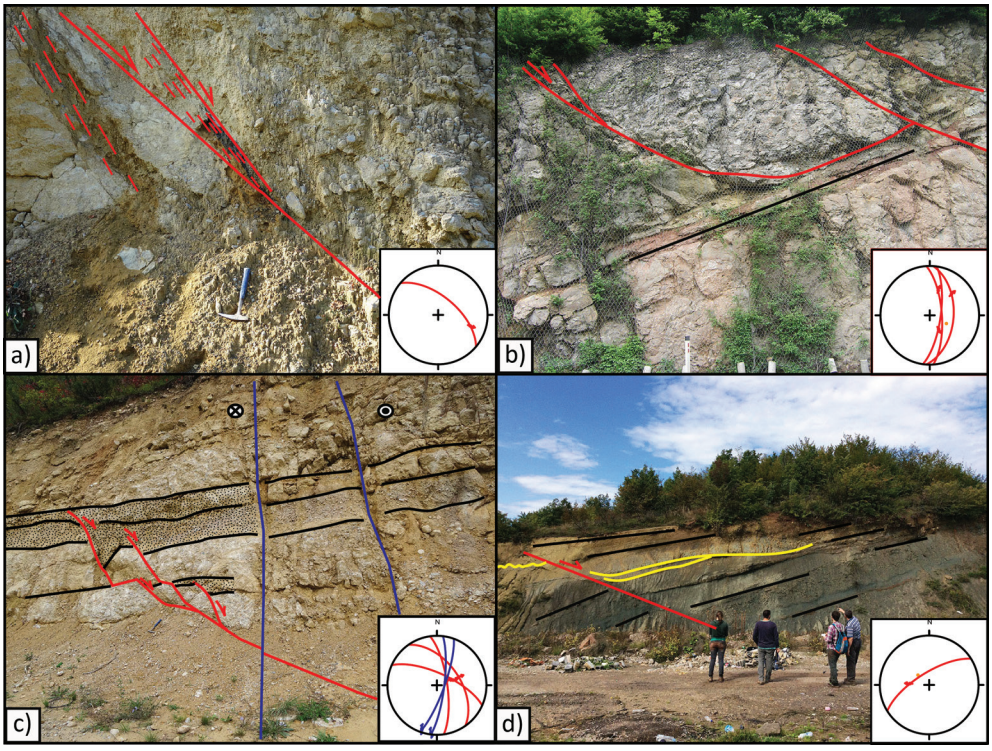

Figure 2.8: Field examples of the relationship between normal faulting and sedimentation. Location of outcrops is shown in Fig. 2.3. Note the orange dots represent pole of the bedding plane used to back-tilt the fault. a) Fault gouge with internal cataclastic foliation in unconsolidated clays and sandstones within syn-kinematic conglomeratic deposits; b) Listric ramp-flat geometry truncated by subsequent higher angle normal faults in syn-kinematic conglomeratic deposition. The decollement layer is made up by siltstones; c) Back-stepping migration of normal faulting at outcrop scale in syn-kinematic deposition. The latter are visible by a wedge geometry in the local deposition; d) A top to the NE normal fault cross-cutting the pre-kinematic Oligocene continentalclastics with paleosoil horizons marking the bedding (black line) and lacustrine marls deposited above an erosional unconformity (yellow line).

kinematics and fault evolution with time was possible because the separation of these events and grouping of faults is based on the superposition of the numerous available syn-kinematic wedges with stratigraphic time and not on the consistency of extensional directions.

The first event of normal faulting (Fig. 2.4b1) indicate a NE-SW extensional direction with limited deviations likely related to local rotations around vertical axis during the subsequent phase of latest Miocene - Pliocene contraction. These faults have large offsets, usually more than 10 m, but locally exceed the 10-20 m scale of outcrop observation. These faults were also tilted by subsequent normal faulting near the SW margin of the basin or by later contractional thrusts and folds. The second event of extension was generally ENE-WSW oriented (Fig. 2.4b2). The normal faults have NW-SE to NNE-SSW strikes with a significant component of oblique slip along N-S oriented faults (Fig. 2.4b2). In outcrops, the inclination of these faults range from 25° to 70°, but this value becomes always around 60° after back-tilting of bedding to its original depositional position. This indicates that similar oriented extensional faults were subsequently tilted by the last extensional event or the subsequent phase of contraction. The third event of normal faulting indicates ESE-WNW oriented extension (Fig. 2.4b3), fault orientation showing deviations from N-S to NNW-SSE with oblique slip to strike-slip components of movement. These faults indicate less to no subsequent tilting from their original 60° dip in rheologically strong lithologies, such as conglomerates, near the SW margin of the basin.

Normal faults have planar or listric surfaces defining high or low-angle fault planes with respect to the (tilted) stratigraphy (Fig. 2.8). High-angle normal faults dip 50-60° in conglomerates. Whenever fault gouge material is made up by softer sediments (such as marls), it forms a clear foliation subsequently truncated by a shear fabric showing a kinematic direction of transport (Figs. 2.6e, 2.8a). A large number of normal faults display low angle segments in the soft sediments, particularly well visible in the NE part of the basin (e.g., Fig. 2.8b). This indicates either original low-angle normal faulting in rheologically weak sediments (LANF segments, e.g., Pedrera et al., 2012) or subsequent exhumation of the listric low-angle level of normal faults. The latter is visible by faults becoming listric and low-angle at rheological contrasts. This geometry is observed, for instance, as decollements accommodating penetrative layer-parallel shear at the contact between coarse (and thick) sedimentary units, such as conglomerates and sandstones, and fine (and thin) sedimentary units, such as siltstones and mudstones (Fig. 2.8b). Low- and high- angle normal faults intersect and provide crosscutting criteria in syn-kinematic wedges (Fig. 2.8b). Normal faults locally truncate earlier syn-kinematic wedges associated with the Oligocene - Early Miocene thrusting and their associated unconformities (Fig. 2.8d). In such situations, tilting of sediments during thrusting can be differentiated from the one created by the subsequent normal faulting. The listric normal faults dipping NE-wards show a gradual migration of deformation towards their SW-ward located footwall, demonstrated by the superposition of syn-kinematic wedges (Figs. 2.7c and 2.8c). This is a critical observation that is valid for the extensional phase at the scale of the entire basin. It can be best studied in two profiles constructed along the main valleys crossing the basin, i.e. the Lašva and Fojnica (Figs. 2.6 and 2.7). In these profiles, the superposition of syn-kinematic wedges demonstrates that faulting gradually migrated in a footwall

direction towards the youngest Busovača Fault. Outside this fault, the geometrical relationships show that numerous outcrop-scale normal faults are generally connected to three major structures at depth that cumulate larger offsets, which correspond to the three successive deformation events (1 to 3 in Figs. 2.6a, b and 2.7a, b). The average normal fault strike is NW-SE with top NE- transport direction indicating an average NE-SW extension, although many variations are observed including oblique and strike-slip faults (Figs. 2.6b and 2.7b). The syn-kinematic sedimentation is frequently coarse conglomeratic and is associated with smaller-offsets synthetic and antithetic normal faults (Figs. 2.6c and 2.7c). Faulting was associated with significant footwall uplift, which is documented by erosion of fault planes that removed large parts of the overlying coarse conglomeratic deposits (Fig. 2.7c). This erosion created gentle slopes buried by subsequent prograding wedges. The overall offsets are variable from few centimetres to more than 10 m (e.g., Fig. 2.8). Hanging-wall antithetic rotations tilted previously formed faults and their footwalls, which resulted in lower inclinations of synthetic fault planes against inclined bedding (Fig. 2.7a). The cumulative offset of all normal faults observed is in the order of 1km, which corresponds roughly with the stratigraphic thickness of the Lašva unit in the proximal conglomeratic area. When adding the offset of the SW-most fault that could not be estimated (Figs. 2.6a and 2.7a), the total offset is likely much higher.

2.4.3. Final basin inversion

The third deformational phase (Fig. 2.4c) produced reverse faults, asymmetric folds and a large number of tear faults that affected both the underlying basement and its Mesozoic cover, and the overlying basin fill (Fig. 2.3). The overall contraction direction is N-S oriented, observed both in faults and folds, with a large number of deviations along structures that display local strain partitioning. This is caused by inversion along oblique ramps, which in fact are the dominantly NW-SE striking normal faults formed in the previous deformation phase. In the basin, this oblique thrusting created a large number of tear faults as observed by N-S striking dextral faults (Figs. 2.3, 2.4c3-4) formed by thrusting over the NW oriented segments of oblique ramps. They are also associated with sinistral conjugate faults with comparatively smaller offsets.

The N - S to NNW-SSE contraction was also accommodated by a large number of folds that are observed mainly in the finer turbiditic or deep-water pelagic sequence, while the coarse grained sequence deformed mainly by thrusting. Individual folds are symmetric, tens of meters wide with generally E-W oriented axial planes (Fig. 2.4c2), often with hinge collapse or parasitic folds along their flanks (Fig. 2.9a). When associated with thrusts, folds become asymmetric (e.g., Fig. 2.9c), with axial planes of variable inclinations from 20-80°. Thrusts vergence is both N- and S-wards. Shortening accommodated by folding is variable, as indicated by wide and open anticlines and synclines that laterally change into tight and overturned folds formed near major thrusts characterized by ramp-flat geometries (Fig. 2.9c). Decollement levels, i.e. flats, are usually localized in finer sediments (shales, silts) that are deformed in wide shear zones with shear-bands like geometry (Fig. 2.9b) accommodating large (i.e. tens of meters) layer parallel offsets. Folding was

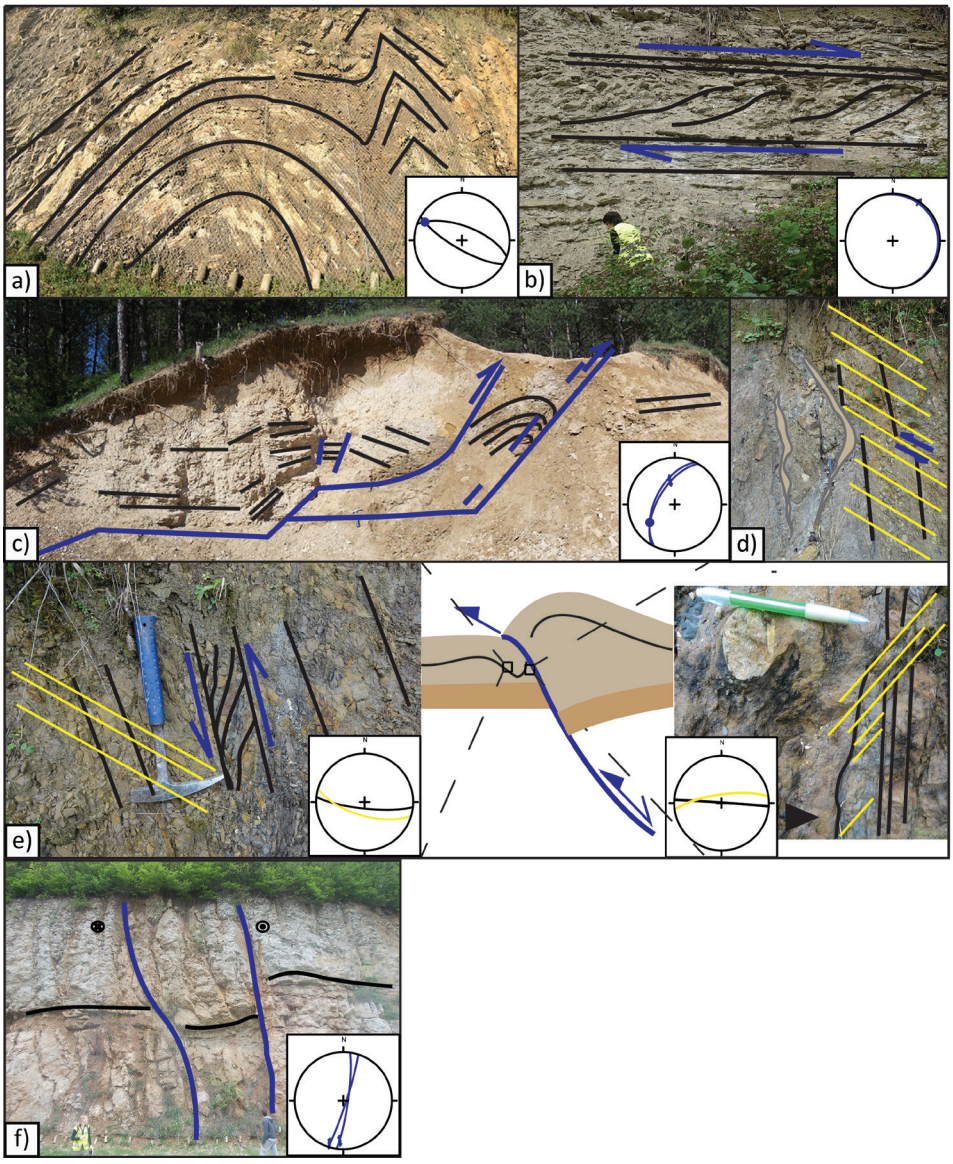

Figure 2.8: Field examples of the relationship between normal faulting and sedimentation. Location of outcrops is shown in Fig. 2.3. Note the orange dots represent pole of the bedding plane used to back-tilt the fault. a) Fault gouge with internal cataclastic foliation in unconsolidated clays and sandstones within syn-kinematic conglomeratic deposits; b) Listric ramp-flat geometry truncated by subsequent higher angle normal faults in syn-kinematic conglomeratic deposition. The decollement layer is made up by siltstones; c) Back-stepping migration of normal faulting at outcrop scale in syn-kinematic deposition. The latter are visible by a wedge geometry in the local deposition; d) A top to the NE normal fault cross-cutting the pre-kinematic Oligocene continentalclastics with paleosoil horizons marking the bedding (black line) and lacustrine marls deposited above an erosional unconformity (yellow line).

associated with the local formation of a pervasive cleavage that was subsequently sheared in the footwall of major thrusts (Fig. 2.9d).

2.5. The evolution of sedimentary environments during the Early – Middle Miocene

The Early-Middle Miocene sedimentary infill consists of successions of alluvial-deltaic conglomerates and sandstones (Lašva series of Milojević, 1964) that are laterally replaced with more distal prodelta lacustrine turbidites, slumps, or more profundal lacustrine deposition (the Transition zone of Milojević, 1964). The sedimentological mapping has separated 18 facies units (Table 2.1), which are grouped in the 13 facies associations (Table 2.2, Fig. 2.10) described below.

2.5.1. Alluvial fan system

The alluvial system is well observed along the entire SW margin of the basin, usually juxtaposed against eroded fault scarps. The overall geometry shows wedging, thickening towards the footwall and pinching out in the opposite hanging-wall direction. The size of wedges is highly variable, from tens of meters to tens of decimetres. The more proximal part of the alluvial system can be generally described by two facies associations (A1 and A2, Table 2.2).

The proximal alluvial fan facies association A1 consists of pebble to boulder breccias and conglomerates (Figs. 2.10 and 2.11a). The base of this facies is a sharp boundary and/or erosional unconformity and is gradational towards the adjacent facies associations (A2 and B1). The angularity and clast size suggest a short distance transport. This is in agreement with clast composition, which corresponds to the metamorphic and magmatic lithologies of the neighbouring Mid-Bosnian Schist Mountains and their Mesozoic cover. Giving the usual location in the immediate hanging-wall of normal faults, this facies association formed due to fault scarp degradation and deposition by rockfalls and debrisfalls (e.g., Postma and Drinia, 1993; Leepard and Gawthorpe, 2006).

The proximal to middle alluvial fan facies association A2 is composed of amalgamated sheets of pebble to cobble size conglomerates and coarse-grained sandstones (Fig. 2.10). Laterally, these conglomerates are interbedded with or overlain by thin layers of fine sandstones and siltstones that contain often water escape structures. The latter structures together with the large grain size and high angularity of clasts indicate rapid deposition near the source area from unconfined sheet floods and mass flows events in the proximal to middle alluvial fan environment (e.g., Nemec and Steel, 1984; Miall, 1985). Laterally, the A2 facies association is inter-bedded with or overlain by B1 and B2 associations.

Facies association B1 comprises of conglomerates and sandstones which are usually amalgamated, cutting each other vertically and laterally forming multi-storeys bodies (Table 2.2, Figs. 2.10 and 2.11b), where each store is bounded by an erosional surface and preservation of the fine-grained intercalations is low. Laterally, B1 passes into B2 facies association. The B2 facies association includes

Table 2.1: Lithofacies units separated in the Sarajevo-Zenica basin. The codes used and their interpretation follow the general standardisation described in previous sedimentological studies (Bouma et al., 1962; Postma, 1990; Miall, 1996; Talling et al., 2012).

facies units	description	interpretation
Gcm	clast-supported cobble (boulder) to pebble size (breccia) conglomerates with low amount of granula matrix; subangular to subrounded clasts; poor sorting; massive; plane base	cohesionless debris flow, granular flow
Gmm	matrix-supported cobble (boulder) to pebble size (breccia) conglomerates in fine sand/mud matrix; subangular to subrounded with/without chaotically distributed mud clasts; poor sorting; lack of vertical grading; non-erosional base with sharp grain size break at the boundaries; bed thickness varies from 0,4 to 1,5 m, very often amalgamated beds with thickness > 10 m	cohesive debris flow
Gh	clast- to matrix-supported pebble to cobble size conglomerates; moderate sorting; weak normal grading, sometimes no grading; crude horizontal stratification; planar base; bed thickness varies from 25 to 40 cm with lateral extension tens of meters	sheet flood deposits, longitudinal bars, lag deposits
Gp	clast- to matrix-supported cobble to pebble conglomerates; subrounded to rounded; weak sorting; planar-cross bedding, imbrication; erosional bases; bed thickness varies 0,3 -1,3 m	transverse bedforms
Gt	clast- to matrix-supported pebble to cobble conglomerates; subangular to subrounded; through cross-bedding; weak sorting; erosional basal surface; graded or ungraded; bed thickness varies from 0,3 to 2 m	channel fill
Sr	coarse to fine sandstones; well sorted with ripple cross-lamination; thickness of bed set is < 20 cm	ripples-lower flow regime, overbank stream-flood deposits
Sm	medium to coarse grained sandstones; poorly sorted; no internal structure with/without scattered granulas and pebbles	subareal to subaqueous cohesionless debris flow;
Sh	fine to coarse grained sandstones; horizontal bedding; slightly erosional base; beds 7 to 20 cm thick	plane-bed deposits under subaerial sheet flows or stream flows
St	medium- to fine-grained sandstones; well sorted; rounded clasts; weak normally graded or ungraded; solitary or grouped cross-bedding	megaripple under subareal sheet flows or stream flows

Table 2.1 (continued): Lithofacies units separated in the Sarajevo-Zenica basin. The codes used and their interpretation follow the general standardisation described in previous sedimentological studies (Bouma et al., 1962; Postma, 1990; Miall, 1996; Talling et al., 2012).

facies units	description	interpretation
Fl	fine sandstones interbedded with siltstones and mudstones sometimes with scattered granulas; laminated or massive; bed set thickness less than 10 cm	deposition from suspension of waning floods or abundant channel
Ta	coarse- to medium-grained (pebbly) sandstones with low matrix content; medium to good sorting; vertical normal grading or no grading; mud chips aligned in certain levels; erosive or planar base	high density turbidity currents
Tb	medium-grained sandstones; parallel lamination; poor vertical overall grading	high/low density turbidity currents
Tc	medium- to fine-grained sandstones; well sorted, low matrix content; asymmetric ripple cross-lamination/climbing ripples; laminae can be convoluted; tapering shape of sandstone beds; sometimes the steeper sides of ripples are draped by organic matter	low density turbidity currents
Td	fine sandstones to siltstones; parallel lamination result of the alternation of 1-2 mm thick fine sandstones and siltstones laminae; can resemble FU grading trends	low density turbidity currents
Te	fine siltstones and mudstones; not stratified, but may exhibit parallel lamination marked by well sorted silt; dark grey to light grey color	suspension fall-out from waning low density turbidity currents or cohesive density flow
L	beige mudstones; laminated with wavy to planar bedding; upper and lower boundaries are sharp and plane; sometimes can be mottled with reddish fakes; lens body geometry; include fossil fragments (ostracods); thickness varies from > 1 to 15 cm	lagoon, shallow lake to back-swamp suspension, background deposition
Md	mudstones, light brown; lack of internal structure; no fossils; tabular with gradual contact with units above and below; bed thicknesses is up to 1m	inorganic lake precipitation

Table 2.2: Summary of facies associations interpreted in the Sarajevo-Zenica basin.

Depositional environment		Facies associations code	Facies code (see Table 2.1)	Description	Inferred depositional process
Alluvial fan	proximal	A1	Gcm, Gmm	Wedge-like packages of red structureless coarse-grained conglomerates with variable amounts of matrix. Angular to subangular basement-derived clasts varies from 2 cm to 2 m in size with scarce blocks of 2,5 to 3 m. Tectonic (i.e. fault scarps) or erosional contact towards the adjacent basement or basin fill. It may exceed 20 m in thickness. Locally truncates A2 and B1.	Colluvial rockfall and debrisfall deposits originated from variable degree of rolling and sliding of fragments down the slope before deposition. They are deposited in the lower part of the slope (fault escarpment). The lithological nature of the clasts suggests small catchment area restricted to BSMts (footwall, e.g., Postma and Drinia, 1993; Longhitano et al., 2015).
		A2	Gmm, Gcm, Sm, Sh, minor Gp, Sr, Gh	Sheet-like packages of red coarse- to medium-conglomerates intercalated with coarse-grained sandstones. Subrounded to subangular polimictic clasts may show imbrication. The lower and upper boundaries are plane and slightly erosional. Thickness varies from 2 to 5 m. Locally truncates B1 and B2.	Deposition from flood-related braided flows dominated by sheet flows combined with debris flows. This association of depositional processes is typical for deposition in the proximal to middle alluvial fan (e.g., Miall, 1985; Nemec and Postma, 1993).
	distal	B1	Gp, Gcm, Sm minor Gh, Sh	Channelized to sheet like packages of red medium- to fine-grained conglomerates and sandstones with scarce siltstones. The lower and upper boundaries of channelized conglomerates and sandstones are wavy and erosional. The sheet-like packages show subhorizontal bedding marked by abrupt change in the grains size.	Deposition from dominantly subareal braided-stream flows and sheet flows, rarely intercalated with debris flow deposits i.e. high-energy and bedload dominated flows in the bride-plain environment (e.g., Nemec and Postma, 1993).
		B2	Sm, Fl, Sh, St	Tabular packages of (wavy or parallel) laminated siltstones and (organic-rich) claystones intercalated with fine-grained sandstones. The siltstones and claystones may have mudcracks or iron crust and/or be mottled. They are irregularly intercalated with poorly sorted medium-grained sandstones and granula-conglomerates. The geometry of these intercalations varies from channel- to lobe- and sheet-like. Alternates with B1 and C0.	Deposition from subareal waning flows combined with suspension fall-out in the overbank environment often interrupted by flooding events (e.g., DeCelles et al., 1991; Ielpi, 2012).

Table 2.2 (continued): Summary of facies associations interpreted in the Sarajevo-Zenica basin.

Depositional environment		Facies associations code	Facies code (see Table 2.1)	Description	Inferred depositional process
Pond/shallow water lake system		C0	Fl, L, Sh, Sm	Lense-like packages of (wavy or parallel) laminated beige mudstones intercalated with single bed, or subordinately bed sets of fine- to medium - grained sandstones or angular granula conglomerate. The mudstones can be bioturbated with mottled upper surface. The mudstones include Ostracodes.	Deposition by particle settling in low energy environment; lagoon or ponds in the marginal lake environment with rare debris flows resulting from flood events (e.g., Melchor, 2007; Ielpi, 2012)
Deltaic system	delta plain	C1	St, Gcm, Sh, Sr, Gt	Channelized packages of trough-cross bedded medium- to coarse-grained conglomerates interbedded with sheet-like packages of coarse- to medium-grained sandstones and conglomerates. The clasts are subrounded to rounded. The channel lag comprises of pebble to cobble size conglomerates. The layers thickness varies from 0.5 to 2 m. These layers are intercalated with thin (up to 20 cm) medium- to fine-grained sandstones with wavy and ripple-cross lamination. The packages are organized in the coarsening- and thickening-upward sequences. Gradually passes into D1 downslope.	The thick layers of sandstones and conglomerates were deposited from stream, sheet and debris flows recording periods of bedload river floods at the river mouth. The sandy intercalations resulted from lower flow regime, waning flows or by reworking during periods of quiescence (e.g., Collela, 1990; García-García et al., 2006).
	delta slope	D1	Gcm, Sm, minor Ta-c	Sheet-like packages of coarse- to medium-grained conglomerates and sandstones. The bed thickness varies from 0,3 m to 2, 5 m. The scattered pebbles (even boulders of BSMts) suggest horizontal bedding in amalgamated beds. They are interbedded with 5 to 15 cm thick fine-grained sandstones and siltstones.	Combination of multiple depositional processes: dominated by the debris flow, grain flow and lesser influence of turbidity currents typical for aggradational and progradational delta slope. The flows originated by hyperpicnal mixing of river and lake water due to high sediment input during fluvial flooding events (e.g., Prior and Bornhold, 1988; Collela, 1990).
		D2	Gcm, Sm, Ta-e	Channelized to sheet like packages coarse-to medium- grained sandstones engulfed in fine-grained sandstone to siltstones. Package thickness varies from 3 m to 5 m. The package show coarsening- and thickening-upwards.	Deposition dominantly from high energy and concentrated turbidity and debris flows on the erosional slope of a delta (e.g. Leppard and Gawthorpe, 2006).

Table 2.2 (continued): Summary of facies associations interpreted in the Sarajevo-Zenica basin.

Depositional environment		Facies associations code	Facies code (see Table 2.1)	Description	Inferred depositional process
Deltaic system	proximal prodelta	E1a	Sm, Gmm, Ta-e	Sheet- to wide lobate and channel - like packages of coarse- to medium-grained sandstones, siltstones and mudstones with rare influxes of medium-to fine-grained conglomerates with/without rip-ups. Subordinately, this unit may include lobe-like geometry of the layers and slumped intervals. This is an downslope equivalent of D1.	Deposition from turbidity currents and debris flow deposits in the toe of the slope, proximal prodelta settings (e.g., Leppard and Gawthorpe, 2006; Strachan et al., 2013).
		E1b	Sm, Ta-e	Isolated channel-like layers of medium-grained sandstones interbedded fine-garained sandstones, siltstones and mudstones. The succession may be interrupted by poorly sorted coarse-to medium-grained sandstones with the intrabasinal rip-up or out-sized clasts. It may contan plant remains and coal particles. The package coarsens and thickens up-section. Upslope it passes into D2.	Deposition from unidirectional subaqueous turbiditic currents interrupted with debris flows. The channel-like geometry and intrabasinal rip-ups suggest erosional slope (e.g. Leppard and Gawthorpe, 2006).
		E1c	Ta-e	Sheet-like packages of parallel to wavy laminated fine- to medium-grained sandstones and siltstones intercalated with mudstones. This packages include slumped layers with variable thicknesses from 0.25 cm to 15 m. The slumped layers contained intrabasinal rip-ups, blocks and folded beds. Laterally truncates D2 and E2b.	Deposition from alternating of high - and low-density turbidity flows intercalated with mass flows resulted from slope instability (e.g., Postma, 1984; Strachan et al., 2013).
	distal prodelta	E2a	Ta-c, L, Md	Parallel to wavy laminated beige mudstones regularly interbedded with well-sorted medium-grained calcarenite sandstones. The sandstones are structureless with plane base, sometimes may show coarsening-upwards and/or, parallel lamination and/or ripple-cross lamination. The sandstones comprises of dominantly Ugar flysch fragments (limestone) with subordinate amount of organic matter and coal particles. The mudstones contain ostracodes. The whole succession is irregularly interrupted with structureless mudstones up to 1 m thick. Usually, this facies association forms a base of coarsening upwards sequence gradually passing into E1b.	Combined deposition from low-density turbidity currents and suspension fall-out with cyclic high-density turbiditic flows in the distal prodelta environment. The lithic fragments in cyclic sandstones suggest catchment area restricted to pre-rift coal-rich succession and Ugar flysch (e.g., Benvenuti, 2003; Melchor, 2007).
		E2b	Tc-e, Md	Sheet-like packages of parallel laminated mudstones intercalated with fine-sandstones, siltstones and ripple cross-laminated sandstones associated with organic-rich mud drapes. Bed thickness varied from 5 to 15 cm. This facies association includes Ostracodes.	Cyclic alternation of low density-turbidity currents and suspension fall-out in the distal prodelta and basin plane setting of the underfilled basin (with low sedimentary input, e.g. Melchor, 2007)

laminated siltstones and claystones intercalated with thin layers of organic rich clay or isolated channels of fine- to medium-grained sandstone and pebbly sandstone crevasses (Table 2.2). The immersion surfaces are marked by red iron-rich crusts and mottled structures developed in silts and palustrine carbonates. The channelized system of B1 facies association has an unconfined character and was deposited in a high energy/discharge braided plain of a delta fan (e.g., Nemec and Postma, 1993). Furthermore, B2 facies association are floodplain deposits deposited in a quiet, low energy environment, with confined channels in the braided plain delta fan (e.g., Miall, 1985; Pavelić and Kovačić, 1999). The distal fan facies often alternates with the C0 facies association described below, which may be the result of avulsion of distributary channels, increasing the sediment discharge due to flooding, or cyclic activity of normal faults (e.g., Gawthorpe and Colella, 1990; DeCelles et al., 1991).

2.5.2. Pond/shallow water lake system

The facies association C0 is composed dominantly of thinly bedded mudstones interrupted by isolated channel-like coarse sandstones and breccias (Table 2.2, Figs. 2.10 and 2.11c). Sometimes, it may contain mottled top part of a layer. This facies association often has a wedge geometry, rarely includes lenses, and is thickening towards the centre of the basin. It is usually intercalated between B2 and C1, and is frequently downlapped by the B1 facies association. Red alteration layers in carbonates indicate local pedogenesis (i.e. mottled, e.g. Ielpi, 2012). The carbonate deposition is often associated with lacustrine ostracods that indicate suspension settling in a shallow lake/pond environment. This is periodically supressed by channels feeding a mouth bar system or occasional flooding events (e.g. Melchor, 2007).

2.5.3. Deltaic system

Facies association C1 consists of channelized and tabular conglomerates and sandstones (Table 2.2, Figs. 2.10 and 2.11d) usually organized in coarsening and thickening upward packages. The observed erosion, trough cross-bedding and finning upwards indicate migration of channels and bars under hyperpycnal flow in the place where a river discharges in a body of stagnating water (Fig. 2.11d) (i.e., a delta plain, e.g. Postma, 1990; García-García et al., 2006).

The facies association D1 consists of cobble to pebble conglomerates and coarse- to medium-grained sandstones (Fig. 2.10), often marked by outsized clasts of Mid-Bosnian Schist Mountains (Fig. 2.11e). The flows were induced on the sedimentological slope by discharging a coarse-grained alluvial bedload during flooding events or more likely by grain flow from an unstable delta slope (e.g., Prior and Bornhold, 1988). They show tabular and wide lobate bed geometries parallel to the basin margin and basin tapering wedges along the flow profile. The D1 may have sharp and flat, or gradational contacts to the adjacent facies associations (B1, C1 up-slope and E1a down-slope) and general coarsening-upwards trends. D2 facies associations include wide channel to sheet-like coarse- to medium- grained sandstones facies (Fig. 2.10). Erosion, stacked channels and scarcity of tabular beds

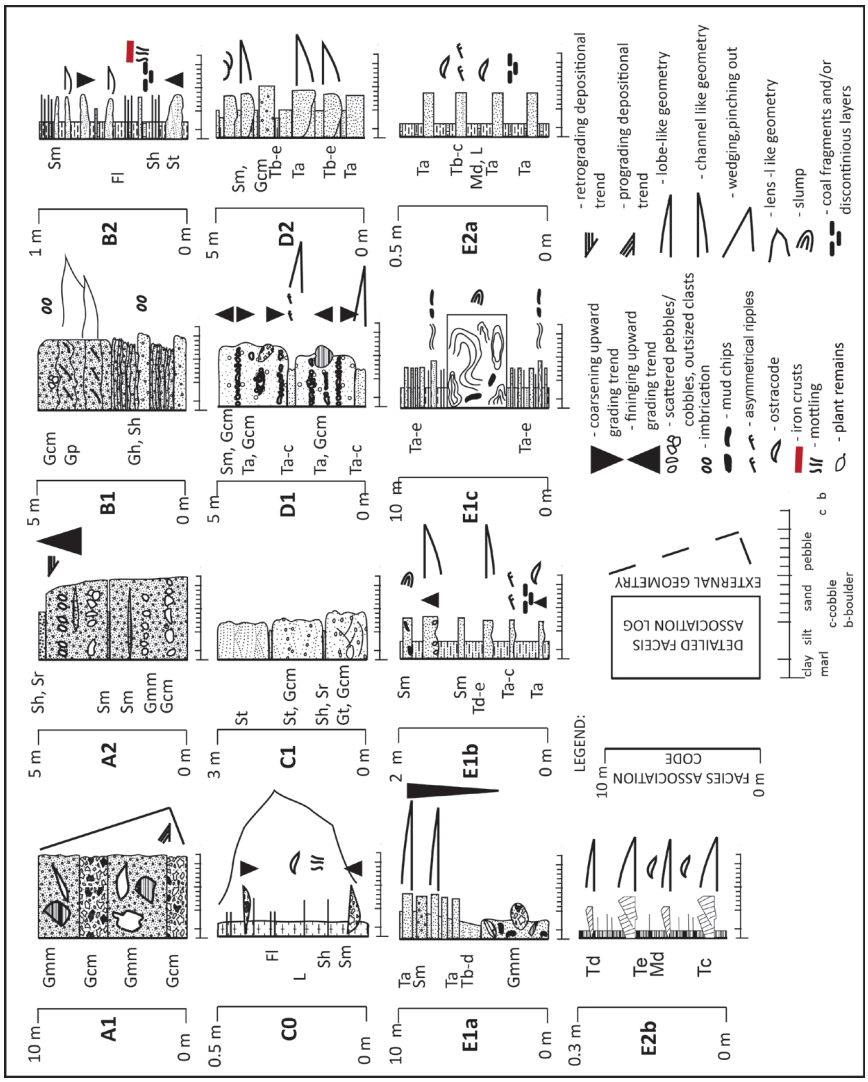

Figure 2.10: Grouping of lithofacies units into facies associations.

Figure 2.11 (facing page): Field examples of facies associations. Location of outcrops is shown on Fig. 2.3 a) Example of the debris flow deposits in the proximal alluvial fan facies association A1. Note basement blocks up to 2m in diameter; b) Sheetflood deposits in the distal part of the fan, facies association B1; c) Example of shallow water carbonates, facies association C0; d) Example of inter-distributary channel and bars facies association C1 with cross-bedded sandstones; e) Example of delta front facies association D1 with outsized clasts (up to 1.5 m in diameter) in a turbiditic sequence; f) Example of toe-slope facies association E1a with sandstone megabeds containing rip-up clasts; g) Example of prodelta facies association E1b with loading structures of fine-grained sandstones over mudstones; h) Example of distal prodelta facies association E2b with starved ripples in distal turbidites; i) Example of prodelta facies association E1c showing slope failure probably caused by fault activity.

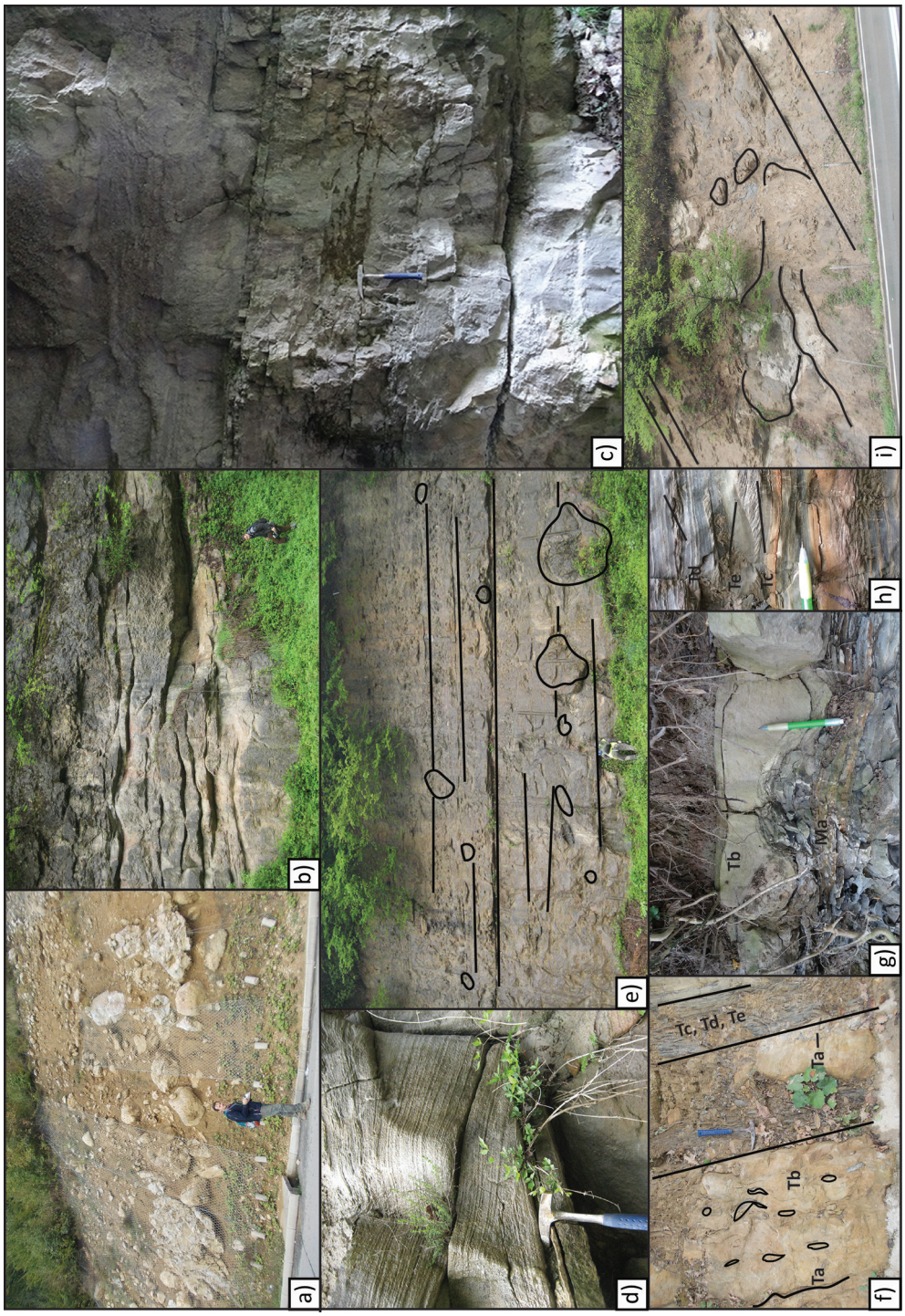
a)
b)
c)
d)
e)
f)
Tc, Td, Te
Ta
Tb
Ta
g)
Tb
Ma
h)
Td
Te
Tc
i)

indicate deposition from unidirectional flows bypassing and depositing material downstream (e.g., Mulder and Alexander, 2001; Leppard and Gawthorpe, 2006). This can be observed also in the lateral transition to facies association E1a and E1b described below.

Facies association E1a contains dominantly coarse- to medium- grained sandstones interbedded with siltstones and mudstones facies (Table 2.2, Fig. 2.10). The tabular to wide lobate and channelized turbiditic layers are interrupted by slumps (Fig. 2.11f). Slumped layers contain a mixture of coarse grained clasts up to boulder size and rip-up clasts of parallel laminated layers of slope sediments supported by a fine sandstone/siltstone matrix. They represent material that was deposited at the toe of the slope due to avalanching along the unstable steep slope (e.g., Postma, 1984; Strachan et al., 2013). Downwards the slope, E1a gradually passes into E1b.

The E1b facies association is characterized by isolated channel-like sandstones facies engulfed within siltstones and mudstones (Table 2.2, Figs. 2.10 and 2.11g). The sandstones are poorly to medium sorted with subangular to subrounded fragments of schists and limestones. The grain size, thickness and frequency of sandstones increases upwards from fine- to coarse-grained. This means an increase of terrigenous material input by erosion of a rejuvenated footwall and deposition by a feeding system with unidirectional concentrated flows further basin-ward (e.g. Lowe, 1982; Mulder and Alexander, 2001). This is documented by a gradual transition into the E2a facies association downwards along the flow direction. Additionally, plant remains and coal fragments suggest hanging-wall directed input as well, most likely by erosion of the previously deposited Oligocene - Lower Miocene coal series. This facies association has a gradual transition to E1a upwards in the stratigraphy.

The facies association E1c is made up by an alternation of sheet-like medium- to fine-grained sandstones, siltstones and mudstones facies (Table 2.2, Figs. 2.10 and 2.11i). This monotonous succession is sometimes interrupted by large scale slumps consisting of folded and broken autochthonous/intra-basinal layers or chaotic deposits. This indicates that the unconfined flows in the distal prodelta environment are obstructed by deposits of seismically triggered failure due to local fault activity (e.g., Postma, 1984; Sharp et al., 2000). The facies association E1c grades upslope into D2 and downslope into E2b.

The facies association E2a is made up by alternations of rhythmic sheet-like calcarenite sandstones and mudstones (Table 2.2, Fig. 2.10). The majority of the beds are structure-less, indicating deposition from steady turbidity currents with rapid aggradation, in most cases suppressing tractional transport or post-depositional reworking (e.g., Talling et al., 2012; Strachan et al., 2013). This suggests significant reworking of the clastic material in a shallow water environment before deposition into a distal delta environment. Some of these flows may represent the dominance of paleoflows draining hanging-wall composed of Bosnian Flysch limestones. This facies association represents periodic broad terminal channel lobes from a more proximal setting prograding into a mud-prone succession of the distal prodelta (e.g., Benvenuti, 2003; Talling et al., 2012).

The facies association E2b is made up of mudstones sometimes intercalated

with medium-grained ripple-cross laminated sandstones (Table 2.2, Figs. 2.10 and 2.11h). The mudstones contain dark and light grey to orange laminae that formed as a result of variable content of organic matter. The alternation of monotonous dark brown to dark grey mudstone are suggestive to anoxic bottom waters (e.g., Melchor, 2007; Ielpi, 2012). The transition between various mudstones is sharp inferring dominant deposition by settling from suspension at the lake bottom with variable redox conditions. Alternatively, these can also represent low density flows and/or mud debrites in the distal part of a basin floor fan (e.g. Talling et al., 2012). In general, this facies association indicates a lack of terrigenous influx and a dominance of the mud flows in the starved, under-filled basin (e.g. Carroll and Bohacs, 1999). In the stratigraphic succession E2b facies association alternates with E1a or D1 facies associations, and their contacts are sharp.

2.6. The link between normal faulting and evolution of facies associations

Our observations in the Sarajevo-Zenica Basin indicate a close link between the activation of normal faults and deposition of various facies associations. This link is best described by three characteristic groups of facies associations. These correspond to the evolution of the depositional environment, controlled by the balance between the rate of creating accommodation space and the rate of sediment supply, during the three main stages of a normal faulting: onset (Fig. 2.12), high displacement rates (Fig. 2.13) and gradual termination of fault activity (Fig. 2.14).

The onset of normal fault activity triggers the coeval deposition of A1, A2 and E2b facies associations (Fig. 2.12). The bulk of deposition consists of proximal to middle fan facies associations localized right next to the normal fault scarp (Fig. 2.12a, d). The footwall is uplifted during faulting and subsequently providing eroded material for deposition of A1 and A2 facies associations. These facies associations show a prograding and aggrading character in the hanging-wall direction forming a steep talus that may reach 30° inclinations (Fig. 2.7c). The overlying strata indicate that the alluvial fan incises and erodes the fault scarp, creating a sub-areal unconformity, which is recognized latter as a sequence boundary (Fig. 2.7c). The coeval deposition in the more distal lacustrine environment is marked by sediment starvation, observed by deep lacustrine deposits conformably overlying pre-faulting littoral limestones (e.g. E2b over pre-faulting strata, Fig. 2.12b, d). The latter infers rapid basin subsidence (Prosser, 1993). The base of this sequence in deep lake deposits (i.e. E2b) was used as a diagnostic marker for a sequence boundary, being correlative to the proximal erosional unconformity marking the maximum flooding surface. Furthermore, the normal fault activation (syntethic and antitethic) is recognized in deep water facies by the presence of large scale slumps (E1c, Fig. 2.11i), or mud-prone slope deposits (E1b) often overlying an angular unconformity (Fig. 2.12c). The wedge shape geometry of sedimentary bodies infers higher subsidence rates in the immediate hanging wall, but also may suggests that tilting was controlled by the listric geometry of the normal fault (García-García et al., 2006).

The period of highest displacement rates (Fig. 2.13) increases the

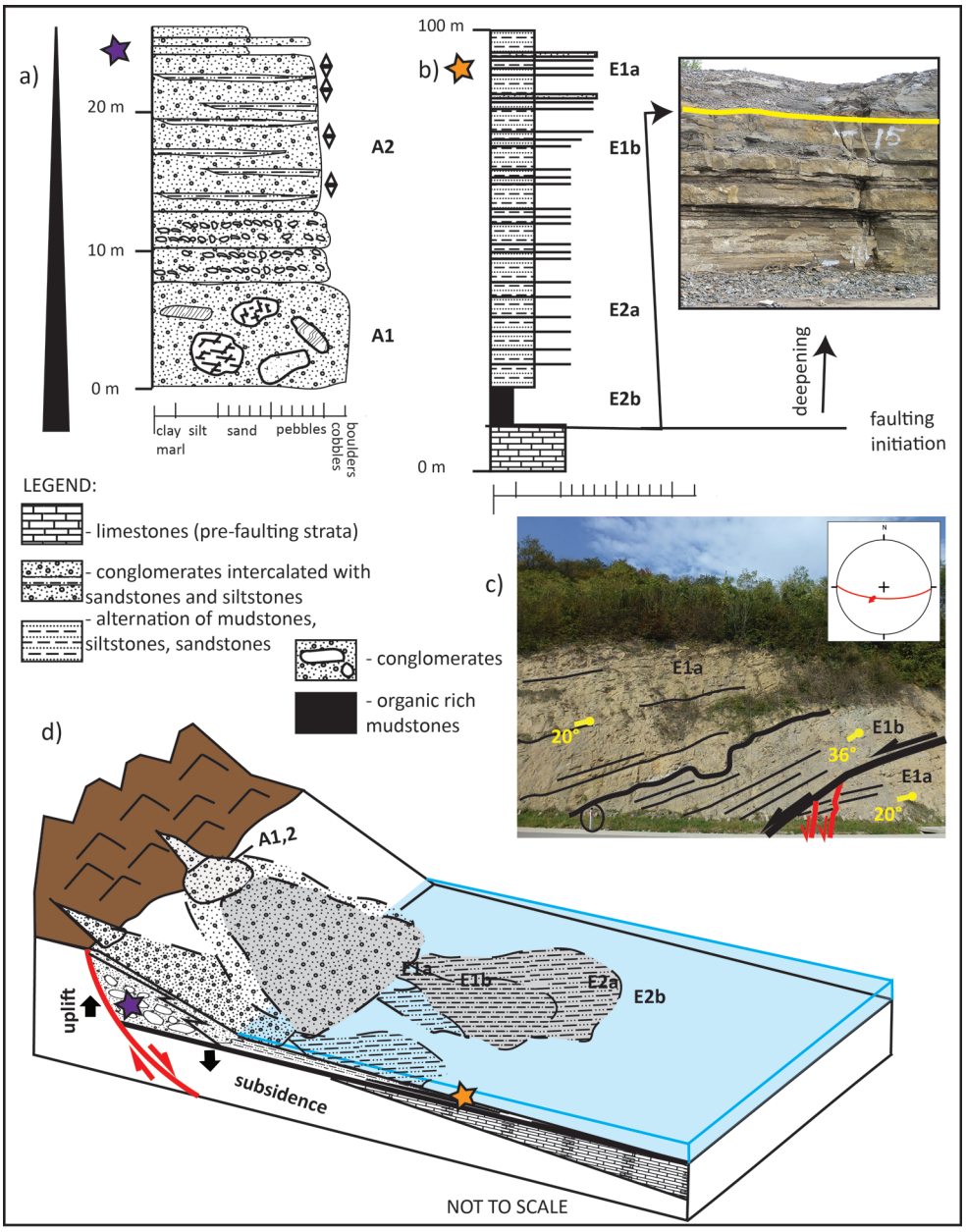

Figure 2.12: Sedimentological evolution of various facies associations of the tectonic systems tract at the onset of fault activity. a) Typical sedimentological log for the proximal units of the onset fault activity systems tracts deposited over eroded fault planes in their hanging-wall; b) Typical sedimentological log illustrating the progradation in deep lacustrine environment at the base of the slope created by the normal faults. This progradation follows the initial transgression recorded over the organic rich marls and is observed as a transition from immature to well-developed turbidites. Note the high amount of organic matter in the mudstones probably reflecting stratigraphic condensation due to rapid deepening.

Figure 2.12 (continued): The yellow line marks correlative maximum flooding surface at the base of the new sequence dividing pre-faulting mudstones (E2b) and shallow water carbonates (pre-rift deposits); c) toe slope décollement triggered by antitethic faulting in the basin. The thick black line (i.e. angular unconformity) represents the previous décollement surface. The activity of the normal fault created steep fault scarp and tilting of the pre-existing slope which combined with the basin ward dip of the bedding in the uplifted footwall behaves as a décollement surface. The created accommodation space was partly filled by the prograding and aggrading hanging-wall directed mudflows (E1b). The erosional surface and scouring (wavy black line) at the top of the E2b suggests erosional and bypass flows before higher amount of coarse material (E1a) fill up the previously created space and decrease the slope gradient. The scale of the outcrop is shown by the traffic sign (0.7 m high) in the black. The red line with arrow on the stereoplot indicates orientation of the fault plane and sense of movement; d) Interpreted sedimentological environment combining the A, E1 and E2 facies associations. See Fig. 2.10, Tables2.1 and 2.2 for the meaning of the facies association codes.

accommodation space rapidly. This leads to simultaneous deposition of immature terrestrial material in the proximal to middle alluvial fan facies associations (A1 and A2) and delta slope (D1, D2 and E1a) settings restricted to a narrow zone in the immediate hanging wall. The progradation of irregular flows of immature terrestrial material in the lake indicates erosion of the steep uplifting footwall and material transport via bypass flows without significant reworking and residence time (e.g. Leppard and Gawthorpe, 2006). Consequently, more distal and lateral facies associations (B1,B2, D2, E1b) record a decrease in channel amalgamation and channel/overbank ratio up in the section, with higher frequency coarsening-upwards influxes within the overall fining-upwards grading trend (Fig. 2.13a). Such higher frequency influxes may indicate short term flooding-events (e.g. Støren, 2010), or short periods of tectonic quiescence and further transport of material eroded from the footwall (e.g. Catuneanu, 2002). Similarly, periodic lobes in the distal prodelta environment (E2a, E2b) can also be interpreted to be transported by flows draining both the hanging-wall and the footwall, or are events of hanging-wall tilting during normal fault activity (Fig. 2.12b, 2.13d). The shallow water lacustrine carbonates with Ostracode fauna mark the maximum flooding surface (Fig. 2.10c, C0 in Fig. 2.13b, c). The facies beneath this surface show retrogradational and fining upward grading trends (Fig. 2.13a, c), while the overlying facies associations display progradational stacking patterns and coarsening upwards (Figs. 2.13b, c and 2.14b).

The final stage of fault activity (Fig. 2.14) is characterized by lower rates of creating accommodation space when compared with sedimentation rates and ultimately end of fault activity (e.g. Sweet et al., 2003, 2005). The subsidence of the hanging-wall extent over the immediate footwall at low rates. The effect is that only in the most proximal areas the facies associations A1 is replaced by A2 and B1 in the vertical succession, which onlap the slope and the eroded fault scarp with general retrogradational and aggradational deposition, and fining-upwards grading trends as the fault activity dies out (Fig. 2.7c, 2.14a). This retreat is caused by the erosion of the fault scarp and general lowering of the source area relief when the activity of the fault and thereby exhumation of the footwall terminates. In the more distal areas, the accommodation space is outpaced by the sedimentation rate, the effects being observed in the dominance of coarse-grained material, coarsening-upwards grading due to progradational depositional trends

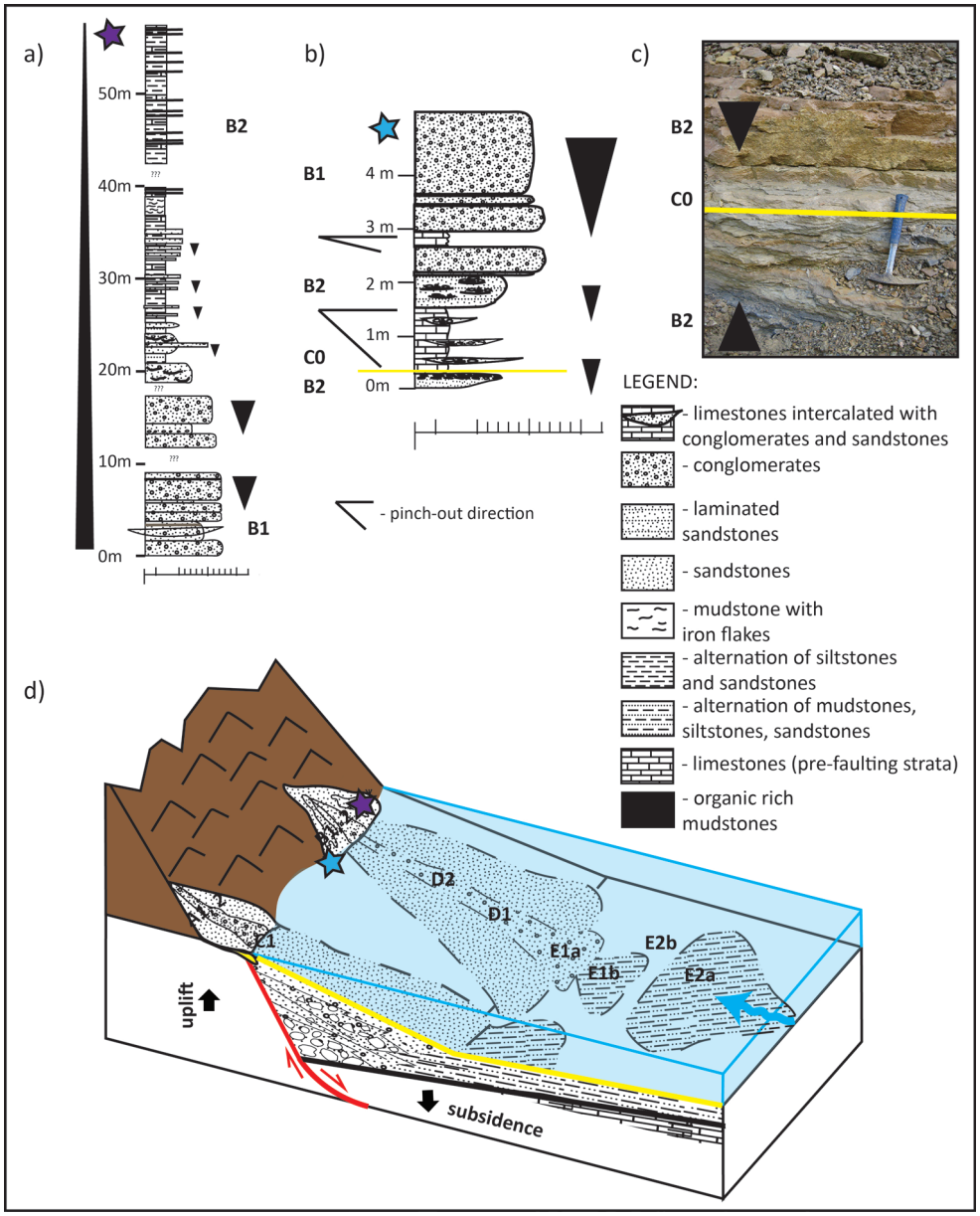

Figure 2.13: Sedimentological evolution of various facies associations of the systems tract formed during highest displacement rates of faults. a) typical sedimentological log of distal fan facies deposited during the rapid transgression associated with the subsidence of the normal faults hanging-wall. An upward transition from channelized distal alluvial fans to flood plains and shallow lacustrine deposition is observed; b) Sedimentological log illustrating a maximum flooding surface formed during the highest displacement rates of normal faulting, observed by shallow water lacustrine carbonates rich in ostracodes separating a distal alluvial facies associations. See also Fig. 2.12c; c) isolated crevasses and channels in overbank deposits (lower part of the section below yellow line). The amount of the

Figure 2.13 (continued): channels and crevasses increases up in the section. These are separated by a maximum flooding surface marked by shallow water limestones with ostracodes (yellow color); d) Interpreted sedimentological environment combining the A, B, C and E facies associations. The blue arrow suggests hanging-wall directed drainage. See Fig. 2.10, Tables 2.1 and 2.2 to for the meaning of the facies association codes.

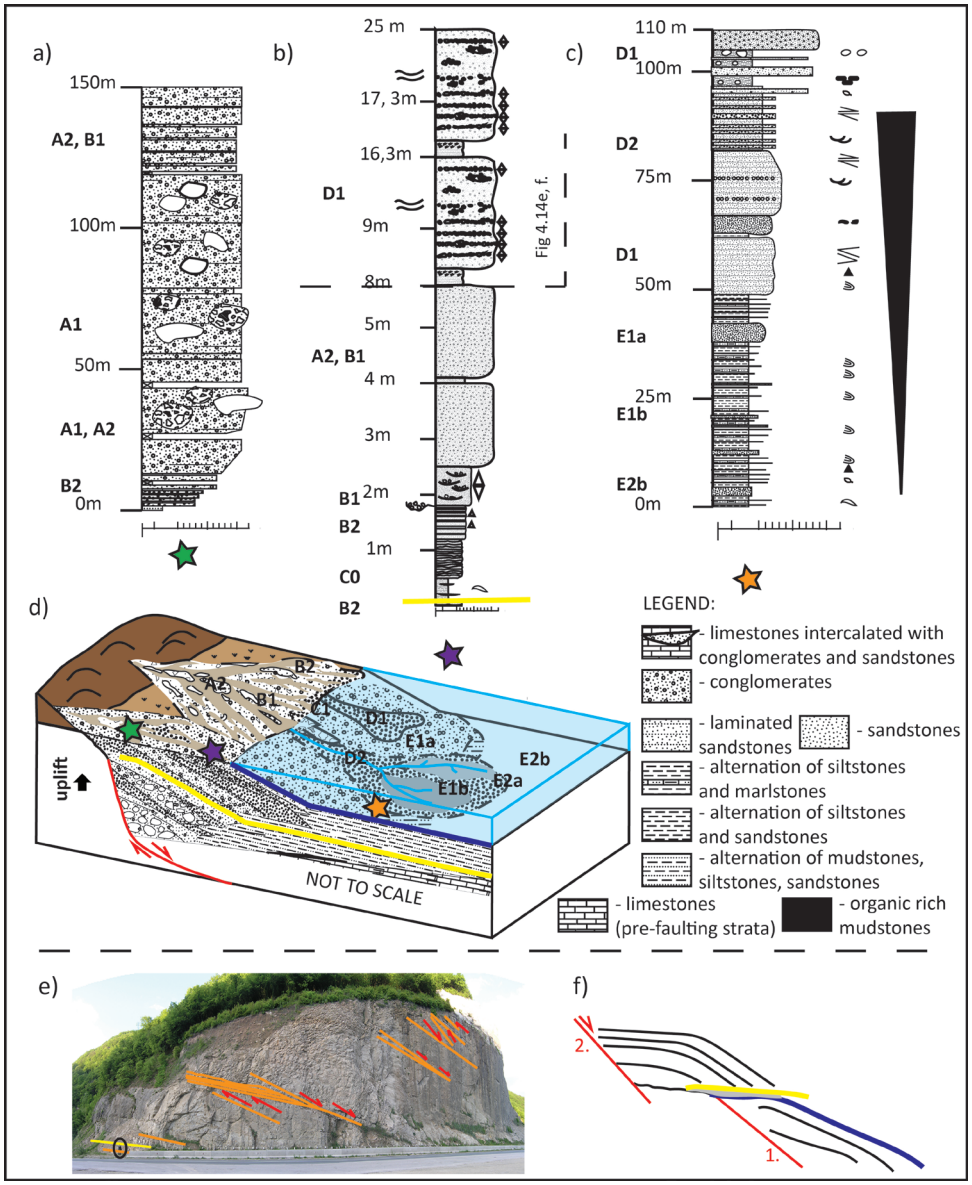

Figure 2.14: Sedimentological evolution of various facies associations during low displacement rates and after faulting. a) A typical sedimentological log for the proximal part of the post-rift systems tract burying the earlier formed normal faults; b) Sedimentological log illustrating an intermediate position in the sedimentological environment around the river

Figure 2.14 (continued): discharge area with coarsening upwards patterns and aggradation in the braided plain environment during normal regression (below dashed line) and progradation of delta slope deposits which are syn-kinematic to the subsequent faulting event (above dashed line). Yellow line marks the maximum flooding surface formed during highest displacement rates of the fault; c) Sedimentological log illustrating a basin-ward position in the sedimentological environment with coarsening - upwards patterns near the transition from prodelta to delta slope caused by sedimentation rate outpacing accommodation space creation rate and transport of material further into the basin; d) Interpreted sedimentological environment combining the B, C, D and E associations. Yellow line marks the maximum flooding surface developed during highest displacements rates of the fault. The dark blue line represents the maximum regressive surface; e,f) Illustration of the sedimentological response at the transition between the ceasing the activity of one fault system and initiation of the next one in its footwall. This results in a backstepping migration of the extensional deformation; e) a high frequency progradation-retrogradation pulses (red arrows) formed due to rapid changes in sedimentation rates and/or accommodation space with an overall prograding character. The yellow line marks the maximum flooding surface, the orange line delineates bedding planes. Geologists for a scale (inside black cycle); f) Interpretative sketch showing the onset of activity of next faulting event caused by the deformation migration in to footwall of the previous fault leading to drowning of previous deltaic system. The grey polygon represents transgressive system, based by the maximum regressive surface (dark blue line) and maximum flooding surface (yellow line) towards the top. The numbers 1 and 2 represent the younging trend of faulting events. See Fig. 2.10, Tables 2.1 and2.2 for the meaning of facies association codes.

accompanied by low rates of aggradation in the delta plain (Fig. 2.14b, c, d). Often the vertical succession finishes with smaller fining-upwards trend, especially visible in the distal facies associations. The distal faces associations (C1, D2, E1b) indicate an increase in channel amalgamation and channel/floodplain sediments ratio up in the section (Fig. 2.14b). Laterally, progradation can be followed along a gradual or sharp transition from E1a,b to D1 facies associations (Fig. 2.14c). The sediment was supplied by the high energy bedload-dominated rivers that show a gradually decreasing in energy in response to exhaustion of the source area which resulted in small fining-upward packages capping the sequence.

The next faulting event occurs into footwall of the previous fault. The onset of this next event causes drowning of previous deltaic system. The change from prograding to retrograding (syn-kinematic) depositional trend during fault migration is marked by a change at the maximum regressive surface. This migration and subsequent progradation during the next cycle is visible in the basin in a outcrop (Fig. 2.14e,f).

2.7. A coupled tectonic and sedimentological model of the Sarajevo - Zenica Basin during the asymmetric Early - Middle Miocene extension

Field observations demonstrate that the second depositional cycle in the Sarajevo - Zenica Basin was dominantly controlled by the Early - Middle Miocene extension. This is proved by the observed features of syn-depositional normal faulting and associated clastic wedges. The response of facies associations (Fig. 2.15) to each event of normal faulting is rapid overall deepening. The asymmetry

of extension created the dominant deposition of coarse proximal delta facies associations against the SW margin of the basin and the deposition of coarsening- and fining-upwards cycles in the vertical profile. In most of the observed situations, rapid changes in facies associations are driven by coeval normal faulting and, therefore, there is a direct link between extensional tectonics and sedimentation. Obviously, this does not completely exclude the influence of other external forcing factors, such as climatic lake level variations driven by the balance between precipitation and evapo-transpiration, which may incorporate questionable global or regional eustatic effects in such an enclosed intra-montane basin (e.g., Leever et al., 2011).

At the level of one extensional event, we interpret the onset of fault activity and the period of maximum displacement rates to correspond to a transgressive systems tract, while the final stage of fault activity corresponds to a regressive systems tract (Fig. 2.16). They are separated by a maximum flooding surface and together form a TR cycle. These cycles are bounded by a composite surface that includes a sub-aerial unconformity and the correlative maximum regressive surface. In the distal lake facies, the maximum regressive surface may be missing or overlap with the maximum flooding surface due to overlapping activity of the two subsequent faults, such as for instance at the highest displacement rate of one and onset of another faulting event. This cycle is controlled by the activity of a normal fault or a group of genetically related normal faults in the studied basin (Fig. 2.15). The thickness of such a cycle varies from 80 to 150 m as a function of the amount of accommodation space created by each event of normal faulting. In our specific studied case of the Sarajevo - Zenica basin, each normal faulting event back-stepped in the footwall and, therefore, the basin was progressively enlarged. Our analysis has detected three main transgressive-regressive cycles that are linked with the three major normal fault sets grouping the outcrop-scale faults formed during the three extensional events. These three sets are progressively younger SW-wards, i.e. in a footwall direction. The activation of the fourth set (3b in Figs. 2.6 and 2.7, i.e. the Busovača Fault stricto-senso) is associated with an incomplete developed cycle, either due to its deposition in an already filled basin with dominant proximal alluvial deposition, or due to subsequent erosion during the following post-Middle Miocene inversion of the basin. A similar backstepping pattern of fan deposits has been documented elsewhere in the neighbouring Sava Basin of the northern Dinarides (Pavelić and Kovačić, 1999).

The higher-order cycles are bounded by sub-aerial unconformities in what was the proximal part of the basin at the time of deformation and maximum regressive surfaces in more distal parts. They have net upper boundaries. The high-order sequence boundaries are created by a renewed activation of normal faults. The migration of listric normal faulting in a footwall direction resulted in antithetic tilting of older cycles of sedimentation. The overall depositional trend of multiple cycles is retrogradation governed by the back-stepping migration of subsequent faults, whereas the proximal facies of one event is sealed by the distal facies of the next event of normal faulting (Figs. 2.14e, f and 2.15). Such a retrogradational pattern driven by progressive basin enlargement has been observed also in other extensional basins (e.g., Postma and Drinia, 1993; García-García et al., 2006).

The internal structure of one high-order cycle reflects the evolution of each

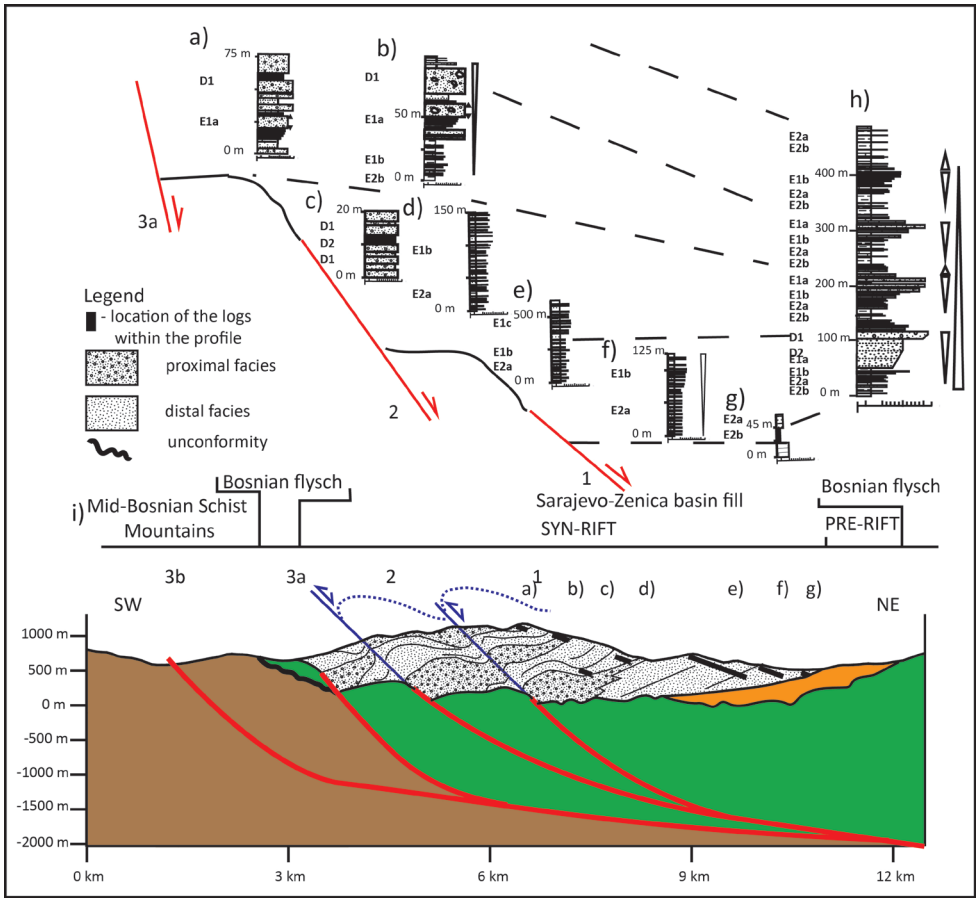

Figure 2.15: An interpretative sketch of abackstepping alluvial-deltaic system following deformation migration towards the basin margin. a-g) sedimentary logs along the Hum profile; h) fining-upward cycle in the basin centre. The black dashed lines represent boundaries of the Transgressive-Regressive (T-R) cycles in column a-g. See Fig 2.10 for the meaning of the facies association codes; i) Hum profile. Numbers 1, 2, 3a and 3b represent faulting events correlated with the profiles in Figs.2.6 and 2.7. See locations in Fig. 2.3.

Figure 2.16 (facing page): a) Evolution of the Sarajevo - Zenica Basin illustrated as a conceptual model. 1 - A fordeep basin formed in front of an advancing nappe. The onset and evolution of the basin is controlled by the thrust; 2 - Tectonic inversion and formation of the asymmetric extensional basin; 3 - The final basin inversion; b) Idealized sequences of the asymmetric extensional basins. 1 - basin margin(s), showing overall coarsening - upward cycle internally arranged into smaller fining - upwards cycles; 2 - basin depocentre with overall fining - upwards cycle including of smaller coarsening - upwardscycles; 3 – T-R cyclicity induced by the backstepping migration of deformation.

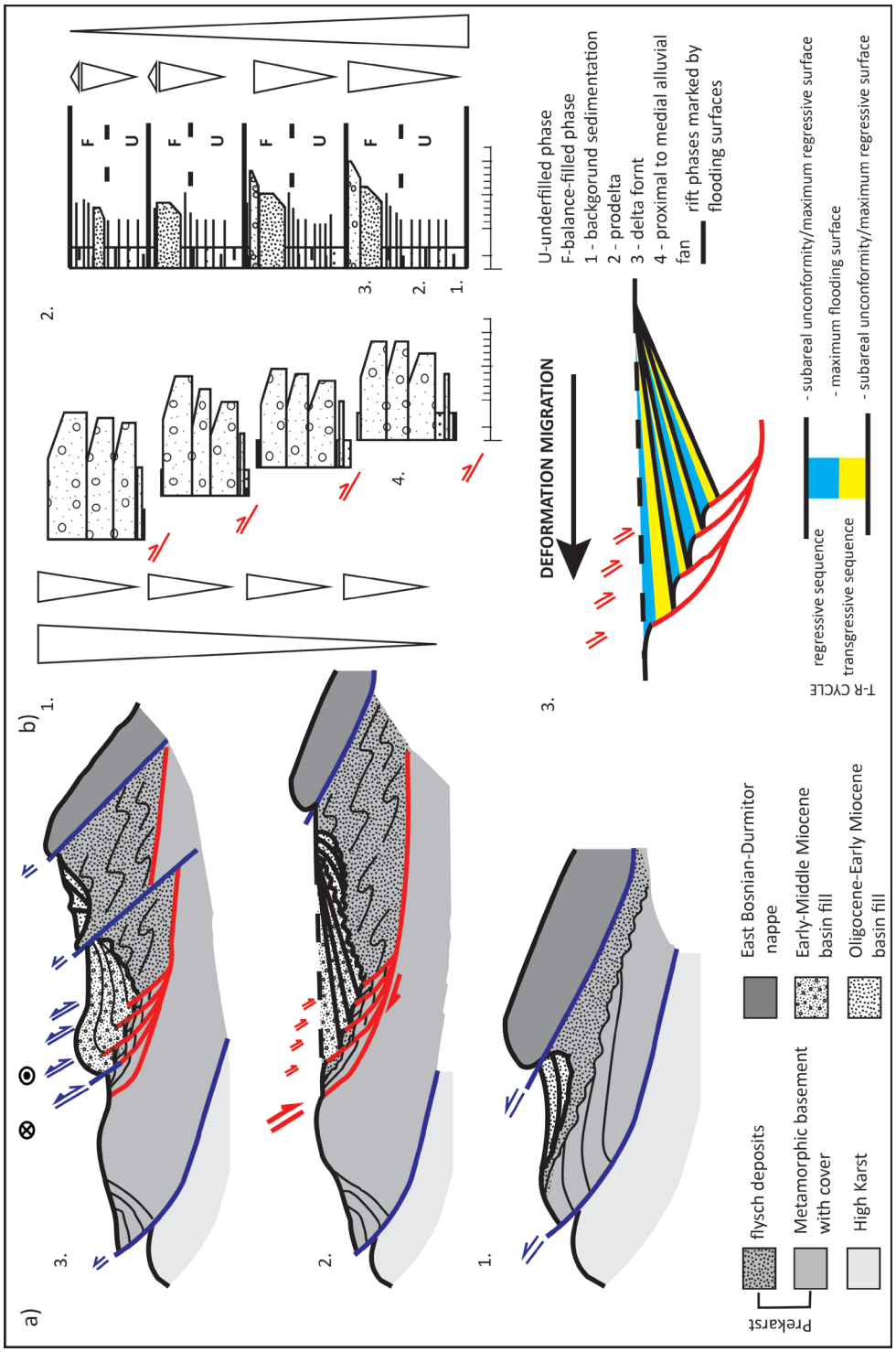
a)
3.
2.
1.
b)
1.
2.
3.
4.
F
U
DEFORMATION MIGRATION
U-underfilled phase
F-balance-filled phase
1 - backgorund sedimentation
2 - prodelta
3 - delta fornt
4 - proximal to medial alluvial fan
rift phases marked by flooding surfaces
T-R CYCLE
regressive sequence
transgressive sequence
- subareal unconformity/maximum regressive surface
- maximum flooding surface
- subareal unconformity/maximum regressive surface
flysch deposits
Metamorphic basement with cover
High Karst
Prekarst
East Bosnian-Durmitor nappe
Early-Middle Miocene basin fill
Oligocene-Early Miocene basin fill

major normal fault. The initial transgression is characterized by a fining upwards grading profile in the proximal part of basin and aggradation in more distal areas. Most of the deposition continued in alluvial environment, trapping material next to the adjacent fault scarp and cutting off supply to the distal lacustrine part of the basin (e.g., Loutit et al., 1988, Galloway, 1989). This shows that sedimentation generally kept pace with subsidence during the onset of normal faulting (Jackson et al., 2002). The onset was followed by a period of rapid subsidence in the hanging-wall of the normal fault, which was associated with aggradation and smaller scale prograding episodes. All facies associations display an overall fining upwards pattern. The short-term coarse fluxes of alluvial sediments may result in increase of the sediment supply, generally interpreted to be the result of wet climate or record of source rejuvenation due to normal fault slip (e.g., Blum, 1993). In our studied case, the latter acceleration of subsidence is rather obviously driven by the activation of normal faults. The under-filled nature of the basin during this period is a result of accommodation outpacing sediment supply due to high fault displacement rates. Similar with what was observed elsewhere (e.g., Leeder et al., 2002; Leppard and Gawthorpe, 2006), the basin is characterized by the steep, bypass and sometimes erosional slope controlled by the marginal fault and limited, narrow coastal area created by the specific geometry of the normal faults and their rapid footwall exhumation. This stage can be generally characterized as an under-filled stage, where the rate of creating accommodation space is generally higher than the sediment supply (e.g., Carroll and Bohacs, 1999; Withjack et al., 2002). The gradual cessation of fault activity is recognized by a regression marked by rapid progradation of the delta front within the basin, creating the overall coarsening-upwards grading profile. Pre-dating and on-going exhumation of normal fault footwalls increased the profile of the source area and produced high energy rivers with strong erosional character. These bedload dominated rivers carried coarse-grained material further away from the source filling up the basin and create a diachronous basal progradation surface, which is younger in a distal direction (Sweet et al., 2003, Ramaekers and Catuneanu, 2004). This stage can be generally characterized as an over-filled stage, when the rate of creating accommodation space was lower that the increased rate of sediment supply, resulting from the exhumation of the footwall (e.g. Carroll and Bohacs, 1999; Withjack et al., 2002).

At even higher resolution, the activation of faults with smaller offset observed in outcrops may be related to the definition of a higher-order cyclicity. However, such very high order cycles are difficult to discriminate from autocyclic processes, such as lateral shifting of the main channel or flooding events.

The low-order extensional cycle at the scale of the entire Lower - Middle Miocene basin fill shows an overall coarsening-upwards pattern that is superposed over the high-order transgressive-regressive cyclicity (Figs. 2.15 and 2.16). Given the similar distribution of facies associations inside the basin, this overall coarsening-upwards pattern reflects changes in the dominant SW-ward migration of the source area. The system of normal faults gradually exhumed an increasingly active source area in their footwall (i.e. the Mid-Bosnian Schist Mountains), which increased the sediment input and filled the created accommodation space. The resulting transgressive-regressive cycles are increasingly coarser. Grading of the higher-order cycles is not always visible in the hanging-wall near the fault (e.g.,

Fig. 2.13a), whereas such grading is better documented in more distal sediments (e.g., Fig. 2.13b). This inference is in agreement with previous interpretations that most proximal sediments adjacent to the source area do not exhibit coarsening-upwards grading trends (e.g. Miall, 1996). Similar with what was inferred in others sedimentological studies of normal faulting (e.g., Leeder and Gawthorpe, 1987; Gawthorpe and Colella, 1990), these cycles have a wedge shape geometry due to the larger subsidence in the vicinity of normal faults.

The provenance and maturity of the material sourcing clastic wedges indicate a catchment area of the fluvial system that was dominantly located in the footwall of the normal faults (i.e. the Mid-Bosnian Schist Mountains). These are mainly local short streams sourcing small fans in the immediate hanging-wall of normal faults. Such a drainage style was observed in other extensional basins, such as the Suez Rift (Leppard and Gawthorpe, 2006), Gulf of Corinth (Gawthorpe and Leeder, 2000), or Barent Sea (Prosser, 1993). In addition to small isolated drainages, the fan systems along the Lašva and Fojnica valleys mirrors the much larger Mid-Bosnian Schists Mountains catchment area supplying large fan complex by carrying high amount of coarse material into the Sarajevo - Zenica Basin. The continuous lateral correlation between the similar deltaic succession retreating in the direction of normal faulting means that the incision kept pace with footwall uplift and maintained the sediment transport into the basin. Similar observations are available in the modern examples of Akrata and Xylokastro Deltas in Gulf of Corinth rift (e.g., Seger and Alexander, 1993). Alternatively, they can also be associated with relay ramps connecting normal fault segments (e.g. Young et al., 2002; Trudgill, 2002). We cannot fully exclude that the basin was sourced from a hanging-wall direction or by an axial drainage, but the observations of asymmetric depositional bodies show that such influxes are likely suppressed by streams with massive influx draining the footwall.

2.8. Tectonic and sedimentary evolution of the Sarajevo - Zenica Basin

Our study shows that sedimentation in Sarajevo-Zenica Basin during Oligocene - Miocene times was controlled dominantly by tectonically induced changes in the geometry of the accommodation space and changes in the source area. The general extensional and contractional trends in the basin have been observed or inferred also by previous studies (e.g. Hrvatović, 2006; de Leeuw et al., 2012 and references therein), but our analysis provides a much higher resolution and is able to discriminate the succession of events with time (Fig. 2.16), which is critical for understanding not only the tectono-sedimentary evolution of the basin, but also the larger area of the Dinarides.

2.8.1. Thrusting during the onset of Oligocene - Early Miocene basin deposition

Our study shows a novel demonstration that the Oligocene - Early Miocene onset of basin deposition was associated with NW-SE oriented thrusts, folds and

the formation of local unconformities during sedimentation. This NE-SW oriented contraction shows a dominantly SW tectonic transport. Grouping deformation structures and the provenance of sediments shows a direct relationship with the thrusting at a larger scale of more internal Dinarides units (East Bosnian - Durmitor and/or Drina - Ivanjica) over the basin sediments. These sediments were deposited unconformably over the Mesozoic cover of the Pre-Karst unit and over the younger, more external parts of the Bosnian Flysch (i.e. its Ugar - Durmitor Cretaceous interval). These geometries indicates that the older, more internal parts of the Bosnian Flysch (i.e. late Jurassic - Earliest Cretaceous Vranduk interval) served as a decollement horizon for the Oligocene - Early Miocene thrusting. In fact, this decollement is an inherited weakness zone from older Late Jurassic - Cretaceous thrusting that was coeval with the overall deposition of the Bosnian Flysch. In this context, the initiation of the Oligocene - Early Miocene sedimentation of the Sarajevo-Zenica basin took place in a foredeep basin that formed in the footwall of more internal Dinarides units (Fig. 2.16a1). At higher resolution, this Oligocene - Early Miocene sedimentation reflects likely the syn-kinematic deposition of the two sedimentary cycles described by previous studies (Muftić, 1963; Milojević, 1964). Their position in the footwall of the main thrust of more internal Dinarides units and the relative constant sediment influx infer that the cyclicity is related to two different pulses of thrusting inside the foredeep basin. This may reflect successive thrust loading and unloading events, as typically observed in many other foredeep areas (e.g., Ballato et al., 2008; Catuneanu et al., 2001 and references therein).

At a more regional scale, the Dinarides contraction took place during successive late Jurassic - Eocene shortening events, generally migrating towards its foreland, but also associated with moments of out-of sequence deformation (e.g., Schmid et al., 2008; Ustaszewski et al., 2010). Later, (Late) Miocene - Quaternary contractional deformations is documented by structural studies either in the external, offshore and neighbouring parts of the Dinarides or in their internal-most parts by inverting the sediments of the Pannonian Basin. The latter deformation has variable effects along the strike of the Dinarides, apparently increasing SE-wards in their external-most parts and NW-ward in the internal zone (e.g., Placer, 1999; Tomljenović and Csontos, 2001; Matenco and Radivojević, 2012; van Gelder et al., 2015 and references therein). The prolongation of contractional deformation during the Oligocene - Miocene times was quite uncertain until our study (see discussion in de Capoa et al., 1995; Mikes et al., 2008a), mostly because the bulk exhumation of the Dinarides took place earlier, combined with similar contractional directions and uncertainties in dating the Miocene sediments in the intra-montane basins. Therefore, our study is a first clear demonstration of a link between contraction and sedimentation that post-dated the main Eocene event in the central part of the Dinarides. Although affected by age uncertainties, the syn-kinematic Oligocene - Early Miocene sediments that document this contraction must predate the ~18 Ma onset of deposition of the second cycle representing the initiation of the Dinaride Lake System and the start of the main extensional phase in the Pannonian Basin (de Leeuw et al., 2012; Mandic et al., 2012). Although the Late Oligocene Climatic Optimum that stalled in the Aquitanian may have imprinted the sedimentation of the Dinaride Lake System (de Leeuw et al., 2012), the coeval first depositional cycle in the Sarajevo – Zenica Basin was primarily controlled by tectonics.

2.8.2. Early - Middle Miocene extension

The earlier contraction was followed in the Sarajevo-Zenica Basin by the deposition of a new low-order tectono - sedimentary cycle. This extensional deposition is slightly shifted SW-wards in respect to the earlier tectono-sedimentary cycle by directly overlying the pre-Oligocene basement and sedimentary cover of the Pre-Karst unit (Fig. 2.16a2). The overall NE-SW to E-W direction of extension has local variations during the successive normal faulting events. The geometry of the normal faults and the antithetic tilting of their hanging-walls indicate that the four major listric normal faults merge at depth into one major decollement level (Figs. 2.6, 2.7, 2.15 and 2.16b) that is rooted somewhere in the Bosnian Flysch, most likely in its younger Ugar - Durmitor component. Once again, the presence of this decollement horizon located at the contact between the basement and dominantly carbonatic cover of the pre-Karst and East Bosnian – Durmitor units has facilitated its reactivation by the NE-SW oriented extension.

The coeval exhumation of the Mid-Bosnian Schists Mountains located in the footwall of the normal fault system is inferred by eroded footwalls and the geometry of these faults. Exhumation studies in the Mid-Bosnian Schist Mountains show a few late Miocene – early Pliocene apatite U-Th/He ages (5-7Ma) in the immediate footwall of the Busovača Fault, while zircon fission fission-tracks are generally older than 27-28Ma in the Mid-Bosnian Schists Mountains (Casale, 2012). A more recent study derived zircon fission track ages of 24-29 Ma in the immediate footwall of the main Busovača fault (Hrvatović et.al, 2015). This means that zircon fission track and higher temperature thermochronological Eocene-Oligocene and older ages must reflect also the first stage of contraction observed also in the Sarajevo-Zenica Basin. The Late Miocene - Pliocene lower temperature thermochronological ages reflect exhumation coeval with the last observed stage of contraction. The ages predate and post-date with a few million years the main Early - Middle extensional basin formation. Given the partial retention zones of zircon and apatite fisson track and U-Th/He, this limits the Mid-Bosnian Schist Mountains exhumation during the Early - Middle Miocene extension somewhere between 3-5 km at normal geothermal gradients. The Busovača fault system reflects the brittle deformation associated with this exhumation. Therefore, we conclude that this represents an uni-directional low-angle listric normal fault system that is associated with footwall exhumation. Obviously, this asymmetry is facilitated by pre-existence of the rheological weakness of the Bosnian Flysch.

The extensional depositional cycle observed in the Sarajevo-Zenica Basin is regionally coeval with the initiation of the Dinaride Lake System. The lacustrine phase took place from 18 to ~13 Ma (de Leeuw et al., 2012), culminating at ~15.5 Ma when the lake system gained its maximum extent, interpreted to be an effect of favourable conditions during the Miocene Climatic Optimum (Zachos et al., 2001). The coeval evolution of the Sarajevo-Zenica Basin was almost entirely controlled by the extension. The Miocene Climatic Optimum might have enhanced the favourable conditions of extending the lake, but its subsidence is certainly tectonically controlled. At a more regional scale, this phase of extension was coeval with the

overall Miocene extension that started at ~20-18 Ma in the main depocentres of the Pannonian Basin. The northern margin of the Dinarides adjacent to the Pannonian Basin was affected by coeval large scale extensional exhumation along detachments that indicate top-N to top-E extension along the Dinarides strike. This extension peaked ~15-11Ma and its onset is generally older in the eastern areas of Serbia, such as Fruška Gora or the Morava corridor (Ustaszewski et al., 2010; Stojadinović et al., 2013; Toljić et al., 2013; van Gelder et al., 2015). Closer to our studied area, Miocene extension affected also the internal units of the Dinarides (Ilić and Neubauer, 2005; Schefer et al., 2011). This overall extension resulted in the formation of asymmetric extensional basins, where the hanging-wall subsidence was associated with significant exhumation in the footwall of detachments or normal faults (e.g., Matenco and Radivojević, 2012). These studies have shown that the location of these detachments is controlled by the weakness of various inherited Dinarides nappe contacts, most often made up by contractional trench turbidites. This is strikingly similar with the Sarajevo - Zenica Basin, whose Early - Middle Miocene normal faulting was associated with footwall exhumation of the Mid-Bosnian Schist Mountains was controlled by the inherited weakness of the Bosnian Flysch unit. Therefore, the observed extension must have the same genetic cause. The Sarajevo - Zenica Basin is the most external area in the Dinarides documented so far by a field study to be affected by the extension of the Pannonian Basin.

2.8.3. Late Miocene and subsequent inversion

The overall basin fill was inverted by a post-Middle Miocene stage of contractional deformation that was observed in many other areas of the Dinarides (Tomljenović and Csontos, 2001; Ustasewski et al., 2014 and references therein) and is likely still active at present (Bennett et al., 2008). In our studied case of the Sarajevo - Zenica Basin, the basin was inverted with a N-S oriented direction of contraction (Fig. 2.16a3). The obliquity of this inversion direction to the NW-SE oriented structural grain of the inherited normal fault system resulted in the inversion of this system over oblique ramps associated with a large number of tear and transfer faults. It is rather clear that the distribution of sedimentological facies from coarse alluvial in the SW to more distal turbiditic to pelagic in the NE inherited from extensional phases controlled the geometry of the subsequent contractional deformation. The resulted geometry is the one of en-echelon thrusts and folds accommodated by transfer zones or tear faults. Most of the deformation has a S-ward vergence, but opposite N-verging back-thrusts or folds are also observed, although accommodating lower amounts of shortening. Unsurprisingly, their prolongation at depth appears to be connected at depth into a larger offset decollement that is rooted, yet again, in the Bosnian Flysch thrust contact. In the SW parts of the Sarajevo-Zenica basin (Figs. 1 and 3), coeval deposition in several synforms suggests that sedimentation took place in fordeep basins, although sedimentological patterns, dominated by alluvial and other continental sub-aerial deposition, are not fully diagnostic. The deposition in the basin was also associated or post-dated by the final contractional exhumation of the Mid-Bosnian Schist Mountains, as documented by the apatite U-Th/He low temperature

thermochronology data (~5-7 Ma, Casale, 2012).

2.9. Conclusions

Our study of the Sarajavo - Zenica Basin, a large isolated Oligocene - Miocene basin situated in the centre of the Dinarides orogen, has demonstrated a novel succession of deformation events, with critical inferences for the evolution of this mountain chain, and serves as a quantitative example of analysing the link between normal faulting and sedimentological evolution in asymmetric extensional basins.

The Oligocene - Early Miocene contraction was responsible for the onset of deposition in a basin that formed as a foredeep in the footwall of the coeval thrust displacing more internal Dinarides units over the Pre-Karst nappe situated in its footwall, and reactivating the inherited Bosnian Flysch Late Jurassic - Cretaceous tectonic contact. This thrusting has resulted in the creation of two transgressive-regressive cycles that reflect pulses of deformation during the overall contraction. At regional scale, this observation solves a long-standing controversy and shows that contractional deformation continued during Oligocene - Early Miocene times after the main Late Eocene orogenic phase in the central part of the Dinarides. More precise dating of this cycle of deposition is required for an accurate age determination of this deformation. The contraction was subsequently followed by a new cycle of deposition in the basin driven by the activation of a system of NE-dipping normal faults and the creation of an asymmetric extensional basin associated with significant exhumation in the SW-ward located footwall of normal faults. Deformation migrated towards this footwall with time, enlarging the basin and creating the space for the repetition of a higher order transgressive-regressive cyclicity observed in the alluvial to deep water turbiditic and pelagic coeval depositional system. At a larger scale, the observation of this extensional evolution proves that the extension of the Pannonian Basin was felt much further SW-wards than previously thought, re-activating thrust contacts inherited from the previous contractional evolution. The basin was affected ultimately by the overall indentation of Adriatic units and inversion observed in more internal units, a process that continued and is active today in most of the Dinarides (e.g., Pinter et al., 2005; Bennett et al., 2008; Handy et al., 2010).

The Early - Middle Miocene basin fill and extensional kinematics serve as a very good example of understanding systems tracts in asymmetric extensional basin. Our analysis demonstrates that the first order pattern of basin fill is regressive, coarsening-upwards, driven by the increasing and coeval exhumation during extension of a source area situated in the footwall of the normal faults, i.e. the Mid-Bosnian Schist Mountains. This gradually growing source area ensured an almost uni-directional sourcing of the basin and a marked asymmetry of the distribution of the sedimentological facies inside the basin, that is almost exclusively coarse grained alluvial to deltaic fan in the SW and more distal in the NE. Over this overall first order pattern (or low order cycle), a higher order cyclicity grouping transgressive and regressive systems tracts is observed to be directly associated with the activity of individual normal faults. These cycles have characteristic sedimentological patterns during the onset, maximum rate of slip along normal

faults and their gradual ceasing, from alluvial facies and wedges in proximal parts of normal faults to deeper water deposition at higher distances in their footwall. Sequence boundaries are formed during moments when the normal faults migrate further in a footwall direction and created a drowning of pre-existing alluvial fans and proximal deltaic facies and their shift in the same direction. Increasing the source area by footwall exhumation results in a massive SW-ward sourcing that ultimately fills the basin completely at very high rates during the final regression.

The overall analysis of such extensional basins shows that asymmetry and footwall exhumation changes significantly the sequence stratigraphy of extensional systems, which is almost exclusively studied so far in basins buried beneath passive continental margins (e.g., Martins-Neto and Catuneanu, 2010 and references therein). It shows that sedimentation in asymmetric basins, often observed in back-arc or intra-montane areas, is dominantly controlled rheologically by the inherited weakness of pre-existing nappe contacts (e.g., Tari et al., 1992; Brun and Faccenna, 2008). The asymmetric depositional geometry is imprinted in the high resolution transgressive-regressive cycles. The source input increases by footwall exhumation until the basin is completely filled during the rapid extension. Such basins deserve further studies and a better expression in current research of depositional characteristics in active tectonic settings.

Chapter 3. Variability of orogenic magmatism during continental collision: A numerical modelling approach

This chapter is based on Andrić, N., Vogt, K., Matenco, L., Cvetković, V., Cloetingh, S., Gerya, T., in revision in Gondwana Research.

3.1. Introduction

The mechanics of continental collision have been analysed in numerous analogue and numerical studies that have revealed the critical influence of several key parameters on orogenic build-up, such as the rheology of the continental lithosphere, the thermal age of the subducted oceanic lithosphere, the convergence rate and external forcing factors, such as the rate of erosion and/or sedimentation (e.g., Burov and Yamato, 2008; Ueda et al., 2012; Willingshofer et al., 2013; Erdös et al., 2014 and references therein). Most of these studies have focused on the mechanical growth of orogens, which is influenced by a number of processes, such as continental subduction (e.g., Vogt et al., 2017), delamination of continental lithosphere (e.g., Ueda et al., 2012), crustal relamination (e.g., Hacker et al., 2011), slab detachment (e.g., Duretz et al., 2011), eduction (e.g., Andresen et al., 1991; Duretz and Gerya, 2013) and exhumation of continental crust (e.g., Brun and Faccenna, 2008; Beaumont et al., 2009; Sizova et al., 2012).

The compositional evolution of magma during continental collision is less understood and analysed by means of thermomechanical models on a lithospheric scale. However, the mechanics of subduction and subsequent collision control the location of magma, their composition and emplacement mechanism (e.g., Vogt et al., 2012; Dymkova et al., 2015; Menant et al., 2016a). A broad variability of magmatism in terms of volume, composition, spatial and temporal distribution was observed in many collisional systems (e.g., Ducea, 2001; DeCelles et al., 2009; Cvetković et al., 2015; Menant et al., 2016b). Previous numerical studies have analysed the compositional change of magmas and their production rate (e.g., Vogt et al., 2012; Zhu et al., 2013), the effects of magmatic weakening on lithospheric strength and its control on lithospheric deformation (e.g., Gerya and Meilick, 2011; Gerya et al., 2015). Regional subduction dynamics and 3D asthenospheric flow during slab retreat and tearing were shown to impact magma generation, migration, transport and emplacement (e.g., Menant et al., 2016b). In contrast, the tectonic mechanisms driving the magmatic diversity found in orogenic areas are still not fully understood and are difficult to quantify solely by conventional field studies and geochemical techniques. Hence, self-consistent numerical approaches, which are able to quantify the temporal and spatial generation of melts during subduction and collision, offer an important additional tool to address complex interactions between magma production and lithospheric scale processes.

In this study, we present a series of 2D magmatic-thermomechanical experiments designed to quantitatively couple subduction and collision with magma generation, focusing on its compositional changes. Our setup is designed to simulate rapid subduction of a narrow ocean, followed by continental collision. By starting from a reference model, we further perform a parametric analysis on the role of crustal rheology, ocean size and thermal age, and convergence rate. The results are compared with the Dinarides Mountains, a European orogen affected by subduction, collision and back-arc extension, which have a well-preserved record of temporal and spatial changes in magma composition.

3.2. Numerical modelling methodology

Our magmatic-thermomechanical model is based on the i2vis Code and solves a series of thermal and mechanical equations by combing a finite difference approach and a marker in cell technique (Gerya and Yuen, 2003, see also Appendix 1, Tables 3.1 and 3.2). The model incorporates effects that are essential for the study of orogenic magmatism, such as mineralogical phase changes, fluid release and consumption, partial melting, melt extraction and emplacement. The mechanical equations of momentum (Stokes equation for creeping flow) and mass (continuity equation) are solved for a compressible non-Newtonian, visco-plastic fluid. Solving the energy equation, which accounts for latent, adiabatic, radiogenic and shear heat production, simulates the thermal evolution of the model. A detailed description of the numerical approach is given in Gerya and Yuen (2003, 2007) and Gerya (2010).

3.2.1. Initial configuration

The 2D computational domain covers 4000 km X 1400 km with a resolution of 1361 X 351 nodal points (Fig. 3.1). The numerical resolution decreases from 10 X 10 km to 1 X 1 km toward the centre of the domain, i.e. area undergoing subduction and collision. All boundaries are free slip. The setup simulates subduction beneath a passive continental margin and includes a gradual change in crustal and sediment composition (Fig. 3.1a, e.g., Regenauer-Lieb et al., 2001). An imposed constant convergence velocity of 5 cm/yr induces subduction. This velocity condition is deactivated at the onset of collision, i.e. after ocean closure. Subsequent collision is driven by the pull of the subducted slab.

The oceanic crust is composed of a 2 km thick layer of hydrothermally altered basalt and a 5 km thick layer of gabbro (Tables 3.1 and 3.2, Appendix 1). The upper plate is composed of a 20 km thick upper and a 20 km thick lower crust (e.g., Kelemen and Behn, 2016) of varying rheology (Fig. 3.1b; Table 3.3). The underlying lithospheric mantle is 80 km thick and composed of anhydrous peridotite. The thermal distribution of the oceanic lithosphere is calculated from its thermal cooling age (Table 3.3, Turcotte and Schubert, 2002). The thermal distribution of the continental lithosphere is calculated following a linear increase from 273 K at the surface to 767 K at the Moho and 1617 K at the lithosphere/asthenosphere boundary. For the asthenospheric mantle, a thermal gradient of 0.5 K/km is used. The setup simulates rapid subduction of a medium to small sized ocean (400-800 km in 8-16 My).

The model assumes instantaneous melt propagation and emplacement after extraction. Processes modifying the primary magma composition, such as fractional crystallization, crustal assimilation and magma mixing are not included. Furthermore, the model assumes partial melting of individual sources (Fig. 3.1) and does not account for more complex interactions resulting in melting processes such as for instance vein + wall - rock melting (Foley, 1992). However, the variability of the magmatic source and the nature of partial melting and/or melt extraction are resolved to a first order by our numerical approach.

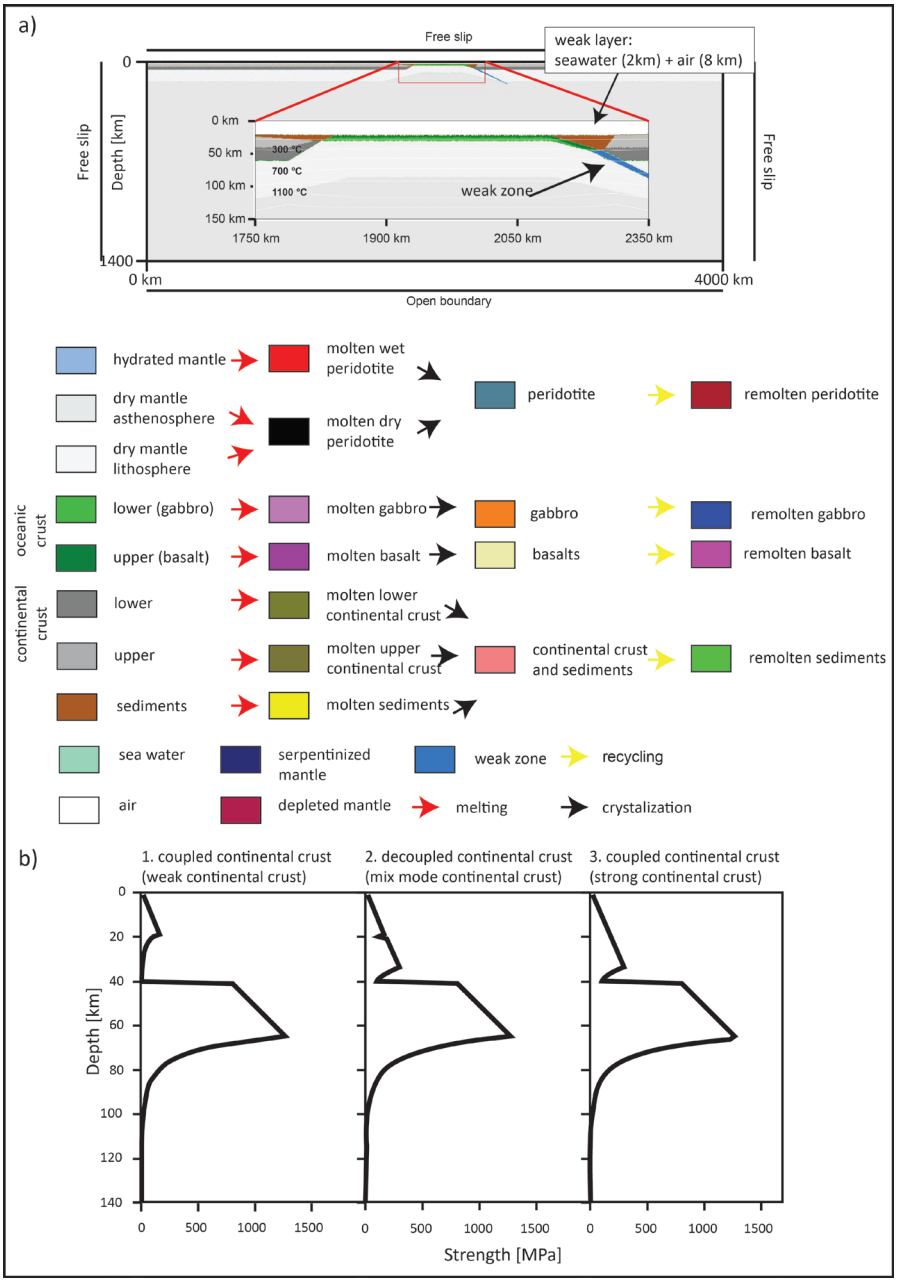

Figure 3.1: a) Initial model setup (see text for details). White lines represent isotherms in °C in increments of 200 °C starting from 100 °C. Materials (e.g., rock, melt, air) that appear in the following figures are defined by colours. The mantle is represented by two colours (two layers with same physical properties) to illustrate mantle flow; b) Initial strength profile of the continental lithosphere for a constant strain rate of = 10-14 s^{-1}. Three initial strength profiles are used (1) coupled weak continental crust, (2) decoupled mixed mode continental crust and (3) coupled strong continental crust.

Table 3.1: Thermal parameters used in the experiments. k is thermal conductivity (Clauser and Hieges, 1995). Hr is the radioactive heat production and H_L represents latent heat production. Tsolidus and Tliquideus,respectively, are solidus and liquidus temperatures of the rocks at given pressure and rock composition. For all rocks: Coefficient of thermal expansion $\alpha = 3\times10^{-5}$ (1/K), coefficient of thermal compressibility $\beta = 1\times10^{-5}$ (1/MPa).

Material; melt generated by melting of that material; magmatic rock crystalized from those melts	k [W/(m* K)] (at T_K, P_{MPa}) (1)	H_r [μW/m^3] (2)	H_L [kJ/kg] (2, 3)	$T_{solidus}$ [K] (at P_{MPa}) (4)	$Tl_{iquidus}$ [K] (at P_{MPa}) (4)
sediments; melt	$[0.64 + \frac{807}{T+77}] * \exp(4 * 10^{-6} * P)$	2	300	at P<1200 MPa: $889 + \frac{1.79*10^4}{P+54} + \frac{2.02*10^4}{(P+54)^2}$ at P>1200 MPa: 831 + 0.06 * P	1262 + 0.09 * P
upper continental crust; melt	$[0.64 + \frac{807}{T+77}] * \exp(4 * 10^{-6} * P)$	1.8	300	at P<1200 MPa: $889 + \frac{1.79*10^4}{P+54} + \frac{2.02*10^4}{(P+54)^2}$ at P>1200 MPa: 831 + 0.06 * P	1262 + 0.09 * P
lower continental; lower oceanic crust; melt	$[1.18 + \frac{474}{T+77}] * \exp(4 * 10^{-6} * P)$	0.18	380	at P<1600 MPa: $973 - \frac{7.04*10^4}{P+354} + \frac{7.78*10^7}{(P+354)^2}$ at P>1600 MPa: $935 + 35 * 10^{-4} * P + 62 * 10^{-7} * P^2$	1423 + 0.105 * P
upper oceanic crust (basalt); melt	$[1.18 + \frac{474}{T+77}] * \exp(4 * 10^{-6} * P)$	0.18	380	at P<1600 MPa: $973 - \frac{7.04*10^4}{P+354} + \frac{7.78*10^7}{(P+354)^2}$ at P>1600 MPa: $935 + 35 * 10^{-4} * P + 62 * 10^{-7} * P^2$	1423 + 0.105 * P
Lithospheric/asthenospheric dry mantle	$[0.73 + \frac{1293}{T+77}] * \exp(4 * 10^{-6} * P)$	0.022	-	$1394 + 0.133 * P_{MPa} + 51 * 10^{-7} * P^2_{MPa}$	2073 + 0.114 * P
wet mantle; melt (dry and wet mantle)	$[0.73 + \frac{1293}{T+77}] * \exp(4 * 10^{-6} * P)$	0.022	300	at P<1600 MPa: $973 - \frac{7.04*10^4}{P+354} + \frac{7.78*10^7}{(P+354)^2}$ at P>1600 MPa: $935 + 35 * 10^{-4} * P + 62 * 10^{-7} * P^2$	2073 + 0.114 * P
serpentinized mantle	$[0.73 + \frac{1293}{T+77}] * \exp(4 * 10^{-6} * P)$	0.022	-	at P<1600 MPa: $973 - \frac{7.04*10^4}{P+354} + \frac{7.78*10^7}{(P+354)^2}$ at P>1600 MPa: $935 + 35 * 10^{-4} * P + 62 * 10^{-7} * P^2$	2073 + 0.114 * P
depleted mantle	$[0.73 + \frac{1293}{T+77}] * \exp(4 * 10^{-6} * P)$	0.022	-	at P<1600 MPa: $973 - \frac{7.04*10^4}{P+354} + \frac{7.78*10^7}{(P+354)^2}$ at P>1600 MPa: $935 + 35 * 10^{-4} * P + 62 * 10^{-7} * P^2$	2073 + 0.114 * P

Table 3.2: Ductile creep parameters of different rheologies involved in experiments. Density - ρ0; reference viscosity - η0; activation energy - Ea; stress exponent – n; activation volume - Va; cohesion – C; fruction angle – sin(ϕdry). The flow laws are defined in Ranalli (1995) and references therein.

Material	ρ_0 [kg/m^3]	flow law	η_0 (Pa^n * s)	E_a [kJ/mol]	n	V_a [J/bar/mol]	C [MPa]	sin(ϕdry)
sediments	2600	wet quartzite	$1.97 * 10^{17}$	$1.54 * 10^5$	2.3	0.8	10	0.15
upper continental crust	2700							
upper oceanic crust (basalt)	3000							
melts derived from sediments, upper and lower continental crust	2400	wet quartzite	$5 * 10^{15}$	0	1	0	10	0
lower continental crust	2900	plagioclase (An75)	$4.8 * 10^{22}$	$2.38 * 10^5$	2.3	0.8	10	0.15
lower oceanic crust	3000	plagioclase (An75)	$4.8 * 10^{22}$	$2.38 * 10^5$	3.2	0.8	10	0.6
melt derived from subducted oceanic crust	2900	wet quartzite	$1 * 10^{13}$	0	1	0	10	0
Lithosphere/asthenospheric dry mantle	3300	dry olivine	$3.98 * 10^{16}$	$5.32 * 10^5$	3.5	0.8	10	0.6
depleted mantle	3200							
hydrated mantle and weak initial shear zone	3200	wet olivine	$5.01 * 10^{20}$	$4.70 * 10^5$	4	0.8	10	0.1
serpentinized mantle	3000							
melt derived from wet peridotite	2900	wet olivine	$1 * 10^{13}$	0	1	0	10	0

Table 3.3: Summary of all performed numerical experiments.

ocean length	400 km	800 km	400 km	400 km	400 km	400 km	400 km	400 km
age of oceanic lithosphere/convergence rate	5 cm/yr (lower plate)	5 cm/yr (lower plate)	5 cm/yr (lower plate)	5 cm/yr (lower plate)	5 cm/yr (lower plate) + 3 cm/yr (upper plate)	symmetric convergence, 2.5 cm/yr	2.5 cm/yr (lower plate)	7.5 cm/yr (lower plate)
20 Ma	sofi							
40 Ma	sofa							
60 Ma	sofb							
80 Ma	sofc	vicc	ijac	spfc	migc	symd	slac	dorc
100 Ma	sofd							
120 Ma	sofe							
duration of the push	until collision	until 400 km of ocean was consumed	until collision	until collision	until 400 km of ocean was consumed	until collision	until collision	until collision
continental crust	mix mode *	mix mode *	weak *	strong *	mix mode *	mix mode *	mix mode *	mix mode *

mix mode * - upper (wet quartzite) and lower (An75_Ranalli 1995) crust
weak * - upper and lower crust (wet quartzite)
strong * - upper and lower crust (An75_Ranalli 1995)

3.3. Results

We performed a series of numerical experiments (Table 3·3) to investigate the dynamics and physical controls of magmatism during subduction and subsequent collision. We first describe a reference model that exhibits patterns of magma migration and compositional changes. This is followed by a parametric study, in which we analyse the influence of varies rheologies, thermal slab ages, ocean sizes and convergence rates.

3.3.1. Reference model

The reference model (sofc, Table 3·3, Fig. 3·2) contains a compositionally and rheologically layered continental crust: weak felsic upper crust (wet quartzite) and strong mafic lower crust (plagioclase), which results in low coupling at their interface (Fig. 3·1b2). In this model, the initial ocean is 400 km wide and has a thermal age of 80 Ma. The lower plate is pushed with 5cm/year towards the upper plate, which remains fixed. The results show a complex spatial and temporal pattern of compositionally variable magmatic sources activated during oceanic subduction, continental collision and after slab detachment (Figs. 3.2 and 3.3).

At the onset of oceanic subduction (< 3 My) partial melting of the subducting slab forms adakites within the upper plate (sensu Defant and Drummond, 1990; Durmmond et al., 1996). After 5 My, the oceanic lithosphere releases volatiles and hydrates the overlying mantle wedge as it sinks deeper into the mantle. The addition of volatiles at depths of ~100 km triggers fluid-fluxed melting of hydrated peridotite in the mantle wedge, which is also associated with melting of the subducted oceanic crust (Figs. 3·2a and 3·3, stage 1). These melts penetrate the overriding plate and form flattened plutons at the transition between the lower and upper continental crust and/or by building a volcanic arc at the surface. In our reference model the magmatic arc is observed in the upper plate at ~250 km distance from the trench (position 1 in Fig. 3.2a). The continuous generation and propagation of melts weakens the overlying continental lithosphere, which results in localized extension and subsidence. The total magmatic addition rate during this phase equals to 35 km^3/km/My.

The closure of the ocean at 8 My is followed by continental subduction of the lower plate (Fig. 3.2c), driven by the pull of the slab before slab break-off which ceases subduction at 32 My. Rheological decoupling between the upper and lower continental crust activates a basal decollement at their interface. This decollement facilitates the incorporation of most of the upper crust of the lower plate into the orogenic wedge by a sequence of foreland propagating thrusts (such thrusts migrate towards the left in Fig. 3.2c). The lower crust of the lower plate remains coupled to its mantle lithosphere and, therefore, subducts beneath the upper plate. Slivers of upper crust (thin light-grey stripes in Figs. 3.2c) are dragged into the subduction channel along with sediments from the accretionary wedge and may reach mantle depths of up to 120 km. These slivers are incorporated into a mélange that includes parts of oceanic crust and serpentinized and hydrated mantle.

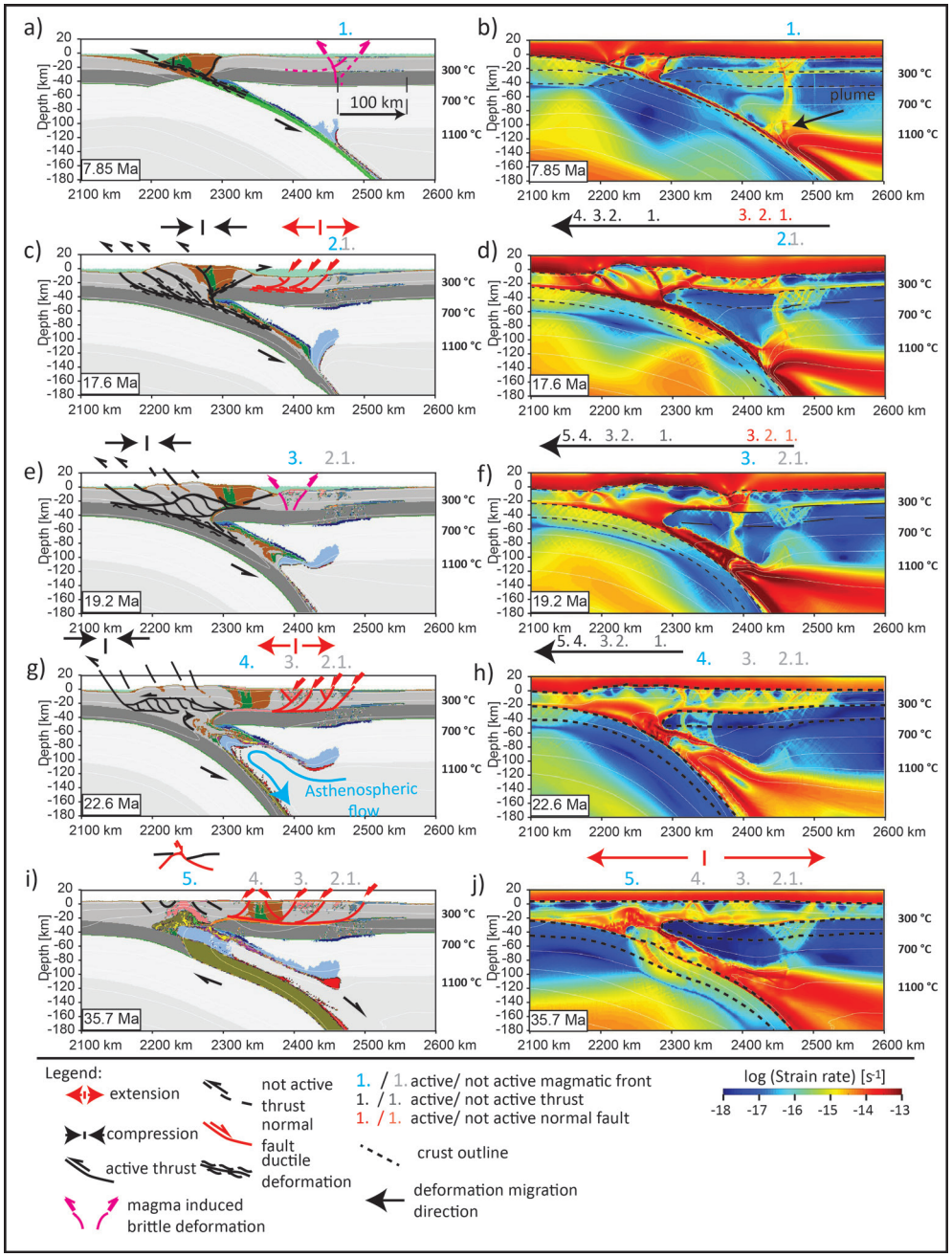

Figure 3.2: Evolution of the reference model (sofc, Table 3.2). The left and right column represent composition and strain rate, respectively. a, b) the first magmatic stage forms by partial melting of wet peridotite during oceanic subduction; c) the second magmatic stage forms during continental subduction and is located 20 km trenchward from the first magmatic arc; d) contemporaneous shortening in the foreland and extension in the hinterland; e,f) the third magmatic stage is syncontractional and forms by partial melting in

Figure 3.2 (continued): subduction channel; g) the fourth magmatic stage represents the most felsic magma end-member during continental collision, associated with extension in the hinterland during relamination; h) foreland propagating deformation front; i) the fifth magmatic stage during overall extension driven by eduction; j) eduction triggers exhumation of mid-crustal rocks to the surface along low-angle detachments. Thick black arrows highlight the sense of shear on the subduction plane. See Fig. 3.1 for colour (material) description.

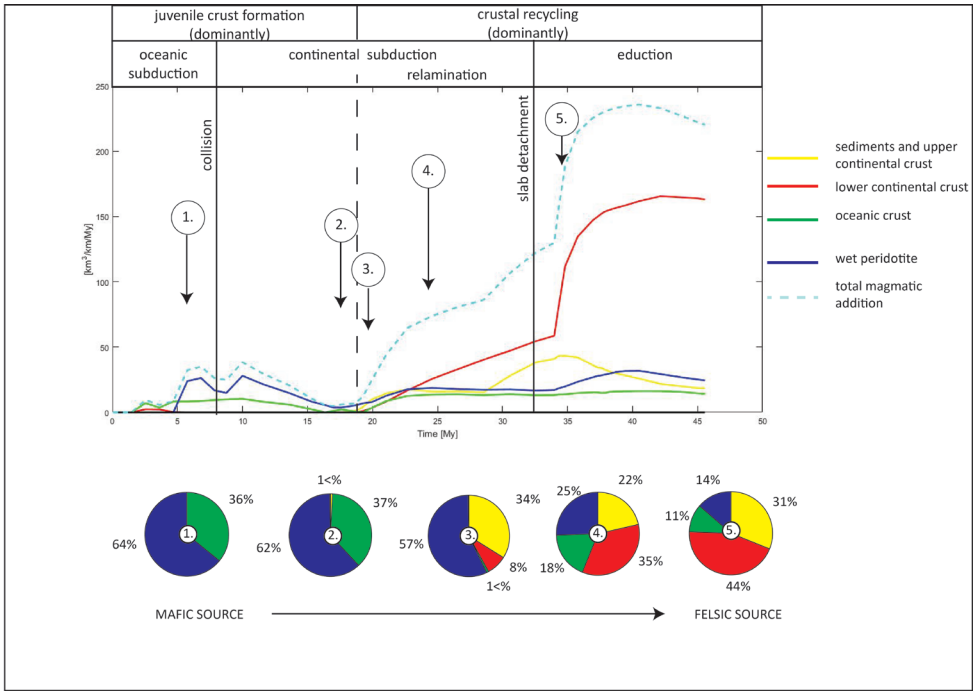

Figure 3.3: Source variability and magmatic addition rates for the reference model. Note that 1 to 5 represent the magmatic stages described in Fig. 3.2, from oldest to youngest.

In the hinterland of the upper plate (right side of Fig. 3.2c), extension is localized along large scale listric normal faults that are rooted in a basal décollement at the transition between the upper and lower continental crust. The activation of normal faults migrates gradually towards the foreland (to the left in Fig. 3.2c). Interestingly, the lower crust of the upper plate remains relatively little deformed. The difference in shortening between the upper and lower crust results in lower crustal indentation of the orogenic wedge, composed of the oceanic suture, accretionary wedge and upper crust. Consequently, the orogenic wedge is pushed over a significant distance towards the hinterland (to the right in Fig. 3.2c-g). This creates a gradual shift between the former suture created during oceanic subduction and the currently active continental subduction zone that increases with time (Figs. 3.2c,e,g). Because of its positive buoyancy and low viscosity, the mélange moves upwards along the subduction channel, and relaminates (sensu

Hacker et al., 2011) the base of the crust at the core of the orogen at around 18 My (~40 km depth, Figs. 3.2c,e,g). At the same time, the lower plate detaches from the mantle lithosphere of the upper plate, which results in slab steepening and asthenospheric upwelling. The asthenospheric upwelling is initially associated with partial melting of wet peridotite, resulting in the creation of small volumes of basaltic melt. These melts are emplaced in the upper plate using normal faults as transport pathways (position 2, Figs. 3.2c and 3.3). The large temperature contrast between the subducted crust and hot asthenosphere causes partial melting of the rock melange in the subduction channel and the lower continental crust. The resulting felsic melts are emplaced in the hinterland of the upper plate ~120 km away from the tip of the lower crust indentor (position 3 in Fig. 3.2e). During this continental subduction stage melting occurs from three compositionally different components: a decreasing proportion of wet peridotite (57% to 25%), an increasing proportion of lower continental crust (8% to 35%) and slightly increasing proportion of rock mélange (cumulative sediments, upper continental crust, oceanic crust, 35% to 40%) sources (positions 3 and 4 and stages 3 and 4 in Figs. 3.2e,g and 3.3). During later collisional stages, the back-arc hinterland of the upper plate records shortening. Reverse faults and folds are formed that act as magma transport pathways (Fig. 3.2e). The continuation of subduction brings more continental material into the subduction channel, generating melts that are increasingly more felsic (position 4 in Figs. 3.2g and 3.3). At this stage, the deformation in the back-arc of the upper plate changes from compression to extension. Normal faults are formed allowing for magma transport and emplacement (Fig. 3.2g).

Finally, slab detachment separates the oceanic and continental part of the slab at 33 My. Slab detachment is followed by exhumation of the lower plate by reversing the motion of the subduction plane (i.e. by eduction, sensu lato Andresen et al., 1991, Fig. 3.2i). Slab detachment combined with exhumation and partial melting of large parts of the lower continental crust induce a decrease in the slab dip. Eduction uplifts the previously relaminated mélange and reactivates the former thrusts as low-angle normal faults or detachments. These structures exhume upper crustal material from depths of ~15-20 km and temperatures of T=500°C-550°C (position 5 in Fig. 3.2i). The exhumation is associated with partial melting of the upper continental crust and emplacement of felsic melts (stage 5 in Fig. 3.3). Furthermore, low-angle normal faults or detachments are used as magma transport pathways, resulting in the formation of either core-complexes or extensional domes (e.g., Tirel et al., 2004, position 5 in Fig. 3.2i).

3.3.2. The influence of rheological stratification of the continental crust

The rheological stratification of the continental lithosphere has a fundamental impact on the kinematics, evolution and geometry of continental collision. Starting from the reference model, two extreme scenarios were performed. First, (Fig. 3.4a-c) we consider the collision of weak continental plates. The entire crust has a wet quartzite rheology in this experiment (Figs. 1b1, 3.4a-b and Table 3.3). Second, we examine the collision of two strong continental plates. In this experiment the entire crust has a plagioclase rheology (Figs. 3.1b3, 3.4d-f and Table 3.3). Although the occurrence of such homogeneous crustal profiles

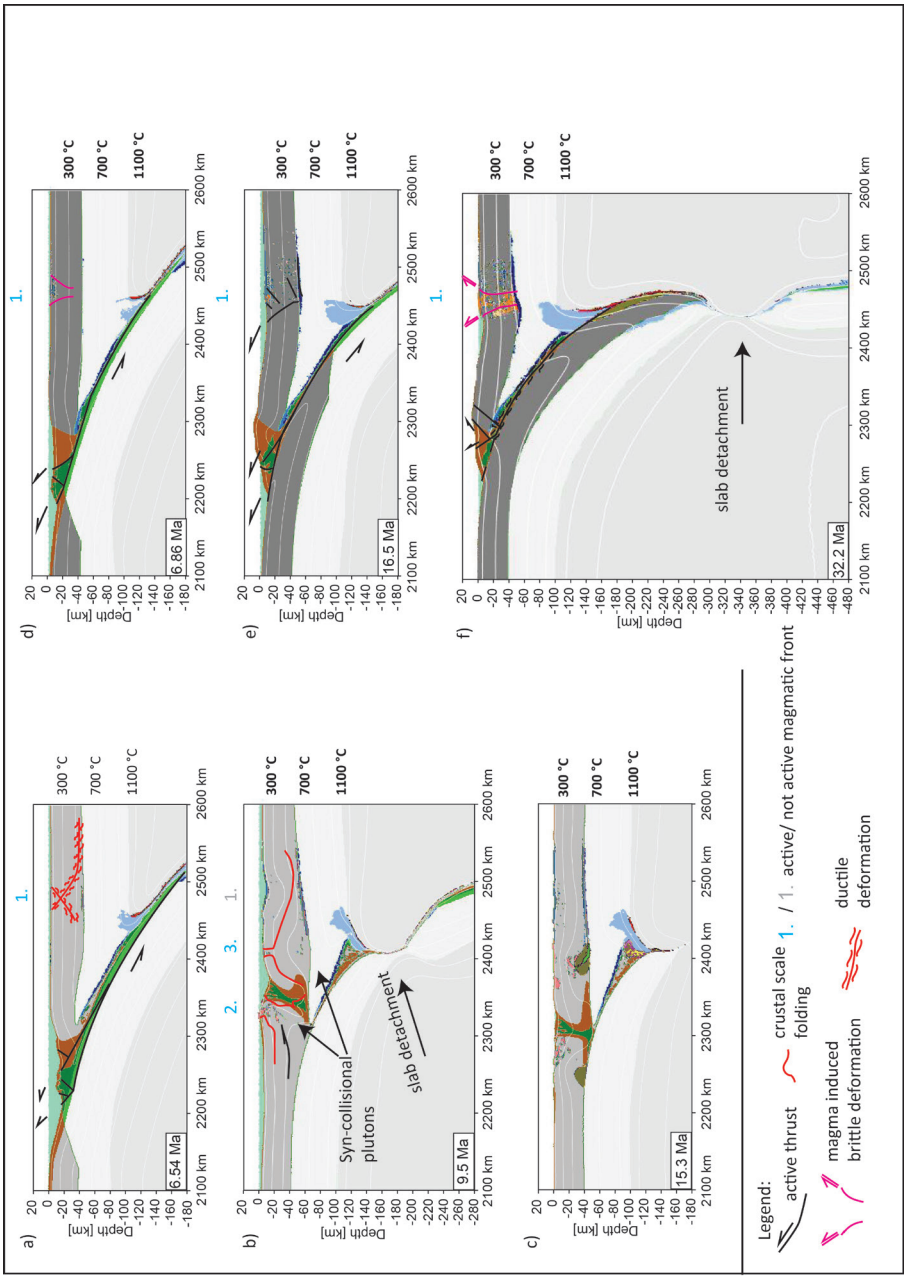

Figure 3.4: Evolution of the rheologically weakest (ijac, a-c) and strongest (spfc, d-f) end-member. a) formation of the first magmatic arc during oceanic subduction; b) intrusion of melts derived from partial melting of the subducted melange during crustal scale folding; c) isostatic rebound after slab detachment followed by partial melting of the lower crust; d) flux melting during oceanic subduction forms a magmatic arc; e) during continental subduction the magmatic front remains fixed; f) partial melting of the subducted slab following slab detachment. See Fig. 3.1 for color (material) description.

is unlikely in nature, we consider these scenarios suitable for illustrating extreme collisional geometries and associated magmatism. In both cases, parts of the upper oceanic crust and accretionary wedge sediments are incorporated into the subduction channel during oceanic subduction (Fig. 3.4a,d). Magmatism results in minor amounts of extension in the hinterland of the upper plate and melt production is restricted to fluid-fluxed melting of the hydrated mantle wedge, similar to the reference model. In the weak-rheology scenario these melts form intrusions at the base of the crust and extrusions at the surface. In the strong-rheology scenario intra-crustal intrusions and surface extrusions are formed instead (position 1 in Figs. 3.4a and 3.4d, respectively).

In the weak-rheology scenario, collision is characterized by decoupling of crust and mantle (Fig. 3.1b1). Only minor amounts of crust and sediment from the accretionary prism are transported into the subduction channel. Thickening of the entire crust accommodates crustal shortening and no continental subduction is recorded (Fig. 3.4b). Slab detachment at the transition between continental and oceanic lithosphere at depths of ~160 km occurs shortly after the onset of collision (~1.5 My) (Fig. 3.4b) and is followed by isostatic rebound (Fig 3.4c). Melting of wet peridotite, subducted melange and crust of the lower plate creates dominantly felsic magmas that are emplaced as intrusions and extrusions in the core of the thickened orogen and in its frontal parts (positions 2 and 3, Fig. 3.4b). The continued orogenic thickening is associated with a gradual increase in temperatures at the base of the crust, triggering additional melting at the base of the crust (position 4, Fig. 3.4c).

In contrast, collision of two strong continental plates results in large amounts of continental subduction due to the large degree of rheological coupling. This creates large volumes of crust-derived melts that are emplaced roughly in the same position when compared with magmas formed during oceanic subduction (Fig. 3.4e,f). Subsequent continental subduction continues until slab detachment ceases convergence at ~32 My. The slab detaches at the transition between continental and oceanic lithosphere at depths of ~300 km (Fig. 3.4f).

3.3.3. The influence of the ocean size and thermotectonic age, and the convergence velocity

We have performed an additional experiment in which the width of the ocean was enlarged (800 km). All other parameters were kept the same when compared to the reference model (Fig. 3.5 and Table 3.3). Deformation geometries, magmatic sources and migration patterns of the magmatic source region are comparable to the reference model (Fig. 3.5). However, a wider ocean increases the slab-pull force and drags the subducted continental lithosphere to larger depths. Consequently, slab detachment occurs earlier at ~22 My and at greater depth (~450 km) when compared with the reference model (Fig. 3.5c). One of the important factors observed to control the kinematics of subduction is the thermal age of the subducting oceanic lithosphere. Starting from the reference model (i.e. thermal age of 80 Ma), we have tested three other scenarios: two with younger (20 and 40 Ma) and one with an older (120 Ma) oceanic plate age (Figs. 3.6a,b,c). In the first scenario no continental subduction is recorded and no deformation

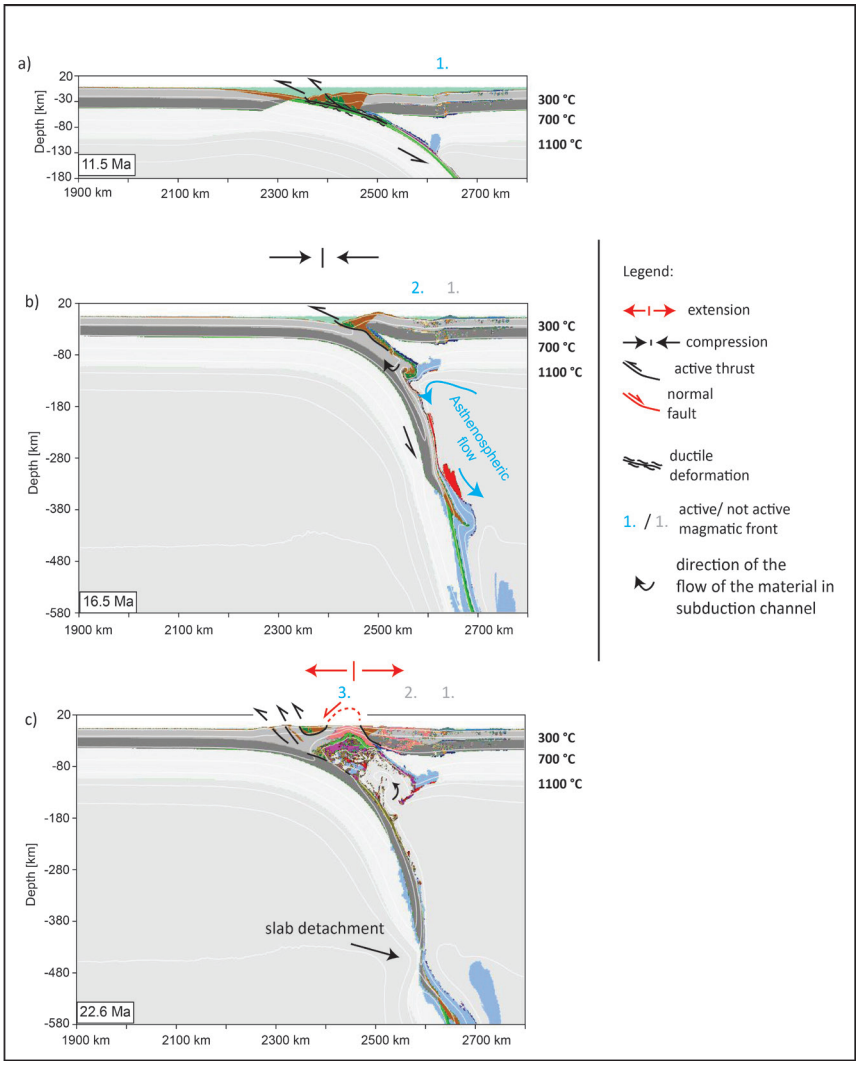

Figure 3.5: Evolution in the 800 km wide ocean setting. a) Partial melting of wet peridotite forms the first magmatic arc during oceanic subduction; b) partial melting of the subducted melange forms second magmatic arc; c) reactivation of former thrusts as asymmetric low-angle detachments and exhumation of syn-kinematic magmatic bodies. See Fig. 3.1 for color (material) description.

is observed after the closure of the ocean ("arrested" orogen, sensu Ueda et al., 2012). Subduction terminates because of the insignificant slab pull. Melting of wet peridotite and partial melting of the subducting slab forms magmas in the hinterland of the upper plate ~220 km away from the trench. Subduction of slightly older slabs (40 Ma Fig. 3.6b), on the other hand, enables continental subduction, generating melts in a position closer to the trench (position 2 in Fig. 3.6b).

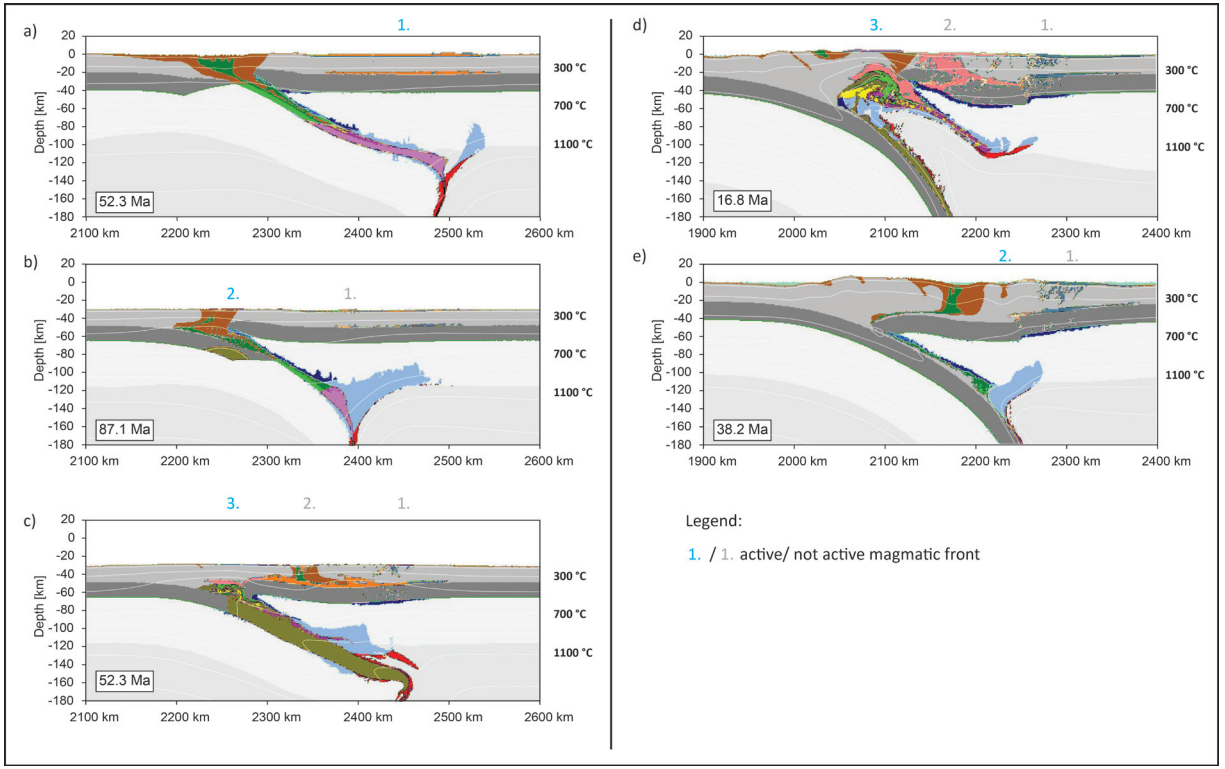

Figure 3.6: Variations in lithospheric cooling age (a-c) and convergence rate (d-f); a) Partial melting of hot and young oceanic lithosphere forms a magmatic arc (20 Ma, sofi); b) second magmatic stage caused by partial melting of the lower crust (40 Ma, sofa); c) three stage magmatic evolution without exhumation of syn-kinematic magmatic bodies for old slabs (120 Ma, sofe); d) step-wise migration of the magmatic arc towards the lower plate (migc, asymmetric convergence, 8 cm/yr (lower plate), 3 cm/yr (upper plate); e) syn-contractional magmatism formed during second magmatic phase (symd, symmetric convergence, 2,5 cm/yr). See Fig. 3.1 for color (material) description.

Subduction of older lithosphere (120 Ma Fig. 3.6c) results in similar collisional and magmatic patterns when compared to the reference model. It also records indentation of the orogenic wedge by the lower crust of the upper plate as described for the reference model. Indentation of the orogenic wedge results in subduction zone and magma source migration. However, much larger amounts of melt are released when compared to the reference model, particularly during the late collisional stage. These melts are emplaced dominantly in the upper plate, at the base of the upper crust (Fig. 3.6c).

The effects of the convergence velocity were tested in two models. In a first model the upper and lower plate converge with 3 cm/yr and 5 cm/yr, respectively. This model shows a shallow dipping subduction zone during oceanic subduction and no significant lower crustal indentation. During continental subduction, the model is characterized by a low degree of coupling between the lower and upper plate, which ultimately leads to more pronounced slab steepening, larger asthenospheric uprise and the formation of larger volumes of melt when compared to the reference model. These melts are emplaced in the upper plate and the magmatic front gradually migrates towards the foreland with time (Fig. 3.6d). The final geometry is similar to the one obtained by subduction of a wider ocean (compare with Fig. 3.5c). The second model assumes symmetric convergence velocities of 2.5 cm/y (Fig. 3.6e). The model shows indentation of the orogenic wedge by the lower crust of the upper plate during collision. Consequently, significant amounts of shortening are recorded in the upper plate and a gradually increasing shift between the slab and the position of the former oceanic suture zone is observed. The observed magmatism is related to fluid-fluxed melting during oceanic subduction and relamination during continental subduction.

3.4. Discussion

Our results confirm that continental subduction in collisional settings is driven by the rheological coupling between lower crust and mantle lithosphere, as suggested by previous studies (e.g., Burov and Yamato, 2008; Vogt et al., 2017). In contrast, rheological decoupling between crust and mantle lithosphere leads to crustal accretion (e.g., Vogt et al., 2017). Our reference model shows that a compositionally layered lithosphere creates a mixed collisional mode, in which the upper crust is accreted to form a collisional orogen, while the lower crust is subducted. The resulting orogen is characterized by a sequence of outward propagating thrusts in the orogenic foreland and low-offset extensional (listric) normal faults in the hinterland of the upper plate. The localisation of extension is driven by magma emplacement in multiple episodes (see also Gerya and Meilick, 2011; Vogt et al., 2012). The depth to which the lower crust is subducted depends on the thermal age of the oceanic lithosphere and on the convergence velocity (see also Duretz et al., 2011). The older the slab or the higher its subduction velocity, the greater is the depth of subduction (Duretz, 2011). Deep subduction of the lower crust leads to slab steepening and slab retreat.

Indentation of the orogenic wedge by the lower crust of the upper plate transports crustal material towards the hinterland (Fig. 3.2c,e,g,i) and creates an

increasing shift between the position of the suture zone and the slab, together with its associated deformation and magmatism. In most of our experiments, magma migrates towards the foreland with respect to the former suture zone. Only in situations in which very young oceanic lithosphere is subducted, or collision of unusually strong and coupled continental lithosphere takes place a fixed magmatic arc is observed (Figs. 6a and 4d-f). The link between magma migration and slab retreat relative to the positions of the suture zone has been inferred for many Mediterranean orogens such as the Aegean, Apennines or Dinarides (e.g., Schefer et al., 2011; Menant et al., 2016a).

The overall magmatic evolution suggested by our models is in agreement with existing numerical modelling and observational studies (e.g., Defant and Drummond, 1990; Vogt et al., 2012). In more detail, migration of magmatism and deformation towards the orogenic foreland is driven initially by the indentation of the lower continental crust in models with a compositionally layered continental lithosphere. Slab retreat is a mechanism observed at later stages of collision and is mostly driven by relamination and eduction (Fig. 3.2g,i). The migration of magmatism is accompanied by compositional changes that are controlled by melting of different sources, which vary from simple mafic (wet peridotite and oceanic crust) during oceanic subduction, to complex combinations (wet peridotite, oceanic crust, subducted mélange and lower continental crust) during continental subduction and, ultimately, to a dominantly felsic source (upper crustal material) during eduction (Fig. 3.3). In contrast, the formation of adakite-like magmas is inferred for collisional areas where young and hot slabs were consumed (20-40 My, Fig. 3.6a, b).

3.4.1. Variability of the magmatic source during continental subduction and exhumation

Magma production is dominated by partial melting of wet peridotite at early stages of subduction and remains active during later stages of collision, but with gradually decreasing contributions in the overall magmatic budget (Fig. 3.3). Subduction of continental crust involves its partial melting and separation of melts into a mafic residue and a felsic fraction (e.g., Jull and Kelemen, 2001; Kelemen et al., 2003). Driven by its intrinsic buoyancy, this felsic fraction may relaminate to the base of the crust (Hacker et al., 2011). In our models, partial melting of the subducted mélange and lower continental crust becomes progressively more important once relamination is triggered. This relamination is driven by the interaction between the asthenospheric mantle and the mélange in the subduction channel. The buoyant upraise of material from the subducted mélange along the subduction channel stops at the base of the orogen at ~40 km depth. This allows for the emplacement of dominantly felsic magma over a large area (Fig. 3.2g and i).

Mixtures of wet peridotite, sediment, and other crustal rocks have been generally suggested to explain the source variability of post-collisional (ultrapotassic to calc-alkaline) magmatism in the Mediterranean domain and in Tibet, mostly based on geochemical and isotopic signatures (e.g., Conticelli et al., 2011; Prelević et al., 2013; Zhengfu Guo et al., 2014). In addition, field and geochemical studies

of collisional granitoids in many orogens suggest that these rocks are derived from metaluminious magmas originated from partial melting of mafic lower continental crust (e.g., Christofides et al., 2007).

After slab detachment, the sense of shear along inherited thrust contacts is reversed triggering extension by the formation of major low-angle normal faults or detachments reactivating the former subduction zone or other pre-existing nappe contacts. Footwall exhumation along these structures brings felsic magma from mid-crustal levels to higher structural positions. Coeval decompressional melting of dominantly crustal material produces peraluminious felsic magmas that are emplaced as syn-kinematic granites or extensional gneiss domes, such as inferred for the Aegean domain during the migration of subduction and back-arc extension (e.g., Tirel et al., 2004; Brun and Faccenna, 2007; Dilek and Altunkaynak, 2009). In our models, slab detachment and shear reversal of the subduction plane are not directly responsible for exhumation of the rocks along the subduction channel (see also Duretz et al., 2012; Duretz and Gerya, 2013). Here the exhumation of rocks starts earlier by buoyant rise of material towards the surface in the subduction channel (see also Burov et al., 2001). In other words, we observe a two-stage uplift of material from the subduction channel. At first, relamination uplifts the subducted melange from depths of ~120km to the base of the orogen (40 km). Subsequent shear reversal transports this material from the base of the orogen to middle crustal levels. This process has been also suggested for the exhumation of UHP-HP terranes, such as in the Western Gneiss Region of Norway (e.g., Liou et al., 1996; Ota et al., 2000).

3.4.2. The Dinarides Mountains: an example of migration of magmatism in orogens

The Dinarides Mountains (Fig. 3.7a) formed during the late Mesozoic - earliest Cenozoic closure of the Neotethys Ocean and subsequent continental collision between Europe and Adria (e.g., Dimitrijević, 1997; Karamata, 2006; Schmid et al., 2008). This evolution was followed by the Miocene extension of the Pannonian Basin and its subsequent latest Miocene – Quaternary inversion

Figure 3.7 (facing page): Interpretative tectono-magmatic evolution of the Dinarides based on our study and petrological-geochemical results (Cvetković et al., 2013 and references therein). a) tectonic map of the Alpine-Carpathian-Dinaridic system (simplified after Schmid et al., 2008). Black thick line (A-B) represents the location of the reconstructed profile; b) production of calc-alkaline magmas in typical continental arc setting during oceanic subduction in the Late Cretaceous ; c) monogenic alkaline magmas resulted from partial melting of a metasomatised lithospheric mantle during continental subduction in the (latest Cretaceous?)-Paleogene; d) magma production is driven by partial melting of multiple sources (wet peridotite, subducted melange and lower continental crust) in the subduction channel during relamination in the Eocene – Oligocene; e) generation of magmas produced by multiple sources due to relamination during continental subduction, and subsequent formation of syn-kinematic peraluminious magmas triggered by eduction during the Miocene; f) present day profile. Note that patterns of magmatic bodies reflect different magma sources and not the petrology of crystallized rocks.

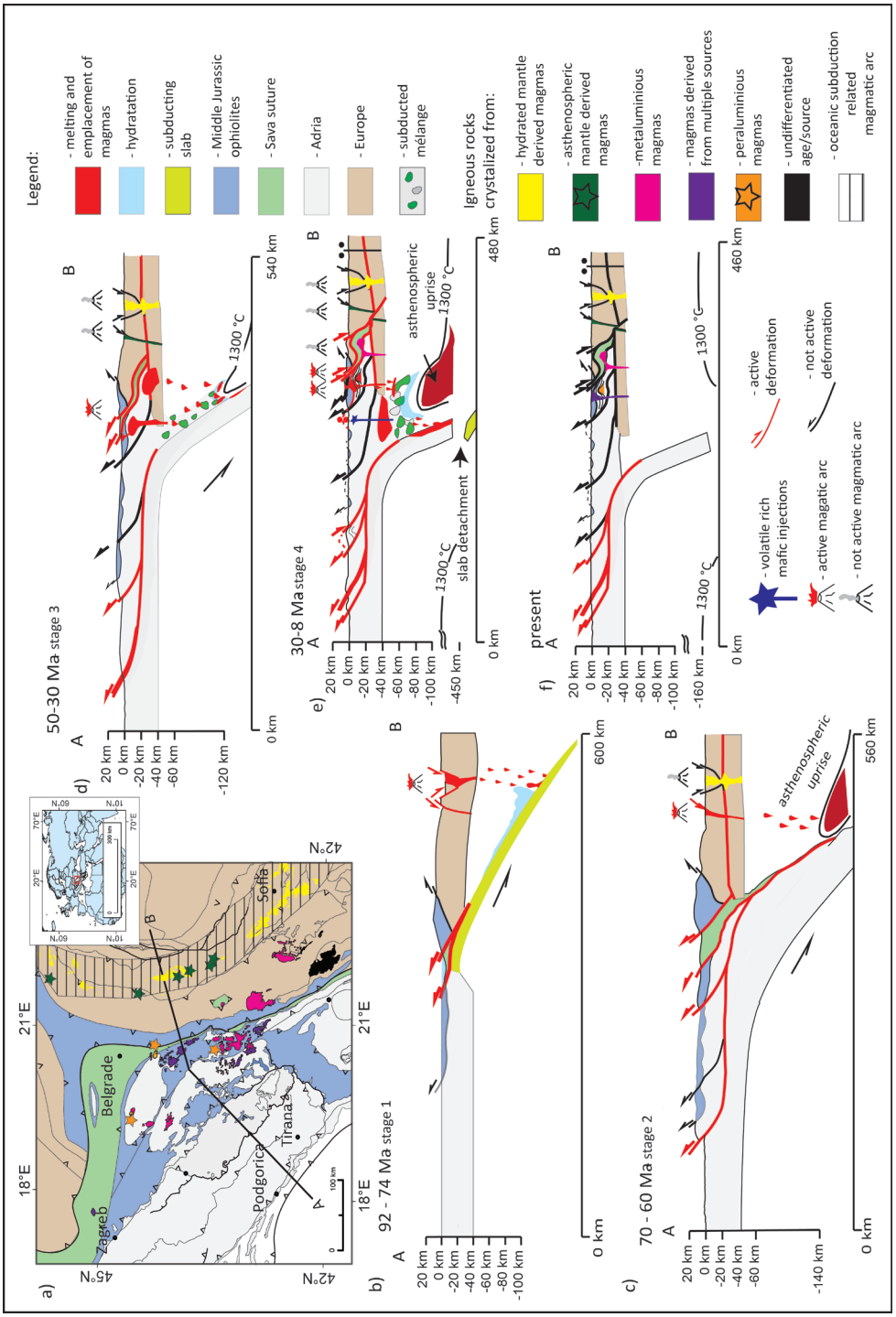
Legend:
- melting and emplacement of magmas
- hydratation
- subducting slab
- Middle Jurassic ophiolites
- Sava suture
- Adria
- Europe
- subducted mélange
Igneous rocks crystallized from:
- hydrated mantle derived magmas
- asthenospheric mantle derived magmas
-metaluminious magmas
- magmas derived from multiple sources
- peraluminious magmas
- undifferentiated age/source
- oceanic subduction related magmatic arc
- volatile rich mafic injections
- active magatic arc
- not active magmatic arc
- active deformation
- not active deformation
a)
18°E
21°E
45°N
42°N
Belgrade
Zagreb
Podgorica
Tirana
Sofia
b)
92 - 74 Ma stage 1
c)
70 - 60 Ma stage 2
d)
50-30 Ma stage 3
e)
30-8 Ma stage 4
f)
present
1300 °C
slab detachment
asthenospheric uprise

(Horváth and Cloetingh, 1995), which modified the initial thrusting geometry of the Dinarides units (e.g., Matenco and Radivojević, 2012; Balázs et al., 2016). The tectonic evolution of the Dinarides was associated with significant magmatism that occurred in several successive stages during late Cretaceous-Miocene times (Cvetković et al., 2013). These stages are generally organized in lineaments roughly parallel with the strike of the orogen and show an overall trend of increasing crustal input towards the orogenic foreland (e.g., von Quadt et al., 2003; Cvetković et al., 2013; Gallhofer et al., 2015). These general observations bear strong similarities with the inferences of our study.

In more detail, oceanic subduction created the first stage of Late Cretaceous (~92-67 Ma) magmatism that is observed in the Apuseni - Banat - Timok - Srednogorie (ABTS) belt, located in the hinterland of the Dinarides orogen (e.g., von Quadt et al., 2005; Gallhofer et al., 2015). This stage produced calc-alkaline rocks with a subordinate adakite-like geochemical signature formed by partial melting of wet peridotite in the mantle wedge (e.g., von Quadt et al., 2002; Kolb et al., 2013, Fig. 3.7b). A general foreland age progression is inferred across ~100km, which is interpreted as the result of either oblique subduction or slab retreat (e.g., von Quadt et al., 2005; Kolb et al., 2013; Gallhofer et al., 2015). Field studies have demonstrated a genetic link between magmatic emplacement and the formation of local extensional/transtensional basins/structures, where extrusive and intrusive magmas were emplaced or re-deposited. This is particularly clear in the Timok and Srednogorie sectors of the ABTS belt (e.g., Georgiev et al., 2009; Naydenov et al., 2013). There are no quantitative studies on the amounts of Late Cretaceous extension in these Timok - Srednogorie sectors, but the overall stretching appears to be minor at the orogenic scale. The character of this magmatism and its kinematic relationships are comparable with the initial formation of a stable magmatic arc in our models, where such an arc forms by melting of wet peridotite and subordinate oceanic crust during early stages of oceanic subduction (Fig. 3.2a). The weakening effect of magma transport and emplacement triggers extension. Subsequent magmas are emplaced beneath or in the overlying (half-) grabens. Therefore, our model infers that slab-retreat is not required to create the observed Late Cretaceous extension and magma migration patterns in the Dinarides. Furthermore, generic back-arc extension driven by slab retreat was shown to affect the hinterland of magmatic arcs, not the magmatic arc itself (e.g., Uyeda and Kanamori, 1979; Dewey, 1980). In other words, all these observations and modelling results suggest that although slab retreat could have taken place during Late Cretaceous times, it is not intrinsically required by the observed relationship between magmatism and tectonics in the hinterland of the Dinarides.

The final closure of the Neotethys Ocean likely took place during latest Cretaceous - earliest Paleogene times by the creation of an oceanic suture zone (~65 Ma, Sava Zone, e.g., Pamić, 2002; Schmid et al., 2008; Ustaszewski et al., 2010). The convergence continued during Paleogene times, although its kinematic effects and amplitude of deformation in the internal Dinarides are not fully understood (e.g., Matenco and Radivojević, 2012; Stojadinović et al., 2017). At first, the deformation was coeval with the emplacement of a second stage of short-lived latest Cretaceous – earliest Palaeocene (~70-65 Ma) monogenetic mafic alkaline volcanic and subvolcanic bodies. These bodies were emplaced over or intruded into the upper

plate mostly along pre-existing fractures formed during localized extension (Fig. 3.7c, e.g., Tschegg et al., 2010; Cvetković et al., 2013). Xenoliths found in these magmatic rocks suggest lithospheric temperatures of ~1000°C (e.g., Cvetković et al., 2004b, 2007a). This magmatism was shown to have formed by partial melting of hydrous mantle (Cvetković et al., 2010), interpreted as a subduction free source similar to the source of the European Cenozoic anorogenic provinces (e.g., Lustrino and Wilson, 2006; Cvetković et al., 2007a). These observations are in general agreement with our modelling predictions, where melting of wet peridotite in the mantle wedge at temperatures of more than 1000°C continued to produce small volumes of magma (Fig. 3.7c).

Continued shortening during Eocene-Oligocene times is interpreted as a foreland propagation of thrusting and out-of-sequence reactivations in the external and internal Dinarides, respectively (e.g., Ustaszewski et al., 2010; Andrić et al., 2017; Stojadinović et al., 2017). A gradual switch from contraction to extension took place during Oligocene times in areas situated in the vicinity of the Sava suture zone (Erak et al., 2017; Stojadinović et al., 2017). In the same area, the character of deformation is mirrored by the magmatic evolution that recorded a third stage of coeval magmatic emplacement located more to the foreland when compared with the earlier Late Cretaceous - Palaeocene magmatism (Fig. 3.7d). This Eocene - Oligocene magmatism was emplaced as dominantly medium- to high- potassic calc-alkaline plutons and their extrusive equivalents derived from I-type metaluminious granitoid magmas (e.g., Cvetković et al., 2007b). The elevated contents of large ion lithophille elements, low Sr-Nd isotope ratios together with rare earth element patterns suggest a source located in the uppermost mantle or lower crust (e.g., Cvetković et al., 2007b; Schefer et al., 2011). The larger volumes of predominantly acid to intermediate rocks are associated with lower amounts of volcanic and sub-volcanic potassic to ultra-potassic rocks with mafic to even ultramafic compositions. They are thought to be derived from a source composed of depleted peridotite and terrigenous trench sediments accreted beneath the lithosphere of the upper plate (Prelević et al., 2005; 2013), possibly related to slab roll-back (Schefer et al., 2011). These observations are in agreement with our reference model, which predicts the migration of deformation and magmatism towards the foreland with respect to the suture zone before the onset of slab detachment. Here magmatism is triggered by relamination of crustal material to the base of the orogen and partial melting of wet peridotite, tectonic mélange and lower continental crust in the subduction channel (Figs. 3.2d-g).

The Miocene extension reactivated inherited nappe contacts, which led to exhumation of material from mid-crustal levels in the footwall of detachments or low-angle normal faults. This is well observed in large areas in the Dinarides, but with larger offsets in their internal part and neighbouring southern Pannonian Basin, in particular along the pre-existing Sava suture zone (e.g., Ustaszewski et al., 2010; Stojadinović et al., 2017). The exhumation induced decompressional melting and the formation of peraluminous magmas (Fig. 3.7e, e.g., Cvetković et al., 2007a; Schefer et al., 2011). Small volumes of magmatic bodies occurring only in the internal Dinarides characterized this Miocene extension-related magmatic stage. Our modelling demonstrates that the widespread Miocene extension was associated with the emplacement of dominantly felsic melts from the upper

crust (Figs. 3.2i and 3.7e) and the rheological weakening created during previous magmatic stages.

The kinematic and magmatic observations in the Dinarides show that in the Oligocene deformation changed gradually from contraction to extension over ~8 My. Our modelling shows that this gradual change could be controlled by progressive slab detachment, resulting in a change from Eocene relamination and contraction to Miocene eduction and extension. The extension observed near the Sava Zone (sensu Matenco and Radivojević, 2012) has started ~28-29 Ma (Toljić et al., 2013; Erak et al., 2017). When combined with the predictions of our modelling, this imposes that the overall Oligocene - Miocene orogenic extension took place during and after the slab-detachment in the Dinarides.

The Miocene extension was followed by the latest Miocene - Quaternary indentation of Adria. Seismicity, teleseismic tomography, potential field data and active seismic experiments show a present foreland shift of 100 km between the position of the Sava suture zone and the present-day location of the Dinarides slab (Fig. 3.7f, e.g., Bennett et al., 2008; Šumanović and Dudjak, 2016), which is compatible with our model geometry (Fig. 3.2i). Such shifts and plate configurations are also common in other collisional orogens in the Mediterranean domain (Apennines, Betics-Rif, Carpathians) that show retreating subduction boundaries, steep slabs, back-arc extension and migration of magmatic fronts towards the foreland (Brun and Faccenna, 2008; Faccenna et al., 2014; Matenco et al., 2016). Our modelling shows that these shifts can result from a combination of lower crustal indentation followed by slab retreat, relamination and eduction (Figs. 3.2 and 3.7). This novel explanation for the commonly observed shift between the location of the oceanic suture and the position of the slab detected by teleseismic tomography sheds new light on the geodynamic evolution of these Mediterranean orogens.

3.5. Conclusions

We investigated numerically an intimate link between the generation of magmatism, and the kinematics, rheology, geometry and tectonic evolution of orogens during subduction and subsequent collision. Our results suggest that the rheological and compositional layering of the crust imposes a key control on the distribution of magmatic rocks.

We showed that magmatic weakening of the upper plate focuses deformation during subduction and subsequent collision. The influx of more felsic material during continental subduction creates a gradual change to shallower and more crustal magmatic sources that continuously migrate towards the foreland. This change focuses deformation at gradually more shallow lithospheric levels and results in the emplacement of progressively more felsic magmatic products. Interestingly, changes in the character of deformation are not necessarily related to a migration of the subduction interface. During oceanic subduction and early collision changes between shortening and extension at far distances from the subduction interface are driven by the magmatic emplacement rather than by the migration of the slab. The formation of a typical subduction-related large-scale magmatic arc is not observed in our models, which would likely require the

subduction of larger oceans for longer periods of time. Instead, subduction-related magmatism focusses deformation and results in atypical situations, such as the magmatic emplacement in back-arc extensional (half-) grabens.

During collision we observe migration of deformation, movement of the subduction zone and associated magmatism relative to the outcropping location of the former suture zone formed during oceanic subduction. Existing studies generally show that this gradually increasing shift is created by slab retreat (e.g., Doglioni et al., 2007; Duretz and Gerya, 2013). Our results demonstrate an additional component. During early stages of collision the lower crust of the upper plate indents the orogenic wedge, which increases the shift and enables subduction of lower crust. In other words, continental subduction and orogenic build-up are assisted by lower crustal indentation in the overriding plate. This process also explains the migration of magmatism during early stages of collision. At later stages of collision, other processes such as slab detachment may accompany the slab retreat.

Our simulations provide significant new insights for the understanding of the subduction and collision dynamics in the Dinarides. The key characteristics of the Dinarides, such as the foreland propagating deformation and magma front, and the gradual compositional change towards more felsic magmas is explained in our models by lower crustal indentation, relamination and eduction accompanying oceanic and continental subduction. Magmatism in the Timok or Srednogorie grabens that display rather reduced stretching can also be explained by localisation of deformation and rheological weakening during emplacement and does not necessarily require a period of Late Cretaceous slab retreat. Changes in collisional magmatism observed near the Sava Zone can be explained by a transition to melting in the subduction melange and relamination. We attribute the gradual Oligocene transition in the kinematic and magmatic character from relamination - contraction to eduction - extension by coeval slab detachment in the Dinarides.

Appendix 1

1. Governing equations

All numerical experiments are based on the I2VIS code (e.g Gerya and Yuen, 2003a) which uses finite-difference and the marker-in-cell technique to solve momentum, continuity and heat equations.

Continuity equation (conversion of mass):

$$\frac{\partial v_x}{\partial x} + \frac{\partial v_y}{\partial y} = 0,$$

where x and y are horizontal and vertical coordinates, respectively. The terms ∂v_x and ∂v_y indicate components of the velocity vector.

Momentum equation (2D Stokes) takes form:

$$\frac{\partial \sigma'_{xx}}{\partial x} + \frac{\partial \sigma'_{xy}}{\partial y} = \frac{\partial P}{\partial x},$$

$$\frac{\partial \sigma'_{yx}}{\partial x} + \frac{\partial \sigma'_{yy}}{\partial y} = \frac{\partial P}{\partial y} - g\rho \text{ (T, P, C, M)},$$

where σ'_{xx}, σ'_{xy}, σ'_{yy} are the deviatoric stress tensor components. The density ρ (T, P, C, M) depends on temperature (T), pressure (P), composition (C) and mineralogy (M) and g is the acceleration due to gravity.

Heat conservation equation coupled with mechanical equations (Gerya and Yuen, 2003b):

$$\rho C_p (\frac{\partial T}{\partial t}) = -\frac{\partial q_x}{\partial x} - \frac{\partial q_y}{\partial y} + H_r + H_a + H_s + H_L,$$

$$q_x = -k(\text{P, T, C})\frac{\partial T}{\partial x},$$

$$q_y = -k(\text{P, T, C})\frac{\partial T}{\partial y},$$

where C_p is isobaric heat capacity; q_x and q_y are heat fluxes; k (P, T, C) is thermal conductivity, which is a function of pressure, temperature and composition (see Table 1); H_r is radiogenic heat (see Table 3.1); H_a, H_s, H_L are adiabatic, shear and latent heat components, respectively.

$$H_a = T\alpha \frac{DP}{Dt},$$

$$H_s = \sigma'_{xx}\dot{\varepsilon}_{xx} + \sigma'_{yy}\dot{\varepsilon}_{yy} + 2\sigma'_{xy}\dot{\varepsilon}_{xy},$$

where α is the thermal expansion and $\dot{\varepsilon}_{xx}$, $\dot{\varepsilon}_{yy}$, $\dot{\varepsilon}_{xy}$ are components of the deviatoric strain rate tensor.

1.2. Boundary conditions

All boundary conditions are fee slip. The top surface of the oceanic and continental crust is treated as an internal free surface by using a low viscosity (1019 Pa s) and low density (1 kg/m³ for air, 1000 kg/m³ for water) top layer (initially 10 km). The interface between this weak layer and the top of the oceanic/continental crust evolves spontaneously. Further on, the topography of the model (air/crust interface) evolves according to a transport equation. It accounts for sedimentation and erosion and is calculated for each time-step (Gerya, 2010):

$$\frac{\partial y_{es}}{\partial t} = v_y - v_x \frac{\partial y_{es}}{\partial x} - v_s + v_e = 0,$$

where y_{es} is the vertical position of the surface as a function of the horizontal distance x: v_y and v_x describe the vertical and horizontal components of the material velocity vector at the surface. The v_s and v_e are sedimentation and erosion rates, respectively, corresponding to the relation:

v_s = 0 mm/a v_e = 0.3 mm/a for y < 9 km

v_s = 0.03 mm/a v_e = 0 mm/a for y < 10 km

1.3. Rheological model

All rheologies are visco-plastic. Viscous (ductile) deformation is computed as a combination of dislocation and diffusion creep and depends on temperature, pressure and strain rate. A smooth transition between dislocation creep and diffusion creep is assumed to occur at 104 Pa (Turcotte and Schubert, 2002). The viscosity for dislocation creep is defined as follows (Gerya, 2010):

$$\eta_{creep} = \frac{\dot{\varepsilon}_{II}^{\frac{1-n}{n}}}{A_D^{\frac{1}{n}}} \exp\left(\frac{Ea + PVa}{nRT}\right),$$

where $\dot{\varepsilon}_{II} = \sqrt{1/2\,\dot{\varepsilon}_{ij}\,\dot{\varepsilon}_{ij}}$ is the second invariant of the strain rate tensor. The terms A_D (material constant), Ea (activation energy), Va (activation volume) and n (creep exponent) are experimentally determined flow law parameters (Ranalli, 1995). R is the gas constant.

Plasticity (brittle failure) is implemented using a yield criterion, limiting the creep viscosity, $\eta_{creep.}$ Additionally, we assume that fluid and melt lower the plastic strength of rocks in our model. The yield strength is decreased according to the prescribed pore fluid and melt pressure factors, λ_{fluid} and λ_{melt}, respectively.

$$\eta_{creep} \le \sigma_{yield} / 2\dot{\varepsilon}_{II},\ \sigma_{yield} = c + P\sin(\varphi),$$

$$\sin(\varphi) = \sin(\varphi dry)\lambda_{fluid},\ \ \lambda_{fluid} = 1 - P_{fluid} / P_{solid}$$

$$\lambda_{melt} = 1 - P_{melt} / P_{solid},$$

where c is the cohesion, which is the strength at P = 0 and ϕ is effective internal friction angle calculated from the friction angle of dry rock (Table 3.2). The terms P_{solid} and P_{fluid} designate dynamic pressure and pore fluid/melt pressure, respectively.

1.4. Water migration

The model assumes that pore water content decreases due to compaction from 2 wt.% to 0 wt.% at depth of 75 km:

$x(wt.\%) = (1 - 0.013\Delta y)X_{H_2O(p0)}$,

where $X_{H_2O(p0)}$ =2 wt.% is the free water content at the surface and Δy is the depth in km below the surface (0 - 75 km).

Further on, expelled water moves upwards instantaneously, until it reaches rock which assimilates water (e.g. Gorzcyk et al., 2007). This process is formulated by the following equation:

$v_{x(water)} = v_x$, $v_{y(water)} = v_y - v_{y(percolation)}$,

Where v_y and v_x are local velocities of the mantle. The constant relative velocity of upward percolation of water through the mantle is $v_{y(percolation)}$ = 10 cm/a.

1.5. Partial melting and melt extraction processes

Following previous studies, the water transport model does not permit complete hydration of the peridotitic mantle (e.g. Nikolaeva et al., 2008). Therefore, the hydrated mantle solidus is located between the wet and dry peridotite solidi. Both, hydrous and dry melting increases linearly with temperature and pressure (Gerya and Yuen, 2003). The volumetric amount of melt, M0, for a given pressure and rock composition is based on:

$M_0 = 0$ when $T < T_{solidus}$,

$M_o = (T - T_{solidus})/(T_{liquidus} - T_{solidus})$ when $T_{solidus} < T < T_{liquidus}$,

$M_0 = 1$ when $T < T_{liquidus}$.

$T_{solidus}$ is the solidus temperature where wet and dry solidi are used for the hydrated and dry mantle. $T_{liquidus}$ represents the dry liquidus temperature at a given pressure and rock composition (Table 3.1). Melt extraction from partially molten rocks occurs where the melt extraction exceeds, a pre-defined melt threshold of M_{max} = 4%. A non-extractable amount of melt M_{min} = 2% remains in the source (e.g. Sizova., 2010; Vogt et al., 2012).The total amount of melt, M, for every marker considers the amount of previously extracted melt and is calculated as:

$$M = M_0 - \sum_n M_{ext} \ ,$$

where $\sum_n M_{ext}$ is the total melt fraction extracted during previous n extraction episodes. Rocks are considered refractory when the extracted melt fraction is larger than the standard one (i.e. when $\sum_n M_{ext} > M_0$). When the total amount of melt M exceeds the threshold M_{max}, the melt fraction $M_{ext} = M - M_{min}$ is extracted and is M_{ext} updated. Extracted melts are transported instantaneously to the near surface environment. Here they from volcanic arcs (20 %) or emplace within continental crust (80 %) at levels of highest possible intrusion rate (i.e. highest possible local crustal divergence rate, div_{crust}). The emplacement level is calculated by evaluating the ratio of the effective melt overpressure and the effective viscosity of the crust above the extraction region:

$$div_{crust} = \left[Py_{melt} - g_y \rho_{melt} \left(y_{melt} - y \right) - Py \right] / \eta_y \ ,$$

where Py_{melt} is pressure at the extraction level y_{melt} and Py is the pressure at the current level y, g is gravitational acceleration in y-direction [m/s^2], ρ_{melt} is the melt density and ηy is the effective local crustal viscosity at the current level y.

The effective density, ρ_{eff}, of partially molten rocks is defined by:

$$\rho_{eff} = \rho_{solid} \left(1 - M + M \frac{\rho_{0molten}}{\rho_{0solid}} \right),$$

where ρ_{osolid} and $\rho_{omolten}$ are the standard densities of solid and molten rocks, respectively (Table 3.1) and ρ_{osolid} is the density of solid rocks at given P(MPa) and T(K) calculated from:

$$\rho_{P,T} = \rho_0[1-\alpha(T-T_0)][1+\beta(P-P_0)],$$

where α and β denote the thermal expansion and compressibility coefficients, respectively (Table 3. 1).

The effect of the latent heat is defined by an increased effective capacity of partially molten rocks (C_{peff}) computed by the following equation:

$$C_{peff} = C_p + H_L/(T_{liquidus} - T_{solidus}),$$

where C_p indicates heat capacity of the rock; H_L is latent heat, J/kg.

Chapter 4. Structural controls on sedimentation during asymmetric extension: the case of Sorbas Basin (SE Spain)

This chapter is based on Andrić, N., Matenco, L., Hilgen, F., de Bresser, H., in revision in Global and Planetary Change.

4.1. Introduction

The architecture of sedimentary basins is controlled by the balance between the rate of creating accommodation space and the rate of sediment supply (e.g., Schlische, 1991; Schlager, 1993; Gawthorpe et al., 1994). The kinematics and offset of normal faults dominantly control the sediment production and dispersal patterns in extensional basins by creating the accommodation space, influencing the basin physiography, drainage network and sediment transport pathways (e.g., Gawthorpe and Hurst, 1993; Gupta et al., 1999; Gawthorpe and Leeder, 2000; García-García et al., 2006). The variability and evolution of normal fault offsets or migration across fault arrays creates tectonic-induced sedimentation cycles that have a wide range of time scales, from millions to several thousand years (e.g., Gawthorpe and Leeder, 2000; Petersen et al., 2010).

Sediment dynamics during initiation of normal faulting is generally less quantified at the scale of outcrops, when compared with the conceptual availability of tectonic system tracts or other more general syn- and post- rift deposition cyclicity (e.g, Prosser, 1993; Nottvedt et al., 1995; Martins-Neto and Catuneanu, 2010; Balazs et al., 2016; Andric et al., 2017). This initiation is often associated with the deposition of coarse-grained alluvial fans and/or fan deltas sourced from uplifting footwalls and deposited along extensional margins at the base of fault scarps (e.g., Colella, 1988; Postma and Drinia, 1993; Leppard and Garwthorpe, 2006). Owing to the proximity to the active normal fault, these relatively small-scale depositional systems respond rapidly to slip events, which are observed in the cyclic alternation of vertical coarsening- and/or finning- upwards trends (e.g., Rohais et al., 2008). The initiation of normal faulting creates a gradually increasing depositional slope that delivers gravity flow sedimentation to the deep-water environment (e.g., Nemec, 1990; Fugeli and Olsen, 2007; Strachen et al., 2013). During rapid sedimentation associated with normal faulting, terrigenous or shallow marine material may be delivered as out-sized coarser-grained events into an otherwise contrasting deep-water facies, for instance coarse deposition in distal prodelta mudstones (Young et al., 2000) or distal deep marine lobes (Kane et al., 2017). Furthermore, large-scale slide and debris flow deposits are shed by slope collapse into the deep-water facies (e.g., Kleverlaan, 1987). However, a direct observation of the relationship between these types of flows and their changes controlled by the activity of normal faults is very rare in outcrop studies (Henstra et al., 2016). Such observation is highly relevant for discriminating the tectonic-induced cyclicity from other external forcing factors (eustasy, climate, runoff precipitation) or autocyclic depositional processes.

One excellent example retaining extended exposures of sedimentary facies deposited during the initiation of extension is the Miocene - Pliocene Sorbas Basin, part of the extensional system overlying the internal parts of Betic Cordillera in the SE Spain (Fig. 4.1; e.g., Dewey et al., 1989; Rosenbaum et al., 2002; Vissers, 2012). Exposures of normal faults and associated syn-kinematic sedimentary facies deposited during the Miocene initiation of extension are available in the SE part of the Sorbas Basin (e.g., Haughton, 1994; Do Couto et al., 2014 and references therein). In this part of the basin, we have studied the link between normal faulting and continental to deep-water deposition by means of a high resolution kinematic and sedimentological study. The aim is to quantify the influence of the change in

slope and bathymetry induced by normal faulting, and the associated sedimentary flow dynamics and lobe stacking patterns. The results are integrated in a dynamic model of sedimentation during initiation of extension and are discussed in the overall context of the Betic Cordillera evolution.

4.2. Geological settings

The Betic-Rif orogenic system (Fig. 4.1a) formed in response to the subduction and closure of the Tethyan ocean during the convergence between Iberia and Africa continental units (e.g., Duggen et al., 2004; Vissers, 2012). The late Mesozoic to Cenozoic shortening resulted in the creation of a nappe stack affecting Palaeozoic - Mesozoic sediments derived from the southern Iberian margin in the External Betics or derived from the southern Iberian and Alboran margins in the Internal Betics (the Nevado-Filabride, Alpujarride and Malaguide units, García-Hernandez et al., 1980; Banks and Warburton, 1991; Platt et al., 2003; Balanyá et al., 1997; Torres-Roldán, 1979). The Oligocene - Early Miocene shortening in the External Betics was largely coeval with extensional deformation in the Internal Betics. This extension partly reactivated former thrusts as detachments and induced a rapid exhumation of metamorphic cores (e.g., Martínez-Martínez and Azañón, 1997; Platt et al., 1989; 2005; Garcia-Dueñas et al., 1992; Augier et al., 2005). This exhumation was kinematically associated with the formation and evolution of several extensional basins that presently separate the metamorphic sierras of the SE Spain (Fig. 4.1a, Garcia-Dueñas et al., 1992; Lonergan and Platt, 1995; Crespo-Blanc, 1994; Augier et al., 2005; Meijninger, 2006; Pedrera et al. 2012; Giaconia et al., 2014). The overall extension is generally thought to be driven by removal of lithospheric mantle beneath the Internal Betics or by roll-back associated with slab detachment of the Gibraltar slab (e.g., Faccenna et al., 2004; Spakman and Wortel, 2004; Jolivet et al., 2008; Gutscher, 2012; Vissers, 2012). The initial Early Miocene (~22 to 18 Ma) N-S to NNE-SSW oriented extension was associated with the exhumation of the neighbouring Alpujarride and Nevado - Fillabrides nappe complex (e.g. Monié et al., 1991; Crespo-Blanc et al., 1994; Platt et al., 2005) and was followed by an E-W oriented Middle - Late Miocene (~15 to 9 Ma) extension driving the main subsidence observed in the basins (e.g., de Jong, 1991; Jabaloy et al., 1992; Johnson et al., 1997; Augier et al., 2005; Platt et al., 2005; Vázquez et al., 2011).

In the Internal Betics, the Sorbas Basin (Fig. 4.1b) was extensively analysed in numerous studies, owing to extended and almost complete exposure of its Middle Miocene - Pliocene fill (e.g., do Couto et al., 2014 and references therein). The sediment deposition was driven by an initial extension, followed by inversion and influenced by the large sea-level changes during the Messinian Salinity Crisis (Fig. 4.1b, Martin and Braga, 1994; Stapel et al., 1996; Hodgson and Haughton, 2004). The late exhumation of the Nevado-Filabrides during upper Serravallian to lower Tortonian was coeval with the onset of sedimentation in the Sorbas Basin (~ 12-11 Ma, Johnson et al., 1997; Vazquez et al., 2011; Augier et al., 2013). The extension has created an asymmetric geometry, controlled by the activity of a

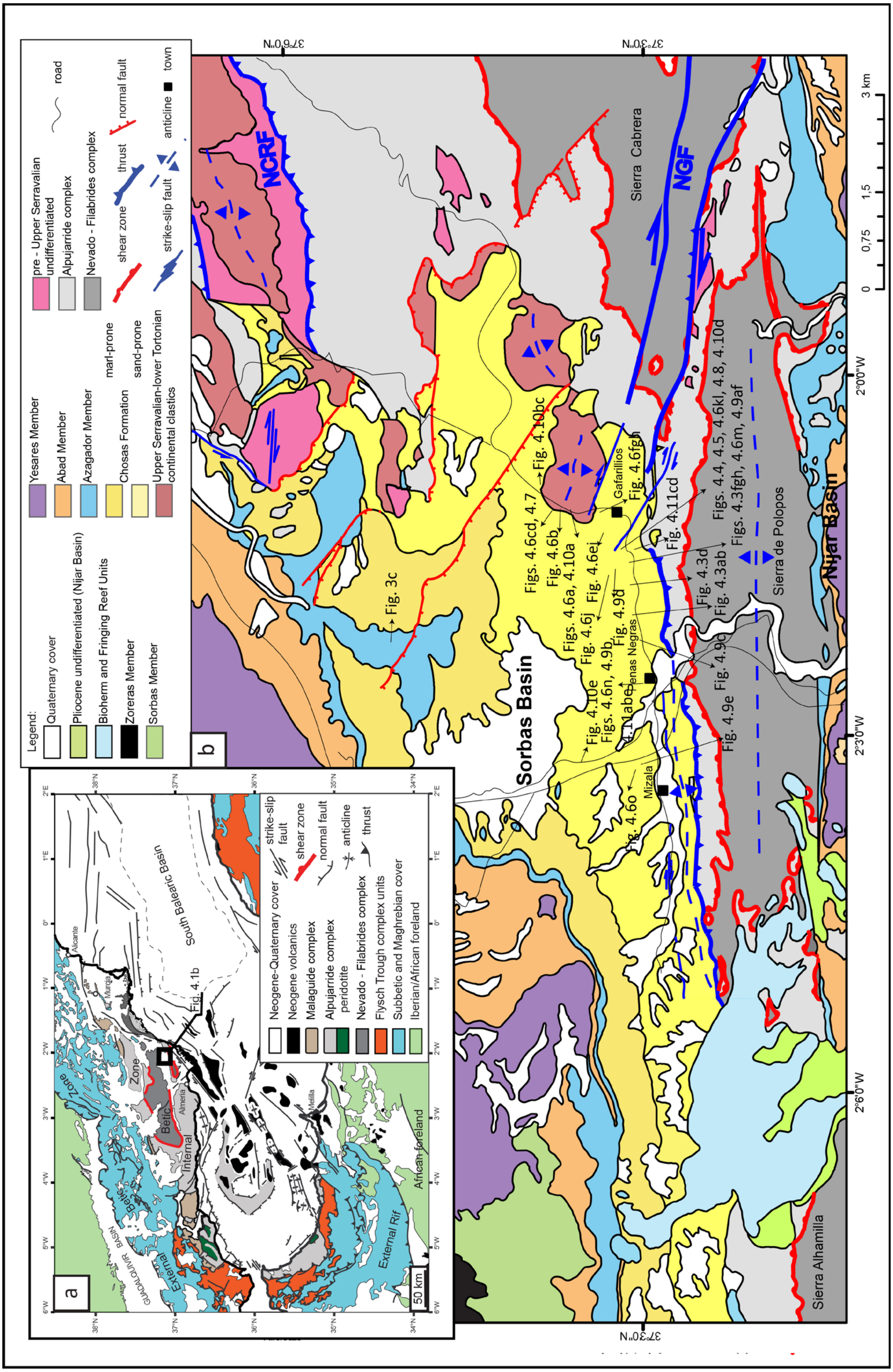
a
Neogene-Quaternary cover
Neogene volcanics
Malaguide complex
Alpujarride complex
peridotite
Nevado - Filabrides complex
Flysch Trough complex units
Subbetic and Maghrebian cover
Iberian/African foreland
strike-slip fault
shear zone
normal fault
anticline
thrust
South Balearic Basin
Fig. 4.1b
Betic Internal Zone
External Betic Zone
External Rif
African foreland
Alicante
Murcia
Almeria
Melilla
50 km
b
Legend:
Quaternary cover
Pliocene undifferentiated (Nijar Basin)
Bioherm and Fringing Reef Units
Zoreras Member
Sorbas Member
Yesares Member
Abad Member
Azagador Member
Chosas Formation
marl-prone
sand-prone
Upper Serravalian-lower Tortonian continental clastics
pre - Upper Serravalian undifferentiated
Alpujarride complex
Nevado - Filabrides complex
road
normal fault
thrust
anticline
town
shear zone
strike-slip fault
Sorbas Basin
Sierra Cabrera
Sierra de Polopos
Sierra Alhamilla
Nijar Basin
NCRF
NGF
Gafarillos
Peñas Negras
Mizala
Fig. 3c
Fig. 4.10bc
Figs. 4.6cd, 4.7
Fig. 4.6b
Figs. 4.6a, 4.10a
Fig. 4.6ei
Fig. 4.6j
Fig. 4.9d
Figs. 4.6n, 4.9b,
Fig. 4.10e
4.11abc
Fig. 4.6o
Fig. 4.6fgh
Fig. 4.11cd
Fig. 4.3d
Fig. 4.3ab
Fig. 4.9c
Fig. 4.9e
Figs. 4.4, 4.5, 4.6kl, 4.8, 4.10d
Figs. 4.3fgh, 4.6m, 4.9af
37°6'0"N
37°3'0"N
2°0'0"W
2°3'0"W
2°6'0"W
0 0,75 1,5 3 km

Figure 4.1 (opposing page): a) Tectonic map of the Betic-Rif orogenic system (modified after Comas et al., 1999). The thick rectangle shows the study area of Fig. 4.1b; b) Geological map of the SE part of Sorbas basin (modified after Do Couto et al., 2012). NGF-North Gafarillos fault, NCRF-North Cabrera reverse fault.

N-dipping fault most likely rooted into the main Alhamilia detachment or its more brittle equivalents (Fig. 4.1b, e.g., Garcia-Dueñas et al., 1992; Martinez-Martinez and Azonon, 1997; Do Couto et al., 2014, Giaconia et al., 2014). The Sorbas Basin subsidence was driven by successive episodes of extension with NW-SE and NE-SW presently observed directions, which controlled the upper Serravallian - Tortonian sedimentation (e.g., Do Couto et al., 2014 and references therein). The southern boundary of the basin (the northern limit of Sierra de Polopos and Sierra Alhamillia, Fig. 4.1) is part of a transpressive fault system with top NW sense of shear that formed during the subsequent late Tortonian - Messinian basin inversion, which possibly reactivated an earlier extensional normal fault (e.g., Ott d'Estevou and Montenant, 1990; Haughton, 2001; Giaconia et al., 2012, 2013; Jonk and Biermann, 2002; Booth-Rea et al., 2004). The inversion is thought to have migrated southwards with time (e.g. Jonk and Biermann, 2002; Giaconia et al., 2012) and was associated with the deposition of upper Tortonian sediments (e.g., Weijermars et al., 1985; Kleverlaan, 1989). The overall inversion is thought to have started at ~8Ma and was driven by N-S contraction and transcurrent deformation post-dating the back-arc extension and observed regionally in the Alboran Domain (e.g., Comas et al., 1999; Jolivet et al., 2008).

4.2.1. Structure, stratigraphy and sedimentological evolution of the Sorbas Basin

The Sorbas Basin is flanked by the metamorphic rocks of Sierra Alhamillia, Sierra de Polopos and Sierra Cabrera to the south and Sierra de los Filabres to the north (Fig. 4.1). These sierras are generally slightly asymmetric domes with structurally steep northern flanks and gentle dipping southern ones (e.g., Platt et al., 1989). On the southern flank of Sorbas basin, the Gafarillos strike-slip fault system has a northern and a southern branch, the latter being kinematically connected with the transpressive system observed at the northern margin of Sierra Alhamilla and Sierra de Polopos (Fig. 4.1, e.g., Giaconia et al., 2012; 2013).

The basement of sierras is made up by Alpujarride low-temperature and locally high-pressure meta-sediments (Permian phyllites and Triassic marbles and dolomites, Martínez-Martínez and Azañón, 1997; Booth-Rea et al., 2002, 2005) and Nevado-Filabride high-temperature and locally high-pressure meta-sediments and magmatics overprinted by a greenschist facies retromorphism (Johnson et al., 1997; Vázquez et al., 2011). This nappe stack was overprinted by a high-temperature and low pressure metamorphic event that took place most likely during the onset of exhumation (e.g., Vissers, 2012; Platt et al., 2013). The Nevado-Filabride nappe stack (from bottom to top Ragua, Calar-Alto and Bedar-Macael units) contains Paleozoic micaschists intercalated with quartzites and marbles, Permo-Triassic meta-pelites and quartzites, and Triassic marbles (e.g., Garcia-Dueñas et al.,1988; de Jong, 1991;

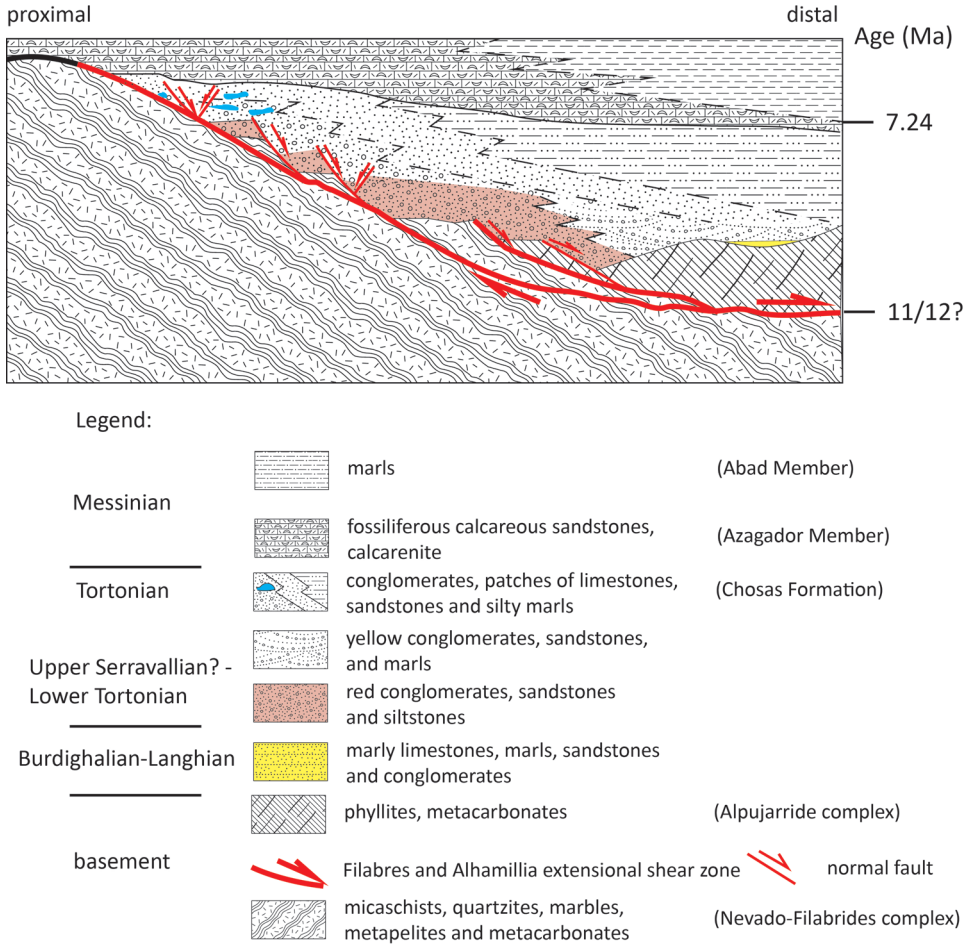

Figure 4.2: General lithostratigraphic scheme of the Sorbas Basin, modified from Puga – Bernabeu et al., (2007), Ott d'Estevou and Montenat (1990) and the results of the present study.

Martinez-Martinez and Azanon, 1997; Martinez-Martinez et al., 2002).

The oldest Miocene sediments are poorly preserved Burdigalian (-Langhian?) marly limestones, sandstones, conglomerates and marls observed as isolated patches overlying the basement of Sierra Cabrerra (pre-Upper Serravalian in Fig. 4.1b, Ott d'Estevou and Montenant, 1990; De Galdeano and Vera, 1992). Their deposition is thought to have been controlled by an earlier extensional episode associated with the exhumation of the basement nappe stack (22-18 Ma, e.g., Crespo-Blanc, 1994).

The main extensional evolution started in the Sorbas Basin at ~12-11 Ma (Fig. 4.2) during the extensional exhumation of the Nevado-Filabrides unit (e.g., Johnson et al., 1997; Augier et al., 2013). The associated sedimentation is made up

of fluvial conglomerates, sandstones and siltstones that laterally grade into deltaic conglomerates, sandstones and marls that reach thicknesses of ~ 100m (e.g., Ott d'Estevou and Montenant, 1990). The gradually increasing Tortonian normal faulting accelerated the basin subsidence and created an open marine environment (e.g., Dabrio et al., 1990; Poisson et al., 1999), where a deltaic system was shedding conglomerates and sandstones transported further into the basin by turbiditic submarine fan systems interbedded within pelagic marls (e.g. Haughton, 2001). These sediments are ~2 km thick and are generally grouped into the generic Chosas Formation (e.g., Völk, 1966; Ott d'Estevou and Montenant, 1990; Barragán, 1997; Booth-Rea et al., 2004). During the late Tortonian, the basin was predominately supplied by north to south directed flows (i.e. sediments derived from Sierra de los Filabres). Further into the basin, the flows were deflected along the northern margin of Sierra Alhamillia, which resulted in a dominant west to east flow direction (e.g., Weijermars et al., 1985; Haughton, 2001). The Chosas Formation shows progressive youngening westwards, while the eastern part of the basin was deformed and inverted during the late Tortonian (e.g., Haughton, 2001). Therefore, the upper part of the turbiditic sequence is considered to have been deposited during the subsequent inversion and strike-slip faulting observed with larger effects near the southern basin margin, which has influenced the depositional character of this sequence (e.g., Kleverlaan, 1989; Poisson et al., 1999; Haughton, 2001).

The Upper Tortonian turbidites are overlain by shallow-water temperate ramp carbonates, generally grouped into an uppermost Tortonian to earliest Messinian Azagador Member (Fig. 4.2, e.g., Ruegg, 1964; Martin et al., 1999; Braga et al., 2006; Puga-Bernabéu et al., 2007). The contact between the Chosas Formation and Azagador Member is thought to be an unconformity, which recorded the latest Tortonian- earliest Messinian basin inversion (e.g., Possion et al., 1999). The Azagador carbonates prograded basin-wards, have a gradual transition to and are overlain by more distal marls (the Lower Abad Member, e.g., Ruegg, 1964; Riding et al., 1991; Martin and Braga, 1994). At the beginning of Messinian times both the southern and the northern basin margins were overstepped by reef deposits (Bioherm Unit and Fringing Reef Unit, respectively), which were locally deposited unconformably over the Azagador Member (e.g., Ruegg, 1964; Martin and Braga, 1994, Riding et al., 1991). These reef units grade laterally into silty marls and marls intercalated with diatomites (the Upper Abad Member, e.g., Ruegg, 1964, Krijgsman et al., 2001). During the Messinian Salinity Crisis, the Sorbas Basin reached a semi - isolation that started at 5.971 Ma and led to deposition of 120 m thick selenite gypsum, interbedded within clay and marly laminites (the Yesares Member, Dronkert, 1976; Manzi et al., 2013). These evaporites are buried by lagoonal coarse carbonates that laterally grade into Gilbert-type of delta deposits (the Sorbas Member, e.g., Roep et al., 1998). The whole succession was overlaid by red continental conglomerates that reach ~60 m thickness (the Zorreras Member, Montenat et al., 1980; Martin-Suarez et al., 2000).

4.3. Field observations of extensional fault kinematics

Similar with previous studies (Do Couto et al., 2014; Giaconia et al., 2014), our field observations show that the onset of extension and subsidence of the

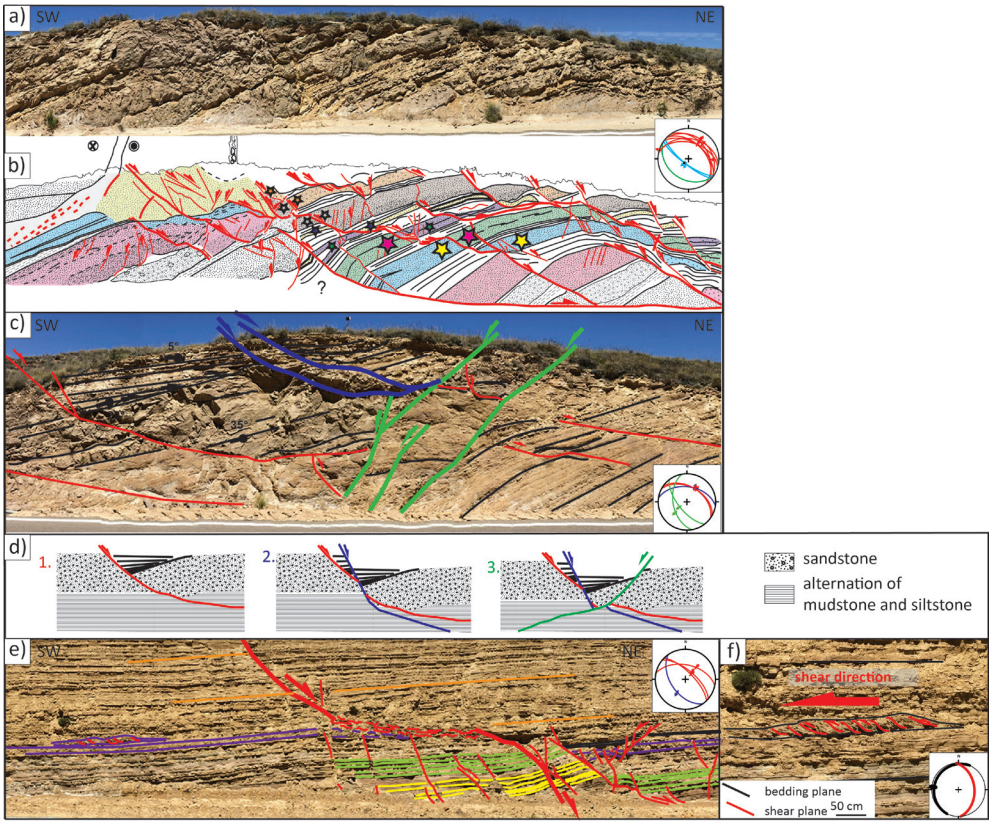

Figure 4.3: Extensional geometries and kinematics of normal faulting in the turbiditic succession of the Chosas Formation in the SE part of Sorbas Basin. Locations in Fig. 4.1b. a) panoramic photo and b) interpretation of normal faulting associated with deformation along an extensional ramp-flat system and associated syn-kinematic deposition in the submarine fan environment. Green line, blue and red lines on the stereonet represent bedding plane, antithetic and synthetic faults; c) intersection of successive stages of high- and low- angle normal faults. Note the refraction at the transition between thick sandstones and mudstones/siltstones layers; d) Evolutionary sketch of the three successive deformation events depicted in Fig. 4.3c. The oldest faults are associated with syn-kinematic sedimentation; e) extensional ramp-flat geometry formed in sediments of the C5 facies association, where the flat segment truncates mud-rich sandstones; f) raft of thrusts that formed originally in the lower part of a toe slope décollement.

Figure 4.4 (facing page): Extensional geometries and kinematics of normal faulting in the shallow water deltaic to submarine fan transition cropping out in the SE part of Sorbas Basin. Locations in Fig. 4.1b. a) panoramic photo and b) interpretation of a listric normal fault system dipping ENE-wards truncated by subsequent strike-slip structures formed during basin inversion. Note the antithetic tilting of hanging-walls that created the main depositional slope of the basin; c) intersection between two normal fault sets cross-cutting a thick event bed (location is the blue star in Fig. 4.4b); d) inset of Fig. 4.4c illustrating layer parallel shearing in the fine-grained sediments; e) a possible solution for the temporal evolution of fault sets depicted in Fig. 4.4b: the flat segment forms in a layer-parallel shear zone that formed

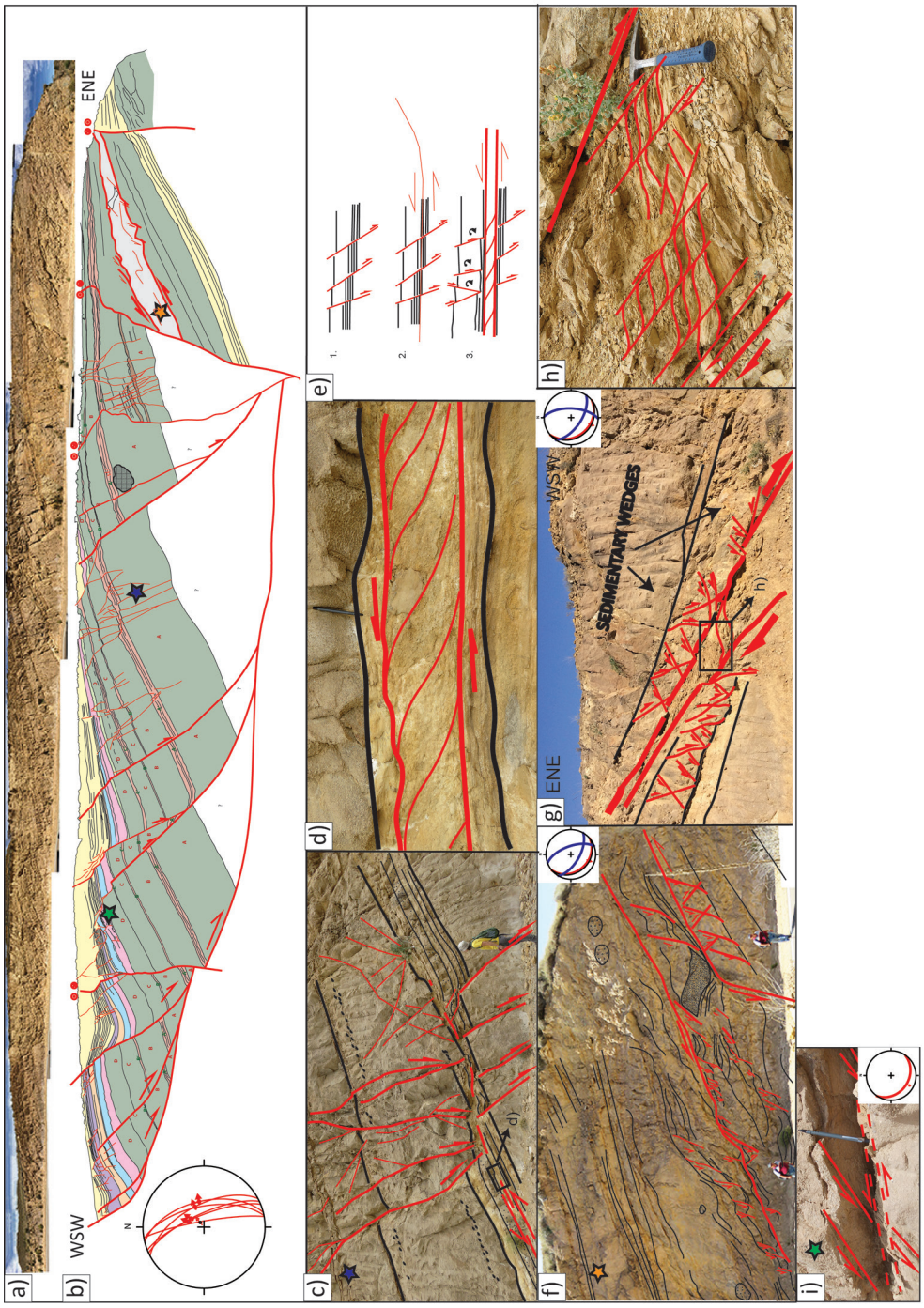
a)
b)
WSW
ENE
c)
d)
e)
1.
2.
3.
f)
g)
WSW
ENE
SEDIMENTARY WEDGES
h)
h)
i)

Figure 4.4 (continued): subsequently and cross-cuts the earlier domino-style normal faults; f) large-scale extensional shear zone formed along a SW dipping normal fault (location is the orange star in Fig. 4.4b). Riedel shears are domains where less deformed, but rheologically strong layers (sandstones and conglomerates) form sigmoidal clasts that may reach up to 2 m; g) The variability of the same shear zone as in Fig. 4.4f towards the south. Earlier formed conjugate normal faults are truncated by the shear zone; h) inset of Fig. 4.4g illustrating CS structural fabrics developed within shear zone; i) layer parallel shearing developed within rheologically weak layers (location is the green star in Fig. 4.4b).

Sorbas Basin during upper Serravallian - Tortonian times was associated with successive NW-SE and NE-SW oriented normal faults that are often organized in conjugate sets and are locally associated with less frequent E-W oriented strike-slip transfer faults. Furthermore, a large number of normal faults were mapped in the SE part of the basin (Figs. 4.3 – 4.5), where the upper Serravallian-Tortonian fluvial, deltaic and offshore marine successions crop out. Many of these faults are syn-depositional, demonstrating the coeval nature of deformation and sedimentation, and have variable offsets up to few tens of metres in studied outcrops (e.g., Figs. 4.3b, 4.4b, 4.5f). No observed contractional or transpressional structures have syn-kinematic character in the outcrop exposures of Chosas Formation in this part of the basin, inferring that inversion post-dated their deposition.

The oldest upper Serravalian - Tortonian exposed sequence near the

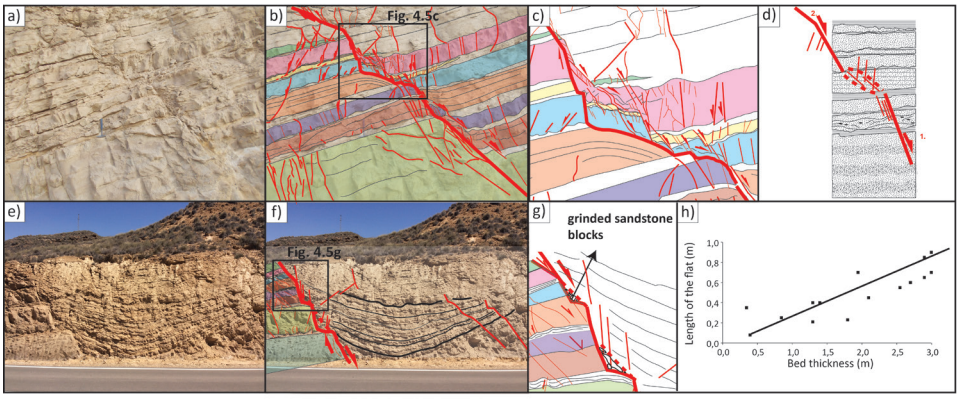

Figure 4.5: Illustration of normal faults with staircase geometry. Locations in Fig. 4.1b. a) photo and b) interpretation sketch of a fault with a staircase geometry. The transition between segments is observed along layer parallel flats that truncate a sandstone/silty lithology; c) Inset of Fig. 4.5b illustrating an extensional horse formed along a step in the staircase geometry. Well-cemented sandstone blocks are rotated, while the weaker silty sandstones and mudstones are sheared, forming an overall sigma-like clast geometry; d) sketch illustrating the mechanisms of connecting two highly-inclined segments of the staircase geometry by deforming a restraining vertical overlap zone (red dashed line); e) photo and f) interpretation of a large offset normal fault with a staircase geometry; g) inset of Fig. 4.5f, illustrating shortcutting the steps of a staircase geometry forming grinded sandstone and mudstone in the damage area; h) the observed correlation between the length of the flat segment and the thickness of underling rheological strong layers observed along the staircase fault trace geometry.

Gafarillos village (Fig. 4.1b) is affected by a dense array of normal faults. The frequency of these faults rapidly decreases upwards in the stratigraphy. The faults affect the fluvial, deltaic and the transition to submarine fan deposits (Figs. 4.3 and 4.4) and have 2 main directions of extension, NW-SE and NE-SW. The first one is predominant in the older alluvial to deltaic sequence located in the SE part of the basin, while the second is dominant upwards in the stratigraphy. Older normal faults have centimetres to metres offsets, with a few examples reaching more than 10 metres (e.g. Fig. 4.4b). Syn-kinematic deposition is evident on many localities (e.g., Fig. 4.3d and 4.4b), providing an unusual strong age control of deformation, combined with a clear association of deposition with normal faulting. A rheological control of the mechanics of normal faulting is obvious, with high-angle or ramp geometries in conglomerates and thick sandstones, and listric or layer parallel fault segments in finer geometries (Figs. 4.4 and 4.5). Large offset faults are associated with antithetic tilting of hanging-walls, folding and draping geometries in finer sediments, and coarse lithologies deposited near fault planes. In more uniform rheologies, similar antithetic tilting is observed along successive fault arrays ("domino" normal faulting, Fig. 4.10c,e).

Upwards in the stratigraphy of the Chosas Formation (such as exposed along the road linking Penas Negras and Gafarillos, Fig. 4.1b) NW-SE oriented normal faults with variable offsets (cm to > 20 m) have a dominant top to the NE sense of tectonic transport and have more complex geometries when compared with the lower alluvial sequence (Figs. 4.4 and 4.5). The numerous faults observed in this Chosas heterogenous sequence have ramp - flat (Fig. 4.3a,b,e), complex listric (Fig. 4.3c) or staircase (Fig. 4.4) geometries. Simple planar or listric geometries are less frequent (Fig. 4.4c). Low angle normal faulting is observed in matrix-supported, and/or semi-lithified sandstones and conglomerates (Figs. 4.3a,b,e and 4.4). Normal faulting initiated with Riedel shears and created fault gouges and semi-ductile shear zones in finer silt or shale lithologies (Fig. 4.4d-h). Normal faulting is also associated with numerous connecting joints and Riedel shears.

A characteristic ramp - flat geometry of large NE-dipping faults is often observed at the transition between alluvial, deltaic and deep-water deposits, often associated with syn-kinematic clastic wedges (Fig. 4.3a,b). Ramps are observed in sandstones and conglomerates, often at right angles to bedding, suggesting that initiation of faulting took place by dilatation along extensional joints (Fig. 4.3a,b). Flats are observed in finer silt or shale lithologies, where shearing is observed by the formation of brittle shear-bands and sheared clasts geometries in a fault gouge that is usually foliated. Deformation is associated with joints and antithetic Riedel shears, and roll-over anticlines and small (half-) grabens in hanging walls (Figs. 4.3a,b and 4.4a,b).

Foliated fault gouges are made up of silt and clay material, may reach 5 m thickness and show clear shear-sense indicators, such as an obvious brittle shear bands fabric (Fig. 4.4d,h). Along the road from Penas Negras to Gafarillios, these shear zones dip to the SW (Fig. 4.4a,b) and are sub-parallel to bedding in finer grained material (fine sands, silts and muds) that contain intercalated coarse sandstones and conglomerates. These zones contain small extensional duplexes with large sigma-shaped metres-size clasts having geometries consistent with the overall sense of shear, made up of more resistant sandstones and conglomerates,

back-rotated and offset by synthetic Riedel shears (Fig. 4.4d,f,g,h).

One interesting geometry observed in outcrops is that of high- angle (70° - 90°) fault segments developed in 0.15 m - 4 m thick coarse sandstones (mostly granular debris flows) and conglomerates connecting layer sub-parallel (<35°, but general layer parallel) segments in 0.05 m - 0.4 cm thick fine sandstone, siltstones and mudstones bedsets. This creates a staircase fault geometry (Fig. 4.5). A direct relationship between the thickness of the underlying coarse sandstones and conglomerates and the overlying size of the step (or length of the flat) can be observed (Fig. 4.5h). Some faults do not display any apparent offset along individual steps, but the total displacement is obvious if the full stratigraphy is considered (Fig. 4.5). In more details, some displacements along low offset faults are seen to be associated with layer parallel shearing and dragging in finer beds, and shortcutting the steps by creating extensional horses (Fig. 4.5a-d). When displacement increases, these shortcutting features are less or not preserved (Fig. 4.5e,f,g). In other situations of staircase normal faults, we have observed a layer parallel shear confined to fine lithologies that presumably were rheologically weak (Fig. 4.4i). This suggests two stages of movement: first the formation of a high angle normal fault cutting through all layers, followed by layer parallel shearing creating offsets along steps in the normal fault. Deformation along staircase faults is associated with cm-scale faults that have higher dips in the hanging-wall (40°-70°) than the footwall (20°-30°, Fig. 4.5).

The staircase geometry not affected by layer parallel shearing formed in response to the contrasting lithologies cross-cut by normal faulting, possibly enhanced by the unconsolidated, high water-pressure content of finer sediments at the time of deformation (e.g., Childs et al., 2009). Refraction during propagation of normal faulting (e.g., Childs et al., 1996; Schöpfer et al., 2006) is unlikely, because this does not explain the flat layer parallel segment of the staircase geometry. We infer that these observed staircase geometries formed by linking initially shorter Riedel shears or joints across rheologically weak layers in a vertical overlap shear zone, where the faults steps are connected upwards into the footwall across the overlap zone (e.g., Childs et al., 2009; Rykkelid and Fossen, 2002). This interpretation is supported also by synthetic rotation of sigmoidal clasts in the restraining vertical overlap structure. Alternatively, the staircase geometry may also be formed as a result of growth and propagation of the faults nucleated within mechanically stronger layer and linked via weak layers (e.g., Gabrielsen et al., 2016). These faults were initially separated (i.e. soft-linked, e.g., Fig. 4.4c) and become connected when the fault offset exceeds the thickness of the weak layer (i.e. hard-linked, e.g., Fig. 4.5e,f,g).

4.4. The depositional environment associated with extension

The upper Serravallian – Tortonian sediments exposed in the SE part of the Sorbas Basin are characterized by coarse-grained clastics deposited in an alluvial fan and deltaic environment, which laterally changes to shallow marine and further to a deeper marine depositional system. These sediments were transported into the basin by a combination of rock-fall, stream flows and different types of gravity flows

Table 4.1: Lithofacies observed in the studied SW part of the Sorbas basin. Their interpretation follows a standard sedimentological procedure (Bouma et al., 1962; Postma, 1990; Miall, 1996; Talling et al., 2012).

Facies code	General description	Inferred depositional process
F1	clast - supported; boulder to pebble conglomerate; with/without out - sized clasts; matrix: low amount of coarse - grained sandstone; subangular to subrounded clasts; poor to medium sorting; massive; plane base	rapid sedimentation from cohesionless debris flow/granular flow
F2	matrix - supported; cobble (boulder) to pebble conglomerate/sandstone; matrix: fine - grained sandstone/siltstone/mudstone; subangular to subrounded clasts; poor sorting; massive; planar base	sedimentation from cohesive debris flow
F3	clast - to matrix - supported; cobble to granula conglomerate/sandstone; moderate sorting; weak normal grading, imbrication; crude horizontal stratification; planar base	longitudinal - bar or sieve deposits under subareal braided - stream flow
F4	clast - supported; cobble to granula conglomerate; subangular to subrounded clasts; poor to medium sorting; normal grading; erosional base	channel - lag deposits under subareal flashy braided - stream; sedimentation from subaquous high - density turbidity flow
F5	clast - to matrix - supported; cobble to granula conglomerate/sandstone; subrounded to rounded; weak sorting; planar crossbeds, imbrication; planar base	transversal - bar deposits under subareal braided - stream; deltaic growths from older bar remnants
F6	clast - to matrix - supported; pebble to cobble conglomerate/coarse - to fine - grained sandstone; subangular to subrounded; weak sorting; through crossbeds; graded or ungraded; erosional base	channel fill under subareal braided - stream; sedimentation from high - density turbulent flow
F7	coarse - to medium - grained (pebbly) sandstone; low matrix content; medium to well sorting; normal grading/massive; If presents mud rip-ups aligned; erosive/planar base	rapid sedimentation from high - density turbidity currents (Ta division of Bouma, 1962)
F8	medium - to fine - grained sandstone; parallel lamination; planar base	sedimentation from subaerial sheet or stream flow; deposition from high - to low - density turbidity flow (Tb division of Bouma, 1962)
F9	medium - to fine - sandstone; well sorting; ripple - cross lamination; climbing ripples	sedimentation from sheet or stream flow; reworking of the sediments by wave action; deposition from low - density turbidity flow (Tc division of Bouma, 1962);
F10	coarse - to medium - grained sandstone; no internal structure; often with scattered granulas, pebbles	sedimentaion from subareal to subaquous cohesionless debris flow

Table 4.2 (continued): Lithofacies observed in the studied SW part of the Sorbas basin. Their interpretation follows a standard sedimentological procedure (Bouma et al., 1962; Postma, 1990; Miall, 1996; Talling et al., 2012).

F11	medium - to fine - grained sandstone; moderate sorting; planar crossbeds; planar base	sedimentation under sheet or stream flow; deposition from unidirectional, steady high - density turbudity currents
F12	medium - to fine - grained sandstones; well sorting; weak normally graded/ungraded; low - angle crossbeds; planar base	dunes (lower flow regime) under subareal sheet flow or stream flow; deposition from wave and/or tidal currents passing through channel; lateral accretion
F13	fine - grained sandstone interbedded with siltstone; sometimes with scattered granulas; laminated or massive; planar base	sedimentation from suspension of waning floods; suspension fall-out in local overbank flood areas or aboundant channel; sedimentation from low-density turbidity flow (Td division of Bouma, 1962)
F14	fine - grained siltstone to mudstone; planar lamination or massive	sedimentation from waning low - density turbidity flow (Te division of Bouma, 1962) or cohesionless density flow
F15	grey mudstone; massive/weak planar lamination	particles settling from water column
F16	yellow marl; massive/weak planar lamination	particles settling from water column
F17	fine - grained sandstones, structurless	bioturbated sandstone
F18	coarse - to medium - grained sandstones; chaotic; scattered pebbles, mud rip - ups	slump deposit

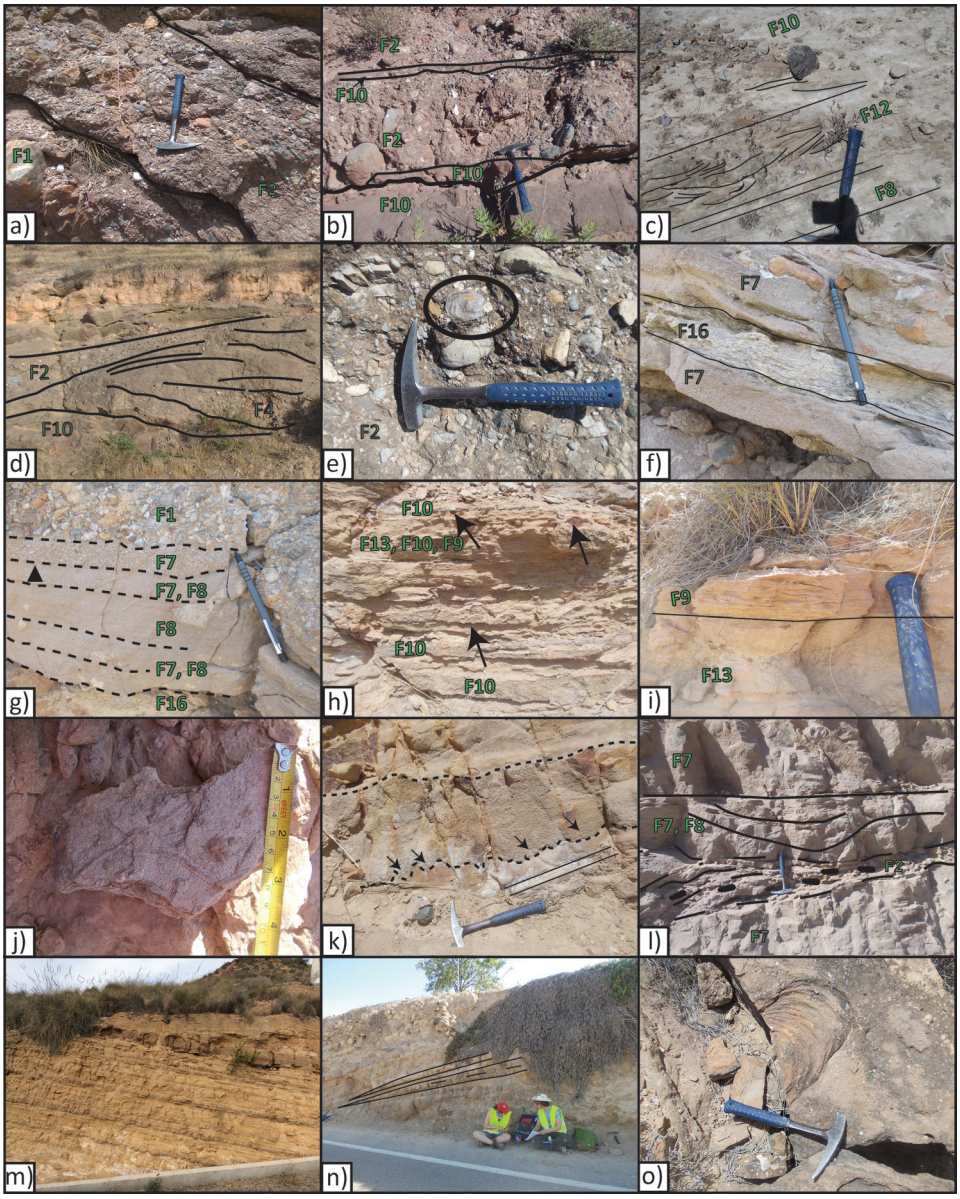

Figure 4.6: Typical examples of the main facies associations. See Table 4.1 for facies details and Fig. 4.1b for photo locations. a) facies association A1 with matrix- to clast- supported conglomerates deposited in a proximal alluvial fan environment. Thick black line marks the bedding; b) facies association A2 with structure-less sandstones and conglomerates deposited in a distal alluvial fan environment; c) facies association B with well sorted mature yellow trough cross bedded sandstones deposited in a shallow water marine (shoreface) environment; d) facies association C1 with channelized delta plain deposits; e) facies association C2 with sheet-like polimict conglomerates deposited in river-dominated delta front environment. Note the oyster shell inside the black ellipse; f) facies association C2

Figure 4.6 (continued): with coarse-grained sandstones containing isolated out-sized clasts intercalated with wavy laminated yellow carbonate mudstone deposited from subaqueous distributary channels and mouth bars affected by a wave and tidal influence; g) facies association C2 with amalgamated sandstones deposited from high-density turbidity currents capped with granular flow deposit in the delta front environment. Dashed lines delineate bed sub-units; h) facies association C3 with burrows in sandstones and mudstones interrupted with pebble to granula clastic episodes; i) facies association C3 with ripple-cross laminated sandstone and bioturbated sandy mudstones deposited in a prodelta settings; j) facies association C3 with horizontal burrows in prodelta sandstones; k) facies association C4 with amalgamated event beds comprised of an alternation of granula sandstones and clast- to matrix-supported conglomerates, whereas the base of the latter is characterized by loading structures (black arrows); l) facies association C4 with interference of amalgamated beds and lateral channels (likely fault perpendicular flow); m) facies association C5 with parallel laminites, siltstones and mudstones deposited on a basin plain; n) isolated medium-grained sandstone lobes deposited from high-density turbidity currents in terminal lobes; o) Zoophycus in distal submarine fan environment.

such as debris flows or high- and low- density turbititic currents. The suspension fall-out deposition took place mainly in deltaic and deeper marine environments, often suppressed by gravity flows. Eighteen lithofacies were identified in the studied outcrops (Table 4.1). These lithofacies are organized in eight facies associations (Figs. 4.6 – 4.10), interpreted as alluvial, shallow marine, deltaic and deeper marine depositional systems.

4.4.1. Alluvial fan and shallow marine systems

The alluvial system crops out in a restricted part of the basin (north of Gafarillos village, Fig. 4.1b) and is made up by red multi-storey bodies displaying sheet-like geometry. The flow was often confined by coeval normal faults, which created centimetres to metres wedge-shaped geometries by thickening towards the fault (Fig. 4.10a).

The facies association A1 is characterized dominantly by thick-bedded (0.5 - 2 m) pebble to cobble conglomerates and coarse-grained sandstones (F1, F2 less common F10, Table 4.1, Fig. 4.6a). They are poorly sorted and immature, and contain a large compositional diversity of clasts (such as quartzite, schists, dolomites, marble, recycled conglomerates and sandstones). The base is planar with small scale erosional relief (<10 cm). The succession is intercalated with thin-bedded (<0.1 m) fine-grained sandstones and siltstones (F9, F13, Table 4.1). This facies association overlies unconformably the pre-Miocene basement and is gradually replaced by the A2 facies association (see below). The facies association A1 is interpreted

Figure 4.7 (facing page): A detailed sedimentary log of the alluvial to shallow water marine environment transition observed in the SE part of the Sorbas Basin. See Table 4.1 for facies details and Fig. 4.1b for the log location. FAA1 and FAA2 – Facies association A1 and A2, respectively; FAB- Facies association B; FAC1- Facies association C1. The grey rectangles with numbers represent stages of fault activity: 1 - high displacement rates; 2 - gradual termination of the faulting activity, and 3 - fault quiescence.

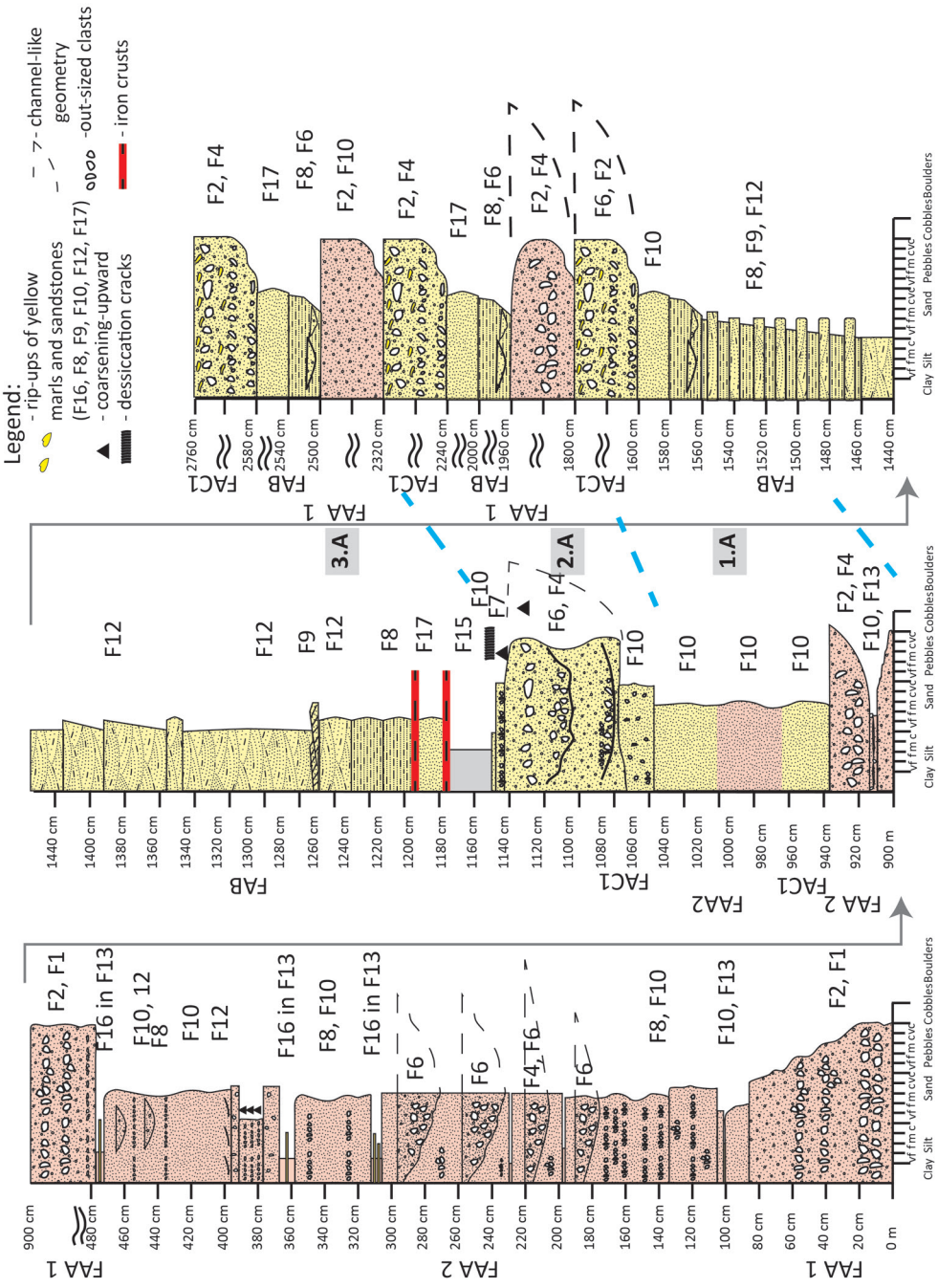
Legend:
- rip-ups of yellow marls and sandstones (F16, F8, F9, F10, F12, F17)
- coarsening-upward
- dessiccation cracks
- channel-like geometry
- out-sized clasts
- iron crusts
FAA 1
FAA 2
FAB
FAC1
FAA2
3.A
2.A
1.A
Clay Silt Sand Pebbles Cobbles Boulders
vf f m c vf f m c vc vf f m c vc

as a proximal alluvial fan system dominated by deposition of debris flows (e.g., Nemec and Steel, 1984; Blair and McPherson, 1994). The angularity and lithological nature of the clasts derived from the surrounding metamorphic basement suggest a proximal source area located in the neighbouring sierras. The clasts derived by eroding the fault scarp indicate that these flows originated from remobilization of colluvial rock-fall deposits at the base of an active fault (e.g., Blikra and Nemec, 1998; Longhitano et al., 2015). Intra-basinal clasts suggest footwall degradation of syn-depositional faults and re-deposition in the same area.

The facies association A2 is characterized by medium-bedded (0.2-1.2 m) sand prone deposits (F2, F3, F7, F8, F10, less common F4, F5, Table 4.1, Fig. 4.6b). These deposits are often channels filled with pebble to cobble conglomerates with erosive base and gradational top. The imbrication and plane cross-bedding indicate a SW-wards flow direction. The sandstones are often interbedded with finer deposits (F9, F11, F13, Table 4.1). This facies association grade into facies association C1 (see below). The facies association A2 is interpreted as deposition in a medial to distal alluvial fan environment dominated by flood-related braided flows alternating with debris flows (e.g., Nemec and Postma, 1993; Barrier et al., 2010). Finer clastics were deposited by combined waning flows and suspension in a lower energy environment. The cross-stratified bed sets and channels with erosive base resulted from migration of small distributary channels within a fan system (e.g., Blair and McPherson, 1994). General alternation of proximal and distal alluvial fan deposits in the vertical succession can be interpreted as self-induced avulsion of an alluvial fan system, change in the sediment supply due to source area uplift or seasonal fluvial discharge (e.g., Gawthorpe and Collela, 1990; DeCelles et al., 1991; Andrić et al., 2017).

The facies association B is characterized dominantly by tabular medium-bedded (0.05-0.4 m) well sorted yellow calcareous sandstones (F8, F9, F12, F17 and minor F10, Table 4.1, Fig. 4.6c). These sandstones may be structure-less or contain climbing-ripples and trough-cross bedding, often draped by mud. Parallel and ripple-cross lamination is less obvious. Beds are separated by thinly-bedded (0.01 - 0.15 m) mudstone layers (F15, Table 4.1). Towards the top, this facies association becomes locally pebbly with strings or isolated outsize clasts. This facies associations shows a general coarsening-upwards trend and is deposited beneath or lateral with respect to delta deposits (i.e. delta channel, C1, see below). This is observed by staked, sharply based, well sorted sandstones with ripples and oppositely directed low-angle cross-bedding that indicate deposition from recurrent flows (e.g., Gowland, 1996; Young et al., 2000). The facies association B is interpreted as shallow marine waves and tidal deposits with low or outside fluvial influence. Mudstone drapes suggest periods of quiescence and deposition from suspension. The relative good sorting and lack of coarser-grained material in the lower part of the succession suggest low clastic sourcing and reworking (e.g., Carr et al., 2003). In the upper part of the coarsening upwards sequence, the occurrence of outsized clasts and pebbly strings infers a higher proximal clastic influx (e.g. Young et al., 2000).

4.4.2. Deltaic system

The facies association C1 is characterized by thick-bedded (0.7-1.5 m) conglomerates and sandstones (F2, F4, F6, F10, F17, minor F3, Table 4.1, Fig. 4.6d). The individual bed geometry varies from wide channels with erosive base and rip-ups of underlying fine sandstones and marls, to less frequent sheet like layers with planar base. They include shell fragments (Pectens, oysters, <5%). This facies association alternate with facies associations A and B by building coarsening-upward successions (Fig. 4.7). The contact with facies association B is gradual (over ~1 m), while the contact with facies association A is sharp. The facies association C1 is interpreted to be deposited from high energy hyperpycnal and debris flows based on the presence of channels, rip-ups fragments and a general coarsening-upward trend. These sedimentary features are typical for deposition at the mouth of river-dominated deltas (i.e. delta plain, e.g., Garcia-Garcia et al., 2006).

The facies association C2 is characterized by alternation of thick-bedded conglomerates and sandstones (0.2-2 m) (F1, F2, F7, F8, F10, Table 4.1, Fig. 4.6e,f,g) and thinly-bedded (0,1 m to 0,2 m) yellow marls (F16, Table 4.1, Fig. 4.6f). The sandstone and conglomerate beds have generally a sheet-like amalgamated geometry, where amount of matrix and grain-size vary vertically and laterally. The amalgamated beds may be up to 8 m thick. Bed bases are plane to slightly erosional. The conglomerates show high textural maturity and roundness and may be imbricated. Most sandstones are normally graded and contain variety of sedimentary structures, parallel lamination, climbing ripples, flaser lamination and ripple cross-lamination. Occasionally, sandstones are structure-less with floating clasts or pebble to cobble strings. Well rounded outsized clasts (up to 1 m) are common. This facies association passes into facies association C1 upslope and C3 downslope. This association commonly forms upward coarsening units of tens of meters. The facies association C2 is interpreted to be result of deposition from concentrated, high-energy flows (dominated by debris flows and granular flows and where turbulent flows are less common) during high discharge episodes in delta front environment (e.g., Young et al., 2000; Schomacker et al., 2010). These flow episodes are separated by periods of low discharge that allow sediment redistribution and reworking by waves and tides, colonization and bioturbation (e.g., Dabrio et al., 1990; Aschoff et al., 2016). Relatively small bedset thicknesses indicate deposition in shallow water environment (~10`s of meters of water), where the absence of clinoforms suggests deposition in a coarse-grained shoal water type of fan delta (e.g., Lewis et al., 2015; Postma, 1990).

The facies association C3 is characterized by alternation of thin-bedded (0.01 m to 0.15 m) of medium- to fine- grained sandstones, siltstones, mudstones and marlstones (F7, F8, F9, F13, F16, F17, Table 4.1, Fig. 4.6h,I, j). Individual beds have a sharp planar base. The medium- to fine-grained sandstones are well sorted, usually showing ripple-cross lamination (climbing, symmetric and asymmetric), wave ripples and horizontal lamination (Fig. 4.6i). These sandstones have rare convolution or hummocky lamination and contain locally burrows and plant material (Fig. 4.6j). Near the transition with facies association C2, these sandstones may contain floating clasts or strings. The facies association C3 is interpreted to be deposited in a low energy prodelta environment, with periodic low- and high-

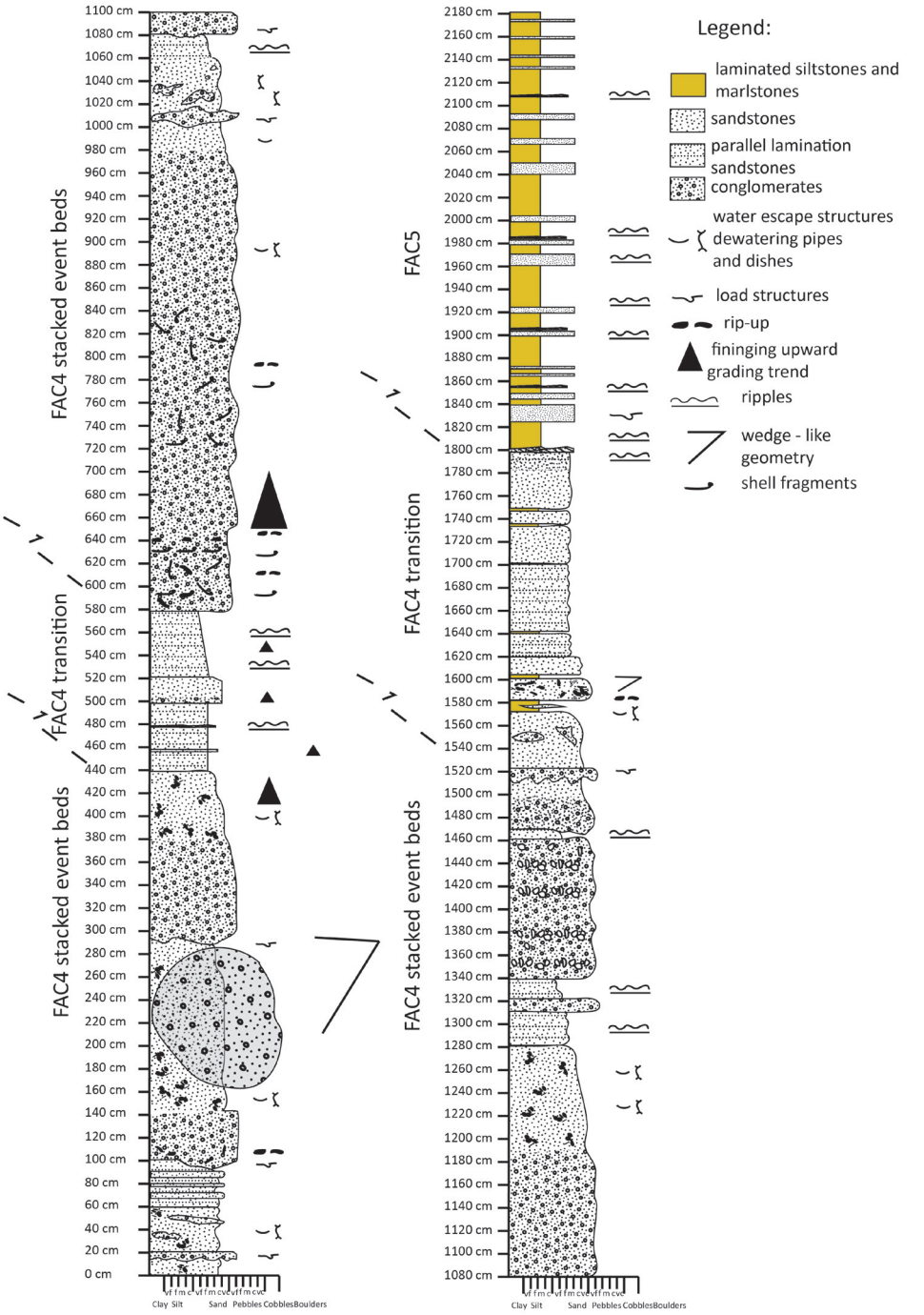

Figure 4.8: Detailed sedimentary log of a prograding submarine-fan into the basin plain environment in the SE part of the Sorbas Basin. See Fig. 4.1b for the log location. FAC4- Facies association C4; FAC5- Facies association C5.

density turbidity currents derived from a continental source (e.g., Mulder and Alexander, 2001; Garcia-Garcia et al., 2011). The rare hummocky bedforms indicate an influence of storm waves due to either combined flows (waves and currents) or complex oscillatory flows (e.g., Arnott and Southard, 1990). The presence of benthic organisms (i.e. vertical and horizontal burrows, Skolithos) together with wave and tide generated sedimentary structures indicate deposition above fair-weather wave base in sublittoral zone (e.g., Aschoff et al., 2016).

4.4.3. Deeper marine system

The facies association C4 is characterized by an alternation of tabular and wedge shaped thick-bedded (0.5 - 1.2 m) facies dominated by sandstones and conglomerates (F7, F8, F18, occasionally F1 and F2, Table 4.1, Fig. 4.6k,l) and medium to thick-bedded (0.1 - 1 m) fine-sandstone and siltstone facies (F8, F9, F13, Table 4.1). The base of individual beds is sharp and partially loaded. Locally, this association contains wide channel-like geometries and scours with erosional base and granular/pebble lag and rip-ups (Fig. 4.6l). Sandstone-rich beds are often stacked, which creates 4 - 8 m thick units (Fig. 4.8). The internal division surfaces are represented by aligned mud rip-ups, shells and/or grain-size breaks. Water escape structures, sand injections and mud rip-ups are common (hybrid beds, H1 division of Haughton et al., 2009). The fine-sandstones/siltstones include up to 40 cm thick hybrid beds with an upper banded division (H2 division of Haughton et al., 2009). The internal banded structure is marked by monotonous variation in clay matrix in sandstones. Sandstones are structure-less or may show parallel lamination. The succession is organized in coarsening- (and finning-) upward sequences that alternate vertically and laterally with facies association C5 (Fig. 4.8). The facies association C4 is interpreted to be result of rapid deposition from high density turbidity and debris flows at high aggradation rates, deposited in the lower part of the slope and axial part of proximal submarine lobes (e.g., Kneller and Branney, 1995; Prélat et al., 2009; Talling et al., 2012). Unusually, thick coarse-grained sandstone and fine-grained sandstone/siltstone are deposited from hybrid flows showing evidence of flow transformation from poor to more cohesive flows (e.g., Haughton et al., 2009). Locally, these deposits are reworked by distributary channels which bypass material further into the basin (e.g. Stevenson et al., 2015). The fine sandstone/siltstone unit suggest deposition from dilute turbidity currents and hybrid flows outside the main lobe (off-axis or fringes, e.g., Prélat et al., 2009). The presence of boulders and slumps indicate deposition along a relatively steep slope (e.g. Blair and McPherson, 1999).

The facies association C5 is characterized by thin bedded (0.01-0.1 m) heterolithic packages of mudstones, siltstones, fine thin sandstones (F13, F14, F15, Table 4.1, Fig. 4.6m,n,o) intercalated with fine- to medium- grained sandstones (F7, F8 and F9, Table 4.1). Bedding is marked by sharp vertical alternations of dark yellow and light grey beds, mm to cm scale. Sandstones (0.1 - 0.2 m thick) intercalations divide this monotonous succession on packages of variable thicknesses (0.1 - 0.9 m). Beds are continuous tabular to lobate. Channel-like bed geometries are rare and associated with medium- to coarse - grained sandstones (Fig. 4.9f). Thicker and coarser sandstone layers occur more frequently in close stratigraphic proximity

(within 1 - 2 m) of proximal submarine fan facies association (C4). This facies association is commonly observed as tens of meters' thick intervals that can be interrupted by chaotically deformed packages of autochthonous material (up to 2 m thick) or sandstones (F18, Table 4.1, Figs. 4.3g,h and 4.9a). They include folded heterolithic beds and rip-ups enclosed in a poorly sorted silty/sandy matrix. They have sharp to erosive contact towards the surrounding undeformed heterolithic packages. This chaotic facies is associated with normal faults up slope and reverse fault down slope. The facies association C5 is interpreted as a product of combined deposition from dilute turbidity currents and suspension fallout in a distal submarine fan environment over the basin plain (e.g., Bouma, 1962; Talling et al., 2012). Planar, climbing-ripple and ripple lamination resulted from bed tractional reworking under moderate to high aggradation rate (e.g., Southard, 1991; Mutti, 1992; Talling et al., 2012). Isolated sandstones beds represent the expression of the distal-most progradation of high density turbidity flows bypassing the lobe environment (e.g., Talling, et al., 2012; Stevenson et al., 2015). The intercalated chaotic packages suggest syn-depositional deformation due to remobilization of autochthonous intra-basinal material (e.g., Spychala et al., 2017). When combined with normal faults up slope and reverse faults downslope, this facies association shows periods of gravitational sliding, i.e. toe slope decollements (e.g., Postma, 1984).

4.4.4. Sedimentological events during deposition

We use the term 'event-bed' in the sense of a depositional event characterized by contrasting lithologies that reflects the stacking of one or multiple flow types, which does not necessarily mean that beds are isolated or unusually thick. Such event beds are rather frequent in the studied sedimentary succession (Fig. 4.9). Near the source area, these beds are observed as thick packages of proximal alluvial fan deposits deposited over distal alluvial or deltaic sediments (Fig. 4.7). The rapid transition of facies associations, angularity and nature of the clasts suggests that the deposition was interrupted by moments of rapid uplift and erosion of normal fault footwall scarps and sedimentation in their proximity (e.g. Longhitano et al., 2015). In more distal marine environment, six types of event beds are marked by clear and contrasting sedimentation.

The event bed type 1 is characterized by chaotically deformed (i.e. folded, bed raft, rip-ups, Fig. 4.9a) thin bedded heterolithic packages enclosed within a poorly sorted silt to clay matrix. These beds have sharp upper and lower boundaries. They occur within distal submarine fan facies associations C5 and reach 2 m thicknesses. Deformation along such beds is often connected along a decollement to a break-up zone made up by normal faults, while frequent isolated rafts affected by thrusts or normal faults are observed in the field (Figs. 4.3f, left part and 4.3g). In some instances, the close association with normal faulting is observed by the decollement starting at these faults in their syn-kinematic deposits. The event bed type 1 is interpreted as a toe-slope decollement created by gravitational sliding which evolved into debris flow along the depositional slope on the way to the submarine fan environment (e.g., Talling et al., 2012). In such an environment, slides and debris flows could be initiated by intra-basinal slope steepening, liquefaction

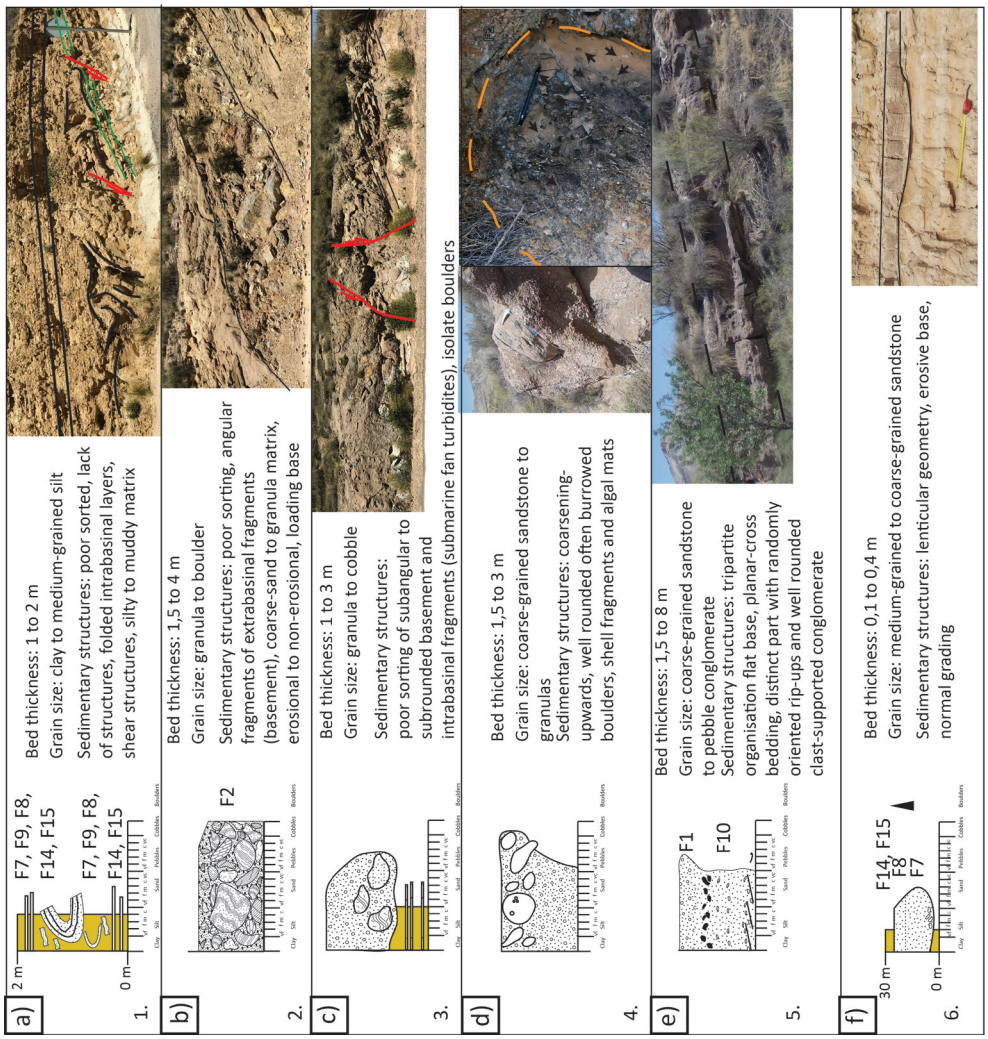

Figure 4.9: Typical examples of event beds. See Table 1 for facies details and Fig. 4.1b for photo locations. a) event bed type 1 resulted from seismically triggered slope collapse, leading to remobilization and embedding of intra-basinal layers and clasts within a distal submarine fan environment (facies association C5) ; b) event bed type 2 resulted from uplift and erosion of the footwall, leading to direct delivery of the extra-basinal material into a distal submarine fan environment by debris flows; c) event bed type 3 resulted from slope failure due to activity of intra-formational faults; d) event bed type 4 deposited from debris flows, which were main drivers for re-deposition of material from shallow environment further into the basin; e) event bed type 5 resulted from debris flow partitioning on the long run out path; f) event bed type 6 formed as isolated distributary channels within a distal submarine fan environment.

of underlying mud-rich deposits and/or failure generated by overpressure due to high sedimentation rate on the slope (e.g., Gee et al., 1999; Bull et al., 2009). In our

studied case, the close association with normal faulting demonstrate that sliding was driven by tectonics. These slides were most likely triggered by fault induced seismicity (e.g., Bugge et al., 1988; Spychala et al., 2016), similarly with what has been previously discussed in the neighbouring Tabernas Basin (such as the "Gordo mega-bed" of Kleverlaan, 1987). However, when compared with the large-scale Tabernas chaotic mega-beds, our type 1 event is smaller and do not appear to have a basin-wide continuity.

The event bed type 2 is characterized by angular out-sized extra-basinal clasts (up to 2 m) enclosed within poorly sorted sandy matrix (Fig. 4.9b). Beds are often isolated and interbedded within relatively finer layers abundant with water escape structures. The event bed type 2 is observed in the apical parts of coarsening-upward sequences in submarine fan deposits (Fig. 4.11a,b). The event bed type 2 is interpreted as a result of rapid deposition from land-derived debris flows bypassing the shallow water and slope and depositing material in the submarine fan environment (e.g. Leppard and Gawthrope, 2006). The character of beds (oversized angular extra-basinal clasts) indicated that these flows were generated in alluvial environment by remobilisation of rock-fall material eroded from the uplifting footwall of the basin bounding fault.

The event bed type 3 is characterized by a bipartite organisation. The lower division is comprised of sandy matrix supported outsized clasts, extra-basinal (dolomites, schists, marbles) and intra-basinal (medium- to coarse-grained turbidites). The upper division consists of structure-less sandstones (Fig. 4.9c). The event bed type 3 is interpreted to reflect cohesion-less debris flow deposition that was followed by high-density turbidites deposited as part of the same general waning event (e.g. Talling et al., 2012). The intra-basinal clasts resulted from footwall uplift and degradation of normal faults, shedding material towards the distal submarine fan environment. Faulting caused coeval slope instability, leading to remobilisation of reworked extra-basinal clasts that are mixed with the intra-basinal material along the slope on the way to the distal submarine fan environment. The location of intra-basinal normal faults localized the gravity flows on the basin plain (Fig. 4.9c).

The event bed type 4 is characterized by out-sized well rounded cobbles and boulders of extra-basinal clasts (dolomites, schists, marbles), whereas some dolomite clasts contain lithophaga borings (Fig. 4.9d). They have bipartite organisation with a matrix-supported pebbly sandstone that is coarsening-upwards to a cobble - boulder conglomerate. The event bed type 4 is interpreted to result from redistribution of avalanching material along an unstable slope (e.g., Postma, 1984). Frequent borings suggest storage and reworking of the material from a delta plain or beach environment before re-deposition further into the basin (e.g., Puga-Bernabeu, Martin and Braga, 2007; Lewis et al., 2015). The remobilization of material stored in the shallow water environment can be induced by the seismically triggered slope failure or high fluvial discharge (e.g., Haughton et al., 2009; Garcia-Garcia et al., 2011).

The event bed type 5 is characterized by a tripartite organisation (Fig. 4.9e). The lower part of the bed may include planar cross-bedding formed by alternating matrix-supported conglomerates and pebbly sandstones flat bands (F1, F2, F10,

Table 4.1). The middle of the event bed is composed of sandstones with silt to clay matrix and narrow zones of randomly oriented marls (often yellow) rip-ups and scattered pebbles. The upper part is made up of a clast-supported conglomerate. The event bed type 5 is interpreted to be result of partitioning the debris flow along the slope (hybrid flow, e.g. Haughton et al., 2003; Kane and Pontén, 2012). Our observations suggest that the debris flow may transform partially to an independent forerunner turbidity current on long run out paths (i.e. long transport far into the basin, e.g., Haughton et al., 2003; Haughton et al., 2009). During such transport, the turbidity current decelerates and becomes dilute enough to develop planar cross-bedding at the base of event beds (Fig. 4.9e). Similar bed types (i.e. turbidites linked with debrites) are common in distal and lateral margins of deep water systems caused by failure of a syn-tectonic slope (e.g., syn-rift Jurassic submarine fans of the North Sea Basin, Haughton et al., 2003). This scenario is inferred by extra-basinal components and rip-ups of shallow water marls.

The event bed type 6 is characterized by isolated medium- to coarse- grained sandstones interbedded within a finer distal submarine fan facies association C5 (Fig. 4.9f). This event bed has often a channel-like geometry, granular at the base, general coarsening-upwards pattern and climbing ripple-cross lamination. The event bed type 6 is interpreted as an episodic influx of land-derived material into a distal submarine fan environment. The material was transported along distributary channels in a distal terminal lobe, most likely derived from turbidity currents originated from concentrated hyperpycnal flows during a high discharge (e.g. Garcia-Garcia et al., 2011).

4.4.5. Syn-kinematic sedimentation

Clear syn-kinematic deposition is observed in sedimentary wedges deposited against normal faults and sealed by finer grain sediments. As a function of the direction of normal faulting and the related attitude of the slope along which the basin was supplied by terrestrial material, we distinguished two types of syn-kinematic wedges: synthetic (same directions) and antithetic (opposite directions). This means that synthetic wedges are supplied by terrestrial material across or along a footwall slope created by normal faults, while antithetic wedges were supplied by terrestrial material along a slope created by antithetic tilting of hanging-walls against normal faults. Both synthetic and antithetic wedges thicken towards the fault and pinch out in a hanging wall direction, but are oriented differently relative to source area, i.e. they thicken SW-wards and NE-wards, respectively. Both are locally observed to be associated with footwall uplift and erosion.

In the alluvial and deltaic succession, synthetic wedges are controlled by centimetres to decimetres offset of low- and high- angle normal faults (Fig. 4.10a-c), while antithetic wedges are less common. These wedges are matrix-supported (cobble to pebble) sandstones and conglomerates that have often outsized clasts derived from cohesive debris flows (F2, Table 4.1, Fig. 4.10a-c). These observations show rapid deposition driven by the instability of a syn-tectonic slope. An increase in mud content enhances the flow strength, which enables the transport of out-sized clasts (e.g., Talling et al., 2012). The inter-bedding or sealing of wedges with finer

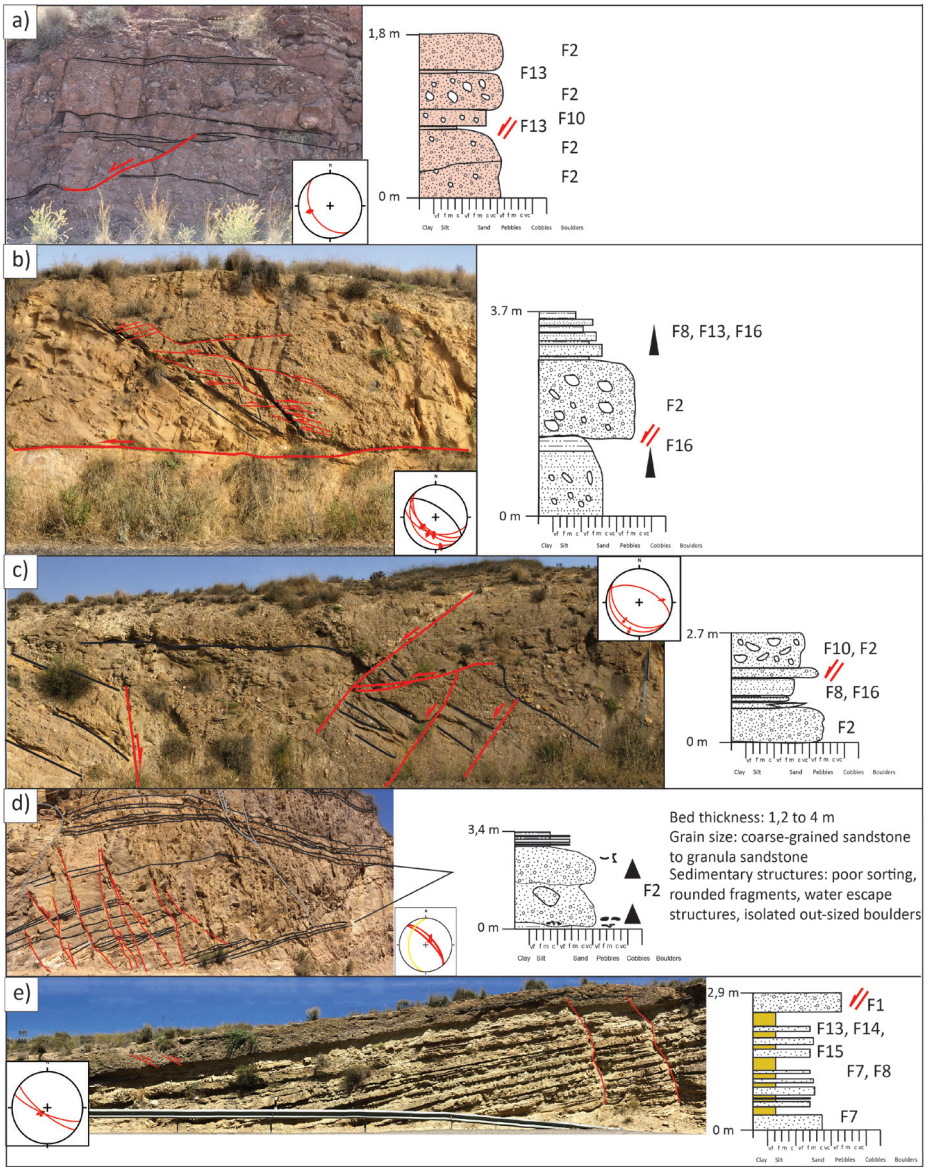

Figure 4.10: Typical examples of syn-kinematic wedges associated with normal faults. See Table 4.1 for facies details and Fig. 4.1b for photo locations. a) syn-kinematic wedges developed in a distal alluvial environment associated with synthetic normal faulting; b) syn-kinematic wedges developed in a delta front environment associated with synthetic normal faulting; c) syn-depositional domino normal faults triggering a deposition of matrix - supported sandstones in a delta plain environment; d) a syn-kinematic wedge that is controlled by antithetic rotation of a hanging-wall during faulting in a submarine fan environment; e) a coarse-grained debris flow event confined by the activity of normal faults in a distal submarine fan environment.

clastic sediments is interpreted to result from diluted or waning turbidity currents and/or suspension fall out during moments of tectonic quiescence (F14, F15, F16, Table 4.1). Rapid changes of sedimentary facies across these wedges show local forced progradation of more proximal (higher energy) over distal (lower energy) facies, driven by the activity of normal faults. However, these faults may confine distributary channels and influence the lateral migration of the fan system.

A large number of synthetic and antithetic wedges was observed in the marine succession (Figs. 4.3a,b and 4.10d,e). Some of these wedges illustrate a rapid transition from distal to proximal positions even at the level of one bed or bed set (Fig. 4.10e). Such wedges are made up of debris flow and high-density turbiditic flow deposits. More complex, larger scale antithetic wedges grouping several syn-kinematic layers are related to large offset ramp-flat normal fault systems (Fig. 4.3a,b). Several simultaneous wedges with variable ramp offsets are associated with a coarse influx of debris flows, which is sealed by finer grained lithologies in the overall submarine fan environment (Fig. 4.3ab). Successive offsets along these faults are clearly observed to be associated with high-frequency sedimentary cycles, which are otherwise very similar in expression with the autogenic cyclicity created by a submarine lobe shifting, driven by migration or instability of distributary channels (e.g., Prélat et al., 2009).

4.5. Discussion

4.5.1. Normal faulting controlling high – order tectonic cyclicity in the Sorbas basin

Observations of normal faults offsets in the studied part of the Sorbas basin shows that the subsidence and the associated accommodation space was created mainly by NE dipping normal faults, i.e. dipping towards the location of the exposed basement not affected significantly by the subsequent inversion (Figs. 4.3 and 4.4). This observation means that the accommodation space was created by hanging-wall tilting and filled dominantly by antithetic wedges. The sedimentation observed in the basin was controlled by the rate of displacement along normal faults, influencing the evolution of the slope, together with the amount and character of the sediment supply (Fig. 4.11).

High displacement rates along normal faults were associated with a sedimentation dominated by a discharge of coarse-grained material in shallow water environment (Fig. 4.11f1, i.e. facies associations A1, A2, C1 and C4, Table 4.1). The subsidence and slope failure by normal faulting resulted in narrowing the shelf and a retrograding depositional trend observed in proximal areas by the transition from alluvial to deltaic associations (Fig. 4.7, location 1.A). The deltaic material previously trapped in shallow water environment during tectonic quiescence stages is remobilized during fault steepening and slope failure deeper into the basin by toe-slope decollements and debris flows (Fig. 4.11a,b). Such debris flow mixing sand and clay material create the relatively isolated event beds type 1, 3 and 4 embedded within distal submarine fan deposits (Fig. 4.9a,c,d). Immediately after slope failure, the debris flows incorporate ambient water and material on

a)
fault quiescence
low displacement rates
high displacement rates
fault quiescence
70cm
42°
35°
30°
b)
fault quiescence
low displacement rates
high displacement rates
fault quiescence
25 m
20 m
15 m
10 m
5 m
0 m
Clay Silt Sand Pebbles
c)
fault quiescence
low displacement rates
10°
20°
d)
4 m
0 m
fault quiescence
low displacement rates
vf f m cvf f m cvf f m cvf
Clay Silt Sand Pebbles
e)
f)
1.
2.
3.
Legend
load structures
rip-ups
lobe-like geometry
fining- /coarsening-upwards grading trend
channel-like geometry
soft sediment deformation
water escape structures
retrograding depositional trend
progradational depositional trend
hanging-wall rotation
erosion of uplifting basement and subsequent deposition into the basin

Figure 4.11 (opposing page): Field examples of deposition controlled by slope steepening and shallowing, illustrating the concepts of system tracts formed during high- and low- displacement rates along normal faults, as well as during tectonic quiescence. See Fig. 4.1b for photos location. a) coarsening-upward succession reflecting the overall prograding and aggrading depositional trend at the toe of the slope, formed during slope steepening to more than 10°. The orange lines mark the location of the sedimentary log in Fig. 4.11b. The thick blue line marks the start of the sequence controlled by normal faulting. Dashed blue lines mark the separation between system tracts. Green star represents the position of backsets in Fig. 4.11e; b) detailed sedimentary log of the coarsening-upward succession in Fig. 4.11a; c) retrogradational depositional trend following slope shallowing and exhaustion of source area formed during the transition from the low displacement rates to tectonic quiescence system tracts. Red arrows indicate aggradational onlapping geometry (1. 5 m high traffic sign for a scale); d) detailed sedimentary log showing a fining upward succession deposited during gradual termination of faulting activity and subsequent slope shallowing; e) Inset of Fig. 4.11a showing scour fill with up dip sigmoidal backset stratification formed due to hydraulic jump (20 cm long measuring tape for scale). Black dashed line shows the sigmoidal stratification. Black thick line shows the background bedding; f) interpretative sketches showing sedimentary response to hanging - wall antithetic rotation during three main stage of fault activity that separate individual system tracts controlled by tectonics: 1 - high displacement rates; 2 - low displacement rates, and 3 - fault quiescence.

the way leading to their partial transformation into a high-density turbitidic flow. This high-density turbiditic flows becomes stratified, due to inability to support all particles by turbulence (e.g., Sumner et al., 2008; Postma et al., 2014). The lower layer remains concentrated and becomes supercritical. The upper layer is a low concentrated flow that transports finer fractions further into the basin plain (F8, F9, F13 and F14 facies, Table 4.1). The lower supercritical flow undergoes an erosive hydraulic jump and decelerate at the base of the slope (e.g., Postma et al., 2009; 2014), observed by coarse-grained deposits with soft-sediment deformation, rip-ups and scours filled with upslope dipping sigmoidal crude layering (Fig. 4.11a,b,f; backfill, Postma et al., 2009; 2014). These scours are typical for toes of steep slopes where incoming supercritical turbulent flows suddenly decelerate and experience erosive hydraulic jump producing a cut - and - fill architecture (e.g., Mutti and Normark, 1987; Cartigny et al., 2014; Henstra et al., 2016). This is followed by the flow being transformed back to supercritical, which carry coarse-grained material further into the basin by deposition in an event bed type 5 (e.g. Postma et al., 2009; 2014). These processes create a general progradation and growth of the fan.

During the same stage of high displacement rates, the sedimentation is characterized by finning upward cycles (e.g., Fig. 4.7, location 1.A), due to rates of creating accommodation space higher than the sediment supply. The exception is deposition at the toe of the slope, where sedimentary succession is characterized by sharp contacts and a coarsening-upward grading trend (Fig. 4.11a, b, f1). Here, the base of the succession is marked by a sudden appearance of thick high-density turbidites and cohesion-less debris flows, overlaying the fine-grained sediments of the distal submarine fan and basin plain (Fig. 4.11b). This toe deposition is coeval with a slope steepening that may increase to 10° inclinations (Fig. 4.11a, b). This steepening was created mainly by normal faulting and associated antithetic rotations, combined to a lesser extent with autocyclic processes such as

compensational stacking (Mutti and Sonnino, 1981; Prélat et al., 2009) or upslope knickpoint retreat (e.g. Haughton et al., 2009).

At lower displacement rates, when normal faulting gradually decreases, the creation of accommodation space is overpassed by the sediment supply (Fig. 4.11f2). This stage is associated with enhanced erosion in the footwall of synthetic normal faults and degradation of the source area, observed by dry mass-waste transport (i.e. rock-fall) to the immediate hanging-wall (e.g. Longhitano et al., 2015) and syn-kinematic clastic wedges filled with basement material (Fig. 4.10a). These sediments are subsequently remobilized and transported further into the basin by land-derived concentrated hyperpycnal flows that often bypass the delta plain and are deposited at the base of the slope or in the basin plain. This sedimentation is observed by the deposition of event beds type 3 or smaller counterparts, which are often located in the apical parts of an overall coarsening-upwards trend (Figs. 4.9b and 4.11a,b). Some material was temporarily stored in the delta plain and later transported by debris flows that underwent a transformation from high- to low-density turbidity flows, sending material to the basin plain. The overall sedimentation of this stage is characterized by a prograding and aggrading depositional trend, observed as a coarsening-upward succession (Figs. 4.7, location 2.A and Fig. 4.11a,b,f2). This is observed in proximal environment by a gradual transition from shoreface to deltaic and alluvial facies, and by an increase of basement derived material (Fig. 4.7, location 2.A).

The periods of active normal faulting are separated by stages of tectonic quiescence, when the source area is already degraded (Fig. 4.11f3). This is observed by the dominantly coeval deposition of the facies associations A2, B, C1, C2, C5 (Table 4.1). The material shed by the source area is mainly trapped and reworked by fluvial, wave and tidal processes in a proximal shoreface environment. Intercalations of carbonate rich mudstones with abundant burrowing fauna (oysters, pectin, lithophaga borrings) reflect a low energy environment. The main mechanisms of deposition in deep-water environment are diluted turbiditic currents and suspension fall out, irregularly interrupted by high density flows (e.g., event bed type 6, Figs. 4.6n and 4.9f), further on transformed in diluted flows. These high density flows were most likely created by the down-dip transformation of cohesion-less to cohesive debris flows by incorporation of fine grained material (e.g., Henstra et al., 2016). This is observed by the transition from clast- to matrix-supported conglomerates in the upper part of the slope that are laterally replaced with normally graded and horizontally bedded sandstones. The decrease in the slope inclination initiated during the gradual cessation of fault activity is also continued during the tectonic quiescence stage, observed by a retrogradation and fining-upwards trend at the toe of the slope (Fig. 4.11c,d,f3). In the deep water, the main mechanism of deposition is by axial flows, which rework existing sediments, facilitated by the reduction of coarse-grained fault perpendicular sourcing. This is visible by the direction of transport in channels observed in the fining upward sequence of the proximal submarine fan (Figs. 4.5l and 4.8).

In general, the higher order tectonic cyclicity in Sorbas basin is created by the normal faulting is observed by successive coarsening- and fining-upward grading trends surpassing the inherent autocyclic character of the turbidictic deposition. The coarsening-upward trend is associated with a submarine fan growth and a net

prograding depositional trend in the basin following the deceleration of faulting activity. The fining-upward trend is observed by retrogradation due to source exhaustion during tectonic quiescence moments.

4.5.2. Low - order tectonic cyclicity in the Sorbas basin

The upper Serravallian – Tortonian extension of the Sorbas Basin created an overall transgressive sedimentation that gradually changed from alluvial to deltaic and deeper marine. Normal faults footwall uplift and hanging-wall tilting enhanced the pre-existing orogenic source area that shed in 4 My the 2km thick coarse clastic influx observed in the basin (e.g., Ott d'Estevou and Montenant, 1990; Do Couto et al., 2012). The initial transgression was followed by a generalized regression during the gradual ceasure of normal faulting that changed ultimately the depositional environment to the shallow-water deposition of the Azagador member. Our observations show that this low-order cycle was clearly controlled by tectonics that surpassed sea-level oscillations, such as the observed global drop of ~ 50 m (~11 – 9 Ma, Miller et al., 2005) and rise of ~35 m (~9 - 8 Ma, Miller et al., 2005).

The high-order cycles controlled by normal faulting described above can be grouped in three stages of coupled tectonic and sedimentological evolution observed in the upper Serravallian – Tortonian sediments (Fig. 4.12). In terms of rift sequence stratigraphy, these stages correspond to rift initiation, early rift climax and middle-late rift climax tectonic system tracts (e.g., Prosser, 1993).

Similar with what was observed elsewhere (e.g., Leeder and Gawthorpe, 1987; Ravnas and Steel, 1998; Gawthorpe and Leeder, 2000), the first stage of rift initiation is associated with the formation of isolated fault-bounding depocentres with relatively small rates of subsidence. Alluvial fan sediments were deposited in such symmetric depocentres bounded by normal faults with small displacement. The succession is characterized by a rapid transition from distal to proximal alluvial fan sediments in the close proximity to the active fault (e.g., Figs. 4.10a and 4.12a). The dominant sedimentation mechanisms are rock fall and debris flows transporting footwall derived material further into the basin by a river system flowing along the axis of these depocentres. Sediments have simple wedge-shaped geometries that are directly dependent on the available accommodation space created in the normal faults hanging-walls and the sediment supply from the immediate footwalls (e.g., Quirk, 1996).

The early rift-climax stage is composed of alluvial and delta fan deposits (Fig. 4.12b). Hanging-wall antithetic tilting is the main driver for basin subsidence, sedimentation and the creation of a gentle slope into the basin. The basin slope creates a shoal-type fan delta (2-5° slope dip, e.g. Garcia-Garcia et al., 2006), where sedimentation is dominated by gravitational flow processes such as debris and grain flows that transform into high-density turbidity currents in the deeper water (Fig. 4.5g). The deltaic system was deposited at the shoreface, with water depths of ~10 - 15 m, controlled by the subsidence created by normal faults and influenced by fluvial, wave and tide processes.

The middle-late rift climax stage is predominately composed of delta slope and basin plain deposits (Fig. 4.12c). This is when the normal faulting took place

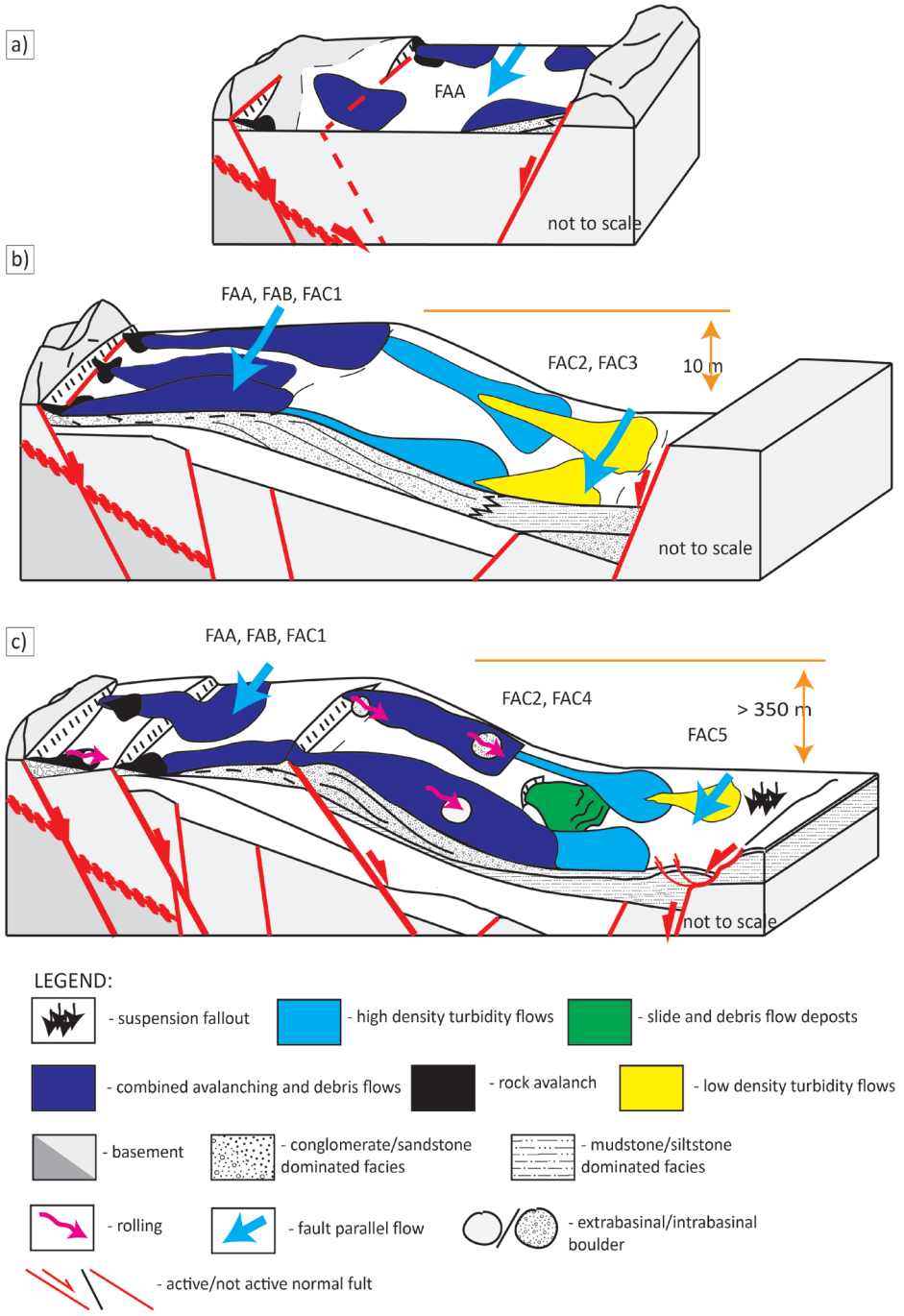

Figure 4.12: Evolution of depositional environments during three stages of evolution of an asymmetric extensional basin. a) The rift initiation stage characterized by progradational and aggradational of alluvial fans sourced from immediate footwalls of normal faults creating multiple depocentres formed by the distributed deformation. No marked asymmetry is

Figure 4.12 (continued): observed during this stage; b) the early rift – climax stage, when hanging – wall antithetic tilting drives the subsidence and creates an asymmetric depocenter. The depositional system is dominated by alluvial fans and shoal type fan deltas delivering material into the basin along the hanging – wall slope; c) the middle – late rift climax stagedominated by coeval deposition of prograding and aggrading alluvial, delta and submarine fans, similarly controlled dominantly by the continuation of tilting by hanging-walls antithetic rotation. FAA – facies association A; FAB – facies association B; FAC1 – facies association C1; FAC2 – facies association C2; FAC3 – facies association C3; FAC4 – facies association C4; FAC5 – facies association C5.

dominantly inside the basin, enhancing the subsidence and creating a deeper marine environment that reached ~350 m (e.g., Ott d` Estevou et al., 1981). Normal faults offsets reach ~30 m, increasing the observed hanging-wall depositional slope to around 10°. This leads to slope failure recorded by event-beds 1, 3 and 4 (Fig. 4.9), the formation of a narrow shelf and dominant deposition at the toe of the slope.

These three successive stages of maximum fault activity were followed in the Sorbas Basin by a continuation of the Tortonian sedimentation that is dominantly observed by a cyclic alternation of packages containing high- and low- density turbidites, which were shed from a gradually degrading source area. The low number of normal faults and the architecture of observed background turbiditic sedimentation indicate a predominant high-resolution autocyclic nature of deposition, combined with episodic tectonic induced cycles (see also Haughton, 2001). The generalized regression ultimately led to the deposition of the shallow water Azagador Member.

4.6. Conclusion

Our combined kinematic and sedimentological study of the extensive outcrop exposures in the lower sedimentary infill of the Sorbas Basin has quantified the balance between the evolution of normal faults and the cyclic character of sedimentation.

The extension changed gradually its direction from NW-SE to NE-SW during the overall transition from continental to marine sedimentation. The mechanics of normal faulting was strongly controlled by the rheological contrast between relatively strong conglomerates and sandstones layers, and weaker finer siltstones and more pelagic deposits. This control is illustrated by the combined presence of high- and low-angle normal faults, ramp-flats and staircase geometries. Deformation affected partially un- or poorly- consolidated sediments that locally resulted in the formation of a fault gouge with a clear foliation and brittle shear bands, incorporating rheologically stronger conglomerates and sandstones blocks in wider shear zones.

Moments of activation of normal faults are associated with the formation of clastic syn-kinematic wedges, composed of coarse - grained material supplied from fault perpendicular and axial drainages and formed predominantly by antithetic tilting of hanging-walls. Deposition took place in alluvial, deltaic, shallow and deep

marine environment during three successive phases of rift initiation and climax, followed by a generalized stage of regression where autocyliclic depositional processes were the main depositional mechanism. Initiation of extension was associated with the formation of isolated depocentres in continental alluvial environment, moments of fault activation being characterized by a transition to rock-fall and proximal alluvial fans. The continuation of extension led to the creation of a shallow-water marine environment dominated by shoal-type deltas and to a deeper environment dominated by turbiditic deposition. The overall deposition was dominated by coarse-grained heterogeneous sediments originated from rock-fall, debris flow, turbiditic flow, hybrid flows and slumps initiated on the deforming basin margin and transported along the hanging-wall slope into the deep marine environment.

These low order stages of basin evolution are composed of a higher order coarsening- and fining- upward cyclicity, controlled by the activity of normal faulting. These patterns reflect the main gravity flow transformation formed in the response to three main faulting stages: the ones of high displacement, gradual termination of the faulting activity and tectonic quiescence. The highest fault displacement rates are characterized by slope failures producing large-scale intra-basinal slumps, co-genetic debris flows and turbiditic flows that resulted in the deposition of event beds embedded within basinal plain sediments. Moreover, the slope steepening induces partial transformation of the debris flows and deposition of linked turbidites and debrites at the toe of the slope. During termination of the faulting activity, the system is dominated by concentrated land-derived hyperpicnal and debris flows, which did not suffer significant transformations before being deposited at the base of the slope. The tectonic quiescence is dominated by down-dip transformation of the non-cohesive to more cohesive flows. The debris flows evolved to low-density turbiditic flows along the slope and continued as a low density further into the basin. In the sedimentary record, these flow transformations are represented as coarsening- and fining- upward grading cycles that reflect prograding and retrograding depositional trends within a submarine lobe environment during the evolution of normal faulting.

Chapter 5. Concluding remarks: integrated geological observations and numerical modelling results

The research presented in this thesis aims to better understand the effects of tectonics on sedimentation in asymmetric extensional basins and magmatism in collisional systems. A detailed, field study has led to a new generic sedimentological model for extensional asymmetric basins typical for the late stage evolution of an orogen. This model is based on case studies from non-marine (Sarajevo - Zenica Basin, Dinarides) and marine (Sorbas Basin, Betic Cordillera) depositional systems. The proposed model suggests certain sedimentological patterns commonly found in asymmetric extensional basins. These findings, provide better understanding of process - response interactions between accommodation space and sediment supply controlled by the normal faulting.

The numerical modelling results emphasize the importance of rheological stratification of the continental crust on the variability of magmatism across the collisional zone. This has led to a new model explaining the migration of magmatism across the orogen by relatively strong lower crustal indentation. Numerical simulations also showed that magmatism has a strong impact on the overall geodynamic evolution of collisional zones, especially in localizing deformation and changing its style. Furthermore, the gradual change of magmatic sources during collisional stages is explained as a response to certain lithospheric-scale processes, i.e. relamination, slab detachment and eduction which followed subduction of oceanic and continental lithosphere along the colliding margins.

Although the numerical modelling setup represents a simplified reality, and our models were not designed to fit a particular natural system, they do serve to better understand the collisional dynamics of the Dinarides. Additionally, the field results from the Sarajevo - Zenica Basin, help to better constrain crustal - scale processes operating during the late – and post – collisional stages in the Dinarides. Particularly, this applies to deformation styles and their migration patterns in relation to surface processes during the Neogene.

5.1. The sedimentation in asymmetric extensional basins

A detailed, field study in the Sorbas Basin has led to a new generic sedimentological model for extensional asymmetric basins. The reactivation of faulting leads to slope formation and changes in behavior of subaqueous gravity flows. The onset of faulting produces slope failures, large-scale intra-basinal slumps, co-genetic debris flows and turbiditic flows resulting in the deposition of chaotic units intercalated with distal facies. These units are present in various tectonic and depositional settings (e.g., Kleverleen, 1987; Moernaut et al., 2014; Ezquerro et al., 2015).

Steep slope gradients induce partial transformation of debris flows and deposition of linked turbidites and debrites at the toe of the slope. These flows are often erosional and bypass flows. The gradual termination of the fault activity and coeval destruction of the uplifted source area influence concentrated land-derived hyperpicnal plumes. Debris flows which did not suffer transformations before deposition, may still be deposited directly at the base of the slope. As the basin becomes filled during tectonic quiescence, the slope becomes shallower and the dominant processes along the slope are transformations of the flows from non-

cohesive to more cohesive flows.

5.2. Tectonically induced cyclicity in asymmetric extensional basins

The observations in the Sarajevo-Zenica and Sorbas basins show the evolution of tectonically induced sedimentary cycles at different scales. In the Sarajevo-Zenica basin, the basin - scale depositional cyclicity is controlled by the migration of extensional deformation. The subsequent foreland-directed migration of extension controlled the back-stepping of the normal faults and basin widening. The gradual exhumation of the source area leads to the source-ward shift of sedimentary environments and basin depocenter. Upon the next faulting event within the footwall of the previous fault triggers a new tectonic cycle that drowns the previous cycle. This results in an overall retrogradational trend in the basin and a complex basin architecture where every low-order tectonic cycle represents one step in the deformation migration. In contrast, a basinward migration of deformation leads to narrowing of the basin and exhumation of sedimentary cycles in the footwall of the active fault and their subsequent destruction by erosion, as observed in the Corinth rift (e.g., Nixon et al., 2016).

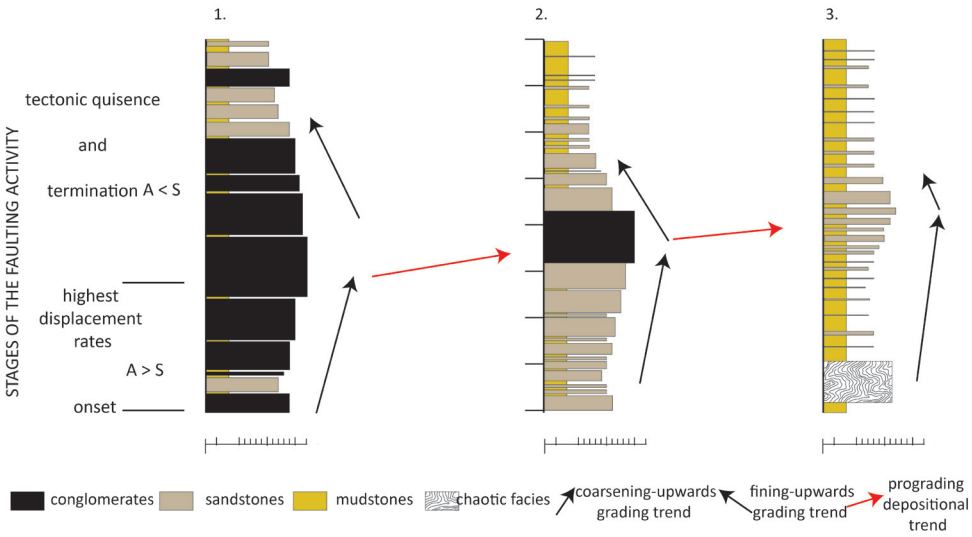

Figure 5.1: Idealized tectonically induced cycles in as asymmetric extensional basin.

Furthermore, lateral variability of the sedimentary patterns perpendicular to the fault in both the Sarajevo-Zenica and Sorbas basins suggests higher order tectonically induced sedimentary cycles that are superimposed on the lower order cycles. Here, high – order cycles describe the balance between accommodation space and sediment supply controlled by the activity of the individual normal

fault (Fig. 5.1). The stages of fault activity, (onset, high displacement rate and tectonic quiescence) control the internal architecture of the high-order tectonically induced sedimentary cycles in the basin. In general, documented tectonic cycles are dominated by prograding depositional trends separating two relatively short retrograding depositional trends, which are described as a coarsening- and two fining-upwards gradational trends, respectively. The basal fining-upward trend reflects the faulting activity (i.e. rapid subsidence outpacing sediment supply). The coarsening-upward succession corresponds to periods when sediment supply outpace accommodation space and fill the basin. The upper, fining-upward trend, suggests a gradual decrease in depositional energy due to exhaustion of the source area during tectonic quiescence. These depositional trends are diachronous across the basin showing a youngening trend basinwards (red arrow on the Fig. 5.1). This diachronous prograding depositional trend reflects the lag time of 2-3 Ma between exhumation of the source area (footwall) and re-deposition of the material further into the basin (e.g., Stojadinović et al., 2017).

At a higher resolution in clastics systems, at the level of one delta or submarine fan for instance, it is often difficult to discriminate cycles driven by fault slip events, climate driven cycles (i.e. high discharge periods) or autocyclic processes such as avulsion. The examples from the Sorbas basin suggest that complex fault geometries may provide a basin floor defect to focus distributary channels and produce even higher order cycles. In the absence of complex fault system, those cycles would be the result of the autocyclic processes or fluvial discharge.

5.3. Magmatism in subduction-collision systems: inferences from numerical modelling

Lithospheric-scale numerical modelling results confirm that magmatism and rheological stratification of the continental crust highly influence the broad geometry and dynamics of collisional zones (see also Gerya and Melik, 2011; Vogt et al., 2012; Vogt et al., 2017). Furthermore, numerical simulations show how percolation of magmatic melts weakens the lithosphere and influences the change of deformational style in the interior of the upper plate (i.e. local extension in the hinterland and formation of back-arc basins coeval with regional crustal shortening in the foreland). Therefore, these changes are not necessarily driven by the migration of the subduction interface, such as significant slab roll-back. For example, the subduction of relatively small oceans is associated with small amounts of retreat which are not enough to produce extension necessary for opening of back-arc basins (e.g., Magni et al., 2014). Therefore, in such cases the melt weakening plays key role for enabling extensional deformation and back – arc basins initiation.

In the case of colliding rheologically stratified continents, the numerical models suggest that foreland-directed migration of deformation and magmatism may be driven by the indentation of the lower continental crust. In such systems, the relatively strong lower crust of the upper plate indents the orogenic wedge and transports material towards the hinterland. There, shortening is accommodated within the upper continental crust favored by rheological decoupling between relatively weak upper and relatively strong lower continental crust. In addition, the

lower continental plate plays an important role in the overall heat budget of such orogens by decreasing the heat flow (i.e. blocking the asthenospheric rise; e.g., Andrić et al., in prep.). In contrast, the orogens in which significant slab-retreat drives magmatic migration show relatively high heat flows (e.g., Aegean, ~ 90 mW/m2, Stiros, 1991; Pannonian region, Balázs et al., 2017). In such cases, the asthenospheric flow freely modulates the thermal state of the lithosphere without interferences from the lower crust.

A noteworthy feature of the numerical models is a gradual change in the magmatic sources from predominately mantle to crust derived. In more detail, the composition of the magmatic source progresses from a relatively simple mafic composition (wet peridotite and oceanic crust) during the closure of the ocean, to a complex composition (wet peridotite, oceanic crust, subducted mélange and lower continental crust) during continental subduction and, finally, to a predominantly crustal composition (upper crust) during eduction. It appears that this dynamics is dominantly controlled by interplay of the slab-pull and positive buoyancy forces (Andrić and Vogt, in prep).

5.4. Inferences for the tectonic evolution of the Dinarides

This thesis provides significant new insights for the understanding of subduction, collision and subsequent post – collisional dynamics of the Dinarides. The thermo - mechanical numerical modelling shows that the late Cretaceous – Miocene magmatism in the Dinarides can be explain as a principally driven by subduction and associated mantle flow mechanisms. Additionally, the late Cretaceous magmatic phase seems to induce the lithospheric weakening leading to a short, small scale – episode of extension and formation of grabens in the Timok and Srednogorie regions. This idea is supported by the relatively low amount of extension in the back-arc region (e.g., 100 km, Georgiev et al., 2009), compared to the extensional back-arc regions where extension was driven by slab retreat (e.g. amount of extension in Mediterranean back-arcs, ranges from 400 km to 700 km, Faccenna et al., 2014).

The modelling suggests that the major orogenic phase was controlled by continental subduction. The inferences from the Sarajevo - Zenica Basin indicates that this stage lasted until Oligocene. The whole system was subjected to extension after slab detachment, probably in the early Miocene. Eduction is proposed to be the driving mechanism of extension. It triggered the reactivation of the structural fabrics and the opening of the intramountain basins. Both, thermo-mechanical modelling and field studies indicate migration of extensional deformation towards the exterior of the orogen. This relatively short extensional phase (~ 17 – 14 Ma, Sant, Andrić et al., in prep) was followed by basin inversion. The inversion was dominantly N – S directed. Similar to the previous extensional phase, it was controlled by pre-existing orogenic fabric and rheological heterogeneities of the sedimentary infill.

In addition, the modelling explains the compositional changes of the magmatic sources during continental collision as a result of a change in melting from a flux melting and to a lesser degree asthenospheric derived melts during

subduction stage (late Cretaceous - Paleogene) to melting of subducted mélange and lower continental crust (of the lower plate) source and their relamination within the crust during Eocene – lower Miocene times. Finally, after slab detachment, the overall extension leads to exhumation and melting of mid - crust material.

Ultimately, this thesis proposes that the migration of deformation and magmatism in the Dinarides could be driven by the indentation of the lower continental crust of the upper plate into the orogenic wedge, rather than the retreat of the Dinaridic slab. As already mentioned, one of the major features of this type of orogens appears to be relatively low surface heat flow as in the case of the Dinarides (~ 50 mW/m^2, Ravnik et al., 1995).

References

Andersen, T.B., Jamtveit, B., Dewey, J.F., Swensson, E., 1991. Subduction and eduction of continental crust: major mechanisms during continent-continent collision and orogenic extensional collapse, a model based on the south Norwegian Caledonides. Terra Nova 3, 303-310.

Andrić, N., Sant, K., Matenco, L., Mandic, O., Tomljenović, B., Pavelić, D., Hrvatović, H., Demir, V., Ooms, J., 2017. The link between tectonics and sedimentation in asymmetric extensional basins: Inferences from the study of the Sarajevo-Zenica Basin. Marine and Petroleum Geology, in press doi 10.1016/j.marpetgeo.2017.02.024.

Aubouin, J., Blanchet, R., Cadet, J.-P., Celet, P., Charvet, J., Chorowicz, J., Cousin, M., Rampnoux, J.-P., 1970. Essai sur la géologie des Dinarides. Bulletin de la Société Géologique de France 12, 1060-1095.

Augier, R., Jolivet, L., Negro, F., 2013. From ductile to brittle, late-to post-orogenic evolution of the Betic Cordillera: Structural insights from the northeastern Internal zones. Bulletin de la Société Géologique de France 184, 405-425. Augier, R., Jolivet, L., Robin, C., 2005. Late Orogenic doming in the eastern Betic Cordilleras: Final exhumation of the Nevado-Filabride complex and its relation to basin genesis. Tectonics 24.

Augier, R., Jolivet, L., Robin, C., 2005. Late Orogenic doming in the eastern Betic Cordilleras: Final exhumation of the Nevado-Filabride complex and its relation to basin genesis. Tectonics 24.

Aschoff, J., Olariu, C., Steel, R., 2016. Recognition and significance of bayhead delta deposits in the rock record: A comparison of modern and ancient systems. Sedimentology.

Balázs, A., Burov, E., Matenco, L., Vogt, K., Francois, T., Cloetingh, S., 2017. Symmetry during the syn-and post-rift evolution of extensional back-arc basins: The role of inherited orogenic structures. Earth and Planetary Science Letters 462, 86-98.

Balázs, A., Matenco, L., Magyar, I., Horváth, F., Cloetingh, S., 2016. The link between tectonics and sedimentation in back-arc basins: New genetic constraints from the analysis of the Pannonian Basin. Tectonics 35, 1526–1559.

Balanyá, J.C., García-Dueñas, V., Azañón, J.M., Sánchez-Gómez, M., 1997. Alternating contractional and extensional events in the Alpujarride nappes of the Alboran Domain (Betics, Gibraltar Arc). Tectonics 16, 226-238.

Ballato, P., Strecker, M.R., 2014. Assessing tectonic and climatic causal mechanisms in foreland-basin stratal architecture: insights from the Alborz Mountains, northern Iran. Earth Surface Processes and Landforms 39, 110-125.

Ballato, P., Nowaczyk, N.R., Landgraf, A., Strecker, M.R., Friedrich, A., Tabatabaei, S.H., 2008. Tectonic control on sedimentary facies pattern and sediment accumulation rates in the Miocene foreland basin of the southern Alborz mountains, northern Iran. Tectonics 27, TC6001.

Banješević, M., 2010: Upper Cretaceous magmatic suites of the Timok Magmatic Complex, Ann. Géol. Péninsule Balk., 71, 13–22.

Banks, C.J., Warburton, J., 1991. Mid-crustal detachment in the Betic system of southeast Spain. Tectonophysics 191, 275287-281289.

Bargnesi, E.A., Stockli, D.F., Mancktelow, N., Soukis, K., 2013. Miocene core complex development and coeval supradetachment basin evolution of Paros, Greece, insights from (U–Th)/He thermochronometry. Tectonophysics 595–596, 165-182.

Barragán, G., 1997. Evolución geodinámica de la Depresión de Vera. Provincia de Almería. Cordilleras Béticas. PhD thesis, Univ. Granada, Spain (unpublished), 698 pp.

Barrier, L., Proust, J.-N., Nalpas, T., Robin, C., Guillocheau, F., 2010. Control of alluvial sedimentation at foreland-basin active margins: a case study from the northeastern Ebro Basin (southeastern Pyrenees, Spain). Journal of Sedimentary Research 80, 728-749.

Bastesen, E., Braathen, A., 2010. Extensional faults in fine grained carbonates–analysis of fault core lithology and thickness–displacement relationships. Journal of Structural Geology 32, 1609-1628.

Beaumont, C., Jamieson, R.A., Butler, J., Warren, C., 2009. Crustal structure: A key constraint on the mechanism of ultra-high-pressure rock exhumation. Earth and Planetary Science Letters 287, 116-129.

Bennett, R.A., Hreinsdóttir, S., Buble, G., Bašic, T., Bačić, Ž., Marjanović, M., Casale, G., Gendaszek, A., Cowan, D., 2008. Eocene to present subduction of southern Adria mantle lithosphere beneath the Dinarides. Geology 36, 3-6.

Benvenuti, M., Bertini, A., Conti, C., Dominici, S. 2007. Integrated analyses of litho- and biofacies in a Pliocene cyclothemic, alluvial to shallow marine succession (Tuscany, Italy). Geobios, 40(2), 143-158

Bertotti, G., Podladchikov, Y., Daehler, A., 2000. Dynamic link between the level of ductile crustal flow and style of normal faulting of brittle crust. Tectonophysics 320, 195-218.

Bird, J.M., Dewey, J.F., 1970. Lithosphere plate-continental margin tectonics and the evolution of the Appalachian orogen. Geological Society of America Bulletin 81, 1031-1060.

Bittner, D., Schmeling, H., 1995. Numerical modeling of melting processes and induced diapirism in the lower crust.Geophysical Journal International, 123, 59–70.

Blum, M. D., 1993. Genesis and Architecture of Incised Valley Fill Sequences: A Late Quaternary Example from the Colorado River, Gulf Coastal Plain of Texas: Chapter 10: Recent Applications of Siliciclastic Sequence Stratigraphy.

Blair, T.C., McPherson, J.G., 1994. Alluvial fans and their natural distinction from rivers based on morphology, hydraulic processes, sedimentary processes, and facies assemblages. Journal of sedimentary research 64.

Blikra, L.H., Nemec, W., 1998. Postglacial colluvium in western Norway: depositional processes, facies and palaeoclimatic record. Sedimentology 45, 909-960.

Bouma, A. H., Kuenen, P. H., Shepard, F. P., 1962. Sedimentology of some flysch deposits: a graphic approach to facies interpretation (Vol. 168). Amsterdam: Elsevier.

Booth-Rea, G., Azañón, J.M., Martínez-Martínez, J.M., Vidal, O., García-Dueñas, V., 2005. Contrasting structural and P-T evolution of tectonic units in the southeastern Betics: Key for understanding the exhumation of the Alboran Domain HP/LT crustal rocks (western Mediterranean). Tectonics 24.

Booth-Rea, G., Azaón, J.M., Goffé, B., Vidal, O., Martínez-Martínez, J.M. 2002. High-pressure, low-temperature metamorphism in Alpujarride units of southeastern Betics (Spain). Comptes Rendus - Geoscience Volume 334, Issue 11, Pages 857-865

Braga, J.C., Martín, J.M., Betzler, C., Aguirre, J., 2006. Models of temperate carbonate deposition in Neogene basins in SE Spain: a synthesis. Geological Society, London, Special Publications 255, 121-135.

Brouwer, F., Burri, T., Engi, M., Berger, A., 2005. Eclogite relics in the Central

Alps: PT-evolution, Lu-Hf ages and implications for formation of tectonic mélange zones. Schweizerische Mineralogische und Petrographische Mitteilungen 85, 147-174.

Brun, J.-P., Faccenna, C., 2008. Exhumation of high-pressure rocks driven by slab rollback. Earth and Planetary Science Letters 272, 1-7.

Bugge, T., Belderson, R., Kenyon, N., 1988. The storegga slide. Philosophical Transactions of the Royal Society of London A: Mathematical, Physical and Engineering Sciences 325, 357-388.

Bull, S., Cartwright, J., Huuse, M., 2009. A subsurface evacuation model for submarine slope failure. Basin Research 21, 433-443.

Burov, E., Jolivet, L., Le Pourhiet, L., Poliakov, A., 2001. A thermomechanical model of exhumation of high pressure (HP) and ultra-high pressure (UHP) metamorphic rocks in Alpine-type collision belts. Tectonophysics 342, 113-136.

Burov, E., Poliakov, A., 2003. Erosional forcing of basin dynamics: new aspects of syn-and post-rift evolution. Geological Society, London, Special Publications 212, 209-223.

Burov, E., Yamato, P., 2008. Continental plate collision, P–T–t–z conditions and unstable vs. stable plate dynamics: insights from thermo-mechanical modelling. Lithos 103, 178-204.

Cagnioncle, A.M., Parmentier, E., Elkins-Tanton, L.T., 2007. Effect of solid flow above a subducting slab on water distribution and melting at convergent plate boundaries. Journal of Geophysical Research: Solid Earth 112.

Cao, S., Neubauer, F., Bernroider, M., Liu, J., Genser, J., 2013. Structures, microfabrics and textures of the Cordilleran-type Rechnitz metamorphic core complex, Eastern Alps. Tectonophysics 608, 1201-1225.

Calvert, A., Sandvol, E., Seber, D., Barazangi, M., Roecker, S., Mourabit, T., Vidal, F., Alguacil, G., Jabour, N., 2000. Geodynamic evolution of the lithosphere and upper mantle beneath the Alboran region of the western Mediterranean: constraints from travel time tomography. Journal of Geophysical Research: Solid Earth 105, 10871-10898.

Carr, I.D., Gawthorpe, R.L., Jackson, C.A., Sharp, I.R., Sadek, A., 2003. Sedimentology and sequence stratigraphy of early syn-rift tidal sediments: the Nukhul Formation, Suez Rift, Egypt. Journal of Sedimentary Research 73, 407-420.

Carroll, A. R., Bohacs, K. M., 1999. Stratigraphic classification of ancient lakes: balancing tectonic and climatic controls. Geology, 27(2), 99-102.

Cartigny, M.J., Ventra, D., Postma, G., Den Berg, J.H., 2014. Morphodynamics and sedimentary structures of bedforms under supercritical-flow conditions: New insights from flume experiments. Sedimentology 61, 712-748.

Casale, G.M., 2012. Core complex exhumation in peri-Adriatic extension and kinematics of Neogene slip along the Saddle Mountains thrust. University of Washington, p. 93.

Catuneanu, O., 2001. Flexural partitioning of the Late Archaean Witwatersrand foreland system, South Africa. Sedimentary Geology 141, 95-112.

Catuneanu, O., 2002. Sequence stratigraphy of clastic systems: concepts, merits, and pitfalls. Journal of African Earth Sciences 35, 1-43.

Catuneanu, O., Eriksson, P.G., 2002. Sequence stratigraphy of the Precambrian Rooihoogte-Timeball Hill rift succession, Transvaal Basin, South Africa. Sedimentary Geology 147, 71-88.

Childs, C., Nicol, A., Walsh, J.J., Watterson, J., 1996. Growth of vertically segmented

normal faults. Journal of Structural Geology 18, 1389-1397.

Childs, C., Manzocchi, T., Walsh, J.J., Bonson, C.G., Nicol, A., Schöpfer, M.P., 2009. A geometric model of fault zone and fault rock thickness variations. Journal of Structural Geology 31, 117-127.

Christofides, G., Perugini, D., Koroneos, A., Soldatos, T., Poli, G., Eleftheriadis, G., Del Moro, A., Neiva, A., 2007. Interplay between geochemistry and magma dynamics during magma interaction: an example from the Sithonia Plutonic Complex (NE Greece). Lithos 95, 243-266.

Clausen, J.A., Gabrielsen, R.H., Johnsen, E., Korstgård, J.A., 2003. Fault architecture and clay smear distribution. Examples from field studies and drained ring-shear experiments. Norwegian Journal of Geology/Norsk Geologisk Forening 83.

Clauser, C., Huenges, E., 1995. Thermal conductivity of rocks and minerals. In: Rock Physics and Phase Relations. AGU Reference Shelf 3 (ed. Ahrens, T.J.), pp. 105–126. American Geophysical Union, Washington, DC.

Cloetingh, S., Ziegler, P., Beekman, F., Andriessen, P., Hardebol, N., Dèzes, P., 2005. Intraplate deformation and 3D rheological structure of the Rhine Rift System and adjacent areas of the northern Alpine foreland. International Journal of Earth Sciences 94, 758-778.

Cloetingh, S., Haq, B.U., 2015. Inherited landscapes and sea level change. Science 347, 1258375.

Cloetingh, S., Willett, S.D., 2013. TOPO-EUROPE: Understanding of the coupling between the deep Earth and continental topography. Tectonophysics 602, 1-14.

Cloetingh, S.A.P.L., van der Beek, P.A., van Rees, P., Roep, Th.B., Biermann, C., and Stephenson, R.A., 1992. Flexural interaction and the dynamics of Neogene extensional basin formation in the Alboran Betic region, Geo-Marine Letters, 12, 66-75.

Cloetingh, S., McQueen, H., Lambeck, K., 1985. On a tectonic mechanism for regional sealevel variations. Earth and Planetary Science Letters 75, 157-166.

Colella, A., 1988. Pliocene-Holocene fan deltas and braid deltas in the Crati Basin, southern Italy: a consequence of varying tectonic conditions. Fan deltas: Sedimentology and tectonic settings 152, 50-74.

Comas, M., Platt, J., Soto, J., Watts, A., 1999. The origin and tectonic history of the alboran basin: insights from leg 161 results, Proceedings of the Ocean Drilling Program Scientific Results, pp. 555-580.

Condie, K., 2014. Growth of continental crust: a balance between preservation and recycling. Mineralogical Magazine 78, 623-638.

Condie, K.C., Aster, R.C., 2010. Episodic zircon age spectra of orogenic granitoids: the supercontinent connection and continental growth. Precambrian Research 180, 227-236.

Conticelli, S., 1998. The effect of crustal contamination on ultrapotassic magmas with lamproitic affinity: mineralogical, geochemical and isotope data from the Torre Alfina lavas and xenoliths, Central Italy. Chemical Geology 149, 51-81.

Conticelli, S., Avanzinelli, R., Marchionni, S., Tommasini, S., Melluso, L., 2011. Sr-Nd-Pb isotopes from the Radicofani Volcano, Central Italy: constraints on heterogeneities in a veined mantle responsible for the shift from ultrapotassic shoshonite to basaltic andesite magmas in a post-collisional setting. Mineralogy and Petrology 103, 123-148.

Crespo-Blanc, A., Orozco, M., and García-Dueñas, V., 1994. Extension versus compression during the Miocene tectonic evolution of the Betic chain. Late folding of

normal fault systems, Tectonics, 13, 78-88, 1994.

Cvetković, V., Prelević, D., Downes, H., Jovanović, M., Vaselli, O., Pécskay, Z., 2004a. Origin and geodynamic significance of Tertiary postcollisional basaltic magmatism in Serbia (central Balkan Peninsula). Lithos 73, 161-186.

Cvetković, V., Downes, H., Prelević, D., Jovanović, M., Lazarov, M., 2004b. Characteristics of the lithospheric mantle beneath East Serbia inferred from ultramafic xenoliths in Palaeogene basanites. Contributions to Mineralogy and Petrology 148, 335-357.

Cvetković, V., Downes, H., Prelević, D., Lazarov, M., Resimić-Šarić, K., 2007a. Geodynamic significance of ultramafic xenoliths from Eastern Serbia: Relics of sub-arc oceanic mantle? Journal of Geodynamics 43, 504-527.

Cvetković, V., Poli, G., Christofides, G., Koroneos, A., Pécskay, Z., Resimić-Šarić, K., Erić, V., 2007b. The Miocene granitoid rocks of Mt. Bukulja (central Serbia): evidence for Pannonian extension-related granitoid magmatism in the northern Dinarides. European Journal of Mineralogy 19, 513-532.

Cvetković, V., Downes, H., Höck, V., Prelević, D., Lazarov, M., 2010. Mafic alkaline metasomatism in the lithosphere underneath East Serbia: evidence from the study of xenoliths and the host alkali basalts. Geological Society, London, Special Publications 337, 213-239.

Cvetković, V., Pécskay, Z., Šarić, K., 2013. Cenozoic igneous tectonomagmatic events in the Serbian part of the Balkan Peninsula: inferences from K/Ar geochronology. Acta Volcanologica, 10, 111-120.

de Capoa, P., Radoičić, R., D'Argenio, B., 1995. Late Miocene deformation of the Exter-nal Dinarides (Montenegro and Dalmatia). New biostratigraphic evidence. Mem.Sci. Geol. 47, 157–172.

de Leeuw, A., Mandic, O., Krijgsman, W., Kuiper, K., Hrvatović, H., 2012. Paleomagnetic and geochronologic constraints on the geodynamic evolution of the Central Dinarides. Tectonophysics 530-531, 286-298.

de Leeuw, A., Mandic, O., Vranjković, A., Pavelić, D., Harzhauser, M., Krijgsman, W., Kuiper, K.F., 2010. Chronology and integrated stratigraphy of the Miocene Sinj Basin (Dinaride Lake System, Croatia). Palaeogeography, Palaeoclimatology, Palaeoecology 292, 155-167.

Dabrio, C., 1990. Fan-Delta Facies Associations in Late Neogene and Quaternary Basins of Southeastern Spain. Coarse-grained deltas, 91-111.

DeCelles, P. G., Gray, M. B., Ridgway, K. D., Cole, R. B., Pivnik, D. A., Pequera, N., Srivastava, P., 1991. Controls on synorogenic alluvial-fan architecture, Beartooth Conglomerate (Palaeocene), Wyoming and Montana.Sedimentology, 38(4), 567-590.

DeCelles, P.G., Ducea, M.N., Kapp, P., Zandt, G., 2009. Cyclicity in Cordilleran orogenic systems. Nature Geoscience 2, 251-257.

De Jong, K., 1991. Tectono-metamorphic studies and radiometric dating in the Betic Cordilleras (SE Spain) - with implications for the dynamics of extension and compression in the western Meditarranean area, PhD Thesis, Free University Amsterdam, 204 p., 1991.

Defant, M.J., Drummond, M.S., 1990. Derivation of some modern arc magmas by melting of young subducted lithosphere. Nature 347, 662-665.

Delvaux, D., Sperner, B., 2003. Stress tensor inversion from fault kinematic indicators and focal mechanism data: the TENSOR program. In: Nieuwland, D. (Ed.), New Insights into Structural Interpretation and Modelling. Geological Society, London.

Dewey, J., Helman, M., Knott, S., Turco, E., Hutton, D., 1989. Kinematics of the western Mediterranean. Geological Society, London, Special Publications 45, 265-283.

Dewey, J. F. 1980. Episodicity, sequence and style at convergent plate boundaries. In: STRANGEWAY, D. W. (ed.) The Continental Crust and Its Mineral Deposits. Geological Association of Canada, Special Papers, 20, 553–576.

Dilek, Y., Altunkaynak, Ş., 2009. Geochemical and temporal evolution of Cenozoic magmatism in western Turkey: mantle response to collision, slab break-off, and lithospheric tearing in an orogenic belt. Geological Society, London, Special Publications 311, 213-233.

Dimitrijević, M.D., 1997. Geology of Yugoslavia, 2nd edition. Geoinstitute, Belgrade, Belgrade.

Dimitrijević, M.N., Dimitrijević, M.D., 1987. The turbiditic basins of Serbia, Serbian Academy of Sciences and Arts Department of Natural & Mathematical Sciences.

Dimitrijević, M.N., Dimitrijević, M.D., 1991. Triassic carbonate platform of the Drina-Ivanjica element (Dinarides). Acta Geologica Hungarica 34, 15-44.

De Galdeano, C.S., Vera, J.A., 1992. Stratigraphic record and palaeogeographical context of the Neogene basins in the Betic Cordillera, Spain. Basin Research 4, 21-35.

Đerić, N., Gerzina, N., Schmid, S.M., 2007. Age of the Jurassic Radiolarian Chert Formation from the Zlatar Mountain (SW Serbia). Ofioliti 32, 101-108.

Đoković, I., 1985. The use of structural analysis in determining the fabric of Paleozoic formations in the Drina - Ivanjica region. Geol. an. Balk. poluos. 49, 11-160.

Do Couto, D., Gumiaux, C., Augier, R., Lebret, N., Folcher, N., Jouannic, G., Jolivet, L., Suc, J.P., Gorini, C., 2014. Tectonic inversion of an asymmetric graben: insights from a combined field and gravity survey in the Sorbas basin. Tectonics 33, 1360-1385.

Dronkert, H. (1976), Late Miocene evaporites in the Sorbas basin and adjoining areas, Mem. Soc. Geol. Italiana, 16, 341–361.

Drummond, M., Defant, M., Kepezhinskas, P., 1996. Petrogenesis of slab-derived trondhjemite–tonalite-dacite/adakite magmas. Geological Society of America Special Papers 315, 205-215.

Ducea, M.N., 2001. The California arc. GSA today 11, 4-10.

Ducea, M.N., Barton, M.D., 2007. Igniting flare-up events in Cordilleran arcs. Geology 35, 1047-1050.

Duggen, S., Hoernle, K., van den Bogaard, P., Harris, C., 2004. Magmatic evolution of the Alboran region: the role of subduction in forming the western Mediterranean and causing the Messinian Salinity Crisis. Earth and Planetary Science Letters 218, 91-108.

Duggen, S., Hoernle, K., van den Bogaard, P., Garbe-Schönberg, D., 2005. Post-collisional transition from subduction-to intraplate-type magmatism in the westernmost Mediterranean: evidence for continental-edge delamination of subcontinental lithosphere. Journal of Petrology.

Duretz, T., Gerya, T.V., May, D.A., 2011. Numerical modelling of spontaneous slab breakoff and subsequent topographic response. Tectonophysics 502, 244-256.

Duretz, T., Gerya, T., Kaus, B., Andersen, T., 2012. Thermomechanical modeling of slab eduction. Journal of Geophysical Research: Solid Earth 117.

Duretz, T., Gerya, T., 2013. Slab detachment during continental collision: Influence of crustal rheology and interaction with lithospheric delamination. Tectonophysics 602, 124-140.

Dymkova, D., Gerya, T., Burg, J.-P., 2016. 2D thermomechanical modelling of continent–arc–continent collision. Gondwana Research 32, 138-150.

Embry, A., Johannessen, E., 1992. TeR sequence stratigraphy, facies analysis and reservoir distribution in the uppermost TriassiceLower Jurassic succession, Western Sverdrup Basin, Arctic Canada. In: Arctic Geology and Petroleum Potential, Special Publication, 2, pp. 121e146.

Erdős, Z., Beek, P., Huismans, R.S., 2014. Evaluating balanced section restoration with thermochronology data: A case study from the Central Pyrenees. Tectonics 33, 617-634.

Evans, A., Hutchinson, J., 1984. On the mechanics of delamination and spalling in compressed films. International Journal of Solids and Structures 20, 455-466.

Ezquerro, L., Moretti, M., Liesa, C., Luzón, A., Simón, J., 2015. Seismites from a well core of palustrine deposits as a tool for reconstructing the palaeoseismic history of a fault. Tectonophysics 655, 191-205.

Faccenna, C., Becker, T.W., Auer, L., Billi, A., Boschi, L., Brun, J.P., Capitanio, F.A., Funiciello, F., Horvàth, F., Jolivet, L., 2014. Mantle dynamics in the Mediterranean. Reviews of Geophysics 52, 283-332.

Faccenna, C., Becker, T.W., 2010. Shaping mobile belts by small-scale convection. Nature 465, 602-605.

Faccenna, C., Piromallo, C., Crespo-Blanc, A., Jolivet, L., Rosetti, F., 2004. Lateral slab deformation and the origin of the western Mediterranean arcs. Tectonics 23, TC1012, doi:1010.1029/2002TC001488.

Faccenda, M., Gerya, T.V., Chakraborty, S., 2008. Styles of post-subduction collisional orogeny: influence of convergence velocity, crustal rheology and radiogenic heat production. Lithos 103, 257-287.

Faccenda, M., Minelli, G., Gerya, T., 2009. Coupled and decoupled regimes of continental collision: numerical modeling. Earth and Planetary Science Letters 278, 337-349.

Fodor, L., Csontos, L., Bada, G., Györfi, I., Benkovics, L., 1999. Tertiary tectonic evolution of the Pannonian basin system and neighbouring orogens: a new synthesis of paleostress data, in: Durand, B., Jolivet, L., Horvath, F., Seranne, M. (Eds.), The Mediteranean basins: Tertiary extension within the Alpine orogen. The Geological Society, London, pp. 295-334.

Foley, S., 1992. Vein-plus-wall-rock melting mechanisms in the lithosphere and the origin of potassic alkaline magmas. Lithos 28, 435-453.

Friedmann, S. J., Burbank, D. W., 1995. Rift basins and supradetachment basins: intracontinental extensional end-members. Basin Research, 7(2), 109-127.

Fugelli, E.M., Olsen, T.R., 2007. Delineating confined slope turbidite systems offshore mid-Norway: The Cretaceous deep-marine Lysing Formation. AAPG bulletin 91, 1577-1601.

Gabrielsen, R.H., Sokoutis, D., Willingshofer, E., Faleide, J.I., 2016. Fault linkage across weak layers during extension: an experimental approach with reference to the Hoop Fault Complex of the SW Barents Sea. Petroleum Geoscience 22, 123-135.

Galloway, W.E., 1989. Calstic facies models, depositional systems, sequences and correlation: a sedimentologists view of the dimensional and temporal resolution of lithostratigraphy, in: Cross, T.A. (Ed.), Quantitative dynamic stratigraphy. Prentice Hall, New Jersey, pp. 113-126.

Gaetani, G.A., Grove, T.L., 2003. Experimental constraints on melt generation in the mantle wedge. Inside the subduction factory, 107-134.

Gallhofer, D., Quadt, A.v., Peytcheva, I., Schmid, S.M., Heinrich, C.A., 2015. Tectonic, magmatic, and metallogenic evolution of the Late Cretaceous arc in the Carpathian-Balkan orogen. Tectonics 34, 1813-1836.

Garcia-Castellanos, D., Verges, J., Gaspar-Escribano, J., Cloetingh, S., 2003. Interplay between tectonics, climate, and fluvial transport during the Cenozoic evolution of the Ebro Basin (NE Iberia). Journal of Geophysical Research 108, 2347, doi: 2310.1029/2002JB002073.

García-Dueñas, V., Balanyá, J., Martínez-Martínez, J., 1992. Miocene extensional detachments in the outcropping basement of the northern Alboran basin (Betics) and their tectonic implications. Geo-Marine Letters 12, 88-95.

García-García, F., Corbí, H., Soria, J., Viseras, C., 2011. Architecture analysis of a river flood-dominated delta during an overall sea-level rise (early Pliocene, SE Spain). Sedimentary Geology 237, 102-113.

García-García, F., Fernández, J., Viseras, C., Soria, J.M., 2006. Architecture and sedimentary facies evolution in a delta stack controlled by fault growth. Sedimentary Geology 185, 79-92.

García-Hernández, M., López-Garrido, A., Rivas, P., Sanz de Galdeano, C., Vera, J.A., 1980. Mesozoic palaeogeographic evolution of the external zones of the Betic Cordillera.

Gawthorpe, R. L., Colella, A., 1990. Tectonic Controls on Coarse-Grained Delta Depositional Systems in Rift Basins. Systems in Rift Basins. Coarse-Grained Deltas: Special Publication 10 of the IAS, 27, 113.

Gawthorpe, R., Hurst, J., 1993. Transfer zones in extensional basins: their structural style and influence on drainage development and stratigraphy. Journal of the Geological Society 150, 1137-1152.

Gawthorpe, R.L., Fraser, A.J., Collier, R.E.L., 1994. Sequence stratigraphy in active extensional basins: implications for the interpretation of ancient basin-fills. Marine and Petroleum Geology 11, 642-658.

Gawthorpe, R. L., Leeder, M. R., 2000. Tectono-sedimentary evolution of active extensional basins. Basin Research, 12, 195-218.

Ge, Z., Nemec, W., Gawthorpe, R.L., Hansen, E.W., 2017. Response of unconfined turbidity current to normal-fault topography. Sedimentology.

Gee, M.J.R., Masson, D.G., Watts, A.B. and Allen, P.A. 1999. The Saharan debris flow: an insight into the mechanics of long runout submarine debris flows. Sedimentology, 46, 315–335.

Giaconia, F., Booth-Rea, G., Martínez-Martínez, J., Azañón, J., Storti, F., Artoni, A., 2014. Heterogeneous extension and the role of transfer faults in the development of the southeastern Betic basins (SE Spain). Tectonics 33, 2467-2489.

Giaconia, F., Booth-Rea, G., Martínez-Martínez, J.M., Joaquín, J.M., Pérez-Romero, VillegasAzañón, I. (2013). Mountain front migration and drainage captures related to fault segment linkage and growth: The Polopos transpressive fault zone (southeastern Betics, SE Spain). Journal of Structural Geology 46, p 76-91 http://dx.doi.org/10.1016/j.jsg.2012.10.005

Giaconia, F., Booth-Rea, G., Martínez-Martínez, J.M., Azañón, J.M., Pérez-Peña, J.V., Pérez-Romero, J., Villegas, I. (2012). Geomorphic evidence of active tectonics in the Sierra AlhamGeorgiev, N., Henry, B., Jordanova, N., Froitzheim, N., Jordanova, D., Ivanov, Z., Dimov, D., 2009. The emplacement mode of Upper Cretaceous plutons from the southwestern part of the Sredna Gora Zone (Bulgaria): structural and AMS study. Geologica

Carpathica 60, 15-33.

Gerya, T.V., Yuen, D.A., 2003a. Characteristics-based marker-in-cell method with conservative finite-differences schemes for modeling geological flows with strongly variable transport properties. Physics of the Earth and Planetary Interiors 140, 293-318.

Gerya, T.V., Yuen, D.A., 2003b. Rayleigh–Taylor instabilities from hydration and melting propel 'cold plumes' at subduction zones. Earth and Planetary Science Letters 212, 47-62.

Gerya, T.V., Burg, J.-P., 2007. Intrusion of ultramafic magmatic bodies into the continental crust: numerical simulation. Physics of the Earth and Planetary Interiors 160, 124-142.

Gerya, T., 2010. Dynamical instability produces transform faults at mid-ocean ridges. Science 329, 1047-1050.

Gerya, T., Meilick, F., 2011. Geodynamic regimes of subduction under an active margin: effects of rheological weakening by fluids and melts. Journal of Metamorphic Geology 29, 7-31.

Gerya, T.V., Stern, R.J., Baes, M., Sobolev, S., Whattam, S.A., 2015. Plate tectonics on the Earth triggered by plume-induced subduction initiation. Nature 527, 221-225.

Gloppen, T.G., Steel, R.J., 1981. The Deposits, Internal Structure and Geometry in Six Alluvial Fan—Fan Delta Bodies (Devonian-Norway)—A Study in the Significance of Bedding Sequence in Conglomerates.

Gorczyk, W., Willner, A.P., Gerya, T.V., Connolly, J.A., Burg, J.-P., 2007. Physical controls of magmatic productivity at Pacific-type convergent margins: Numerical modelling. Physics of the Earth and Planetary Interiors 163, 209-232.

Gower, C.F., 1996. The evolution of the Grenville Province in eastern Labrador, Canada. Geological Society, London, Special Publications 112, 197-218.

Gowland, S. (1996) Facies characteristics and depositional models of highly bioturbated shallow marine siliciclastic strata; an example from the Fulmar Formation (Late Jurassic) UK Central Graben. In: Geology of the Humber Group; Central Graben and Moray Firth UKCS (Eds A. Hurst, H.D. Johnson, S.D. Burley, A.C. Canham, and D.S. Mackertich), Geol. Soc. Spec. Publ., 114, 185±214.

Grove, T., Parman, S., Bowring, S., Price, R., Baker, M., 2002. The role of an H2O-rich fluid component in the generation of primitive basaltic andesites and andesites from the Mt. Shasta region, N California. Contributions to Mineralogy and Petrology 142, 375-396.

Grove, T.L., Chatterjee, N., Parman, S.W., Medard, E. 2006. The influence of H2O on mantle wedge melting. Earth and Planetary Science Letters, 249, 74–89.

Grove, T., Till, C., Lev, E., Chatterjee, N., Médard, E., 2009. Kinematic variables and water transport control the formation and location of arc volcanoes. Nature 459, 694-697.

Grove, T.L., Till, C.B., Krawczynski, M.J., 2012. The role of H2O in subduction zone magmatism. Annual Review of Earth and Planetary Sciences 40, 413-439.

Guo, Z., Wilson, M., Zhang, L., Zhang, M., Cheng, Z., Liu, J., 2014. The role of subduction channel mélanges and convergent subduction systems in the petrogenesis of post-collisional K-rich mafic magmatism in NW Tibet. Lithos 198, 184-201. Gupta, S., Underhill, J., Sharp, I., Gawthorpe, R., 1999. Role of fault interactions in controlling synrift sediment dispersal patterns: Miocene, Abu Alaqa Group, Suez Rift, Sinai, Egypt. Basin Research 11, 167-189.

Gutscher, M.A., 2012. Subduction beneath Gibraltar? Recent studies provide answers. EOS 93, 133-134.

Handy, M.R., M. Schmid, S., Bousquet, R., Kissling, E., Bernoulli, D., 2010. Reconciling plate-tectonic reconstructions of Alpine Tethys with the geological-geophysical record of spreading and subduction in the Alps. Earth-Science Reviews 102, 121-158.

Handy, M.R., Ustaszewski, K. and Kissling, E., 2015. Reconstructing the Alps–Carpathians–Dinarides as a key to understanding switches in subduction polarity, slab gaps and surface motion. International Journal of Earth Sciences, 104(1), pp.1-26.

Hacker, B.R., Kelemen, P.B., Behn, M.D., 2011. Differentiation of the continental crust by relamination. Earth and Planetary Science Letters 307, 501-516.

Harzhauser, M., Mandic, O., 2008. Neogene lake systems of Central and South-Eastern Europe: Faunal diversity, gradients and interrelations. Paleogeogr. Paleoclimatol. Paleoecol. 260, 417-434.

Haughton, P., Davis, C., McCaffrey, W., Barker, S., 2009. Hybrid sediment gravity flow deposits–classification, origin and significance. Marine and petroleum geology 26, 1900-1918.

Haughton, P.D., Barker, S.P., McCaffrey, W.D., 2003. 'Linked'debrites in sand-rich turbidite systems–origin and significance. Sedimentology 50, 459-482.

Haughton, P., 2001. Contained turbidites used to track sea bed deformation and basin migration, Sorbas Basin, south-east Spain. Basin Research 13, 117-139.

Haughton, P.D., 2000. Evolving turbidite systems on a deforming basin floor, Tabernas, SE Spain. Sedimentology 47, 497-518.

Haughton, P.D., 1994. Deposits of deflected and ponded turbidites, currents, Sorbas Basin, southeast Spain. Journal of Sedimentary Research 64.

Helland-Hansen, W., Martinsen, O.J., 1996. Shoreline trajectories and sequences: description of variable depositional-dip scenarios. J. Sediment. Res. 66 (4), 670e688.

Henstra, G.A., Grundvåg, S.-A., Johannessen, E.P., Kristensen, T.B., Midtkandal, I., Nystuen, J.P., Rotevatn, A., Surlyk, F., Sæther, T., Windelstad, J., 2016. Depositional processes and stratigraphic architecture within a coarse-grained rift-margin turbidite system: The Wollaston Forland Group, east Greenland. Marine and Petroleum Geology 76, 187-209.

Herak, D., Herak, M., Tomljenović, B., 2009. Seismicity and earthquake focal mechanisms in North-Western Croatia. Tectonophysics 465, 212-220.

Hernandez, J., F.D. de Larouzière, J. Bolze, and P. Bordet, 1987. Le magmatisme Néogène bético-rifain et le couloir de décrochement Trans-Alboran: Bull. Soc. Géol. France, 3, 257-267.

Hesse, M., Grove, T.L., 2003. Absarokites from the western Mexican Volcanic Belt: constraints on mantle wedge conditions. Contributions to Mineralogy and Petrology 146, 10-27.

Hinsken, S., Ustaszewski, K., Wetzel, A., 2007. Graben width controlling syn-rift sedimentation: the Palaeogene southern Upper Rhine Graben as an example. International Journal of Earth Sciences 96, 979-1002.

Hodgson, D.M., Haughton, P.D., 2004. Impact of syndepositional faulting on gravity current behaviour and deep-water stratigraphy: Tabernas-Sorbas Basin, SE Spain. Geological Society, London, Special Publications 222, 135-158.

Horváth, F., Musitz, B., Balázs, A., Végh, A., Uhrin, A., Nádor, A., Koroknai, B.,

Pap, N., Tóth, T., Wórum, G., 2015. Evolution of the Pannonian basin and its geothermal resources. Geothermics 53, 328-352.

Horváth, F., Cloetingh, S., 1996. Stress-induced late-stage subsidence anomalies in the Pannonian basin. Tectonophysics 266, 287-300.

Hrvatović, H., 2006. Geological Guidebook through Bosnia and Herzegovina. Geological Survey of Federation Bosnia and Herzegovina, Sarajevo.

Hrvatović, H., Pamić, J., 2005. Principal thrust-nappe structures of the Dinarides. Acta Geologica Hungarica 48/2, 133-151.

Hrvatović, H., Dunkl, I., Strmić-Palinkaš, S., Palinkaš, L., 2015. A new research results metamorphic complex of the Mid-Bosnian Schist Mountains. I Kongres geologa u Bosni i Hercegovini sa međunarodnim učešćem, Zbornik radova, 127-132. Udruženje geologa Bosne i Hercegovine, ISSN 1840-4073, Tuzla, 21-23.10.2015.

Ielpi, A., 2012. Anatomy of major coal successions: facies analysis and sequence architecture of a brown coal-bearing valley fill to lacustrine tract (Upper Valdarno Basin, Northern Apennines, Italy). Sedimentary Geology, 265, 163-181.

Ilić, A., Neubauer, F., 2005. Tertiary to recent oblique convergence and wrenching of the Central Dinarides: Constraints from a palaeostress study. Tectonophysics 410, 465-484.

Jackson, C. A. L., Gawthorpe, R. L., Sharp, I. R., 2002. Growth and linkage of the East Tanka fault zone, Suez rift: structural style and syn-rift stratigraphic response. Journal of the Geological Society, 159(2), 175-187.

Jackson, C. A. L., Gawthorpe, R. L., Carr, I. D., Sharp, I. R., 2005. Normal faulting as a control on the stratigraphic development of shallow marine syn-rift sequences: the Nukhul and Lower Rudeis Formations, Hammam Faraun fault block, Suez Rift, Egypt. Sedimentology, 52(2), 313-338.

Jabaloy, A., J. Galindo-Zaldívar, and F. González -Lodeiro, 1992. The Mecina Extensional System: its relation with the post Aquitanian piggy-back Basins and the paleostresses evolution (Betic Cordilleras, Spain), Geo-Marine Letters, 12, 96-103.

Janecke, S. U., C. J. Vandenberg, and J. J. Blankenau (1998), Geometry, mechanism, and significance of extensional folds from examples in the Rock Mountain Basin and Range Province, U.S.A, J. Struct. Geol., 20, 841–856, doi:10.1016/S0191-8141(98)00016-9.

Jiménez-Moreno, G., de Leeuw, A., Mandic, O., Harzhauser, M., Pavelić, D., Krijgsman, W., Vranjkovic, A., 2009. Integrated stratigraphy of the Early Miocene lacustrine deposits of Pag Island (SW Croatia): Palaeovegetation and environmental changes in the Dinaride Lake System. Palaeogeography, Palaeoclimatology, Palaeoecology 280, 193-206.

Jolivet, L., Brun, J.-P., 2010. Cenozoic geodynamic evolution of the Aegean. International Journal of Earth Sciences 99, 109-138.

Jolivet, L., Faccenna, C., Piromallo, C., 2009. From mantle to crust: Stretching the Mediterranean. Earth and Planetary Science Letters 285, 198-209.

Jolivet, L., Faccenna, C., 2000. Mediterranean extension and the Africa-Eurasia collision. Tectonics 19, 1095-1106.

Jolivet, L., Faccenna, C., Goffé, B., Mattei, M., Rossetti, F., Brunet, C., Storti, F., Funiciello, R., Cadet, J.P., d'Agostino, N., 1998. Midcrustal shear zones in postorogenic extension: example from the northern Tyrrhenian Sea. Journal of Geophysical Research: Solid Earth 103, 12123-12160.

Johnson, C., 1993. Contrasted thermal histories of different nappe complexes in

S.E. Spain: evidence for complex crustal extension, in Late Orogenic Extension in Mountain Belts edited by M. Séranne M. and J. Malavielle, Doc. BRGM Fr., 219, 103.

Johnson, C., Harbury, N., and Hurford, A.J., 1997. The role of extension in the Miocene denudation of the Nevado-Filábride complex, Betic Cordillera (SE Spain), Tectonics, 16, 189-204.

Jonk, R., Biermann, C., 2002. Deformation in Neogene sediments of the Sorbas and Vera Basins (SE Spain): constraints on simple-shear deformation and rigid body rotation along major strike-slip faults. Journal of Structural Geology 24, 963-977.

Jovanović., R, Mojićević, M., Tokić, S., Rokić, Lj., 1971. Basic Geological Map of the SFRY, 1:100.000, Sheet Sarajevo (K-34I). Federal Geological Institute, Belgrade.

Jovanović, M., Downes, H., Vaselli, O., Cvetković, V., Prelević, D., Pscskay, Z., 2001. Paleogene mafic alkaline volcanic rocks of East Serbia. Acta Vulcanologica 13, 159-173.

Kane, I.A., Pontén, A.S., Vangdal, B., Eggenhuisen, J.T., Hodgson, D.M., Spychala, Y.T., 2017. The stratigraphic record and processes of turbidity current transformation across deep-marine lobes. Sedimentology.

Kane, I.A., Pontén, A.S., 2012. Submarine transitional flow deposits in the Paleogene Gulf of Mexico. Geology 40, 1119-1122.

Karamata, S., 2006. The geological development of the Balkan Peninsula related to the approach, collision and compression of Gondwanan and Eurasian units. Geological Society, London, Special Publications 260, 155-178.

Kelemen, P.B., Behn, M.D., 2016. Formation of lower continental crust by relamination of buoyant arc lavas and plutons. Nature Geoscience 9, 197-205.

Kelemen, P., Hanghøj, K., Greene, A., 2003. One view of the geochemistry of subduction-related magmatic arcs, with an emphasis on primitive andesite and lower crust. Treatise on geochemistry 3, 593-659.

Kleverlaan, K., 1987. Gordo megabed: a possible seismite in a Tortonian submarine fan, Tabernas basin, Province Almeria, southeast Spain. Sedimentary Geology 51, 165-180.

Kleverlaan, K., 1989. Three distinctive feeder-lobe systems within one time slice of the Tortonian Tabernas fan, SE Spain. Sedimentology 36, 25-45.

Kneller, B.C., Branney, M.J., 1995. Sustained high-density turbidity currents and the deposition of thick massive sands. Sedimentology 42, 607-616.

Kolb, M., Von Quadt, A., Peytcheva, I., Heinrich, C., Fowler, S., Cvetković, V., 2013. Adakite-like and normal arc magmas: distinct fractionation paths in the East Serbian segment of the Balkan–Carpathian arc. Journal of Petrology, 3, 421-451.

Korbar, T., 2009. Orogenic evolution of the External Dinarides in the NE Adriatic region: a model constrained by tectonostratigraphy of Upper Cretaceous to Paleogene carbonates. Earth-Science Reviews 96, 296-312.

Krijgsman, W., Fortuin, A., Hilgen, F., Sierro, F.J., 2001. Astrochronology for the Messinian Sorbas basin (SE Spain) and orbital (precessional) forcing for evaporite cyclicity. Sedimentary Geology 140, 43-60.

Krstić, N., Savić, L., Jovanović, G., Bodor, E., 2003. Lower Miocene lakes of the Balkan Land. Acta Geologica Hungarica 46/3, 291-299.

Labrousse, L., Duretz, T., Gerya, T., 2015. H 2 O-fluid-saturated melting of subducted continental crust facilitates exhumation of ultrahigh-pressure rocks in continental subduction zones. Earth and Planetary Science Letters 428, 151-161.

Lavecchia, G., Bell, K., 2012. Magmatectonic zonation of Italy: a tool to

understanding Mediterranean geodynamics. INTECH Open Access Publisher.

Leeder, M., Collier, R., Abdul Aziz, L., Trout, M., Ferentinos, G., Papatheodorou, G., Lyberis, E., 2002. Tectono-sedimentary processes along an active marine/ lacustrine half-graben margin: Alkyonides Gulf, E. Gulf of Corinth, Greece. Basin Res. 14, 25e41.

Leeder, M. R., Gawthorpe, R. L., 1987. Sedimentary models for extensional tilt-block/half-graben basins. Geological Society, London, Special Publications, 28(1), 139-152.

Leever, K.A., Matenco, L., Garcia-Castellanos, D., Cloetingh, S.A.P.L., 2011. The evolution of the Danube gateway between Central and Eastern Paratethys (SE Europe): Insight from numerical modelling of the causes and effects of connectivity between basins and its expression in the sedimentary record. Tectonophysics 502, 175-195.

Leppard, C. W., Gawthorpe, R. L., 2006. Sedimentology of rift climax deep water systems; lower Rudeis formation, Hammam Faraun fault block, Suez Rift, Egypt. Sedimentary Geology, 191(1), 67-87.

Lewis, M.M., Jackson, C.A.-L., Gawthorpe, R.L., Whipp, P.S., 2015. Early synrift reservoir development on the flanks of extensional forced folds: A seismic-scale outcrop analog from the Hadahid fault system, Suez rift, Egypt. AAPG Bulletin 99, 985-1012.

Le Pourhiet, L., Burov, E., Moretti, I., 2004. Rifting through a stack of inhomogeneous thrusts (the dipping pie concept). Tectonics 23.

Li, Z., Xu, Z., Gerya, T., 2011. Flat versus steep subduction: Contrasting modes for the formation and exhumation of high-to ultrahigh-pressure rocks in continental collision zones. Earth and Planetary Science Letters 301, 65-77.

Liao, J., Gerya, T., 2017. Partitioning of crustal shortening during continental collision: 2-D thermomechanical modeling. Journal of Geophysical Research: Solid Earth.

Lin, J.Y., Hsu, S.K., Sibuet, J.C., 2004. Melting features along the western Ryukyu slab edge (northeast Taiwan): Tomographic evidence. Journal of Geophysical Research: Solid Earth 109, B12

Liou, J., Zhang, R., Eide, E., Maruyama, S., Wang, X., Ernst, W., 1996. Metamorphism and tectonics of high-P and ultrahigh-P belts in Dabie-Sulu Regions, eastern central China. The tectonic evolution of Asia, 300-343.

Lister, G.S., Davis, G.A., 1989. The Origin of Metamorphic Core Complexes and Detachment Faults Formed during Tertiary Continental Extension in the Northern Colorado River Region, USA. Journal of Structural Geology 11, 65-94.

Lonergan, L., Platt, J.P., 1995. The Malaguide-Alpujarride boundary: a major extensional contact in the Internal Zone of the eastern Betic Cordillera, SE Spain. Journal of Structural Geology 17, 16551667-16651671.

Longhitano, S.G., Sabato, L., Tropeano, M., Murru, M., Carannante, G., Simone, L., Cilona, A., Vigorito, M., 2015. Outcrop reservoir analogous and porosity changes in continental deposits from an extensional basin: The case study of the upper Oligocene Sardinia Graben System, Italy. Marine and Petroleum Geology, 67, pp.439-459.

Loutit, T. S., Hardenbol, J., Vail, P. R., and Baum, G. R., 1988. Condensed sections: the key to age-dating and correlation of continental margin sequences. In Sea Level Changes–An Integrated Approach(C. K. Wilgus, B. S. Hastings, C. G. St.C. Kendall, H. W. Posamentier, C. A. Ross and J. C. Van Wagoner, Eds.), pp. 183–213. SEPM Special Publication 42.

Lowe, D. R., 1982. Sediment gravity flows: II Depositional models with special reference to the deposits of high-density turbidity currents. Journal of Sedimentary Research, 52(1), 279-297.

Lustrino, M., Wilson, M., 2007. The circum-Mediterranean anorogenic Cenozoic igneous province. Earth-Science Reviews 81, 1-65.

Magni, V., Faccenna, C., van Hunen, J., Funiciello, F., 2014. How collision triggers backarc extension: Insight into Mediterranean style of extension from 3-D numerical models. Geology 42, 511-514.

Mandic, O., de Leeuw, A., Vuković, B., Krijgsman, W., Harzhauser, M., Kuiper, K.F., 2011. Palaeoenvironmental evolution of Lake Gacko (Southern Bosnia and Herzegovina): Impact of the Middle Miocene Climatic Optimum on the Dinaride Lake System. Palaeogeography, Palaeoclimatology, Palaeoecology 299, 475-492.

Mandic, O., de Leeuw, A., Bulić, J., Kuiper, K., Krijgsman, W., Jurišić-Polšak, Z., 2012. Paleogeographic evolution of the Southern Pannonian Basin: 40Ar/39Ar age constraints on the Miocene continental series of northern Croatia. International Journal of Earth Sciences, 101, 1033-1046.

Manzi, V., R. Gennari, F. Hilgen, W. Krijgsman, S. Lugli, M. Roveri, and F. J. Sierro (2013), Age refinement of the Messinian salinity crisis onset in the Mediterranean, Terra Nova, 25(4), 315–322.

Martín, J.M., Braga, J.C., Sánchez-Almazo, I., 1999. The Messinian record of the outcropping marginal Alboran basin deposits: significance and implications.

Martín, J., Braga, J.C., 1994. Messinian events in the Sorbas Basin in southeastern Spain and their implications in the recent history of the Mediterranean. Sedimentary Geology 90, 257-268.

Martín-Barajas, A., Vázquez-Hernández, S., Carreño, A.L., Helenes, J., Suárez-Vidal, F., Alvarez-Rosales, J., 2001. Late Neogene stratigraphy and tectonic control on facies evolution in the Laguna Salada Basin, northern Baja California, Mexico. Sedimentary Geology 144, 5-35.

Martínez-Martínez, J., Azañón, J., 1997. Mode of extensional tectonics in the southeastern Betics (SE Spain): Implications for the tectonic evolution of the peri-Alborán orogenic system. Tectonics 16, 205-225.

Martins-Neto, M.A., Catuneanu, O., 2010. Rift sequence stratigraphy. Marine and Petroleum Geology 27, 247-253.

Martín-Suárez, E., Freudenthal, M., Krijgsman, W., Fortuin, A.R., 2000. On the age of the continentaldeposits of the Zorreras Member (Sorbas Basin, SE Spain). Geobios 33, 505-512.

Matenco, L., Munteanu, I., Ter Borgh, M., Stanica, A., Tilita, M., Lericolais, G., Dinu, C., Oaie, G., 2016. The interplay between tectonics, sediment dynamics and gateways evolution in the Danube system from the Pannonian Basin to the western Black Sea. Science of the Total Environment 543, 807-827.

Matenco, L., Radivojević, D., 2012. On the formation and evolution of the Pannonian Basin: Constraints derived from the structure of the junction area between the Carpathians and Dinarides. Tectonics 31, TC6007.

Matenco, L., Krezsek, C., Merten, S., Schmid, S., Cloetingh, S., Andriessen, P., 2010. Characteristics of collisional orogens with low topographic build-up: An example from the Carpathians. Terra Nova 22, 155-165.

Meijninger, B.M.L., (2006). Late-orogenic extension and strike-slip deformation in the Neogene of southeastern Spain (Published PhD thesis, University of Utrecht). Geologica Ultraiectina 269. http://dx.doi.org/1874/124135

Meijninger, B., Vissers, R., 2006. Miocene extensional basin development in the Betic Cordillera, SE Spain revealed through analysis of the Alhama de Murcia and Crevillente Faults. Basin Research 18, 547-571.

Melchor, R. N., 2007. Changing lake dynamics and sequence stratigraphy of synrift lacustrine strata in a half-graben: an example from the Triassic Ischigualasto–Villa Unión Basin, Argentina. Sedimentology, 54(6), 1417-1446.

Menant, A., Jolivet, L., Vrielynck, B., 2016a. Kinematic reconstructions and magmatic evolution illuminating crustal and mantle dynamics of the eastern Mediterranean region since the late Cretaceous. Tectonophysics 675, 103-140.

Menant, A., Sternai, P., Jolivet, L., Guillou-Frottier, L., Gerya, T., 2016b. 3D numerical modeling of mantle flow, crustal dynamics and magma genesis associated with slab roll-back and tearing: The eastern Mediterranean case. Earth and Planetary Science Letters 442, 93-107.

Miall, A. D., 1985. Architectural-element analysis: a new method of facies analysis applied to fluvial deposits.

Miall, A. D., 1996. The Geology of Fluvial Deposits. Springer. New York: 582.

Miall, A.D., Miall, C.E., 2001. Sequence stratigraphy as a scientific enterprise: the evolution and persistence of conflicting paradigms. Earth-Science Reviews 54, 321-348.

Mibe, K., Fujii, T., Yasuda, A., 1999. Control of the location of the volcanic front in island arcs by aqueous fluid connectivity in the mantle wedge. Nature 401, 259-262.

Mikes, T., Báldi-Beke, M., Kázmér, M., Dunkl, I., von Eynatten, H., 2008a. Calcareous nannofossil age constraints on Miocene flysch sedimentation in the Outer Dinarides (Slovenia, Croatia, Bosnia-Herzegovina and Montenegro). Geological Society, London, Special Publications 298, 335-363.

Mikes, T., Christ, D., Petri, R., Dunkl, I., Frei, D., Báldi-Beke, M., Reitner, J., Wemmer, K., Hrvatović, H., von Eynatten, H., 2008b. Provenance of the Bosnian Flysch. Swiss Journal of Geosciences 101, 31-54.

Miller, N.C., Behn, M.D., 2012. Timescales for the growth of sediment diapirs in subduction zones. Geophysical Journal International 190, 1361-1377.

Miller, K.G., Kominz, M.A., Browning, J.V., Wright, J.D., Mountain, G.S., Katz, M.E., Sugarman, P.J., Cramer, B.S., Christie-Blick, N., Pekar, S.F., 2005. The Phanerozoic record of global sea-level change. science 310, 1293-1298.

Milojević, R., 1964. Geologic composition and tectonic pattern of Middle-Bosnia coal basin with special review of development and economic value of coal-bearing facies. PhD Thesis, Geological survey Sarajevo special publication, p. 190.

Moernaut, J., Daele, M.V., Heirman, K., Fontijn, K., Strasser, M., Pino, M., Urrutia, R., De Batist, M., 2014. Lacustrine turbidites as a tool for quantitative earthquake reconstruction: New evidence for a variable rupture mode in south central Chile. Journal of Geophysical Research: Solid Earth 119, 1607-1633.

Monié, P., J. Galindo-Zaldivar, F. Gonzalez Lodeiro, B. Goffé, and A. Jabaloy, 1991. 40Ar/39Ar geochronology of Alpine tectonism in the Betic Cordilleras (southern Spain), J. Geol. Soc. London, 148, 289-297.

Montenat, C., d'Estevou, P.O., Masse, P., 1987. Tectonic-sedimentary characters of the Betic Neogene basins evolving in a crustal transcurrent shear zone (SE Spain). Bull. Centres Rech. Explor. Prod. Elf-Aquitaine 11, 1-22.

Montenat, C., P. Ott d'Estevou, J. C. Plaziat, and J. Chapel (1980), La signification des

faunes marines contemporaines des évaporites messiniennes dans le Sud-Est de l'Espagne. Conséquences pour l'interprétation des conditions d'isolement de la Méditerranée occidentale, Géol. Méditerr., 7, 81–90.

Morris, J., Leeman, W., Tera, F., 1990. The subducted component in island arc lavas: constraints from Be isotopes and B-Be systematics. Nature 344, 31-36.

Muftić, M., 1965.Geological relationship between coal terrains between mid-Bosnian coal mines: Bila, Zenica, Kakanj and Breza. Geološki glasnik, Geological survey Sarajevo special publication, p. 108.

Mulder, T., Alexander, J., 2001. Abrupt change in slope causes variation in the deposit thickness of concentrated particle-driven density currents. Marine Geology, 175(1), 221-235.

Mutti, E., 1992. Turbidite sandstones. Agip, Istituto di geologia, Università di Parma. 275pp.

Mutti, E., Normark, W.R., 1987. Comparing examples of modern and ancient turbidite systems: problems and concepts, Marine clastic sedimentology. Springer, pp. 1-38.

Mutti, E., Sonnino, M., 1981. Compensation cycles: a diagnostic feature of turbidite sandstone lobes, Int. Ass. Sed. 2nd European Meeting, Bologna, Abstracts, pp. 120-123.

Naydenov, K., Peytcheva, I., von Quadt, A., Sarov, S., Kolcheva, K., Dimov, D., 2013. The Maritsa strike-slip shear zone between Kostenets and Krichim towns, South Bulgaria—Structural, petrographic and isotope geochronology study. Tectonophysics 595, 69-89.

Nikolaeva, K., Gerya, T.V., Connolly, J.A., 2008. Numerical modelling of crustal growth in intraoceanic volcanic arcs. Physics of the Earth and Planetary Interiors 171, 336-356.

Nixon, C.W., McNeill, L.C., Bull, J.M., Bell, R.E., Gawthorpe, R.L., Henstock, T.J., Christodoulou, D., Ford, M., Taylor, B., Sakellariou, D., 2016. Rapid spatiotemporal variations in rift structure during development of the Corinth Rift, central Greece. Tectonics 35, 1225-1248.

Nemec, W., Postma, G., 1993. Quaternary alluvial fans in southwestern Crete: sedimentation processes and geomorphic evolution. In Alluvial sedimentation (Vol. 17, pp. 235-276). IAS Special Publication.

Nemec, W., 1990. Aspects of sediment movement on steep delta slopes. Coarse-grained deltas 10, 29-73.

Nemec, W., Steel, R., 1984. Alluvial and coastal conglomerates: their significant features and some comments on gravelly mass-flow deposits.

Nottvedt, A., Gabrielsen, R.H., Steel, R.J., 1995. Tectonostratigraphy and sedimentary architecture of rift basins, with reference to the northern North Sea. Marine and Petroleum Geology 12, 881-901.

Olujić, J., Pamić, J., Pamić, O., Milojević, R., Veljković, D., Kapeler, I., 1978. Basic Geological Map of the SFRY, 1:100.000, Sheet Vareš (L-34-133). Federal Geological Institute, Belgrade.

Ota, T., Terabayashi, M., Parkinson, C.D., Masago, H., 2000. Thermobaric structure of the Kokchetav ultrahigh-pressure–high-pressure massif deduced from a north–south transect in the Kulet and Saldat–Kol regions, northern Kazakhstan. Island Arc 9, 328-357.

Ott d'Estevou, P., C.Montenat, and J.-C. Alvado (1990), Le bassin de Vera-Garrucha, in Les bassins Néogènes du domaine Bétique Oriental (Espagne), Documents et Travaux IGAL, vol. 12–13, edited by C. Montenat, pp. 165–187, Inst. Géol. Albert-de-Lapparent, Paris.

Ott d'Estevou, P., G. Termier, and H. Termier (1981), La spongiofaune Néogène de Sorbas (Andalousie orientale, Espagne), Geol. Méditerr., 8(2), 61–78.

Pamić, J., 2002. The Sava-vardar Zone of the Dinarides and Hellenides versus the Vardar Ocean. Eclogae Geol Helv 95, 99-113.

Pamić, J., Balogh, K., Hrvatović, H., Balen, D., Jurković, I., Palinkaš, L., 2004. K–Ar and Ar–Ar dating of the Palaeozoic metamorphic complex from the Mid-Bosnian Schist Mts., Central Dinarides, Bosnia and Hercegovina. Miner Petrol 82, 65-79.

Pavelić, D., Kovačić, M., 1999. Lower Miocene Alluvial Deposits of the Pozeska Mt. (Pannonian Basin, Northern Croatia): Cycles, Megacycles and Tectonic Implications. Geologia Croatica, 52(1), 67-76.

Pedrera, A., Galindo-Zaldìvar, J.s., Lamas, F., Ruiz-Const·n, A., 2012. Evolution of near-surface ramp-flat-ramp normal faults and implication during intramontane basin formation in the eastern Betic Cordillera (the Huercal-Overa Basin, SE Spain). Tectonics 31, TC4024.

Peper, T., Cloetingh, S., 1992. Lithosphere dynamics and tectono-stratigraphic evolution of the Mesozoic Betic rifted margin (southeastern Spain). Tectonophysics 203, 345-361.

Petersen, K.D., Nielsen, S., Clausen, O., Stephenson, R., Gerya, T., 2010. Small-scale mantle convection produces stratigraphic sequences in sedimentary basins. Science 329, 827-830.

Petford, N., Gallagher, K., 2001. Partial melting of mafic (amphibolitic) lower crust by periodic influx of basaltic magma. Earth and Planetary Science Letters 193, 483-499.

Pinter, N., Grenerczy, G., Weber, J., Stein, S., Medak, D., 2005. The Adria Microplate: GPS Geodesy, Tectonics and Hazards (Nato Science Series: IV: Earth and Environmental Sciences). Springer, 413 pp.

Placer, L., 1999. Contribution to the macrotectonic subdivision of the border region between Southern Alps and External Dinarides. Geologija 41, 223–255.

Platt, J.P., Behr, W.M., Johanesen, K., Williams, J.R., 2013. The Betic-Rif arc and its orogenic hinterland: a review. Annual Review of Earth and Planetary Sciences 41, 313-357.

Platt, J., Kelley, S., Carter, A., Orozco, M., 2005. Timing of tectonic events in the Alpujárride Complex, Betic Cordillera, southern Spain. Journal of the Geological Society 162, 451-462.

Platt, J., Whitehouse, M., Kelley, S., Carter, A., Hollick, L., 2003. Simultaneous extensional exhumation across the Alboran Basin: Implications for the causes of late orogenic extension. Geology 31, 251-254.

Platt, J., Vissers, R., 1989. Extensional collapse of thickened continental lithosphere: A working hypothesis for the Alboran Sea and Gibraltar arc. Geology 17, 540-543.

Poisson, A., Morel, J.-L., Andrieux, J., Coulon, M., Wernli, R., Guernet, C., 1999. The origin and development of Neogene basins in the SE Betic Cordillera (SE Spain): a case study of the Tabernas-Sorbas and Huercal Overa Basins. Journal of Petroleum Geology 22, 97-114.

Posamentier, H.W., Allen, G.P., 1993. Variability of the sequence stratigraphic model: effects of local basin factors. Sedimentary Geology 86, 91-109.

Postma, G., 1990. An analysis of the variation in delta architecture. Terra Nova, 2(2), 124-130.

Postma, G., 1984. Slumps and their deposits in fan delta front and slope. Geology, 12(1), 27-30.

Postma, G., Cartigny, M.J., 2014. Supercritical and subcritical turbidity currents and their deposits—A synthesis. Geology 42, 987-990.

Postma, G., Cartigny, M., Kleverlaan, K., 2009. Structureless, coarse-tail graded Bouma Ta formed by internal hydraulic jump of the turbidity current? Sedimentary Geology 219, 1-6.

Postma, G., Drinia, H., 1993. Architecture and sedimentary facies evolution of a marine, expanding outer-arc half-graben (Crete, late Miocene). Basin Research, 5(2), 103-124.

Prélat, A., Hodgson, D.M. and Flint, S.S. 2009. Evolution, architecture and hierarchy of distributary deep-water deposits: a high-resolution outcrop investigation from the Permian Karoo Basin, South Africa. Sedimentology, 56, 2132–2154.

Prelević, D., Foley, S., Romer, R., Cvetković, V., Downes, H., 2005. Tertiary ultrapotassic volcanism in Serbia: constraints on petrogenesis and mantle source characteristics. Journal of Petrology 46, 1443-1487.

Prelević, D., Foley, S., 2007. Accretion of arc-oceanic lithospheric mantle in the Mediterranean: evidence from extremely high-Mg olivines and Cr-rich spinel inclusions in lamproites. Earth and Planetary Science Letters 256, 120-135.

Prelević, D., Jacob, D.E., Foley, S.F., 2013. Recycling plus: a new recipe for the formation of Alpine–Himalayan orogenic mantle lithosphere. Earth and Planetary Science Letters 362, 187-197.

Prior, D. B., Bornhold, B. D. 1988. Submarine morphology and processes of fjord fan deltas and related high-gradient systems: modern examples from British Columbia. Fan deltas: sedimentology and tectonic settings, 125-143.

Prosser, S. 1993. Rift-related linked depositional systems and their seismic expression. Geological Society, London, Special Publications, 71(1), 35-66.

Puga-Bernabéu, A., Braga, J.C. and Martín, J.M. (2007). High-frequency cycles in Upper-Miocene ramp-temperate carbonates (Sorbas Basin, SE Spain). Facies 53, p329–345 http://dx.doi.org/10.1007/s10347-007-0107-3

Puga-Bernabéu, Á. , Martín, J.M. and Braga, J.C (2007). Tsunami-related deposits in temperate carbonate ramps, Sorbas Basin, southern Spain. Sedimentary Geology, Volume 199, Issue 3-4, Pages 107-127

Quirk, D.G., 1996. 'Base profile': a unifying concept in alluvial sequence stratigraphy. Geological Society, London, Special Publications 104, 37-49.

Rabagia, T., Matenco, L., Cloetingh, S., 2011. The interplay between eustasy, tectonics and surface processes during the growth of a fault-related structure as derived from sequence stratigraphy: the GovoraeOcnele Mari antiform, South Carpathians. Tectonophysics 502, 196e220.

Ravnas, R., Steel, R., 1998. Architecture of marine rift-basin successions: American Association of Petroleum Geologists Bulletin, v. 82.

Ramaekers, P., Catuneanu, O., 2004. Development and sequences of the Athabasca basin, early Proterozoic, Saskatchewan and Alberta, Canada. The Precambrian Earth: Tempos and Events. Developments in Precambrian Geology, 12, 705-723.

Rampnoux, J.P., 1970. Regards sur les Dinarides internes yougoslaves (Serbie-Monténégro oriental): stratigraphie, évolution paléogéographique, magmatisme. Bulletin Société géologique de France 12, 948–966.

Ranalli, G., 1995. Rheology of the Earth. Chapman and Hall, London, p. 413.

Ratschbacher, L., Frisch, W., Linzer, H.G., Merle, O., 1991. Lateral extrusion in the Eastern Alps; Part 2, Structural analysis. Tectonics 10, 257-271.

Ravnik, D., Rajver, D., Poljak, M., Živčić, M., 1995. Overview of the geothermal field of Slovenia in the area between the Alps, the Dinarides and the Pannonian basin. Tectonophysics 250, 135-149.

Regenauer-Lieb, K., Yuen, D.A., Branlund, J., 2001. The initiation of subduction: criticality by addition of water Science 294, 578-580.

Riding, R., Martin, J.M., Braga, J.C., 1991. Coral-stromatolite reef framework, Upper Miocene, Almería, Spain. Sedimentology 38, 799-818.

Robertson, A.H.F., 2011. Late Palaeozoic - Cenozoic tectonic development of Greece and Albania in the context of alternative reconstructions of Tethys in the Eastern Mediterranean region. International Geology Review 54, 373-454.

Roep, T.B., Dabrio, C.J., Fortuin, A., Polo, M., 1998. Late highstand patterns of shifting and stepping coastal barriers and washover-fans (late Messinian, Sorbas Basin, SE Spain). Sedimentary Geology 116, 27-56.

Rohais, S., Eschard, R., Guillocheau, F., 2008. Depositional model and stratigraphic architecture of rift climax Gilbert-type fan deltas (Gulf of Corinth, Greece). Sedimentary Geology 210, 132-145.

Rosenbaum, G., Regenauer-Lieb, K., Weinberg, R., 2005. Continental extension: From core complexes to rigid block faulting. Geology 33, 609-612.

Rosenbaum, G., Lister, G.S., Duboz, C., 2002. Relative motions of Africa, Iberia and Europe during Alpine orogeny. Tectonophysics 359, 117-129.

Royden, L.H., 1993. Evolution of retreating subduction boundaries formed during continental collision. Tectonics 12, 629-638.

Rudnick, R., Gao, S., 2003. Composition of the continental crust. Treatise on geochemistry 3, 659.

Rudnick, R.L., 1995. Making continental crust. Nature 378, 571.

Ruegg, G. (1964), Geologische Onderzoekingen in Het Bekken Van Sorbas, S Spanje, 64 pp., Amsterdan Geological Institute, Univ. of Amsterdan

Rykkelid, E., Fossen, H., 2002. Layer rotation around vertical fault overlap zones: observations from seismic data, field examples, and physical experiments. Marine and Petroleum Geology 19, 181-192.

Schefer, S., Cvetković, V., Fügenschuh, B., Kounov, A., Ovtcharova, M., Schaltegger, U., Schmid, S., 2011. Cenozoic granitoids in the Dinarides of southern Serbia: age of intrusion, isotope geochemistry, exhumation history and significance for the geodynamic evolution of the Balkan Peninsula. International Journal of Earth Sciences 100, 1181-1206.

Schlager, W., 1993. Accommodation and supply - a dual control on stratigraphic sequences. Sedimentary Geology 86, 111-136.

Schlische, R.W., 1991. Half-graben basin filling models: new constraints on continental extensional basin development. Basin Research 3, 123-141.

Schomacker, E.R., Kjemperud, A.V., Nystuen, J.P., Jahren, J.S., 2010. Recognition and significance of sharp-based mouth-bar deposits in the Eocene Green River Formation, Uinta Basin, Utah. Sedimentology 57, 1069-1087.

Schöpfer, M.P., Childs, C., Walsh, J.J., 2006. Localisation of normal faults in multilayer sequences. Journal of Structural Geology 28, 816-833.

Sharp, I., Gawthorpe, R., Armstrong, B., Underhill, J., 2000. Propagation history and passive rotation of mesoscale normal faults: implications for synrift stratigraphic development. Basin Research 12, 285-305.

Schmid, S., Bernoulli, D., Fügenschuh, B., Matenco, L., Schefer, S., Schuster, R., Tischler, M., Ustaszewski, K., 2008. The Alpine-Carpathian-Dinaridic orogenic system: correlation and evolution of tectonic units. Swiss Journal of Geosciences 101, 139-183.

Schmidt, M.W., Poli, S., 1998. Experimentally based water budgets for dehydrating slabs and consequences for arc magma generation. Earth Planetary Science Letters 163, 361–379.

Seger, M., Alexander, J., 2009. Distribution of Plio-Pleistocene and Modern Coarse-Grained Deltas South of the Gulf of Corinth, Greece. Tectonic Controls and Signatures in Sedimentary Successions (Special Publication 20 of the IAS), 40, 37.

Seghedi, I., Downes, H., 2011. Geochemistry and tectonic development of Cenozoic magmatism in the Carpathian–Pannonian region. Gondwana Research 20, 655-672.

Seghedi, I., Downes, H., Szakács, A., Mason, P.R., Thirlwall, M.F., Roşu, E., Pécskay, Z., Márton, E., Panaiotu, C., 2004. Neogene–Quaternary magmatism and geodynamics in the Carpathian–Pannonian region: a synthesis. Lithos 72, 117-146.

Sizova, E., Gerya, T., Brown, M., 2012. Exhumation mechanisms of melt-bearing ultrahigh pressure crustal rocks during collision of spontaneously moving plates. Journal of Metamorphic Geology 30, 927-955.

Sharp, I. R., Gawthorpe, R. L., Armstrong, B., Underhill, J. R. 2000. Propagation history and passive rotation of mesoscale normal faults: implications for synrift stratigraphic development. Basin Research, 12(3-4), 285-305.

Sofilj, J., Živanović, M., 1971. Basic Geological Map of the SFRY, 1:100.000, Sheet Prozor (K-33-12). Federal Geological Institute, Belgrade.

Sobolev, S.V., Babeyko, A.Y., 2005. What drives orogeny in the Andes? Geology 33, 617-620.

Sokoutis, D., Corti, G., Bonini, M., Brun, J.P., Cloetingh, S., Mauduit, T., Manetti, P., 2007. Modelling the extension of heterogeneous hot lithosphere. Tectonophysics 444, 63-79.

Sokoutis, D., Willingshofer, E., 2011. Decoupling during continental collision and intra-plate deformation. Earth and Planetary Science Letters 305, 435-444.

Southard, J.B., 1991. Experimental determination of bed-form stability. Annual Review of Earth and Planetary Sciences 19, 423-455.

Šoštarić, S.B., Cvetković, V., Neubauer, F., Palinkaš, L.A., Bernroider, M., Genser, J., 2012. Oligocene shoshonitic rocks of the Rogozna Mts.(Central Balkan Peninsula): Evidence of petrogenetic links to the formation of Pb–Zn–Ag ore deposits. Lithos 148, 176-195.

Spakman, W., Wortel, R., 2004. A tomographic view on western Mediterranean geodynamics, The TRANSMED atlas. The Mediterranean region from crust to mantle. Springer, pp. 31-52.

Spychala, Y.T., Hodgson, D.M., Stevenson, C.J., Flint, S.S., 2017. Aggradational lobe fringes: The influence of subtle intrabasinal seabed topography on sediment gravity flow processes and lobe stacking patterns. Sedimentology 64, 582-608.

Stapel, G., Moeys, R., Biermann, C., 1996. Neogene evolution of the Sorbas basin (SE Spain) determined by paleostress analysis. Tectonophysics 255, 291-305.

Steel, R.J., 1976. Devonian basins of western Norway-sedimentary response to

tectonism and to varying tectonic context. Tectonophysics 36, 207-224.

Stevenson, C.J., Jackson, C.A.-L., Hodgson, D.M., Hubbard, S.M., Eggenhuisen, J.T., 2015. Deep-water sediment bypass. Journal of Sedimentary Research 85, 1058-1081.

Stiros, S., 1991. Heat flow and thermal structure of the Aegean Sea and the Southern Balkans, Terrestrial Heat Flow and the Lithosphere Structure. Springer, pp. 395-416.

Strachan, L.J., Rarity, F., Gawthorpe, R.L., Wilson, P., Sharp, I., Hodgetts, D., 2013. Submarine slope processes in rift-margin basins, Miocene Suez Rift, Egypt. Geological Society of America Bulletin 125, 109-127.

Stojadinović, U., Matenco, L., Andriessen, P., Toljić, M., Rundić, L., Ducea, M.N., 2017. Structure and provenance of Late Cretaceous–Miocene sediments located near the NE Dinarides margin: Inferences from kinematics of orogenic building and subsequent extensional collapse. Tectonophyics in press.

Stojadinović, U., Matenco, L., Andriessen, P.A.M., Toljić, M., Foeken, J.P.T., 2013. The balance between orogenic building and subsequent extension during the Tertiary evolution of the NE Dinarides: Constraints from low-temperature thermochronology. Global and Planetary Change 103, 19-38.

Støren, E.N., Dahl, S.O., Nesje, A., Paasche, Ø., 2010. Identifying the sedimentary imprint of high-frequency Holocene river floods in lake sediments: development and application of a new method. Quaternary Science Reviews 29, 3021-3033.

Strachan, L. J., Rarity, F., Gawthorpe, R. L., Wilson, P., Sharp, I., Hodgetts, D. 2013. Submarine slope processes in rift-margin basins, Miocene Suez Rift, Egypt. Geological Society of America Bulletin, 125(1-2), 109-127.

Sweet, A. R., Long, D. G. F., Catuneanu, O., 2003. Sequence boundaries in finegrained terrestrial facies: biostratigraphic time control is key to their recognition. Geological Association of Canada-Mineralogical Association of Canada joint annual meeting, Vancouver, May 25–28. In Abstracts (Vol. 28, p. 165).

Sweet, A.R., Catuneanu, O., Lerbekmo, J.F., 2005. Uncoupling the position of sequence-bounding unconformities from lithological criteria in fluvial systems, American Association of Petroleum Geologists Annual Convention, pp. 19-22.

Talling, P. J., Masson, D. G., Sumner, E. J., Malgesini, G., 2012. Subaqueous sediment density flows: depositional processes and deposit types. Sedimentology, 59(7), 1937-2003.

Tari, G., Horváth, F., Rumpler, J., 1992. Styles of extension in the Pannonian basin. Tectonophysics 208, 203-219.

Tirel, C., Brun, J.P., Burov, E., 2004. Thermomechanical modeling of extensional gneiss domes, in: Whitney, D.L., Teyssier, C., Siddoway, C.S. (Eds.), Gneiss domes in orogeny. Geological Society of America Special Paper 380, Boulder, Colorado, pp. 67–78.

Toljić, M., Matenco, L., Ducea, M.N., Stojadinović, U., Milivojević, J., Đerić, N., 2013. The evolution of a key segment in the Europe–Adria collision: The Fruška Gora of northern Serbia. Global and Planetary Change 103, 39-62.

Tommasini, S., Avanzinelli, R., Conticelli, S., 2011. The Th/La and Sm/La conundrum of the Tethyan realm lamproites. Earth and Planetary Science Letters 301, 469-478.

Tomljenović, B., Csontos, L., 2001. Neogene-Quaternary structures in the border zone between Alps, Dinarides and Pannonian Basin (Hrvatsko zagorje and Karlovac Basins, Croatia). International Journal of Earth Sciences, V90, 560-578.

Torres-Roldan, R.L., 1979. The tectonic subdivision of the Betic Zone (Betic

Cordilleras, southern Spain); its significance and one possible geotectonic scenario for the westernmost Alpine Belt. American Journal of Science 279, 19-51.

Trudgill, B. D., 2002. Structural controls on drainage development in the Canyonlands grabens of southeast Utah. AAPG bulletin, 86(6), 1095-1112.

Tugend, J., Manatschal, G., Kusznir, N.J., Masini, E., Mohn, G., Thinon, I., 2014. Formation and deformation of hyperextended rift systems: Insights from rift domain mapping in the Bay of Biscay-Pyrenees. Tectonics 33, 1239-1276.

Tschegg, C., Ntaflos, T., Seghedi, I., Harangi, S., Kosler, J., Coltorti, M., 2010. Paleogene alkaline magmatism in the South Carpathians (Poiana Ruscă, Romania): Asthenosperic melts with geodynamic and lithospheric information. Lithos 120, 393-406.

Turcotte, D., Schubert, G., 2002. Geodynamics, Cambridge Univ. Press, Cambridge, UK, 472 pp. doi 10, 0521666244.

Ueda, K., Gerya, T.V., Burg, J.P., 2012. Delamination in collisional orogens: Thermomechanical modeling. Journal of Geophysical Research: Solid Earth 117.

Ustaszewski, K., Kounov, A., Schmid, S.M., Schaltegger, U., Krenn, E., Frank, W., Fügenschuh, B., 2010. Evolution of the Adria-Europe plate boundary in the northern Dinarides: From continent-continent collision to back-arc extension. Tectonics 29, TC6017, doi: 6010.1029/2010tc002668.

Ustaszewski, K., Herak, M., Tomljenović, B., Herak, D., Matej, S., 2014. Neotectonics of the Dinarides–Pannonian Basin transition and possible earthquake sources in the Banja Luka epicentral area. Journal of Geodynamics, 82, 52-68.

van Gelder, I.E., Matenco, L., Willingshofer, E., Tomljenović, B., Andriessen, P.A.M., Ducea, M.N., Beniest, A., Gruić, A., 2015. The tectonic evolution of a critical segment of the Dinarides-Alps connection: Kinematic and geochronological inferences from the Medvednica Mountains, NE Croatia. Tectonics 10.1002/2015TC003937

van Hunen, J., van den Berg, A.P., Vlaar, N.J., 2000. A thermo-mechanical model of horizontal subduction below an overriding plate. Earth and Planetary Science Letters 182, 157-169.

van Wagoner, J.C., Mitchum, R.M., Campion, K.M., Rahmanian, V.D., 1990. Siliciclastic sequence stratigraphy in well logs, cores, and outcrops. Am. Ass. Petrol. Geol. Expl. Ser. 7, 211-240.

van Wijk, J., van Hunen, J., Goes, S., 2008. Small-scale convection during continental rifting: Evidence from the Rio Grande rift. Geology 36, 575-578.

Vázquez, M., Jabaloy, A., Barbero, L., Stuart, F.M., 2011. Deciphering tectonic- and erosion-driven exhumation of the Nevado–Filabride Complex (Betic Cordillera, Southern Spain) by low temperature thermochronology. Terra Nova 23, 257–263. http://dx.doi.org/10.1111/j.1365-3121.2011.01007.x

Verdel, C., Wernicke, B.P., Hassanzadeh, J., Guest, B., 2011. A Paleogene extensional arc flare-up in Iran. Tectonics 30, TC3008, doi:10.1029/2010TC002809.

Vergés, J., Fernàndez, M., 2012. Tethys–Atlantic interaction along the Iberia–Africa plate boundary: The Betic–Rif orogenic system. Tectonophysics 579, 144-172.

Vissers, R.L., 2002. André Dumont medallist lecture 2011 Extension in a convergent tectonic setting: a lithospheric view on the Alboran system of SW Europe. Geologica Belgica 2012, 53-72.

Vogt, K., Gerya, T.V., Castro, A., 2012. Crustal growth at active continental margins: numerical modeling. Physics of the Earth and Planetary Interiors 192, 1-20.

Vogt, K., Matenco, L., Cloetingh, S., 2017. Crustal mechanics control the geometry of mountain belts. Insights from numerical modelling. Earth and Planetary Science Letters 460, 12-21.

Völk, H. R. (1966), Geologie et stratigraphie du Bassin Neogene de Vera, Doctoral thesis, 121 pp., Amsterdam University, Amsterdam.

von Quadt, A., Peytcheva, I., Cvetkovic, V., 2003. Geochronology, geochemistry and isotope tracing of the Cretaceous magmatism of East-Serbia and Panagyurishte district (Bulgaria) as part of the Apuseni–Timok–Srednogorie metallogenic belt in Eastern Europe. Mineral exploration and sustainable development. Millpress, Rotterdam, 407-410.

Watts, A., Piatt, J., Buhl, P., 1993. Tectonic evolution of the Alboran Sea basin. Basin Research 5, 153-177.

Weijermars, R., Th. B. Roep, B. van den Eeckhout, G. Postma and K.Kleverlaan, 1985. Uplift history of a Betic fold nappe inferred from NeogeneQuaternary sedimentation and tectonics (in the Sierra Alhamilla and Almeria, Sorbas and Tabernas Basins of the Betic Cordilleras, SE Spain. Geologie en Mijnbouw, 64, 397411.

Wernicke, B., 1992. Cenozoic extensional tectonics of the U.S. Cordillera, in: B.C., B., Lipman, P.W., Zoback, M.L. (Eds.), The Cordilleran orogen: Conterminous U.S.: Boulder, Colorado,. Geological Society of America, pp. 553-581.

Wiens, D.A., Conder, J.A., Faul, U.H., 2008. The seismic structure and dynamics of the mantle wedge. Annual Review Earth Planetary Sciences 36, 421-455.

Willingshofer, E., Sokoutis, D., Luth, S., Beekman, F., Cloetingh, S., 2013. Subduction and deformation of the continental lithosphere in response to plate and crust-mantle coupling. Geology 41, 1239-1242.

Wilson, P., Gawthorpe, R.L., Hodgetts, D., Rarity, F., Sharp, I.R., 2009. Geometry and architecture of faults in a syn-rift normal fault array: the Nukhul half-graben, Suez rift, Egypt. Journal of Structural Geology 31, 759-775.

Withjack, M.O., Schlische, R.W. and Olsen, P.E., 2002. Rift basin structure and its influence on sedimentary systems. In: Sedimentation in Continental Rifts (Eds R.W. Renaut and G.M. Ashley), SEPM Spec. Publ., 73, 57–81.

Young, M. J., Gawthorpe, R. L., Sharp, I. R., 2000. Sedimentology and sequence stratigraphy of a transfer zone coarse-grained delta, Miocene Suez Rift, Egypt. Sedimentology, 47(6), 1081-1104.

Zachos, J.C., Pagani, M., Sloan, L., Thomas, E., Billups, K., 2001. Trends, Rhythms, and Aberrations in Global Climate 65 Ma to Present. Science 292, 686-693.

Zhu, D.-C., Wang, Q., Zhao, Z.-D., Chung, S.-L., Cawood, P.A., Niu, Y., Liu, S.-A., Wu, F.-Y., Mo, X.-X., 2015. Magmatic record of India-Asia collision. Scientific reports 5, 14289.

Zhu, G., Gerya, T.V., Tackley, P.J., Kissling, E., 2013. Four-dimensional numerical modeling of crustal growth at active continental margins. Journal of Geophysical Research: Solid Earth 118, 4682-4698.

Ziegler, P. A., Cloetingh, S., 2004. Dynamic processes controlling evolution of rifted basins. Earth-Science Reviews, 64(1), 1-50.

Živanović, M., Sofilj, J., Milojević, R., 1967. Basic Geological Map of the SFRY, 1:100.000, Sheet Zenica (L-33-144). Federal Geological Institute, Belgrade.

About the Author

The author of this thesis was born on February 5, 1988 in Kragujevac, Serbia. In 2010 she earned her Bachelor's degree (cum laude) in Geology from Faculty of Mining and Geology, Belgrade, Serbia, followed by a Master's degree (cum laude) in 2012, in Petrology and Geochemistry from the same institution. In March 2014, she started her PhD project at the Department of Petrology and Geochemistry, Faculty of Mining and Geology, University of Belgrade and in the Tectonics Research Group of the Department of Earth Sciences of Utrecht University.